

Investigating a novel  
antifungal drug that inhibits  
fatty acid desaturation

A thesis submitted to  
**University College London**  
in the fulfilment of the requirement for the degree of  
**Doctor of Philosophy**

**Supervisor:** Professor Tim Levine

Department of Cell Biology,  
Faculty of Brain Science

2020

# Declaration

I, Sarah Murphy, confirm that the work presented in this thesis is my own. Where information has been derived from other sources, I confirm that this has been indicated.

---

January 2020

# Abstract

Invasive fungal infections represent a group of diseases that are of increasing worldwide concern. This group of diseases is associated with high mortality rates that can be attributed to widespread clinical drug resistance. Of significant concern, resistance has been recorded against every licenced clinical treatment. F900742 is a member of a novel and hopeful antifungal drug class that exerts activity through the inhibition of fatty acid desaturation. It is likely that F900742 directly targets the fatty acid desaturase  $\Delta 9$  desaturase. F900742 demonstrated broad-spectrum antifungal activity *in vitro* and *in vivo* *G. mellonella* studies at low doses of drug. Ultrastructural analysis established that the inhibition of the OLE1 pathway induced the rapid formation of previously unidentified, lipid-dependent structures that are derived from the ER. It is predicted that these compartments are high in saturated acyl chain content. The sole  $\Delta 9$  desaturase in the budding yeast *Saccharomyces cerevisiae*, Ole1p, relocalised to areas consistent with the aberrant structures. This investigation characterised a novel cellular response to acute inhibition of fatty acid desaturation through the formation of lipo-protective compartments that sequester toxic levels of saturated lipids. F900742 also induced mitochondrial fission and significant ROS production. Together this data suggested that the mechanism of action of F900742 is via lipid-dependent responses that quickly alters the lipidome in favour of saturated lipid content which induces ER and mitochondrial morphological phenotypes and subsequent activation of processes such as ROS production and the UPR.

# Impact statement

The annual mortality as a result of invasive fungal infections has increased over the past few decades. This can largely be attributed to the development of resistance to antifungal treatments, an increase in the number of susceptible patients, and the advent of strains inherently resistant to all clinical options. Of particular clinical concern, resistance has been noted against all antifungal drug classes as such it is predicted that there will be an increase in the number of mortalities worldwide. It is therefore of paramount importance that novel antifungal treatment options are quickly identified and brought to market. However, difficulties in identifying compounds that display sufficient antifungal activity, but limited human toxicity has resulted in an almost 20 year gap since the last novel antifungal drug class was approved for clinical use.

The research presented here identified the likely target of a novel compound, F900742. This drug is predicted to inhibit fatty acid desaturation through competitive inhibition of  $\Delta 9$  desaturase, Ole1p. Ole1p is an essential enzyme within fungi that is not currently targeted by any clinically approved agents. The OLE1 pathway was shown to be a promising antifungal target *in vitro* with a greater than 90% killing rate after a single dose over 24 hours. The antifungal activity of F900742 was corroborated by *in vivo G. mellonella* studies which confirmed that a single dose of F900742 at the MIC was sufficient to ensure a greater than 80% survival rate against a lethal dose of *C. albicans*. This provided powerful evidence for further development of compounds that target Ole1p for use as antifungal agents which could save many thousands of lives each year. However, development of Ole1p inhibitors is significantly hampered by the fact that the fungal desaturase has not been isolated and crystallised to date. Resolving the crystal structure of Ole1p would aid structurally driven design of novel inhibitors that are specific against fungal isoforms only. Although F900742 demonstrated good *in vivo* antifungal activity in the insect model, the addition of serum or BSA reversed the growth inhibitory effect of the drug suggesting it would be of limited use in the clinic. Further to this, and in line with the RRRs for animal testing,



the reversal of antifungal activity highlighted that all hopeful antifungal compounds should undergo *in vitro* testing in relevant serum media to assess activity prior to *in vivo* mammalian studies.

Ultrastructural analysis identified aberrant, ER-derived cytosolic compartments as an acute response to fatty acid desaturation by F900742. Irrespective of its use as a clinical treatment, F900742 represents an informative compound to further our understanding of lipotoxic events. With rising numbers of adverse effects from lipid-related diseases such as obesity, non-alcoholic liver steatosis, and type 2 diabetes, it is essential that research is done to identify mechanisms that underpin both early and late stage lipotoxic events initiated by a range of aberrant lipid profiles.

# Acknowledgments

Wow, what an incredible four years. This PhD has been both stimulating and frustrating, and everything in between - a truly fantastic rollercoaster. It has opened doors into a new field of research and has provided an unexpected career focus. As I start this next chapter of my life, I've been reflecting on those who have helped me to reach this exciting point. I am incredibly fortunate that I have had the support of so many people, so I just wish to say thank you. Completing my PhD would have been a lot more difficult without you all, and my life a lot less fun!

None of my project would have been possible without the brilliant mind of Professor Tim Levine. Tim, thank you. Thank you for offering me the opportunity to work in your group. Thank you for training me with laboratory skills, equipping my mind with alternative ways of thinking, and developing my curiosity. Your endless ideas and enthusiasm have kept me motivated even during the most frustrating of cloning experiments. Your tireless support and guidance have made working in your lab a thoroughly enjoyable experience and a complete privilege. Thank you!

I must also thank my second supervisor, Professor Patric Turowski, for his input in my upgrade which was incredibly useful for the target validation experiments.

Thank you to Mike Birch and Jason Oliver at F2G who provided the opportunity to work in antifungal drug development. I was fortunate enough to gain an excellent insight into the pharmaceutical industry and drug development through time spent at their site. Thank you to Derek Law and Ressa for your help with my experiments at F2G. Thank you to other members at F2G for the useful discussions regarding the drug development process.

Thank you to the BBSRC who funded my studentship.

The UCL Institute of Ophthalmology is bursting with fantastic and friendly scientists: there is no end to the help that people offer. I must extend a huge thank you to Dr Matt Hayes for his continued support with everything microscopy and especially with the EM work in this thesis. Thank you to Diana for your assistance with the

microscopes as well. The Institute would not function without the superwoman that is Claire Cox. Thank you, Claire, for all you have done for me personally and professionally.

Past and present members of Tim's lab have been instrumental in my training. Alberto, thank you for all of your help in the beginning. Banji, it has been great being able to bounce ideas off you and learn from your previous experiences in the more recent years. And to my dear friend, Louise. You've trained me scientifically and supported my research from Day One, offering alternative ideas, training, and guidance. Above all, your friendship has been one of a kind. I have learnt far more than just "science" from you. I cannot thank you enough (or supply enough cookies!) for everything you have done. Thank you!

Dr Emily Eden has also been a fantastic friend and mentor to me, but an extra thank you for your help with all of my HeLa work.

Other past and present members of the Eden-Futter-Levine-Moss office space and the Cell Biology Department have made my time at UCL a lot of fun!

To old friends from school, to new friends that I have met in London, those who have seen me at my weakest after horrendous track sessions, Sarah who was the best housemate, and lifelong friends in the News Team from The University of Birmingham, thank you for all of the great memories, motivation, and encouragement in all areas of my life.

Alice and Sarah, somehow you saw me through the days of undergraduate biochemistry and undoubtedly furthered my enthusiasm for the subject. It seems somewhat poetic that on our 10 year friendship anniversary I have my PhD viva! Thank you for always being such wonderful and supportive friends. I'm endlessly thankful that you both proofread my thesis. I hope that one day you will be using a drug that I have helped to develop in the clinic, Sarah!

I have had an incredibly close group of friends throughout my life. To the "Girlies" from school, and in particular Kate, Holly, Sophie, Lauren, Shalini, Suzie, and Hattie, you are lifelong friends and have been by my side through every achievement (and

commiseration) since we were just four years old. I treasure each and every one of you. I have to thank you all for keeping me sane, and being so understanding, especially during the final stages of my PhD.

James, thank you for all of your love and encouragement even when we've been continents apart. The South American adventures, the beach caipis, and the pasta bakes were instrumental in the completion of writing my thesis!! I cannot wait to explore so much more of the world with you. Also, many apologies for not dedicating the entire thesis to you, but I hope you know how thankful I am for everything you have done for me and for us.

Last and by no means least, my family:

To my Auntie Sabina and Uncle Tim, thank you for showing me so much love and generosity. Thank you for feeding me lots of potatoes(!) and housing me during the final months of my PhD. I absolutely loved staying with you and my cousins, Finn, Emilia, and Indy. I cannot thank you enough for all of the crazy times at "The Mad House".

My sister, Tor, thank you for your infectious positivity and constant encouragement. Whether it's cheering from the side of the netball court or at the track, finding the best wine bars, or being a shoulder through more trying times, you are always there to share the best moments of life with. I've loved you living in London and it has been so wonderful to share this chapter with you just down the road.

Probably (possibly?!) the hardest part of this entire PhD is finding the words to thank my parents. Thank you feels such an inadequate phrase for the sacrifices you made for mine and Tor's education when we were younger; for inspiring our curiosity and constantly supporting our ambitions. Know that we are both forever grateful and thankful that we were so lucky.

# Contents

Declaration.....	1
Abstract.....	2
Impact statement.....	3
Acknowledgments.....	5
Contents.....	8
List of figures.....	11
List of tables.....	14
List of abbreviations.....	15
Introduction.....	17
CHAPTER 1: Introduction.....	18
1.1 The global prevalence of fungal infections.....	18
1.1.1 Epidemiology of fungal infections.....	19
1.1.2 Candidiasis.....	20
1.1.3 Aspergillosis.....	22
1.1.4 Diagnosis of fungal infections.....	23
1.1.5 Antifungal clinical treatments.....	24
1.1.6 Routes to antifungal drug resistance.....	27
1.1.7 Emerging strains.....	34
1.2 Lipids.....	36
1.2.1 Fatty acids.....	38
1.3 $\Delta 9$ desaturases and fatty acid desaturation.....	42
1.3.1 Ole1p.....	42
1.3.2 Structure of $\Delta 9$ desaturases.....	42
1.3.3 Regulation of OLE1 expression.....	50
1.3.4 Ole1p and the mitochondria.....	55
CHAPTER 2: Aims of study.....	57
CHAPTER 3: Materials and Methods.....	58
Results.....	78
CHAPTER 4: F900742 induced Ole1p mislocalisation.....	79

4.1 Introduction.....	79
4.2 Results.....	82
4.2.1 <i>S. cerevisiae</i> was sensitive to F900742.....	82
4.2.2 OLE1 pathway mutants altered the sensitivity to F900742.....	87
4.2.3 Higher temperatures reduced the activity of F900742.....	92
4.2.4 F900742 induced a redistribution of Ole1p.....	96
4.2.5 F900742 induced an increase in expression of Ole1p.....	101
4.2.6 Ole1p relocalisation was specific to F900742.....	103
4.2.7 Unsaturated fatty acids inhibited the redistribution of Ole1p..	106
4.2.7.1 Oleic acid.....	106
4.2.7.2 Palmitoleic acid.....	112
4.2.7.3 Stearic acid.....	121
4.2.8 F900742 induced an increase in Ole1p-GFP protein synthesis.	124
4.2.9 F900742 altered the expression of Ubx2p and Sct1p.....	128
4.3 Discussion.....	131
CHAPTER 5: F900742 target verification.....	134
5.1 Introduction.....	134
5.2 Results.....	135
5.2.1 Deletion of OLE1 reduced the sensitivity of <i>S. cerevisiae</i> to F900742.....	135
5.2.2 OLE1 overexpression reduced the inhibitory capacity of F900742.....	140
5.2.3 F900742 was not active in HeLa cells at concentrations relevant for antifungal activity.....	143
5.2.4 F900742 inhibited Scd1 function in <i>ole1</i> null yeast.....	147
5.2.5 Identification of residues essential for F900742.....	149
5.2.6 Inducing mutations in OLE1.....	157
5.3 Discussion.....	161
CHAPTER 6: Investigating the mechanism of action of F900742.....	168
6.1 Introduction.....	168
6.2 Results.....	169
6.2.1 F900742 inhibited growth in logarithmic phase.....	169

6.2.2	F900742 exerted a fungistatic mechanism of action.....	170
6.2.3	F900742 effects were selective for the OLE1 pathways.....	172
6.2.4	F900742 induced the formation of unidentified structures.....	176
6.2.5	Ole1p-GFP did not relocalise to lipid droplets.....	193
6.2.6	F900742 induced mitochondria fission.....	195
6.2.7	The morphology of other organelles was unaffected by F900742.....	201
6.2.8	Ultrastructural analysis of F900742 treated fungi.....	204
6.2.8.1	<i>S. cerevisiae</i> .....	204
6.2.8.2	<i>C. albicans</i> .....	213
6.2.8.3	<i>A. fumigatus</i> .....	217
6.2.9	Mechanism of action.....	220
6.2.9.1	F900742 induced the production of ROS.....	220
6.2.10	Ole1p-GFP was degraded by the proteasome.....	225
6.3	Discussion.....	235
CHAPTER 7: <i>In vivo</i> analysis of F900742.....		240
7.1	Introduction.....	240
7.2	Results.....	244
7.2.1	F900742 activity in the fungal model <i>G. mellonella</i> .....	244
7.2.1.1	Pilot inoculum study.....	244
7.2.1.2	F900742 tolerance pilot study.....	245
7.2.1.3	F900742 demonstrated <i>in vivo</i> antifungal efficacy.....	247
7.2.2	Fungal burden analysis in <i>G. mellonella</i> treated with F900742.....	250
7.2.3	F900742 activity in mammalian models.....	253
7.2.4	Investigating the activity of novel F6 series compounds.....	254
7.3	Discussion.....	257
Discussion.....		261
CHAPTER 8: Final discussion.....		262
References.....		272

# List of Figures

Figure 1.1 Mechanism of action of the frontline antifungal drug classes for the treatment of invasive fungal infections.....	26
Figure 1.2 Common mechanisms of antifungal drug resistance.....	33
Figure 1.3 F900742 reversal assay.....	36
Figure 1.4 General structure of a phospholipid.....	40
Figure 1.5 <i>De novo</i> synthesis of unsaturated fatty acids.....	40
Figure 1.6 Sequence alignment of mammalian SCD1 isoforms with other $\Delta 9$ desaturases.....	46
Figure 1.7 Sequence alignment of $\Delta 9$ desaturases from fungal strains used in this study and mammalian homologs.....	47
Figure 1.8 Structure of eukaryotic $\Delta 9$ desaturases.....	49
Figure 1.9 Mga2p rotation-based lipid sensing.....	53
Figure 1.10 Model of OLE1 transcription activation.....	53
Figure 1.11 Regulation of fatty acid saturation content by Ole1p and Sct1p.....	55
Figure 4.1 BY Ole1-GFP construct.....	83
Figure 4.2 MICs of <i>S. cerevisiae</i> , <i>S. japonicus</i> , <i>S. pombe</i> .....	85
Figure 4.3 OLE1 pathway mutants altered the sensitivity to F900742.....	90
Figure 4.4 F900742 displayed temperature sensitive activity.....	94
Figure 4.5 Ole1p-GFP localised to the peripheral and nuclear ER.....	97
Figure 4.6 F900742 induced the relocalisation of Ole1p-GFP.....	99
Figure 4.7 F900742 induced an increase in expression of Ole1p-GFP.....	102
Figure 4.8 Relocalisation events were specific between Ole1p and F900742.....	104
Figure 4.9 Oleic acid rescued the activity of F900742.....	107
Figure 4.10 Oleic acid reversed the relocalisation of Ole1p-GFP and the associated increase in expression.....	110
Figure 4.11 Palmitic acid inhibited the activity of F900742.....	113
Figure 4.12 Palmitoleic acid reversed the relocalisation and increased expression of Ole1p.....	116
Figure 4.13 Oleic acid and palmitoleic acid inhibited and reversed F900742 activity.....	119



Figure 4.14 Stearic acid did not reverse F900742 activity.....	122
Figure 4.15 F900742 induced an increase in OLE1 transcription.....	126
Figure 4.16 F900742 induced the relocalisation of Ubx2p-GFP and Sct1p-GFP.....	129
Figure 5.1 Deletion of OLE1 generated an unsaturated fatty acid auxotroph .....	136
Figure 5.2 Deletion of OLE1 altered the sensitivity of F900742.....	138
Figure 5.3 BY $\Delta ole1$ was sensitive to F900742 at high concentrations.....	140
Figure 5.4 Overexpression of Ole1p reduced the inhibitory capacity of F900742.....	142
Figure 5.5 F900742 was not active in HeLa cells at concentrations relevant for antifungal activity.....	145
Figure 5.6 F900742 inhibited Scd1 function in <i>ole1</i> null yeast .....	149
Figure 5.7 OLE1 homologous combination mutagenic cloning strategy.....	152
Figure 5.8 Summary of amino acid substitutions within the OLE1 ORF .....	153
Figure 5.9 Pilot study to determine F900742 concentration for minimal growth of yeast.....	154
Figure 5.10 Ole1p expressed off pOLE1 <sup>wt</sup> did not relocalise .....	156
Figure 5.11 Repeated exposure to F900742 to induce mutation in OLE1.....	159
Figure 6.1 F900742 inhibited growth in logarithmic phase.....	170
Figure 6.2 F900742 exerted a fungistatic mechanism of action.....	171
Figure 6.3 The localisation of ER membrane proteins was unaffected by F900742...	174
Figure 6.4 F900742 induced the relocalisation of RFP-HDEL in wild type yeast.....	177
Figure 6.5 F900742 induced the relocalisation of RFP-HDEL in OLE1 null pathway strains.....	178
Figure 6.6 F900742 induced a rapid relocalisation of RFP-HDEL.....	181
Figure 6.7 Oleic acid inhibited RFP-HDEL relocalisation.....	183
Figure 6.8 Oleic acid reversed RFP-HDEL relocalisation.....	184
Figure 6.9 Deletion of SPT23 was not sufficient to induce the relocalisation of RFP- HDEL.....	187
Figure 6.10 Deletion of OLE1 induced the redistribution of RFP-HDEL.....	189
Figure 6.11 Ole1p-GFP relocalised to RFP-HDEL.....	191
Figure 6.12 Ole1p-GFP relocalised to RFP-HDEL in the diploid Ole1-GFP RFP-HDEL...	192
Figure 6.13 Ole1p-GFP did not relocalise to lipid droplets.....	194
Figure 6.14 Mitochondria morphology and distribution in wild type <i>S. cerevisiae</i> .....	196

Figure 6.15 F900742 induced mitochondrial fission.....	198
Figure 6.16 Oleic acid inhibited F900742-induced mitochondrial fission.....	199
Figure 6.17 Oleic acid reversed F900742-induced mitochondrial fission.....	200
Figure 6.18 F900742 did not induce morphological defects to other organelles.....	202
Figure 6.19 Ultrastructural analysis of F900742-induced morphological phenotypes in <i>S. cerevisiae</i> .....	207
Figure 6.20 Ultrastructural analysis of F900742-induced morphological phenotypes in <i>C. albicans</i> .....	215
Figure 6.21 Ultrastructural analysis of F900742-induced morphological phenotypes in <i>A. fumigatus</i> .....	218
Figure 6.22 F900742 induced the generation of ROS.....	224
Figure 6.23 MG132 did not inhibit oleic acid-induced turnover of Ole1p in BY Ole1-GFP.....	227
Figure 6.24 MG132 did not inhibit the degradation of Ole1p in BY Ole1-GFP.....	229
Figure 6.25 MG132 inhibited Ole1p degradation in $\Delta erg6$ .....	231
Figure 6.26 Ole1p-GFP turnover was not via vacuolar degradation or autophagy.....	234
Figure 7.1 Physiological changes to <i>G. mellonella</i> larvae infected with candidiasis...	243
Figure 7.2 <i>C. albicans</i> inoculum size testing.....	245
Figure 7.3 F900742 had good <i>in vivo</i> efficacy in the <i>G. mellonella</i> model of candidiasis.....	248
Figure 7.4 A second dose of F900742 exerted a greater <i>in vivo</i> protective effect.....	250
Figure 7.5 Fungal burden analysis in <i>G. mellonella</i> .....	252
Figure 7.6 FBS or BSA supplementation was sufficient to inhibit F900742.....	254
Figure 7.7 Antifungal efficacy of novel F6 series compounds.....	256
Figure 8.1 Proposed mechanism of action of F900742.....	269

# List of Tables

Table 1.1	The 10 most common invasive fungal infections.....	19
Table 3.1	Yeast strains used in this study.....	59
Table 3.2	Yeast expression plasmids used in this study.....	61
Table 3.3	Purchased yeast expression plasmids.....	62
Table 3.4	SCD1 image clone.....	62
Table 3.5	Primers used in this study.....	67
Table 3.6	Antibodies used in this study.....	73
Table 4.1	Table of MICs of selected yeast, bacteria, dermatophytes, and moulds.....	79
Table 7.1	F900742 drug tolerance pilot study.....	246

# List of Abbreviations

<b>Aa</b>	Amino acid
<b>ABC</b>	ATP binding cassette
<b><i>A. fumigatus</i></b>	<i>Aspergillus fumigatus</i>
<b><i>A. terreus</i></b>	<i>Aspergillus terreus</i>
<b>AIDS</b>	Acquired immune deficiency syndrome
<b>AmB</b>	Amphotericin B
<b>AU</b>	Arbitrary units
<b>Bp</b>	Base pair
<b>BSA</b>	Bovine serum albumin
<b><i>C. albicans</i></b>	<i>Candida albicans</i>
<b><i>C. krusei</i></b>	<i>Candida krusei</i>
<b>CHX</b>	Cycloheximide
<b>DNA</b>	Deoxyribonucleic acid
<b><i>Ec</i></b>	<i>E. coli</i>
<b>EM</b>	Electron microscopy
<b>ER</b>	Endoplasmic reticulum
<b>ERAD</b>	Endoplasmic-reticulum-associated protein degradation
<b>FA</b>	Fatty acid
<b>FBS</b>	Fetal bovine serum
<b>F9</b>	F900742
<b>Gal</b>	Galactose
<b>GDP</b>	Triose-phosphate dehydrogenase
<b>GFP</b>	Green fluorescent protein
<b>GPI</b>	Glycosylphosphatidylinositol
<b>HIV</b>	Human immunodeficiency virus
<b><i>Hs</i></b>	<i>Homo sapien</i>
<b>IC50</b>	50% inhibitory concentration
<b>IC90</b>	90% inhibitory concentration
<b>IMM</b>	Inner mitochondrial membrane
<b>Kb</b>	Kilobase
<b>MG</b>	MG132
<b>MIC</b>	Minimum inhibitory concentrations
<b>Mins</b>	Minutes
<b>Mut</b>	Mutant
<b>MW</b>	Molecular weight
<b>NAC</b>	N-acetyl cysteine
<b>NAT</b>	Nourseothricin
<b>Ns</b>	Non significant
<b>OA</b>	Oleic acid

<b>OD</b>	Optical density
<b>OLF</b>	Olorofim
<b>ORF</b>	Open reading frame
<b>PA</b>	Phosphatidic acid
<b>PC</b>	Phosphatidylcholine
<b>PCR</b>	Polymerase chain reaction
<b>PE</b>	Phosphatidylethanolamine
<b>PHO5</b>	Phosphate metabolism 5
<b>PI</b>	Phosphatidylinositol
<b>RFP</b>	Red fluorescent protein
<b>ROS</b>	Reactive oxygen species
<b>SA</b>	Stearic acid
<b>SAB</b>	Sabourand
<b><i>S. cerevisiae</i></b>	<i>Saccharomyces cerevisiae</i>
<b><i>S. japonicus</i></b>	<i>Saccharomyces japonicus</i>
<b><i>S. pombe</i></b>	<i>Saccharomyces pombe</i>
<b>Sec61</b>	Secretory61
<b>TGN</b>	Trans Golgi network
<b>TMD</b>	Transmembrane domain

# Introduction

# CHAPTER 1

## Introduction

### 1.1 The global prevalence of fungal infections

Globally, over one and a half million people die every year from invasive fungal infections. The mortality rate from this group of infections is greater than malaria or breast cancer and is similar to tuberculosis and HIV/AIDS. Although the majority of people will experience mild, easy-to-treat fungal infections throughout their lifetime, many millions will contract life-threatening infections that are much harder to diagnose and cure. The mortality rate associated with invasive fungal infections is often greater than 50% and nearing 100% in some cases (Table 1.1). Despite the very high mortality rates, epidemiological data is poor because the World Health Organisation (WHO) does not have a programme for the management of invasive fungal infections and, with the exception of the US Centres of Disease Control and Prevention monitoring coccidioidomycosis (also known as valley fever), no public health agencies conduct surveillance (1).

There is wide availability of multiple antifungal drugs, yet invasive fungal infections remain notoriously difficult to diagnose and treat. Currently there are no rapid clinical tests that can reliably differentiate between fungal strains restricting any scope for strain-specific treatments (2,3). This further exacerbates clinical complications stemming from the inherent difficulties in overcoming the fungi plastic genome and rapid rate of reproduction. These factors, alongside the widespread use of agricultural fungicides, facilitate the selection of strains that rapidly acquire resistance. Of particular concern, there has been resistance recorded against all licenced clinical therapeutics (4). This is discussed further in section 1.1.6, routes to antifungal drug resistance.

Disease (most common species)	Location	Estimated life-threatening infections/ year at that location*	Mortality rates (% in infected populations)*
Opportunistic invasive mycoses			
Aspergillosis ( <i>Aspergillus fumigatus</i> )	Worldwide	>200,000	30–95
Candidiasis ( <i>Candida albicans</i> )	Worldwide	>400,000	46–75
Cryptococcosis ( <i>Cryptococcus neoformans</i> )	Worldwide	>1,000,000	20–70
Mucormycosis ( <i>Rhizopus oryzae</i> )	Worldwide	>10,000	30–90
Pneumocystis ( <i>Pneumocystis jirovecii</i> )	Worldwide	>400,000	20–80
Endemic dimorphic mycoses*†			
Blastomycosis ( <i>Blastomyces dermatitidis</i> )	Midwestern and Atlantic United States	~3,000	<2–68
Coccidioidomycosis ( <i>Coccidioides immitis</i> )	Southwestern United States	~25,000	<1–70
Histoplasmosis ( <i>Histoplasma capsulatum</i> )	Midwestern United States	~25,000	28–50
Paracoccidioidomycosis ( <i>Paracoccidioides brasiliensis</i> )	Brazil	~4,000	5–27
Penicilliosis ( <i>Penicillium marneffeii</i> )	Southeast Asia	>8,000	2–75

\*Most of these figures are estimates based on available data, and the logic behind these estimates can be found in the text and in the Supplementary Materials. †Endemic dimorphic mycoses can occur at many locations throughout the world. However, data for most of those locations are severely limited. For these mycoses, we have estimated the infections per year and the mortality at a specific location, where the most data are available.

**Table 1.1. The 10 most common invasive fungal infections and their associated mortality rates.** Table from (1).

### 1.1.1 Epidemiology of fungal infections

Many of the fungi that elicit life-threatening conditions live as part of the normal fungal flora of healthy humans and are only pathogenic in sufficiently immunocompromised individuals. There are relatively few fungal species that are deemed truly pathogenic - the ability to initiate invasive infection in healthy individuals. Over 90% of reported invasive fungal-related deaths are from species that belong to one of four genera: *Candida*, *Aspergillus*, *Cryptococcus*, and *Pneumocystis*. *Candida* species, in particular *Candida albicans*, are the most common cause of fungal incidence and of life-threatening infections in hospitals (1,5). The epidemiology of fungal diseases is dynamic making it difficult to predict disease course and high-risk groups. Fungal pathogens can initiate a variety of life-threatening invasive diseases (for example through fungaemia, meningitis, and pneumonia), severe chronic conditions (for example chronic pulmonary aspergillosis), and complex chronic respiratory conditions (for example asthma) (6).

The high mammalian body temperature and powerful immune system of healthy individuals are incredibly effective at preventing fungal infection, meaning primary



fungal diseases are uncommon. Ironically, the current prevalence of life-threatening infections can be largely attributed to the substantial developments of modern medicine and procedures. Infection is most often initiated when the host becomes sufficiently immunocompromised, as such the majority of severe fungal infections can be attributed to opportunistic pathogens (such as *Candida* and *Aspergillus* species). In comparison, only a few can be considered true pathogens by causing infection in healthy individuals (for example *Paracoccidioides*) (1). The current prevalence of opportunistic pathogen infections can be attributed to many patients living full lives with immunosuppressing infections (such as HIV/AIDS) (7), as well as treatments, such as chemotherapy, are now relatively well tolerated, but are often associated with severe neutropenia. Alternative aetiologies include exposure to repeated insult, following invasive gut surgery, patients with severe body burns, and premature newborns are at high risk, and therefore the number of susceptible individuals has increased drastically over the last few decades. A recent report suggested that up to 80% of critically ill patients develop candidiasis after just one week in intensive care (8).

For the purpose of this thesis, I will be focusing on *Candida* and *Aspergillus* species.

### **1.1.2 Candidiasis**

*Candida* are yeast that can elicit infections, known as candidiasis, which are most often fatal if left untreated. It is estimated that there is a worldwide annual occurrence of 700000 cases of invasive candidiasis (9). Globally, 92% of candidemia are caused by *Candida albicans* (65.3%), *Candida glabrata* (11.3%), *Candida tropicalis* (7.2%), *Candida parapsilosis* (6%) and *Candida krusei* (2.4%) (10). However, the distribution of these pathogens in clinical isolates is not uniform: the frequency varies with location with *C. glabrata* being more frequent in North America (21% of patients), whilst *C. tropicalis* is more frequent in Asia Pacific (11.7%) and Latin America (13.2%) than the global average (10). There are also variations associated with age of the host and patient characteristics, for example those undergoing chemotherapy compared to those that are not (11).

*Candida* species are often present in the oral cavity, skin, gut, and vulvovaginal flora of healthy humans where these colonies remain relatively benign. Predisposing factors such as use of contraception, wearing dentures, and diabetes mellitus can lead to recurrent, superficial candidiasis for many patients; however, these are non-lethal forms of infection. In contrast, patients with ineffective immunity (for example neutropenia (12)), damage to the gastrointestinal mucosa, and the use of catheters predispose patients to systemic candidiasis which is associated with a high mortality rate despite the availability of multiple lines of treatment (13). There are multiple forms of invasive candidiasis, the course of which depends on the cause of host susceptibility to these opportunistic pathogens. For example, patients receiving chemotherapy often develop systemic candidiasis, but not of the brain, as a result of fungi migration due to a disrupted intestinal epithelium. In contrast, premature newborns often develop abscesses of the brain due to immature blood-brain barrier function and are therefore more at risk of candidiasis of the brain (14).

The ability of *Candida* species to infect humans in a diverse range of locations can be attributed to their ability to survive and thrive in highly disparate microenvironments, as well as possessing a range of virulence factors. These include the ability to transition between morphological hyphal and yeast forms aiding invasion and spreading, the secretion of hydrolytic enzymes, and the ability to form biofilms (15). Furthermore, *Candida* species are able to rapidly adapt to environmental changes in pH and nutrient availability, as well as possess metabolic flexibility and robust stress response mechanisms. Currently, the interplay between fungal invasion and host is poorly understood. As the details of *Candida* pathogenicity mechanisms improves, the potential for novel therapies will expand and patient outcome will undoubtedly improve.

### 1.1.3 Aspergillosis

*Aspergillus* species are moulds that can cause serious invasive infections, as well as allergic conditions. Annually there are 3000000 cases globally of chronic pulmonary aspergillosis, 250000 cases of invasive aspergillosis, and 10000000 cases of fungal-induced asthma (9). *Aspergillus fumigatus* is the species most frequently associated with aspergillosis, accounting for approximately 90% of all global cases. As with candidiasis, global distribution is influenced by location: in the tropical and subtropical regions, *Aspergillus flavus* is isolated as frequently as *A. fumigatus* (16,17). *A. fumigatus* is a sub-species consisting of 63 members. Within this clan there are varying susceptibilities to antifungal therapy, and in particular to azoles (18), highlighting the importance of molecular epidemiology and strain-specific treatments.

*A. fumigatus* is a versatile thermophile that can grow well at human febrile temperatures (39 – 40 °C). *A. fumigatus* spreads as small (3 µm) specialised hyphae (conidiophores). The small size of conidiophores ensures that they can remain airborne for long periods of time and are able to enter the human alveoli. It is estimated that humans encounter several hundred *A. fumigatus* conidia on a daily basis (14), however they are only recognised by the human innate immune system when they are in an air-filled space, such as the lung or sinus, and start to germinate to produce growing hypha (19,20). In such air-filled spaces, a large immune response to *A. fumigatus* can elicit a range of allergic diseases from fungal-sensitising asthma to allergic bronchopulmonary aspergillosis which is associated with severe pulmonary complications, bronchiectasis, and fatal lung damage (21). The innate immunity of healthy humans is sufficient to protect against *A. fumigatus* lethal invasive infection, however when there is a sufficient decrease in the number of functional neutrophils and macrophages to control the germinating conidia, hyphal fragments may be carried to other organs, such as the brain, where metastatic, lethal infection can ensue. An alternative aetiology is *Aspergillus* hyphae can enter blood vessels and cause downstream tissue infarction through clogging of vessels (22).

#### 1.1.4 Diagnosis of fungal infections

A lack of rapid and accurate diagnostic tests for invasive fungal infections remains a fundamental cause of poor patient outcome. However, the accuracy and speed of diagnostic technologies have substantially improved over recent years. Accurate diagnosis is essential for two reasons: firstly, to identify that infection is due to fungal burden and secondly, to identify the strain of fungi eliciting the infection. The second point is vital for guiding treatment options as there are substantial and important differences in susceptibilities between strains as discussed in more detail below. Currently, many laboratories worldwide rely on commercial systems for rapid fungi identification, but the limited number of strains which these tests can identify often leads to misidentification or no identification of clinical isolates (23). Scientists and clinicians have developed several strategies to overcome this barrier. Firstly, patients are characterised into severity of risk to allow for prophylactic, pre-emptive treatments. Secondly, there have been improvements in many diagnostic tools such as matrix-assisted laser desorption/ionisation time-of-flight mass spectrometry (MALDI-TOF MS) and to include the use of histopathology of infected tissues, such culture techniques, PCR and genomic sequencing, as well as biomarker level identification (for example  $\beta$ -D-glucan and galactomannan in bodily fluids), that aid the accurate identification of the invading species and infection severity. These biomarkers guide pre-emptive therapies such that the infection is controlled in the early stages and when the tissue and systemic burden is low. Lastly, and most importantly, for the successful treatment of fungal infections there must be appropriate use of both new and old antifungal drugs (24).

Despite recent advances in the management of fungal infection, many patients remain undiagnosed, receive a misdiagnosis, or are diagnosed late, and these problems are worsened in resource-limited clinics. For example, *Candida auris* is responsible for many of the recent hospital outbreaks, yet accurate identification of this new strain can be difficult as it is often misidentified by commercial identification systems for the common bakers' yeast *Saccharomyces cerevisiae* (25). Furthermore, *in vitro* assays are useful for determining a fungus' susceptibility to a compound, but there are often

discrepancies between the *in vitro* and *in vivo* responses. Susceptibility testing is useful for guiding treatment choices, but many treatment programmes are still largely empirical based in both developed and less developed settings. Despite these advances, the WHO has recognised that many of these newer technologies are, or will be, unaffordable to developing countries and as such have called for new point-of-care diagnostic tests that do not require access to a laboratory (26). Overall, there is a need for improvements in molecular diagnostics for both the identification of fungal pathogens and the detection of specific resistant alleles (27).

### **1.1.5 Antifungal clinical treatments**

Fungi are eukaryotes and evolutionarily similar to humans which somewhat restricts available drug targets to pathways essential to fungi only or risks patient adverse effects and toxicity. The first clinical antifungal, amphotericin B deoxycholate, was approved in the 1950s, but was associated with substantial toxicities. Over recent decades, there have been advances in the number of available antifungal treatments that are less toxic, for example using a lipid formulation of amphotericin B. Despite the generation of new therapeutic classes and the development of third generation drugs, patient survival rates remain modest (Table 1.1). Poor clinical outcomes can be attributed to a lack of early diagnosis and a lack of targeted therapies, along with the rapid rates at which resistance develops in some fungi and innate resistance associated with others. Many antifungal drugs are fungistatic (halt fungal cell growth) and rely on co-antifungal activity of the host immune system which, in many patients, is severely compromised. Exciting new advances in immunotherapeutic treatments have recently been made, but to further develop this line of treatments it is paramount that there is a greater understanding of the protective and antifungal activity of the healthy innate immune system (21). Recent strides have been made which are opening up immunotherapeutic treatment options: enhancing the host's ability to evoke an immune response and enhancing patient recognition of invading fungi are two lines that are currently being explored. It is now widely accepted that phagocytic cells are involved in both the innate and adaptive immunity to provide a protective role against

invasive fungal infections (28,29). Further to this, patients with defects in phagocytic activity, for example chronic granulomatous disease - a result of defects in phagocyte nicotinamide adenine dinucleotide phosphate oxidase, are at risk of life threatening fungal infections (28). One immunotherapeutic treatment currently in development involves enhancing phagocytic activity by soluble immunomodulatory mediators (21). In addition, the importance of fungal pattern recognition receptors, for example C-type lectin receptors, has also been recognised. C-type lectin receptors are involved in host antifungal immunity through the recognition of carbohydrate ligands, such as  $\beta$ -glucans, present on fungal cell surfaces. Upon encountering fungal cells, C-type lectin receptors initiate a proinflammatory immune response, for example through the activation of phagocytosis as well as cytokine and chemokine production. Polymorphisms in the C-type lectin receptors have been linked to enhanced patient susceptibilities to a range of fungal infections (30,31). Further understanding of these receptors, recognition systems, and the fungal ligands will enable the development of vaccines against these diseases.

There are currently just four frontline clinical drug classes for the treatment of invasive fungal infections (Figure 1.1). These are the (i) polyenes, (ii) pyrimidine analogues, (iii) echinocandins, and (iv) the azoles. Of note, the polyenes, echinocandins, and azoles can be used in monotherapy, whereas the pyrimidine analogues are used in combination with another class (32). The polyenes (e.g. amphotericin B) form extramembranous aggregates that extract membrane ergosterol from the lipid bilayer thereby killing the fungi (33). The pyrimidine analogues (e.g. 5-fluorocytosine) inhibit DNA synthesis by disrupting pyrimidine metabolism. The echinocandins (e.g. caspofungin) are the newest antifungal drug class and act via disrupting cell wall biosynthesis by inhibiting (1-3)- $\beta$  glucan synthase. The azoles (e.g. voriconazole) are the largest and most frequently used class. They exert their antifungal effect by inhibiting lanosterol 14- $\alpha$ -demethylase, encoded by ERG11 (CYP51), activity and the subsequent blocking of ergosterol biosynthesis (34). The inhibition of Erg11p simultaneously depletes membranes of ergosterol whilst increasing the amount of toxic sterol precursors, such as 14 $\alpha$ -methylergosta-8,24(28)-dien-3 $\beta$ ,6 $\alpha$ -diol, therefore exerts membrane stress and ultimately arrests cell growth (4). Although there are a

range of antifungals available, complications result from high levels of toxicity, relative ineffectiveness, drug-drug interactions (for example triazoles interact with statins (35)), and poor bioavailability, which are further augmented by the emergence and increase in drug resistance. Therefore, continuous monitoring is required to ensure treatments are at optimum efficacy whilst avoiding unacceptable levels of toxicity (34).

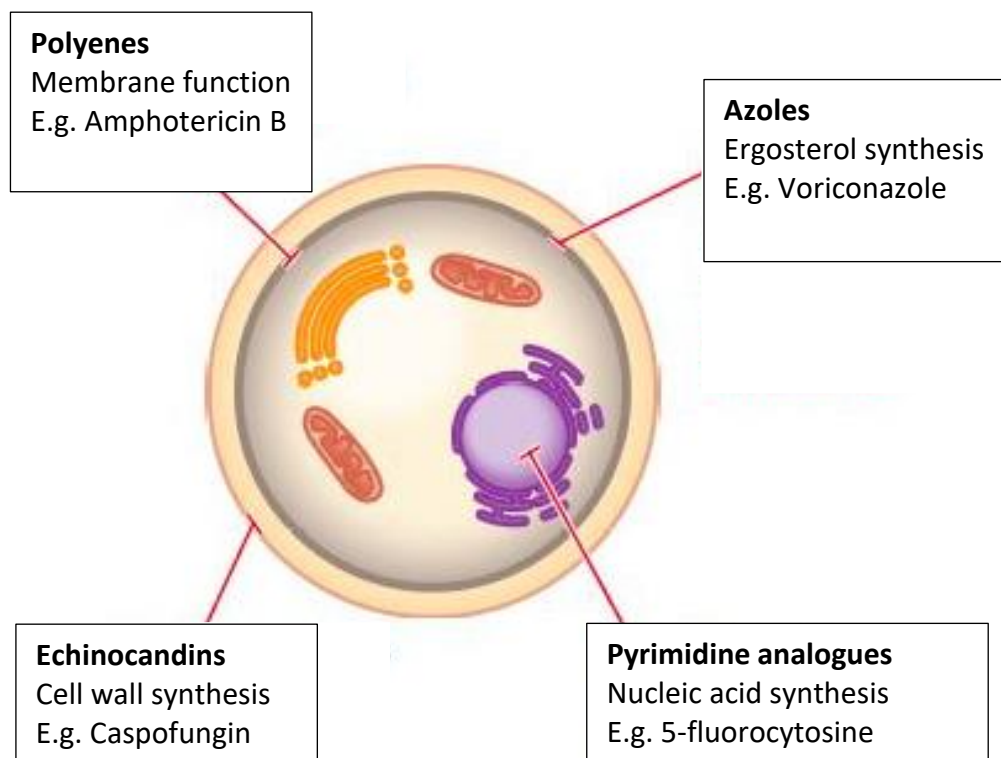


**Figure 1.1. Mechanism of action of the frontline antifungal drug classes for the treatment of invasive fungal infections.** There are four classes of antifungal drug used to treat invasive fungal infections. These are the polyenes, the pyrimidine analogues, the echinocandins, and the azoles. The polyenes, such as amphotericin B, disrupt cellular function through extracting membrane ergosterol. The pyrimidine analogues, such as 5-fluorocytosine, disrupt pyrimidine metabolism and therefore inhibit nucleic acid synthesis. The echinocandins, for example caspofungin, disrupts cell wall synthesis by inhibiting (1-3)- $\beta$  glucan synthase. The azoles, for example voriconazole, inhibit ergosterol biosynthesis. Figure adapted from (36). The polyenes are used in combination therapy with another antifungal drugs class, for example the polyenes. All other classes can be used as monotherapy.

In addition to invasive and potentially lethal fungal diseases, fungi can also elicit non-lethal infections of the skin, hair follicles, and nails. For many of these cases, topical treatments, such as cream or spray formulations, are favoured over oral or intravenous routes of antifungal administration and are suitable for ridding the skin of the fungi. The azoles, such as miconazole, can be used for the treatment of skin infections, however as their antifungal activity is via a fungistatic mechanism, fungicidal options such as the allylamines (for example terbinafine) are often preferred due to the shorter treatment times and associated high cure rates. Like the azoles, the allylamines target the ergosterol synthesis pathway, but at the level of the inhibition of squalene epoxidase (Erg1p) (37). Although skin infections are relatively simple to cure with topical treatments, nail infections can be somewhat more problematic. The morpholines, such as amorolfine, is an antifungal drug class that is used to treat nail infection through the application of the drug via nail lacquer. The morpholines inhibit sterol  $\Delta 14$  reductase and  $\Delta 7$ - $\Delta 8$  isomerase (Erg24p and Erg2p, respectively). However, nail infections are frequently located beneath the nail rather than on top and due to the poor penetration of topical drugs through the nail, systemic treatments can be required (38).

### **1.1.6 Routes to antifungal drug resistance**

The major cause of antifungal treatment failure is the development of resistance. Therapeutic resistance is qualified by a patient not responding to or no longer responding to drug treatment at a standard dose. Host, drug, and microbial factors all contribute to patient outcome. A continuing challenge lies in that we are living alongside a simultaneous rise in the number of new pathogens that are able to evade host immune responses and clinical treatments (for example *C. auris*), as well as the emergence of resistance in existing pathogens (for example *A. fumigatus*) (10).

The battle against antifungal resistance is augmented by the fact that fungal genomes are highly plastic, and fungi reproduce rapidly. This combination results in the rapid selection and infiltration of clones that are resistant to treatment. Although resistance



has been reported against all clinical drug classes, the extent of antifungal drug resistance varies between drug classes and species of fungi. Worryingly, some strains display resistance to all frontline azole therapies: *A. fumigatus* now has an associated mortality approaching 100% and has evolved into an azole-resistant strain due to environmental exposure and selective pressures (39). The azoles have a favourable safety profile with good, broad spectrum activity, but their use is significantly hampered by the fact that they are fungistatic which promotes the clonal expansion on surviving populations. The fungistatic nature of azoles coupled with extensive prophylactic use has facilitated widespread resistance to this drug class (40,41). In contrast, resistance against the polyenes remains rare (42). The polyenes are a potent fungicidal class that inhibit the normal functions of ergosterol. It is likely that resistance remains rare against the polyenes due to the much larger amount of energy required to develop resistance than for the azoles. However, the use of polyenes is clinically limited by adverse toxicity to the host due to structural similarities between the fungal sterol ergosterol and the human major membrane sterol cholesterol (43). Nephrotoxicity is a common side effect of polyene treatment, therefore this drug class is often reserved until other options have proven unsuccessful or are unavailable (44,45).

Parallel to the clinical antifungals, there is a range specific for agricultural use that exert environmental selective pressures. Targets for agricultural chemicals include mitochondria function, the cytoskeleton, and ergosterol biosynthesis. The azoles remain the dominant drug class for the treatment of both agricultural and human fungal infections. The use of agricultural chemicals that target the same pathway as clinical compounds, such as the azoles, exerts an environmental selective pressure for pathogens that would also be resistance to clinical treatments. Although there is a wider range of agricultural fungicides compared to clinical options, resistance to each chemical has still been reported in at least one major pathogen (46,47). In an attempt to overcome the significant selective pressure applied to a single pathway by the use of one drug class, crops are sprayed with multiple classes of antifungals at lower doses (27).

Antifungal drug resistance can be innate (without previous exposure to drug) or acquired (following exposure to drug). The rise in number of inherently and acquired clinically resistant strains stems from several branches: high amounts of selective pressure and only a limited number of clinical treatments available, an increase in the number of susceptible patients alongside an increase in the application of agricultural antifungals, and the ease of global travel facilitates the movement of resistant strains. These points will be discussed further in the following paragraphs.

Firstly, the fungal genome is highly plastic to facilitate survival in the large range of environments that they inhabit, including variations in temperature, pH, and osmolarity. Fungal genome plasticity is also an advantage when responding to agricultural and clinical xenobiotic stress. Each of the available clinical and environmental antifungal drug classes targets just a single pathway. Chemicals that target just one pathway exert a significant selective pressure that results in the clonal expansion of resistant pathogens, namely pathogens that do not depend on the inhibited pathway for survival. Patients deemed at high risk of developing a fungal infection undergo prophylactic treatment, which induces a long-term selective pressure on clinical strains, for example *Candida* and *Aspergillus* species. In turn, antifungal treatments trigger acute stress responses that promote fungal genome instability enabling the development of advantageous mutations, such as amino acid substitutions at the drug binding site as with *C. albicans* developing resistance to the azoles through a Tyr132Phe mutation in ERG11 (CYP51) (48), thereby facilitating strain resistance. The acquisition of resistance to an antifungal drug can be specific to that drug only or it can resonate throughout the entire drug class. The ability of fungi to develop resistance against an entire drug class enables the emergence of strains that initially acquire resistance to environmental antifungals to also be resistant to clinical treatment options. The reduction in genome stability also enhances the ability of fungi to rapidly mutate and develop resistance to the second line treatment as well, therefore forming a multidrug-resistant strain. Further clinical complications arise as prophylactic and empirical use have contributed to the emergence of strains that are innately less sensitive to current treatments, for example *Aspergillus flavus*, *Aspergillus terreus*, *Candida lusitania*, and *Candida auris*, thus further limiting treatment options

(49,50). Resistance to one line of treatment severely limits clinical options, however, multidrug resistance can completely negate any clinical intervention and results in a mortality rate approaching 100%.

Secondly, there has been an increase in frequency of antifungal use both in the clinic and environmentally. The clinical increased use is a result of an expansion in the population of patients susceptible to antifungal infection, and therefore the number of people receiving prophylactic or curative treatment has escalated. This is due to the advances in medical procedures that now facilitate major surgeries, organ transplant, and implantation of devices, alongside an increase in the number of cases of immunosuppressing diseases (HIV/AIDS) and patients undergoing immunosuppressing treatments (chemotherapy) that they are able to tolerate and survive. The increased use of clinical antifungals is paralleled by the increased application of agricultural antifungal treatments. Human population growth and economic expansion have led to more people enjoying a prosperous life, resulting in a huge demand for food (crops), thus an increase in agricultural pesticide treatments. The wide application of agricultural pesticides with identical molecular targets as systemic antifungals ensures that maximum crop productivity can be met, but has bred out plants' innate defence mechanisms and has facilitated the expansion of drug-resistant pathogens outside of clinical settings. Clinical resistance has been observed in parallel with agricultural resistance with the development of the same, but independently acquired, resistance seen from both sources (51). Acquired azole resistance as a result of aneuploidy of a specific segment of chromosome 5 has been observed in both clinical and environmental strains of *C. albicans* and *C. glabrata*. ERG11, the gene encoding the target of azoles, lanosterol-14- $\alpha$ -demethylase, is located on chromosome 5, as such aneuploidy of this chromosome results in an increase in ERG11 mRNA levels which is associated with an increase in azole resistance due to an overwhelming amount of protein for the drug (51). In addition, this region of chromosome 5 also contains the transcription factor TAC1 that activates the expression of the ABC superfamily multi-drug transporter genes CDR1 and CDR2 (52,53). Fluconazole use has been shown to induce aneuploidy of chromosome 5 which also drives the hyperactivity of TAC1 and subsequently the amount of drug efflux through Cdr1p and Cdr2p resulting in a

reduced amount of intracellular drug accumulation and resistance to fluconazole in *C. albicans* (54).

Thirdly, the ease of global travel enables the free flow of pathogens from naïve hosts to susceptible targets. For example, *C. auris* was first isolated from a patient in Japan in 2009. Now, in 2019, it is resistant to all clinical antifungals and is responsible for a worldwide rapid increase in nosocomial, fatal infections (55,56). Alternative hypotheses suggest that *C. auris* developed into a multidrug resistant strain simultaneously but independently on three separate continents (57).

The response of a fungi to antifungal treatment is dependent on the strain, patient status (cause of immunocompromisation and comorbidities), patient genetics (for example, polymorphisms in CYP2C19 are associated with an enhanced metabolism of voriconazole and subsequent treatment failure (58), the drug mechanism of action, dose, and the duration of treatment. Many of the established routes to resistance involve genetic mutation through point mutation, loss of heterozygosity, or aneuploidy most often resulting in alterations to the drug binding site or overexpression of the target (59,60). These responses induce mutations that are stable (inheritable). However, short term, fast responses are also required and are an important part in the acquisition of long-term resistance to give the cell time to develop the permanent genetically stable responses, for example through the overexpression of efflux pumps.

Resistance can be acquired through any single or concurrent mechanism in a clinical isolate and resistance effects can spread within any drug class. Frequently observed mechanisms of resistance are summarised in figure 1.2. (1) Normal binding of drug (blue) to target (purple); (2) Reduced drug internalisation due to a reduction in drug influx proteins. Azole drug influx is an energy-independent process in *C. albicans* and *A. fumigatus* (58,61), however proteins required for drug import have not yet been elucidated; (3) Reduced drug efficacy due to overexpression of target protein overwhelming the inhibitory capacity of the drug (62,63). In *C. albicans*, Upc2 is the transcriptional activator that regulates the expression of ERG11. Gain-of-function mutations (for example A643V) within Upc2 results in constitutive overexpression of

ERG11 and subsequent increased expression of the drug target (45,64,65); (4) Reduced drug efficacy through detoxification of the drug; (5) Conformational changes to the drug binding site (47). This mechanism has been frequently observed in *C. albicans* resistance to the azoles. Multiple mutations in regions adjacent to the active site of ERG11 have been observed in clinical isolates (66) which has also been associated with a loss of heterozygosity. Loss of heterozygosity induces a further azole resistance through the resistant allele (67); and (6) Reduced drug efficacy due to an increase in efflux pump expression resulting in a reduction in intracellular drug concentration (68,69). Cdr1p and Cdr2p are ATP binding cassette (ABC) efflux pumps that are regulated by Tac1 in *C. albicans* (43). Multiple mutations in Upc2 that confer the upregulation of Cdr1p and Cdr2p along with loss of heterozygosity have been reported in clinically resistant isolates (54).

Further to these, poor patient prognostic markers include biofilm formation (70). Of note, there is considerable variation in the development of resistance between and within each class, as well as susceptibility between patients and for the same clinical isolate. Although the genetic mutations and subsequent mechanisms of resistance have been elucidated, the biological factors that induce antifungal resistance are not yet understood.

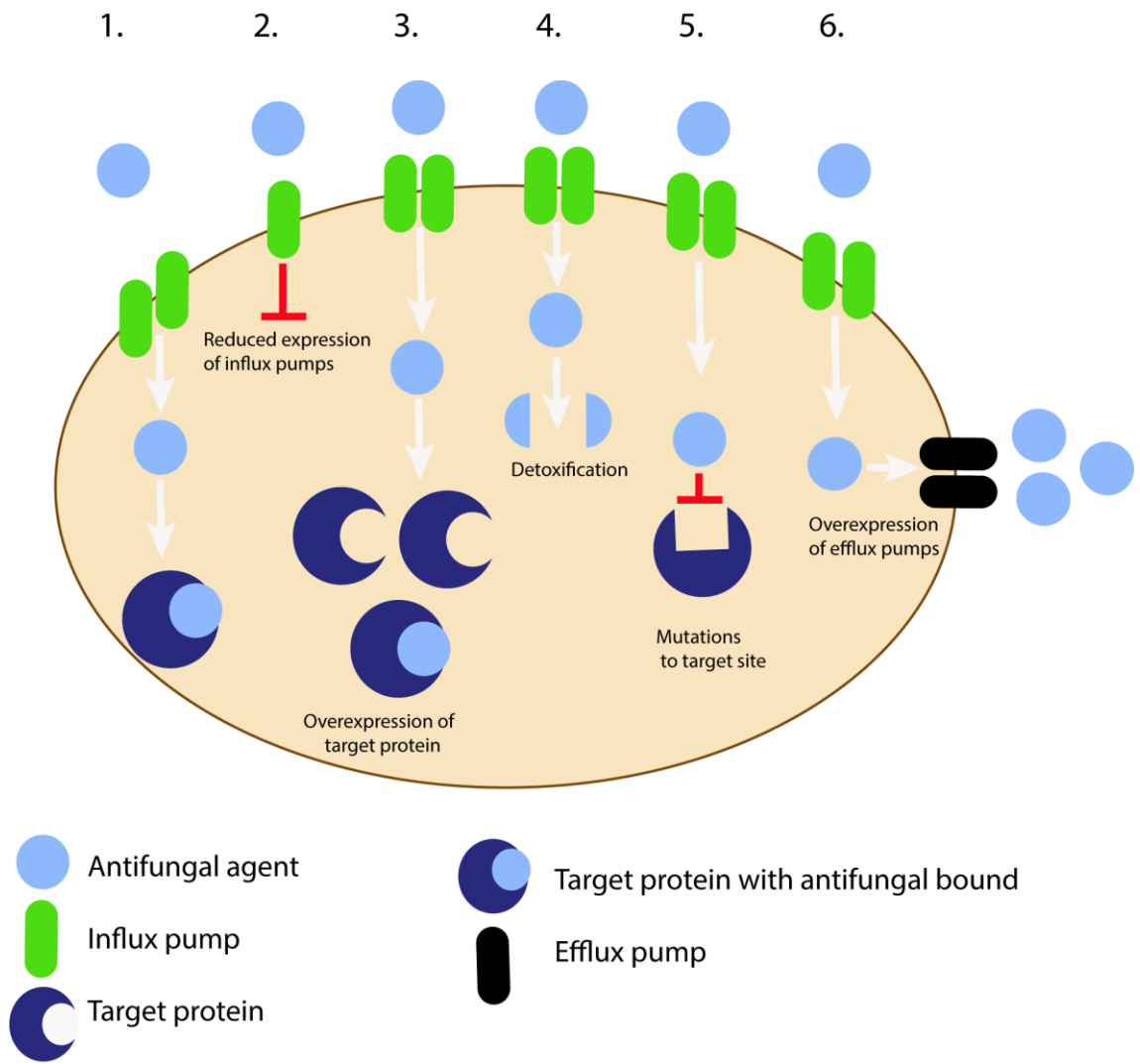


**Figure 1.2. Common mechanisms of antifungal drug resistance.** (1) Normal drug-target binding. (2) Reduced drug influx proteins. (3) Overexpression of target protein. (4) Detoxification of the drug. (5) Conformational changes to the drug site. (6) Overexpression of efflux pump expression.

### 1.1.7 Emerging strains

Over the last decade, the prevalence of new strains, such as *Candida auris*, which are inherently multidrug resistant have emerged as notable pathogens associated with high mortality rates. The widespread use of antifungals is likely to have resulted in the emergence of *C. auris* as such a successful pathogen. *C. auris* was first isolated from the ear canal of a man in Japan in 2009. By 2011, the first case of *C. auris* persistent fungaemia was reported from a patient in Korea on fluconazole and amphotericin B (71). *C. auris* is now resistant to the first-line antifungal fluconazole and displays varying inter-patient susceptibilities to other azoles, echinocandins, and amphotericin B (72). *C. auris* is the only *Candida* species where resistance to all four drug classes has been noted. Therefore, treatment of *C. auris* poses both identification and treatment difficulties, in particular in developing countries where access to more advanced identification systems and a wider range of antifungals than just fluconazole remains limited (73).

At present, the inherent properties of *C. auris* that render this strain resistant to such a range of antifungals remains to be determined. The *C. auris* draft genome revealed the upregulation of genes linked to resistance in other strains, for example the ergosterol synthesis genes ERG3 and ERG11 and the fungal cell wall synthesis gene FSK1-3 (71,72). Of note, the *C. auris* ERG11 gene contains amino acid substitutions (for example F126T, Y132F, K143R) at known azole-resistant codons that are also present in resistant, but not wild type *C. albicans* (74). Furthermore, a significant portion of the *C. auris* genome is devoted to the ABC protein efflux pump family that is consistent with high amounts of drug efflux in this strain (75,76). It, therefore, seems likely that the inherent resistance of *C. auris* stems from the wide use of antifungals which resulted in the successful emergence of this strain. Overall, in light of the development of inherent multidrug resistant strains, it is necessary to reevaluate the prophylactic use of antifungals, in particular azoles, which promotes such profound genome diversity.

Overall, a large rise in the number of resistant strains along with a lack of novel drug classes has resulted in the high mortality rates associated with invasive fungal

infections. Currently there are just 11 new antifungals in clinical stage I or II trials, some of which represent the inaugural member of a novel drug class, for example F901318 (olorofim) that inhibits dihydroorotate dehydrogenase (77), and others are new generation of current drug classes, for example the azole-like tetrazoles VT-1161 (78,79) and VT-1129 (80–82). In order to improve patient outcomes, there needs to be firstly an improvement in the sensitivity and specificity of diagnostic tests; secondly, there needs to be more clinical treatment options through the development of compounds that are highly targeted with lower adverse effects profiles; and thirdly these advances need to be rapid. Such steps are being taken in the right direction, for example the first antifungal vaccine is undergoing clinical trials, however this is yet to receive approval for clinical use by any country in the developed world (83,84). Alongside these pharmaceutical advances, researchers are also investigating the identification of genetic biomarkers that predispose humans to fungal diseases (85).

Our industry partner, F2G, are a biotech company that focus on the development of novel drugs to treat life threatening fungal diseases. One of their recently developed drugs is called F900742. Very little has been disclosed about F900742 and this drug is still under patent. Initially F2G thought that F900742 exerted a non-specific mode of action through lysing cell walls, however a lack of activity in bacteria (see table 4.1) and an inability to haemolyse red blood cells suggested another mechanism was more likely. Haploinsufficiency screens are a useful way to identify the likely target of a drug by reducing the number of copies of a single gene from two to one in a diploid cell resulting in a heterozygote that displays increased drug sensitivity compared to the wild type strain. A haploinsufficiency screen identified a few hits, one of which was a fatty acid  $\Delta 9$  desaturase. The activity of F900742 was then shown to be reversed by the addition of unsaturated fatty acids (labelled in red in Figure 1.3) and lipidomic approaches to analyse whole cell fatty acid content demonstrated an increase in the saturated fatty acid content at the expense of unsaturated fatty acids. All three approaches suggested that  $\Delta 9$  desaturase is the target of F900742.



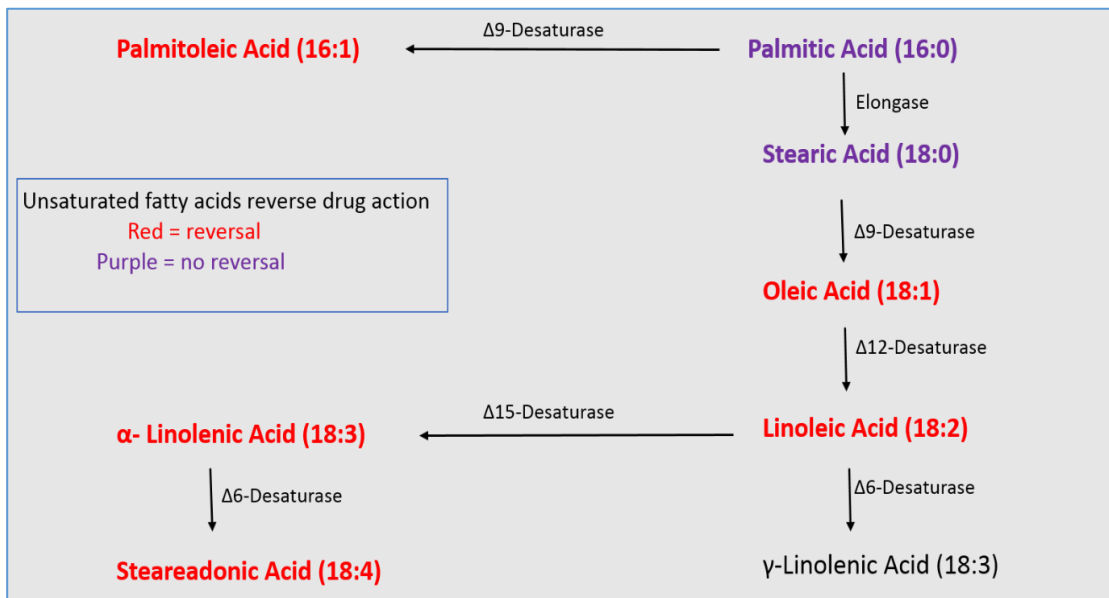


**Figure 1.3. F900742 reversal assay.** The addition of mono- and polyunsaturated fatty acids reversed the action of F900742, whereas the addition of saturated fatty acids did not. This assay suggested that the yeast  $\Delta 9$  desaturase is the target of F900742.

## 1.2 Lipids

The eukaryotic lipidome consists of thousands of different species which facilitates their function in multiple cellular processes (86). Lipids are required for organelle membrane formation, energy storage, signalling molecules, structural integrity, and as mediators of membrane fusion and fission events (87). Variations in lipid requirements are controlled by highly regulated processes that ensures *de novo* synthesis, uptake of exogenous lipids, and degradation of lipids. An excess of lipids can induce lipotoxicity and, in extreme cases, apoptosis. To overcome this, excess lipids are sequestered and stored as lipid droplets. During times of high lipid requirement, for example growth or starvation, lipids can be mobilised from lipid droplets or *de novo* synthesis of lipids initiated to ensure demands are met (88).

In eukaryotes, the plasma membrane or cell wall provides a set boundary that defines the cell and the environment. Inside the cell, organelles are enclosed within a membrane(s) to ensure segregation from each other and the cytoplasm. All

membranes are of defined lipid and protein composition to create a unique identity and ultimately facilitate function. Of particular relevance to this project, proper lipid distribution is paramount for ensuring correct membrane properties, including thickness, fluidity, and curvature which allows processes such as membrane trafficking, yeast budding, and fusion or fission events (86,89,90). A key feature of all biological membranes is their ability to dynamically adapt to their environment. Regulation of membrane properties is required for proper maintenance of cellular processes, including the secretory pathway (90) and the unfolded protein response (91). It is essential that lipids are correctly distributed throughout cellular and organelle membranes as highlighted by the range of lipid-induced diseases (92,93).

The endoplasmic reticulum (ER) is an organelle that is required for protein synthesis, calcium homeostasis, and trafficking. The ER is also the major site of lipid metabolism, including the biosynthesis of the major membrane lipids - sterols and phospholipids. Multiple proteins involved in lipid metabolism are located in the ER, therefore disruption of this organelle can induce severe lipotoxic responses. Crosstalk between the ER membrane and lipid metabolic processes are pivotal in both normal and cell stress states. ER stress has been observed as a result of direct and indirect consequence of alterations to lipid metabolic processes. Further to this, the unfolded protein response (UPR) was first described as a pathway to maintain protein homeostasis. The roles of this pathway have been updated to include essential roles in ensuring correct lipid metabolism (94).

Lipid metabolic processes are highly conserved throughout eukaryotes. The budding yeast *S. cerevisiae* was used as a model organism to study eukaryotic lipid metabolism for the majority of work in this thesis, as such the following sections will focus on lipid metabolism in this yeast. Yeast are single cell, eukaryotic organisms that are comparatively simple in structure compared to humans who have approximately 10 trillion cells. Importantly, many of the intra cellular processes are conserved between yeast and humans, as well as many gene and protein functions, therefore studies in yeast can be used to annotate genes in human and infer protein function. A cooperative effort has resulted in an almost complete set of deletions of every open

reading frame (ORF) in *S. cerevisiae* which were replaced by selectable markers such that each mutation can be traced and used to improve the biological understanding of many genes of unknown function (95). Other *S. cerevisiae* libraries have also been generated, such as a green fluorescent protein (GFP) tag added at the C-terminus of a single gene for every gene such that one protein can be visualised so localisation can be determined under various conditions (36). The relative ease of genetic manipulation of yeast has enhanced the functional understanding of a large number of proteins in both diseased and non-diseased states (96). Since functional information must be obtained by experiment, yeast prove an incredibly useful model as virtually all assays are easier with them than multicellular organisms. Benefits to using yeast include, they are single cell organisms existing in both haploid and diploid form, yeast are easy and cheap to culture, they can cope with a range of environmental conditions, the yeast genome has been sequenced and contains significant homology to other eukaryotes (including humans), and mutants can be easily isolated.

### 1.2.1 Fatty acids

The basic component of complex lipids are fatty acids and a head group (for example choline) (Figure 1.4). A fatty acid is a chain of hydrocarbons terminating with a carboxylic acid. There is a wide variety of fatty acids in eukaryotes with acyl chain length varying between C14-C26 species and taking either a saturated (no double bonds) or unsaturated (1 to 6 double bond(s)) form. All naturally occurring unsaturated fatty acids contain cis double bond(s), that is with both hydrogens on the same side of the double bond. The nomenclature for unsaturation used here is the delta ( $\Delta$ ) labelling system. The position of carbons within an acyl chain can be counted from either the carboxyl end of the fatty acid or from the methyl group. The delta system labels carbon 1 as the carboxyl group and the double bond is indicated as  $\Delta x$ . For example, a double bond between carbon 9 and 10 would be reported as  $\Delta 9$ . Membrane lipid acyl chain saturation is a key determinant of membrane physicochemical properties and is tightly regulated by evolutionarily conserved mechanisms throughout eukaryotes (89,97,98).

Yeast obtain fatty acids either through *de novo* synthesis, the degradation of complex lipids, or uptake from exogenous sources (99). Fatty acids may then take a route to form more complex lipids, such as the membrane lipids phospholipids or sphingolipids, or be stored in triacylglycerols and steryl esters in lipid droplets to serve as an energy reservoir. Free fatty acids can also function as signalling molecules, protein post-translational modifications, and transcriptional regulators (100). The *de novo* synthesis of fatty acids occurs in the cytosol and is highly conserved throughout eukaryotes. Fatty acids are synthesised in a series of energy-dependent carboxylation reactions whereby two carbons are added sequentially. The enzymes required for fatty acid biosynthesis are covalently linked into a multifunctional system known as Type I Fatty Acid Synthase system (FAS). There are two enzymes in this system, acetyl-CoA carboxylase (Acc1p) and fatty acid synthases (Fas1p and Fas2p). The first step in *de novo* synthesis of fatty acids is the generation of the 3 carbon product malonyl-CoA from the two carbon substrate acetyl-CoA catalysed by Acc1p (99). Malonyl-CoA is then used as a C2 donor by the FAS complex to elongate the acyl chain 2 carbons at a time starting from acetyl-CoA. The cyclic addition of the two carbon subunit is repeated until fatty acid chains yield the major yeast saturated acyl-CoAs C16:0 or C18:0 (99). C16:0-CoA and C18:0-CoA may then undergo desaturation in the ER (Figure 1.5). Fatty acid desaturation is an essential process in eukaryotes catalysed by fatty acid desaturase (FADs). There is a range of eukaryotic enzymes that catalyse the desaturation of saturated-CoAs which are named based on where in the hydrocarbon chain the desaturation occurs, for example  $\Delta 6$ ,  $\Delta 9$ ,  $\Delta 12$ . The  $\Delta 9$  desaturase is the only one that appears in all living beings and is essential to life (101). This is also the only desaturase expressed *S. cerevisiae*.

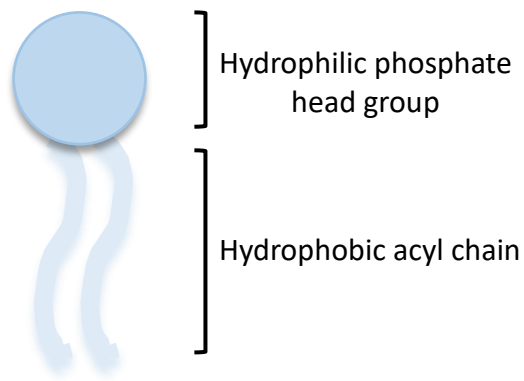


**Figure 1.4. General structure of a phospholipid.** The basic units of lipids are a hydrophobic moiety and a hydrophilic domain. Phospholipids contain two fatty acids covalently bonded to a glycerol backbone. A phosphate group links the glycerol backbone to a hydrophilic head group, for example choline.

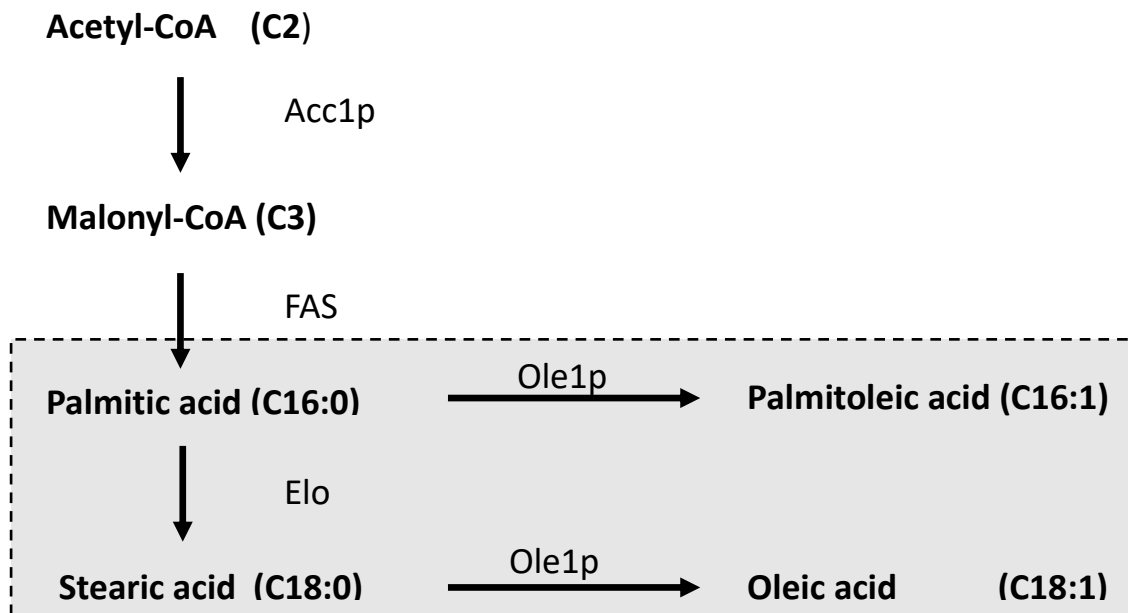


**Figure 1.5. *De novo* synthesis of unsaturated fatty acids.** The *de novo* synthesis of fatty acids proceeds via the cyclic addition of a two carbon subunit donated by malonyl-CoA to the FAS complex such that the fatty acid chain is elongated by two carbons per cycle. This process is repeated until the major saturated fatty acids, palmitic acid and stearic acid (C16:0 and C18:0), are generated. These saturated fatty acid species can be directly incorporated into lipids or may undergo desaturation by a  $\Delta 9$  desaturase (Ole1p in *S. cerevisiae*) to the C16:1 and C18:1 derivatives, palmitoleic acid and oleic acid.

Variations in acyl chain length and saturation as well as the head group give rise to the huge number and diversity of lipids. Yeast contain a few hundred lipid species with monounsaturated fatty acids constituting approximately 70% of the total intracellular lipids (102,103). The major fatty acids in *S. cerevisiae* are unsaturated C16:1 and C18:1,

called palmitoleic acid (20%) and oleic acid (50%) respectively, followed by their saturated counterparts C16:0 palmitic acid and C18:0 stearic acid. Unlike other eukaryotes, plants are unique in that they can synthesise polyunsaturated fatty acids. Mammals meet their polyunsaturated fatty acids dietary requirements by eating plants. Yeast are unusual as they do not require polyunsaturated fatty acids, but if monounsaturated fatty acids are unavailable then they will incorporate polyunsaturated into membranes (104).

As poikilotherms, yeast adapt to extreme temperatures through altering the membrane lipid composition (105,106). It is through alterations to the lipid composition that membrane processes are maintained (107). A key modulator of membrane fluidity is the degree of lipid saturation due to the inherent differences in membrane packing of saturated and unsaturated lipid acyl chains. At higher temperatures, the average acyl chain length and degree of saturation increases which is associated with the incorporation of membrane lipids containing saturated acyl chains with larger head groups, such as phosphatidylcholine (PC) and phosphatidylinositol (PI) at the expense of phosphatidylethanolamine (PE) (98,106,108). In contrast, lower temperatures are associated with a higher degree of desaturated membrane lipids. Desaturation induces a kink in the acyl chain which reduces the membrane packing order thereby increasing membrane fluidity. The importance of the ratio of saturated to unsaturated fatty acids can be determined by the tight regulatory mechanisms controlling this process that are conserved within eukaryotes (105). Aberrant lipid composition that results in an increase in the proportion of saturated fatty acids induces lipid bilayer stress, activation of the unfolded protein response (UPR) (94), and aberrant organelle morphology, for example the mitochondria (109). Conversely, an increase in unsaturated fatty acids is equally detrimental to the cells and, in severe cases, can result in fatty-acid induced necrosis (110). Eukaryotes have sensor proteins to monitor the properties of organelle membranes which can initiate alterations to lipid metabolic processes during times of nutrient starvation, stress, and development. Our understanding of how or indeed what molecular sensors coordinate the degree of lipid saturation and the physiochemical properties of membranes remains incomplete. In the bakers' yeast, *S.*

*cerevisiae*, the modulation of lipid saturation is achieved through the regulation of the sole and essential  $\Delta 9$  desaturase, Ole1p.

### **1.3 $\Delta 9$ desaturases and fatty acid desaturation**

#### **1.3.1 Ole1p**

In 1960, Bloomfield and Bloch described an oxygen and NADPH requiring enzyme that introduced a  $\Delta 9$  double bond into a saturated acyl-CoA substrate in *S. cerevisiae* (111). Since then, other groups have contributed to the understanding that the major eukaryotic pathway synthesising monounsaturated fatty acids occurs in an oxygen-dependent manner catalysed by a microsomal complex consisting of three components – a cytochrome  $b_5$ , an NADH-dependent cytochrome  $b_5$  reductase and the  $\Delta 9$  fatty acid desaturase protein (112–114). Further analysis revealed that the protein complex is integral to the ER membrane and it contains a non-heme iron centre that accepts electrons from the reduced cytochrome  $b_5$  (115). All  $\Delta 9$  desaturases catalyse the insertion of a double bond between carbon 9 and carbon 10 of C16:0 (palmitic acid) and C18:0 (stearic acid) acyl-CoA precursors, yielding C16:1 (palmitoleic acid) and C18:1 (oleic acid) (116,117).

#### **1.3.2 Structure of $\Delta 9$ desaturases**

There is a single cytochrome  $b_5$   $\Delta 9$  desaturase complex in *S. cerevisiae* called Ole1p for OLEic acid requiring (104). Ole1p is an essential 53 kDa, 510 amino acid protein coded for by the OLE1 gene (104,116). Ole1p contains an N-terminal desaturase domain that is linked to a cytochrome  $b_5$  domain (118). The majority of our understanding of the structure of Ole1p is derived from studies performed in the homogeneously purified mammalian homolog, stearoyl CoA desaturase 1 (Scd1) (114). There are currently five known mammalian Scd isoforms of approximately 355 amino acids (SCD1-5). Four SCD isoforms have been identified in mice (SCD1-4) (119–121), whilst two have been characterised in rats (SCD1 and SCD2) (122), and two in humans (SCD1 and SCD5)

(123,124). Comparison of the mammalian and yeast desaturase coding sequences revealed a 36% primary sequence identity with a greater than 70% sequence identity at the active site (Figure 1.6). Stukey et al demonstrated that the rat gene can functionally replace OLE1, but this substitution was only viable in yeast strains expressing cytochrome b<sub>5</sub> (116). Of note, the yeast desaturase domain is fused to a cytochrome b<sub>5</sub> domain, whereas no mammalian  $\Delta 9$  desaturase sequenced to date contain a cytochrome b<sub>5</sub> element within the desaturase complex (118). A possible explanation for this is yeast are poikilotherms - they rely on alterations in their membrane content to adapt to environmental conditions, such as temperature - whereas mammals maintain a constant internal temperature, therefore the incorporation of the cytochrome into the yeast protein could increase the rate of desaturation to ensure rapid membrane lipid adaptation.

Analysis of mammalian primary sequences by Wang et al identified four regions of greater than 10 residues where the sequences display greater than 70% identity, and two additional regions in the same positions of the proteins that contain at least 50 hydrophobic residues (Figure 1.6) (125). These two hydrophobic regions can each be split into two by a small cluster of 5-6 charged residues dividing the halves. The four 18-25 hydrophobic segments span the ER such that the desaturases are anchored to the membrane through four transmembrane passes, positioning the N- and C-termini and the active site on the cytosolic face of the ER as predicted by Stukey (116). The yeast cytochrome b<sub>5</sub> and b<sub>5</sub> reductase motifs are also positioned on the cytosolic face of the ER. In addition, this topology also positions nine conserved histidines, including three regions of conserved histidine box motifs consisting of 'HXXXXH', 'HXXHH' and 'HXXHH' on the cytosolic side of the membrane (126). Site directed mutagenesis studies and crystal structures of the human and mouse Scd1 identified these residues as essential for the enzyme's catalytic activity. The His boxes are thought to be involved in the formation of the catalytic site by interacting with two iron atoms located within the enzyme (127).

Primary sequence conservation shown in figure 1.6 was expanded from Bai et al to include *C. albicans* (Uniprot ID = Q5A747), *A. fumigatus* ([www.aspergillusgenome.org](http://www.aspergillusgenome.org)),




and *S. pombe* (Uniprot ID = O94523) - strains relevant to this study (Figure 1.7). Sequences were taken from Uniprot (homo sapien 1 ID = O00767; homo sapien 5 = Q86SK9; mus musculus 1 ID = P13516) or the [aspergillusgenome.org](http://aspergillusgenome.org) website and a multiple sequence alignment was generated using the entire length of the proteins on [www.ebi.ac.uk](http://www.ebi.ac.uk). Transmembrane domains are indicated (TM1-4) as are the cytoplasmic (amphipathic) helices (A)H1-10. Amphipathic helices are predicted to be at the lipid bilayer-cytosol interface. Helices are predicted to be involved in generating the cytosolic domains, including the active site, of the desaturases. The cytochrome  $b_5$  domain present in fungal  $\Delta 9$  desaturases only is also highlighted.


Sequence homology in figure 1.7 was highlighted using the same colour coding system as in figure 1.6. Sequence homology relating to figure 1.7 only is discussed below. The nine essential histidine residues are conserved in all species at identical positions within the sequences (highlighted in red). All species, apart from *C. albicans*, have a conserved arginine in TM4 (highlighted in grey). This residue relates to arginine 249 in mouse Scd1 which was identified by Bai et al in TM4 in an otherwise highly hydrophobic, transmembrane region and is predicted to be involved in stabilising the kink between TM3 and TM4 (128). Conserved carboxylate groups (highlighted in purple) are involved in the coordination with the iron atoms at the active site are conserved at three positions with all species containing a glutamic acid between AH7 and H8, and an aspartic acid between H2 and H3. There is a second conserved carboxylate between H2 and H3, however the three mammalian proteins all express a glutamic acid, whilst the four fungal species all express aspartic acid at this position. Residues involved in the coordination with the fatty acid acyl chain (highlighted in blue) and in determining the length of the enzyme's tunnel (highlighted in green) are conserved between all species apart from homo sapien Scd5 where there is a single residue in both regions that is not. There are two amino acids in TM2 that are involved in determining the length of the acyl chain binding tunnel (highlighted in green). A tyrosine is conserved throughout human Scd1 and mouse Scd1 and all fungal species, but not human Scd 5. The second amino acid is a glycine in all fungal species, but an alanine in all mammalian proteins shown. Residues highlighted in yellow are the CoA binding site. These are conserved in all mammalian species shown, but the only CoA

binding residue conserved in fungi is an asparagine in TM1 although not in *S. pombe*. *A. fumigatus* has an additional CoA binding site residue that is conserved between the mammalian species, an aspartic acid in H2, but this is not conserved between any of the other fungi shown.


The additional species shown in figure 1.6 all contain the nine conserved histidines in the same position, have identical homology to all mammalian species shown at the acyl chain binding site (highlighted in blue) and at the metal centre (highlighted in purple). Although the residues in TM2 that are involved in determining the length of the acyl chain tunnel (highlighted in green) are not identical, there is conservation of amino acid properties throughout all species making these positions functionally conserved.




**M. musculus (1)** WRNIIILM<sup>Y</sup>LLHLGGLYGIILVPS-CKLYTCLFGIFYMTS<sup>Y</sup>LGITAG<sup>A</sup>HLRWS<sup>E</sup>RTYKARLPLRIFLIANTMA 141  
**M. musculus (3)** WRNIIILM<sup>Y</sup>LLHLVGLALYGITLVPS-CKLYTCLFAFVYVIS<sup>Y</sup>HGIGAGV<sup>R</sup>HLRWS<sup>E</sup>RTYKARLPLRIFLIANTMA 145  
**H. sapiens** WRNIIILM<sup>Y</sup>LLHLGALYGITLIPT-CKFYTWLWGVFYFVS<sup>Y</sup>LGITAG<sup>A</sup>HLRWS<sup>E</sup>RSYKARLPLRIFLIANTMA 145  
**D. rerio** WRNIIILM<sup>Y</sup>LLHIAAVYGLFLIPS-AHPLTLPWAFAC<sup>Y</sup>VYGLGITAG<sup>A</sup>HLRWS<sup>E</sup>RSYKATLPLRIFLAI<sup>G</sup>NSMA 111  
**D. melanogaster** WRNIIILFALVHLAALYGLHSIFTRAKLATLFAAGLYIIG<sup>Y</sup>LVGTAG<sup>A</sup>HLRWA<sup>E</sup>RTYKAKWPLRLLLVIFNTIA 124  
**C. hyperboreus** WQNVAKFVI<sup>Y</sup>IHALFFYGATYLP<sup>S</sup>-MSLNMWIMFLIS<sup>Y</sup>QIIS<sup>Y</sup>LGITMGA<sup>A</sup>HLRWA<sup>E</sup>KTYKAKLPLRIFLTFANSLA 124  
**C. elegans** WK<sup>N</sup>VALFVALHIGALVGLYQLVFAKWATVGVVFL<sup>L</sup>PLTGS<sup>Y</sup>MGVTGG<sup>A</sup>HLRWA<sup>E</sup>RAYKATLSWRVFLMLIN<sup>S</sup>IA 113  
**S. sp. PCC6803** AWTVIFFFTSIHLVALLAFLPQFFSWKAVGMAFLLYVITG<sup>Y</sup>IGITLGFHRCIS<sup>E</sup>RSFNVPKWLEYIFVICGTLA 126  
**A. thaliana** -LDYVKFSASFTVHSLALLAPFFYFWSALWVTFLYT-IG<sup>Y</sup>LGITVSY<sup>R</sup>HLRWA<sup>E</sup>RSFKVPKWLEYLLAYCALLA 110  
**S. cerevisiae** WLNMLVLCGMPMIGWYFALS<sup>G</sup>KVPLHLNVFLFSV<sup>Y</sup>YAVG<sup>Y</sup>VSITAG<sup>A</sup>Y<sup>R</sup>HLRWS<sup>E</sup>RSYSAHWPLRLFYAIFGCAS 186



**M. musculus (1)** F<sup>N</sup>NDVYE<sup>Y</sup>ARD<sup>R</sup>RA<sup>H</sup>HKFS<sup>E</sup>THA<sup>Y</sup>PHNSRRGFF<sup>F</sup>FSHVGVLL<sup>V</sup>VR<sup>K</sup>HPAVKEKGGKLDMSDLKAEKLVMFQRRY 213  
**M. musculus (3)** F<sup>N</sup>NDVYE<sup>Y</sup>ARD<sup>R</sup>RA<sup>H</sup>HKFS<sup>E</sup>THA<sup>Y</sup>PHNSRRGFF<sup>F</sup>FSHVGVLL<sup>V</sup>VR<sup>K</sup>HPAVKEKGGKLDMSDLKAEKLVMFQRRY 217  
**H. sapiens** F<sup>N</sup>NDVYE<sup>Y</sup>ARD<sup>R</sup>RA<sup>H</sup>HKFS<sup>E</sup>THA<sup>Y</sup>PHNSRRGFF<sup>F</sup>FSHVGVLL<sup>V</sup>VR<sup>K</sup>HPAVKEKGGKLDMSDLKAEKLVMFQRRY 217  
**D. rerio** F<sup>N</sup>NDIYE<sup>Y</sup>SRD<sup>R</sup>RV<sup>H</sup>HKYS<sup>E</sup>TD<sup>A</sup>PHNSNRGFF<sup>F</sup>FSHVGVLL<sup>V</sup>VR<sup>K</sup>HPEVIERGRKLE<sup>L</sup>DLKADKVMFQRRF 183  
**D. melanogaster** F<sup>N</sup>DAVYH<sup>Y</sup>ARD<sup>R</sup>RV<sup>H</sup>HKYS<sup>E</sup>TD<sup>A</sup>PHNATRGFF<sup>F</sup>FSHVGVLL<sup>V</sup>CK<sup>H</sup>HPDIKEKGRGLD<sup>L</sup>SDLRADPILMFQRRK 196  
**C. hyperboreus** G<sup>N</sup>NSIYI<sup>Y</sup>SRD<sup>R</sup>RT<sup>H</sup>HKCS<sup>E</sup>KMG<sup>Y</sup>PHNAKRGF<sup>F</sup>FAHMGWLL<sup>V</sup>VR<sup>K</sup>HPEVTRAGK<sup>Y</sup>VNN<sup>T</sup>DL<sup>E</sup>NDL<sup>E</sup>NDK<sup>Y</sup>Q<sup>H</sup> 196  
**C. elegans** F<sup>N</sup>NDIID<sup>Y</sup>ARD<sup>R</sup>RC<sup>H</sup>HKWT<sup>E</sup>TD<sup>A</sup>PHSTNRGMF<sup>F</sup>FAHMGWLL<sup>V</sup>KK<sup>H</sup>DQLKI<sup>Y</sup>QGGKLD<sup>L</sup>SDLYEDPVL<sup>M</sup>FQRRK 185  
**S. sp. PCC6803** C<sup>N</sup>GGVFE<sup>Y</sup>AVG<sup>D</sup>ERM<sup>H</sup>HKFS<sup>E</sup>TT<sup>P</sup>PHDSNKGFW<sup>S</sup>HIGWMMF<sup>E</sup>IP-AKADIPR--YTKDIQDDK<sup>F</sup>YQFCQNN 195  
**A. thaliana** I<sup>N</sup>GDPID<sup>Y</sup>VST<sup>H</sup>RY<sup>H</sup>QFT<sup>S</sup>ER<sup>Y</sup>PHSPKEGFW<sup>S</sup>HLLWYDSAY-LVSKCGRANVEDLKRQWFYRFLQKT 181  
**S. cerevisiae** VEGSAKW<sup>Y</sup>GHS<sup>R</sup>I<sup>H</sup>RYT<sup>D</sup>FLR<sup>Y</sup>PYDARRGLW<sup>Y</sup>SHMGWLL<sup>K</sup>PN---PKYKARADITDMTD<sup>Y</sup>DTW<sup>T</sup>IRFQHRH 255



**M. musculus (1)** YKPGLLMCFILPTLV<sup>P</sup>WYCWGETFVNSLFVST<sup>F</sup>L<sup>Y</sup>YTLV<sup>L</sup>NA<sup>W</sup>LV<sup>N</sup>SA<sup>A</sup>HL<sup>Y</sup>GYR<sup>P</sup>YDKN<sup>I</sup>Q<sup>S</sup>RENILVSLG 287  
**M. musculus (3)** YKPGILLMCFILPTLV<sup>P</sup>WYCWGETFVNSLFVAT<sup>L</sup>L<sup>Y</sup>AVV<sup>L</sup>NA<sup>W</sup>LV<sup>N</sup>SA<sup>A</sup>HL<sup>Y</sup>GYR<sup>P</sup>YDKN<sup>I</sup>DP<sup>R</sup>QNALVSLG 291  
**H. sapiens** YKPGLLMCFILPTLV<sup>P</sup>WYFWGETFQNSV<sup>F</sup>VAT<sup>F</sup>L<sup>Y</sup>AVV<sup>L</sup>NA<sup>W</sup>LV<sup>N</sup>SA<sup>A</sup>HL<sup>Y</sup>GYR<sup>P</sup>YDKN<sup>I</sup>SPRENILVSLG 291  
**D. rerio** YKLSV<sup>V</sup>LMCFV<sup>V</sup>TVV<sup>P</sup>CYM<sup>W</sup>GESLW<sup>I</sup>AYFIPT<sup>L</sup>L<sup>Y</sup>ALGL<sup>N</sup>S<sup>W</sup>LV<sup>N</sup>SA<sup>A</sup>HL<sup>Y</sup>MWGNRPYDGN<sup>I</sup>GPRENRFV<sup>T</sup>FS 257  
**D. melanogaster** YIILM<sup>L</sup>ACFV<sup>L</sup>PTV<sup>I</sup>PMV<sup>Y</sup>WNETLASSW<sup>F</sup>VAT<sup>M</sup>F<sup>Y</sup>WCF<sup>L</sup>NM<sup>W</sup>LV<sup>N</sup>SA<sup>A</sup>HL<sup>Y</sup>KFGNRPYDK<sup>T</sup>MNP<sup>T</sup>QNAFVSAF 270  
**C. hyperboreus** YITSFLLCGFV<sup>I</sup>PTV<sup>L</sup>PYLLWGECLY<sup>T</sup>AYFMA-IF<sup>Y</sup>VITLHV<sup>W</sup>LV<sup>N</sup>SA<sup>A</sup>HL<sup>Y</sup>FGYK<sup>P</sup>YDK<sup>T</sup>IGPTENMLVSL<sup>L</sup> 269  
**C. elegans** YLPLVGI<sup>F</sup>CFALP<sup>T</sup>IFV<sup>V</sup>WLGESAF<sup>I</sup>AYT<sup>A</sup>AL<sup>F</sup>YCF<sup>T</sup>LH<sup>W</sup>W<sup>C</sup>INSV<sup>S</sup>H<sup>W</sup>VGW<sup>P</sup>YD<sup>H</sup>QASSVDN<sup>L</sup>WTS<sup>I</sup>A 259  
**S. sp. PCC6803** LLLIQV<sup>L</sup>GLL<sup>L</sup>FALG-----GW<sup>F</sup>V<sup>I</sup>WGL<sup>F</sup>V<sup>L</sup>V<sup>F</sup>V<sup>H</sup>F<sup>Y</sup>W<sup>F</sup>VNSA<sup>T</sup>E<sup>K</sup>FGYV<sup>S</sup>HESND<sup>Y</sup>SRNC<sup>W</sup>WALL 261  
**A. thaliana** VLFHILGLGF<sup>L</sup>FYLG-----GMS<sup>F</sup>V<sup>T</sup>WGM<sup>V</sup>CA<sup>L</sup>E<sup>V</sup>H<sup>V</sup>W<sup>C</sup>L<sup>I</sup>NSL<sup>C</sup>E<sup>F</sup>W<sup>G</sup>TR<sup>T</sup>W<sup>T</sup>ND<sup>T</sup>SRN<sup>V</sup>W<sup>L</sup>S<sup>V</sup>F 247  
**S. cerevisiae** YILLML<sup>L</sup>TAFV<sup>I</sup>PTLIC<sup>G</sup>YFPN-DYMGGLI<sup>Y</sup>AG<sup>F</sup>I<sup>Y</sup>V<sup>F</sup>VI<sup>Q</sup>QA<sup>F</sup>FC<sup>I</sup>NSL<sup>A</sup>Y<sup>I</sup>GTQ<sup>F</sup>DDRR<sup>T</sup>PRD<sup>N</sup>WIT<sup>A</sup>IV 328



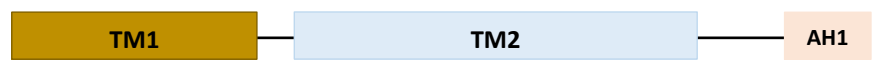
**M. musculus (1)** AVGGGF<sup>N</sup>Y<sup>H</sup>H<sup>H</sup>FP<sup>P</sup>DYSASEY-RWHIN<sup>F</sup>T<sup>T</sup>FFID<sup>C</sup>MAALGLAYDR<sup>K</sup>KVSKATV<sup>L</sup>ARIK<sup>R</sup>TGDGSHK<sup>S</sup> 355  
**M. musculus (3)** SMGGGF<sup>N</sup>Y<sup>H</sup>H<sup>H</sup>AP<sup>P</sup>DYSASEY-RWHIN<sup>F</sup>T<sup>T</sup>FFID<sup>C</sup>MAALGLAYDR<sup>K</sup>KVSKATV<sup>L</sup>ARIK<sup>R</sup>TGDGSHK<sup>S</sup> 359  
**H. sapiens** AVGGGF<sup>N</sup>Y<sup>H</sup>H<sup>H</sup>S<sup>F</sup>PDYSASEY-RWHIN<sup>F</sup>T<sup>T</sup>FFID<sup>C</sup>MAALGLAYDR<sup>K</sup>KVSKAA<sup>L</sup>ILARIK<sup>R</sup>TGDGNYK<sup>S</sup> 359  
**D. rerio** AIGGGFN<sup>Y</sup>H<sup>H</sup>FP<sup>P</sup>DYSTSEYG-WKLN<sup>L</sup>TFIFVD<sup>T</sup>MCFGLASNR<sup>K</sup>KVSKELI<sup>L</sup>ARV<sup>K</sup>RTGDG<sup>S</sup>YR<sup>S</sup>G 325  
**D. melanogaster** TFGGGW<sup>N</sup>Y<sup>H</sup>H<sup>H</sup>FP<sup>P</sup>DYKTA<sup>E</sup>WGCYSLN<sup>I</sup>T<sup>T</sup>AFID<sup>L</sup>FAKIGWAYDL<sup>K</sup>TVAP<sup>D</sup>VIQ<sup>R</sup>RV<sup>L</sup>RTGDG<sup>S</sup>HELW 339  
**C. hyperboreus** AMGGGF<sup>N</sup>Y<sup>H</sup>H<sup>H</sup>FP<sup>P</sup>DYSTSEW-GY<sup>F</sup>NT<sup>T</sup>SRIID<sup>A</sup>MASIG<sup>Q</sup>AYDL<sup>R</sup>TASKAT<sup>E</sup>ARS<sup>V</sup>RTGL<sup>P</sup>ELTA<sup>I</sup> 337  
**C. elegans** AVGGGF<sup>N</sup>Y<sup>H</sup>H<sup>H</sup>FP<sup>P</sup>DYRTSEH-AE<sup>F</sup>LN<sup>W</sup>TR<sup>V</sup>LID<sup>F</sup>ASIG<sup>M</sup>VYDR<sup>K</sup>TP<sup>E</sup>EV<sup>I</sup>QR<sup>C</sup>CK<sup>F</sup>GC<sup>E</sup>TEREK 327  
**S. sp. PCC6803** TFGGGW<sup>N</sup>Y<sup>H</sup>H<sup>H</sup>AY<sup>Q</sup>YSARHGL<sup>Q</sup>-W<sup>W</sup>EV<sup>D</sup>L<sup>T</sup>W<sup>M</sup>TIK<sup>F</sup>LSLLGLAK<sup>D</sup>IK<sup>L</sup>PP<sup>E</sup>TAMANKA----- 318  
**A. thaliana** SFGG<sup>S</sup>W<sup>N</sup>Y<sup>H</sup>H<sup>H</sup>AF<sup>E</sup>SSAR<sup>Q</sup>GLE-W<sup>W</sup>Q<sup>I</sup>DIS<sup>W</sup>YI<sup>V</sup>RF<sup>F</sup>E<sup>I</sup>IG<sup>L</sup>AT<sup>D</sup>V<sup>K</sup>V<sup>P</sup>TEA<sup>Q</sup>RRR<sup>K</sup>AI<sup>V</sup>R----- 307  
**S. cerevisiae** TFGGGY<sup>N</sup>F<sup>H</sup>H<sup>H</sup>FP<sup>P</sup>DYRNA<sup>I</sup>K-W<sup>Y</sup>Q<sup>Y</sup>DP<sup>T</sup>K<sup>V</sup>IY<sup>L</sup>TS<sup>L</sup>VGLAYDL<sup>K</sup>KFSQ<sup>N</sup>AIE<sup>E</sup>ALI<sup>Q</sup>Q<sup>E</sup>K<sup>K</sup>IN<sup>K</sup> 396

**Figure 1.6. Sequence alignment of mammalian SCD1 isoforms with other  $\Delta 9$  desaturases.** Only the regions aligning with SCD1 are shown. TM 1-4 represents the four ER transmembrane domains. (A)H1-10 represents the 10  $\alpha$ -helices which are split into two cytosolic clusters. AH1, AH7, and AH9 are amphipathic and are predicted to be positioned at the lipid bilayer-cytosol interface. H2-6 and H8 are not amphipathic and are involved in the coordination of the diiron metal centre and active site structure. Conserved residues are highlighted in the following colours: Red = histidine; purple = carboxylates in the coordination of the metal centre; blue = acyl chain binding site; yellow = CoA binding site; green = residues involved in determining the length of bound acyl chains; black = mutations that change the substrate specificity; grey = ARG 249 in the transmembrane region. Figure taken from (128).

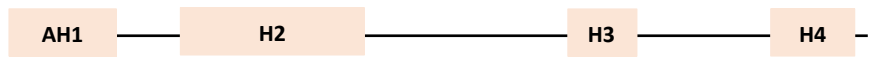
<i>S. c</i>	MPTSGTTIELIDDQFPKDDSSASSGIVDEVLDLLEANILATGLNKKAPRIVNG--FGSLMGS	58
<i>A. f</i>	-----	0
<i>C. a</i>	-----MTTVEQLETVDITKLNIAAAGTNKKVPRVVAAGLGGKLMGT	41
<i>S. p</i>	-----MTAPSATA---FSS---	11
<i>H. s</i> (1)	MPA-----HLLQDDISS-----SYTTTTTITAPPSRVLQNGGDKLE-	36
<i>H. s</i> (5)	-----MPGP-----ATDAG-	9
<i>M. m</i> (1)	MPA-----HMLQ-EISS-----SYTTTTTITAPPSG---NEREKVK-	32



<i>S. c</i>	KEMVSVEFDKKGNEKSNLDRLLLEKDNQEKEEAKTKIHISEQPWTLNNWHQHLNWLNMVL	118
<i>A. f</i>	-----MSAKP-ADASRP-RA-GDPKKVHIADTAITRQNWKVHNWLNWVFL	42
<i>C. a</i>	SDLVKVTAEE---ITKDSMESLAEKDAREKAKYANKKHISEEPWTLDNFAKKINWLNML	98
<i>S. p</i>	-ATTQPTTEGNASMRKRTIP-VVPSVPERKWDPKAPKHIQEQPWTMQNWWRHNLWLCML	69
<i>H. s</i> (1)	---TMPLY-LEDDIRPDIKDDIYDPTYKDKEGPSP-----KVEYVWRNIIL	78
<i>H. s</i> (5)	---KIPFCDAKEEIRAGLESSEGGGPERPGARGQ-----RQNIWVRNVVL	52
<i>M. m</i> (1)	---TVPLH-LEEDIRPEMKEDIHDPTYQDEEGPPP-----KLEYVWRNIIL	74



<i>S. c</i>	VCGMPMIGWYFALSGKVPLHLNVFLFSVFYLAVGVSITAGYHRLWSHRSYSAHWPLRLRF	178
<i>A. f</i>	IIGIPLYGCIQAFW--VPLQLKTAIWAVVYFFTLGITAGYHRLWAHCSYSARLPLRIW	100
<i>C. a</i>	VVFIPVFGAYCAWNY--PPQWKTLVLTFFVMYAFSLISITAGYHRLYSHKSYDAALPVRLF	156
<i>S. p</i>	IFGLPMIAIYGVFT--TPLQTKTLIFAIYYAYSGLGITAGYHRLWSHRAYKAKKPLEYF	127
<i>H. s</i> (1)	MSLLHLGALYGITLI-PTCKFYTWLWGVFVYFVSLGITAGAHRLWSHRSYKARLPLRLF	137
<i>H. s</i> (5)	MSLLHLGAVYSLVLI-PKAKPLTLLWAYFCFLAALGVTAGAHRLWSHRSYRKLPLRIF	111
<i>M. m</i> (1)	MVLLHLGGLYGIILV-PSCKLYTCLFGIFYMTSLGITAGAHRLWSHRTYKARLPLRIF	133



<i>S. c</i>	YALFGCASVEGSAKWWGHSRHHRYTDTLRDPYDARRGLWYSHMGWMLLKPNPKYK---	235
<i>A. f</i>	LAAVGGGAVEGSIKWWGHSRHHRYTDTDKDPYSVRKGLLYSHIGWVMKQNPRI---	157
<i>C. a</i>	FAFFGAGAEGSIKWWGHSRHHRYTDTPRDPYDARRGFWFVSHMGWMLTKANPKNR---	213
<i>S. p</i>	LAAGGAAAFEGSIKWWGHSRHHRYTDTDKDPYNVKKGFVYAHVGMWMIILQNPRI---	184
<i>H. s</i> (1)	LI IANTMAFONDVYEWARHDRAHKKFSETHADPHNSRRGFFFSHVGLLVRKHPAVKEKG	197
<i>H. s</i> (5)	LAVANSMAFONDIFEWSRDHRAHKKYSETDADPHNARRGFFFSHVGLVFRKHRDVIEKG	171
<i>M. m</i> (1)	LI IANTMAFONDVYEWARHDRAHKKFSETHADPHNSRRGFFFSHVGLLVRKHPAVKEKG	193



<i>S. c</i>	ARADITDMTDDWTIRFQHRHYILLMLLTAFFVIPTLICGYFFND-YMGGLIYAGFIRVFVI	294
<i>A. f</i>	GRTDITDLNEDPVVVWQHRNYLKVVLVMGLVVPMLVAGLGWGD-WFGGFYIYAGILRIFV	216
<i>C. a</i>	ARADISDLVADWVTFQHRHYLLMITAAFIFPPTLVAGLGWGD-YWGGFIYAGILKGF	272
<i>S. p</i>	GRSDVSDLNSDPFVMFNHRHFLPIASFMAFIFPPLFCGLLWGD-YRGGYFYAGVCLV	243
<i>H. s</i> (1)	STLDLSDLEAEKLVMFQRRYYKPGLLMCFILPTLVWPYFWGETFQNSVVFATFLRYAVV	257
<i>H. s</i> (5)	RKLDVTDLLADPVVRIQRKYYKISVVLVLCFVPTLVWPYIWGESLWNSYFLASILRYTIS	231
<i>M. m</i> (1)	GKLDMSDLKAEKLVMFQRRYYKPGLLMCFILPTLVWPYCWGETFVNSLWFVSTFLRYTLV	253



<i>S. c</i>	QQATFCVNSLAHYIGTQPFDDRRTPRDNWITAIVTFGEYHNFHHEFFPTDYRNAIKWYQY	354
<i>A. f</i>	QQATFCVNSLAHWLGDQPFDDRNPRDHVITAVTLGEGYHNFHHEFFPSDYRNAIEWHQY	276
<i>C. a</i>	QQATFCVNSLAHWIGVQPFDDRRTPRDHVLTAFTVTFGEYHNFHHEFFPSDYRNALKWYQY	332
<i>S. p</i>	HHATFCVNSLAHLIGSQPFDDTNSARNHFITAVTLGEGNHNYHHAFFPNDYRNGLRWY	303
<i>H. s</i> (1)	LNATWLVNSAAHLYGYRYPYDKNISPRENIVSLGAVGEGFHNYHHSFPDYASAYRWHI	317
<i>H. s</i> (5)	LNISWLVNSAAHMYGNRPYDKHISPRQNPLVALGAIEGFHNYHHTFPDYASAYRWHI	291
<i>M. m</i> (1)	LNATWLVNSAAHLYGYRYPYDKNISRENIVSLGAVGEGFHNYHHTFPDYASAYRWHI	313

	AH9	H10	
<i>S. c</i>	DPTKVI IYLTSLVGLAYDLKFKFSQNAIEEALIQQEQQKINKKKAKINWGPVLTDLPMWDK		414
<i>A. f</i>	DPTKWTIWIWKQLGLAYDLKQFRANEIEKGRIQQQLQKKIDQKRAKLDWGIPLDQLPVMEW		336
<i>C. a</i>	DPTKVTIWCLSKLGLAWNLLKFKFSQNAIEQGLVQQQQKLDLDRMKNKLNWGAEIEKLPVWTR		392
<i>S. p</i>	DPTKIFIIYIASLFLGLAYNLNTPDNEIQKGIVQQKQKVLDRWRKLNWGIPLDQLPVMEF		363
<i>H. s</i> (1)	NFTTFFIDCMAALGLAYDRKKVSKAAILARIKRTGDGNYKSG-----		359
<i>H. s</i> (5)	NPTTWFIDFMCWLGATDRKRATKPMIEARKARTGDSSA-----		330
<i>M. m</i> (1)	NFTTFFIDCMAALGLAYDRKKVSKATVLRARIKRTGDGSHKSS-----		355
<b>Cytochrome b<sub>5</sub> domain</b>			
<i>S. c</i>	QTFLA SKENKGLV I I SGIVHDVSGY I SEHPGGETLIKTALGKDATKAFSGGVYRHSNAA		474
<i>A. f</i>	DDYVEQAKNGRGLIAIAGVVHDVDFIKDHPGGKAMINSIGKDATAMFNGGVYHNSNAA		396
<i>C. a</i>	EEFNERA-KQEGLI I I SGI IHNVKNF I KEHPGGQALVRASLGKDATKAFNGAVYAHSNAA		451
<i>S. p</i>	EDFLEQSKT-RPLVLINGVVHDMTGF-EHPGGQLLRSAFGKDATAAFNGGVYDHTNGA		420
<i>H. s</i> (1)	-----		359
<i>H. s</i> (5)	-----		330
<i>M. m</i> (1)	-----		355
<b>Cyt b<sub>5</sub></b>			
<i>S. c</i>	QNVLADMRVAVIKESKNSAIRMAS-----KRGEIYETGKFF-----		510
<i>A. f</i>	HNLLSTMRVGVIRGGCEVEIWKRAQKESGEYVRDESGQRIIRAGQQVTKIPDPIPTADAA		456
<i>C. a</i>	HNLLATMRVAVVKDGEVNADTFDL-----QEQQM-EKEKQS-----		486
<i>S. p</i>	HNLLSTYRVAVVRGGMEVEVWVKSAGAG-QLPMKDTQGQKIVRVGEQITRIQPPIEAAAAN		479
<i>H. s</i> (1)	-----		359
<i>H. s</i> (5)	-----		330
<i>M. m</i> (1)	-----		355

**Figure 1.7. Sequence alignment of  $\Delta 9$  desaturases from fungal strains used in this study and mammalian homologs.** The entire length of all  $\Delta 9$  desaturases are shown. Fungal strains only contain a cytochrome b<sub>5</sub> domain. Conserved residues are highlighted in the following colours: Red = histidine; purple = carboxylates in the coordination of the metal centre; blue = acyl chain binding site; yellow = CoA binding site; green = residues involved in determining the length of bound acyl chains; black = mutations that change the substrate specificity; grey = ARG 249 in the transmembrane region. Figure adapted from (128). Multiple sequence alignment was generated using [www.ebi.ac.uk](http://www.ebi.ac.uk).

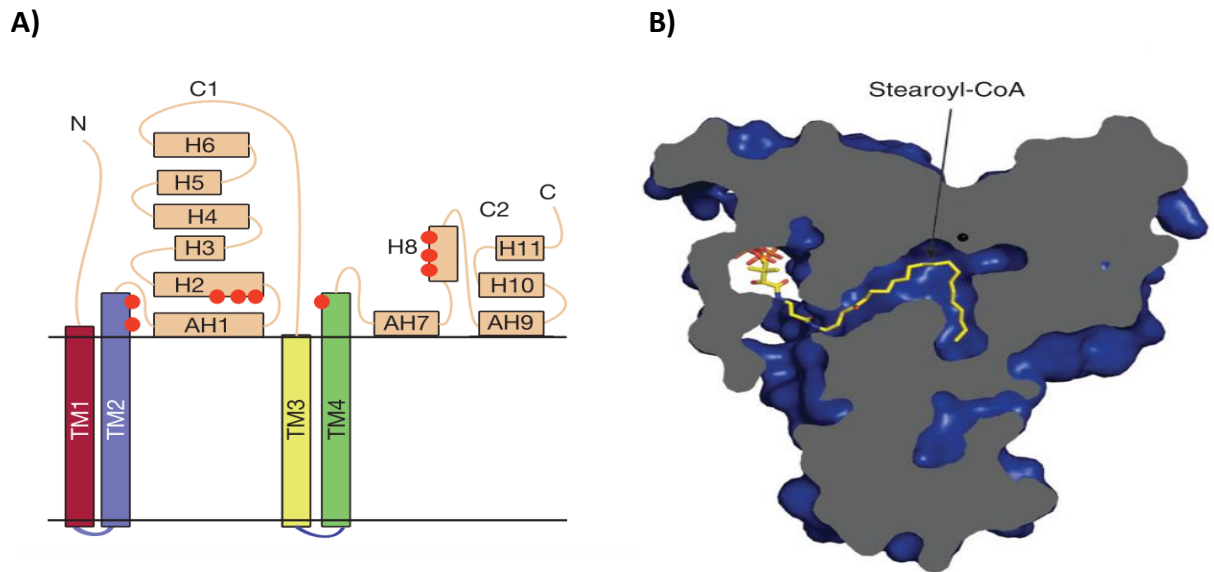


**Figure 1.8. Structure of eukaryotic  $\Delta 9$  desaturase.** A) Cartoon topology of the mammalian  $\Delta 9$  desaturase, Scd1. Scd1 consists of four transmembrane domains that anchor the protein to the ER membrane. The transmembrane domains form a cone-like structure that are capped by cytosolic domains. (A) H1-10 represents 10  $\alpha$ -helices which are split into two cytosolic clusters, C1 and C2. AH1, AH7, and AH9 are amphipathic and are predicted to be positioned at the lipid bilayer-cytosol interface. Red dots indicate conserved histidines that are involved in the coordination of two iron atoms that are required for the formation of the active site. The position of the conserved histidines within the protein sequence can be identified by the residues highlighted in red in figure 1.4. Figure taken from (128). B) Cross-section of human Scd1 showing a tunnel-like pocket where the acyl tail of stearoyl-CoA can dock. The tunnel is lined with hydrophobic residues and contains a sharp kink that ensure only a *cis* desaturation can occur. The length of the tunnel and the sharp kink ensures the correct positioning of carbon 9 and 10 of C16:0 and C18:0 acyl CoA saturated fatty acids for desaturation. Figure taken from (125).

So far, only truncated versions of the mouse and human Scd1 crystal structures have been solved (125,128) and the predicted topologies for both species are consistent. Scd1 contains four transmembrane helices (TM 1-4) arranged in a cone-like formation that are capped by cytosolic domains (C1 and C2) with both the N- and C-termini and the catalytic site on the cytosolic side of the membrane (128,129) (Figure. 1.8). The cap domain consists of ten cytoplasmic helices ((A)H1-10) and interlocks with the cytosolic faces of the four TM domains. The cap contains essential residues that contribute to both metal ion binding and substrate recognition. Consistent with predictions based on sequence conservation, histidines in three histidine-box motifs do participate in metal

ion coordination. Three helical turns of both TM2 and TM4 protrude slightly into the cytosol and provide residues that are essential for the active site.

The fatty acid binding site is a long, hydrophobic tunnel that contains a sharp kink where the active site and dimetal centre are located (Figure 1.8B). The length of the tunnel ensures that only C9 and C10 in the stearyl CoA can align with the catalytic site at kink. The pronounced kink is likely to be involved in holding the substrate in position such that only desaturation between these two carbons is possible. This geometry ensures that only a cis dehydrogenation of the substrate occurs.  $\Delta 9$  desaturases recognise stearyl-CoA via electrostatic and hydrophobic interactions. Wang et al suggest that Scd1 encounters the CoA head group and polar interactions then guide the acyl chain of the fatty acid into the hydrophobic tunnel between transmembrane domains 2 and 4 (125). The acyl chain of stearyl-CoA inserts into the narrow hydrophobic tunnel of Scd1 such that a negatively charged phosphate in the ADP group of CoA is positioned adjacent to a large positively charge surface of the enzyme.

### 1.3.3 Regulation of OLE1 expression

*S. cerevisiae* require highly adaptable membrane compositions to facilitate growth in a range of conditions. Adjustments to membrane lipid saturation occurs through altering the expression of Ole1p in response to sensing of physicochemical properties of the ER membrane. OLE1 is an essential gene - the overexpression or deletion of which is lethal, and as such is tightly regulated (130). Expression of OLE1 is controlled both at the level of transcription (131) and mRNA stability (132). Factors that mediate the expression of Ole1p include temperature (133), hypoxia (134), and high saturated fatty acid content (135). The transcription of OLE1 is regulated by two related homologous factors, Spt23p and Mga2p, that are essential for OLE1 expression. Deletion of either gene is non-lethal, however a double mutation renders the cell non-viable suggesting some form of functional redundancy (136). Neither protein contains a recognisable DNA binding motif as such they are not transcription factors, however Mga2p and

Spt23p have been shown to regulate OLE1 transcription through a fatty acid regulated (FAR) element (131) and subsequent chromatin remodelling (137).

Mga2p and Spt23p are found in two states - one is the inactive p120 kDa protein anchored to the nuclear or peripheral ER membrane via their C-terminus, the other is the soluble p90 kDa that localises to the cytoplasm and nucleus (138,139). Activation of Mga2p and Spt23p is mediated by a cascade of events, however this process is complex, and our understanding remains incomplete. Very little is known about the activation of Spt23p. In contrast, the activation of Mga2p is dependent on a highly flexible, single transmembrane helix that senses lipid desaturation. Mga2p activation is conferred through the dimerisation and rotation of the transmembrane helix within the membrane. The orientation of the transmembrane helix, and in particular of a single tryptophan residue (W1042), is dependent on the lipid desaturation content of the membrane (Figure 1.9). Membranes containing a high degree of unsaturated lipids confer an “off” configuration where the tryptophans are most often orientated away from the dimer interface; whereas these residues are more likely to point towards each other when there is a higher proportion of saturated lipid acyl chains which in turn leads to the “on” configuration of Mga2p and subsequent ubiquitination (97,140). Until recently, it was generally accepted that the rotation of Mga2p was dependent on sensing membrane fluidity. However, it was demonstrated that it is the sensing of lateral pressure by W1042 that induces the rotation of the transmembrane helix of Mga2p as a result of an increase in packing order in membranes with a higher saturated acyl chain lipid content (141). It is not known whether Spt23p activation is also via the sensing membrane lipid saturation using the same rotation-based mechanism as Mga2p. Of note, Mga2p and Spt23p contain 86% sequence identity in the sensory transmembrane helix domains, therefore it is plausible that Spt23p also activated by a similar mechanism (140).

In the “on” confirmation, Mga2p and Spt23p are orientated such that three lysine residues in the cytosolic region can be ubiquitinated by the E3 ubiquitin ligase Rsp5p (142). However, it remains unknown how the membrane sensing domain transmits a signal to recruit the ligase. Following ubiquitylation by Rsp5, Mga2p and Spt23p are



activated by proteasomal processing by the insertion of a flexible, tightly folded loop into the proteolytic chamber of the proteasome to generate the active p90 fragment and a short lived C-terminal fragment (138). It is not currently understood whether the proteolytic cleavage events occur spontaneously or whether it is assisted by ubiquitylation and subsequent recruitment of the ATPase Cdc48p and cofactors Np14 and Ufd1 complex. Following cleavage by the proteasome, the active p90 fragment is mobilised by Cdc48p/ Np14/ Ufd1 for transfer into the nucleus (Figure 1.10). The membrane protein Ubx2p anchors Cdc48p in the ER and has been shown to be a crucial protein in the transcription of OLE1. UBX2 deletion results in a 40% reduction in OLE1 mRNA relative to wild-type cells and an associated shift to saturated fatty acids and a concurrent increase in lipids with small head groups, such as PE at the expense of PC (91). This shift in lipid composition compensates for physical membrane stress induced by the switch to more saturated acyl chains, thereby ensures membrane shape and fluidity. There are two theories for the role of Cdc48p/ Np14/ Ufd1 in the OLE1 pathway: one suggests that Cdc48p complex only acts after the proteolytic processing of Mga2p and Spt23p and acts to release the processed p90 form from the membrane-embedded, unprocessed C-termini (139,143). The second scenario suggests that the Cdc48p complex can co-facilitate the rapid proteolysis of the C-terminal portion of p120 (77,80). Once Mga2 and Spt23 are activated and mobilised from the membrane, they translocate into the nucleus where they activate the transcription of OLE1 through unknown mechanisms (145). The current understanding of how Mga2p or Spt23p activation leads to OLE1 transcription are incomplete.

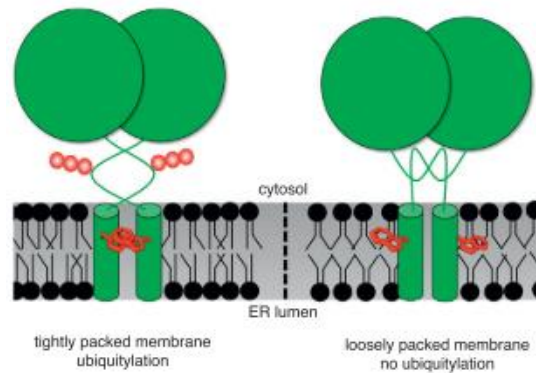


**Figure 1.9. Mga2p rotation-based lipid sensing.** In a more highly lipid saturated membrane (left figure), Mga2p rotates such that W1042 faces inwards to the dimer interface. This positions Mga2p in the “on” conformation by exposing three cytosolic lysines on each Mga2p monomer which can be ubiquitinated by the E3 ligase Rsp5p. Conversely, in highly unsaturated membranes, Mga2p rotates such that W1042 faces away from the dimer interface and the cytosolic lysines are not exposed. Figure taken from (140)

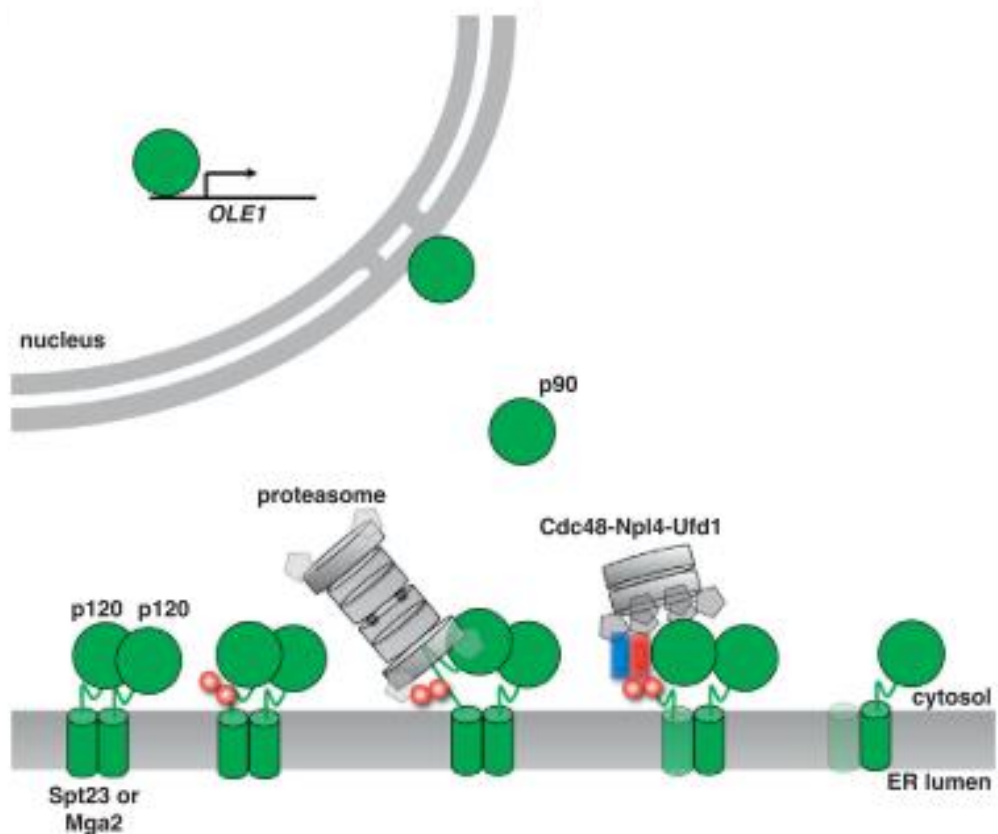


**Figure 1.10. Model of OLE1 transcription activation.** Inactive, P120 Spt23p and Mga2p are ER localised to the ER. On an increase in membrane saturation, Spt23p and Mga2p form homo-dimers which exposes three lysine residues on each monomer. The activation of these proteins occurs via a series of events involving the ubiquitylation of the exposed lysines, activation to the P90 fragment by the proteasome, and mobilisation by the Cdc48 complex. Figure taken from (140).

Cellular fatty acid composition is also regulated by Sct1p. Sct1p is an 86 kDa, ER bound enzyme that is involved in the production of lysophosphatidic acid in the first committed step of glycerophospholipid synthesis. It was initially identified in a screen as a Suppressor of Choline Transport. De Smet et al demonstrated that Sct1p is a novel regulator of fatty acid desaturation through a competition with Ole1p for saturated acyl-CoAs thereby regulating the availability of substrates available for the desaturase and subsequently the degree of fatty acid desaturation (Figure 1.10). De Smet et al identified that both the overexpression and the deletion of SCT1 results in an altered fatty acid profile. The overexpression of SCT1 favours a more saturated fatty acid profile with a fourfold increase in C16:0 and twofold increase in C18:0 at the expense of the unsaturated fatty acid counterparts reported, and an increase in phosphatidyl inositol synthesis at the expense of phosphatidyl ethanolamine. De Smet suggested that this large increase in saturated content would cause a reduction in membrane fluidity and consequently alter essential membrane processes. In line with these observation by De Smet and colleagues, Pineau described significant ER morphological consequences as a result of inactivating heme synthesis. Membrane effects as a result of inhibition of heme synthesis is likely due to a reduction in Ole1p activity. Ole1p contains a di-iron metal centre that is essential to the desaturase catalytic activity through the donation of electrons. Inhibition of the electron transfer from the metal centre of the Ole1p results in a poorly or non-functional desaturase. Pineau used a *Δhem1* strain of *S. cerevisiae* that was confirmed to have an increase in the amount of saturated lipid species at the expense of the unsaturated counterparts. Pineau described the effects of saturated fatty acid accumulation on membranes with aberrant ER morphology and cytosolic, membrane enclosed clefts in the cytoplasm. Pineau also showed that deletion of OLE1 induces the unfolded protein response (UPR) (146).

De Smet et al also showed that the deletion of SCT1 results in a 50% decrease in the amount of C16:0 and an increase in the cellular unsaturated fatty acid content (147). Overexpression of OLE1 has been previously shown by Kajwara to induce an increase in average acyl chain length and a slow growth phenotype (148). Conversely, SCT1 overexpression is associated with a decrease in chain length. Interestingly, co-

overexpression of SCT1 and OLE1 rendered a normal lipid profile and did not affect the growth rate of cells. Overall, these findings suggest that Sct1p competes with Ole1p for C16:0 CoA and C18:0 CoA and it has been proposed that this is by sequestering the saturated CoAs into lipids (Figure 1.11). The role of additional enzymes that also have acyl CoAs as their substrate, for example Gpt2p, in regulating the activity of Ole1p remain to be investigated (149).

The activity of Sct1p is regulated by its phosphorylation state with the enzyme activity being inactivated upon phosphorylation (147). It is likely that this phosphorylation event provides an indirect feedback mechanism that in turn regulates the incorporation of saturated acyl CoA into lipids through the activity of Sct1p. To date, no post-translational modifications have been noted in Ole1p, including phosphorylation events. Future research to identify key kinases and phosphatases that regulate the activity of Sct1p will prove vital to complete our understanding of the maintenance of proper lipid saturation profile.

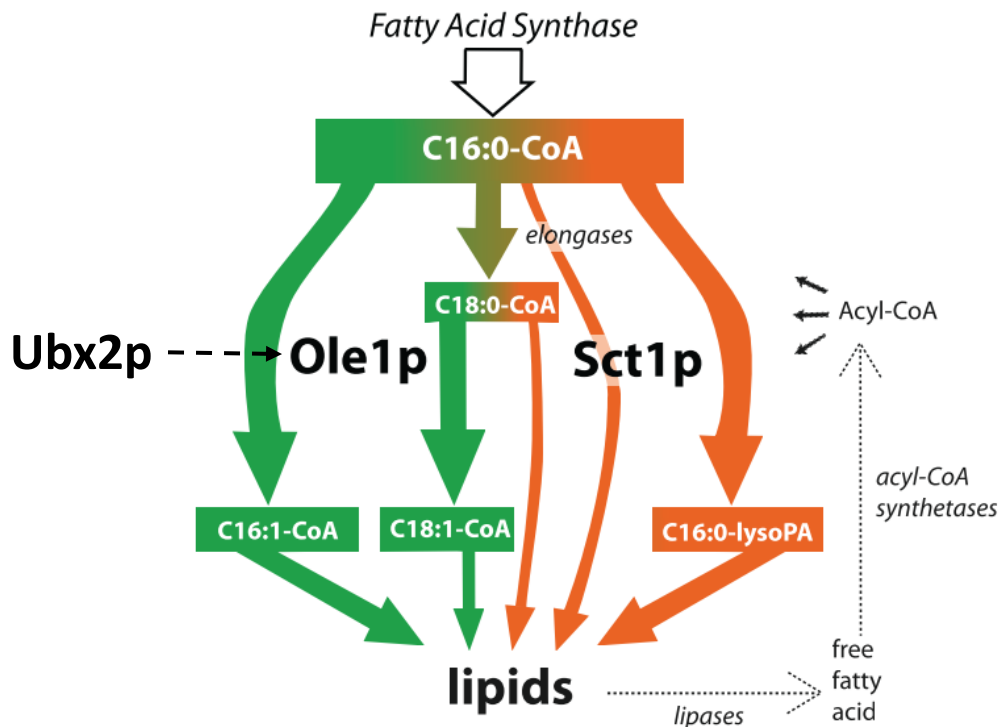


**Figure 1.11. Regulation of fatty acid saturation content by Ole1p and Sct1p.** C16:0 CoA can be directly sequestered into lipids through the activity of Sct1p or Ole1p to render the C16 saturated or unsaturated lipid products. Alternatively, C16:0 can undergo further elongation by elongases to the C18:0 substrate. Sct1p and Ole1p can then compete to sequester the C18:0 CoA substrate into the C18 saturated or unsaturated products. Image taken from (147).

#### 1.3.4. Ole1p and the mitochondria

*S. cerevisiae* reproduce through asymmetric division, known as budding. Initially, cells polarise and a site where the bud will form emerges. Mitochondria enter the bud immediately through movement along actin cables. Once the bud grows to the size of the mother cell, it is severed at the point of joining (150). The distribution of the mitochondria to daughter cells is an essential feature of the yeast mitotic cycle since they proliferate from pre-existing organelles. Each daughter cell is required to receive a sufficient quantity of mitochondria before mother-daughter separation occurs. Stewart et al demonstrated that a mutation to the Mitochondria Distribution and Morphology 2 (MDM2) gene was unable to deliver mitochondria to the bud, but the inheritance of other organelles was maintained (109). Supplementation with oleate was sufficient to rescue to the mutant phenotype. MDM2 was isolated and characterised and shown to encode OLE1. The molecular details by which fatty acids control the inheritance of mitochondria are yet to be described.

# CHAPTER 2

## Aims of study

F900742 is a novel antifungal compound developed by F2G, Manchester, UK. F900742 was identified from a series of drugs in an antifungal screen against *Aspergillus fumigatus* and *Candida albicans*. Initially it was thought that F900742 displayed a non-specific mode of action or exerted its effects through membrane disruption, however it was shown to lack activity in bacteria and an inability to haemolyse red blood cells. F2G had more success in narrowing down the target with reversal assays, haploinsufficiency screens, and fatty acid profile analysis. These three methods suggested that the fatty acid  $\Delta 9$  desaturase was the likely target. The *S. cerevisiae*  $\Delta 9$  desaturase, Ole1p, is the sole copy of an essential enzyme that catalyses the desaturation of fatty acids between carbons 9 and 10.  $\Delta 9$  desaturases are evolutionarily conserved throughout eukaryotes.  $\Delta 9$  desaturases contain 4 membrane spanning ER transmembrane domains making them very difficult to isolate and purify, therefore it is not currently possible to show a drug-protein bound complex.

The overall aim of this study was to confirm the predicted target of F900742 as the fungal  $\Delta 9$  desaturase, Ole1p. This was approached by:

- 1) Test the activity of F900742 in the yeast *Saccharomyces cerevisiae*
- 2) Test the effect varying Ole1p expression has on F900742 activity
- 3) Test that *S. cerevisiae* are functionally viable, but resistant to F900742 when OLE1 is substituted for human SCD1
- 4) Identify residues essential for F900742 binding through the generation of mutations within the OLE1 ORF
- 5) Investigate ultrastructural morphological defects induced by F900742
- 6) Identify the mechanism(s) by which F900742 exerts toxic effects

# CHAPTER 3

## Material and Methods

Unless otherwise stated, all chemicals were purchased from Sigma-Aldrich. Yeast media were purchased from ForMedium.

Unless otherwise stated, all experiments were performed at room temperature (approximately 20 °C).

Unless otherwise stated, *S. cerevisiae* were incubated at 30 °C either on an agar plate or in liquid media. Samples grown in liquid media were shaken at 300 rpm. 14 ml, round bottom falcon tubes with lids that ensure oxygenation were used to grow liquid yeast cultures.

### 1. Yeast strains

The yeast *Saccharomyces cerevisiae* was the model organism of choice used for the majority of experiments to date. *Schizosaccharomyces japonicus* and *Schizosaccharomyces pombe* were also used as a comparison to *Saccharomyces cerevisiae* in some experiments (Table.3.1).

All experiments using *Aspergillus* and *Candida* strains were performed by Sarah Murphy at F2G, Manchester, UK.

*S. cerevisiae* delete strains were obtained from a collection in a BY4741 (MAT a) background.

A collection of C-terminally GFP tagged yeast was kindly gifted to the Levine group by Maya Schuldiner and were synthesised by Huh et al as described in (36). The library was generated by inserting a GFP tag in-frame and immediately after each ORF individually, but before the native stop codon.

BY4741 (BY) Ole1-stop-GFP was made for the purpose of this study. Genomic DNA isolated from BY Ole1-GFP was used as template DNA as described in Methods 10.2. A stop codon was inserted immediately after the OLE1 ORF, but prior to the GFP using the primers OLE1 stop F and OLE1 R (Table 3.5) using the PCR program 5 minutes at 90 °C, 40 x (94 °C 15 seconds, 58 °C 1 second, 52.5 °C 20 seconds, 60 seconds per kb at 72 °C), 7 minutes at 72°C. 400 µl of PCR product was produced, purified using ethanol precipitation and transfected into log phase BY Ole1-GFP. After 48 hours of growth on agar, a single colony was isolated and the OLE1 ORF was amplified by PCR. Successful stop codon insertion was confirmed by both Sanger Sequencing using OLE1 ORF F3 and GFP R1, and confocal microscopy confirmed cells no longer expressed GFP. This colony was streaked on to a fresh plate and used for appropriate experiments.

A cross between BY OLE1-GFP MAT a and BY ERG6-RFP MAT  $\alpha$  was performed by growing a patch of the mixed strains on complete media at 30 °C for 6 hours. A sample from the patch was then streaked to single colonies on a selective agar plate lacking histidine and containing G418 and grown at 30 °C for 48 hours. Confocal microscopy was used to confirm that the cells contained by Ole1p-GFP and Erg6p-RFP.

Strain	Genotype	Source
<b>BY4741</b>	MATa his3 $\Delta$ 1 leu2 $\Delta$ 0 met15 $\Delta$ 0 ura3 $\Delta$ 0	Euroscarf
<b>BY4742</b>	MAT $\alpha$ his3 $\Delta$ 1 leu2 $\Delta$ 0 met15 $\Delta$ 0 ura3 $\Delta$ 0	Euroscarf
<b>R453C</b>	MAT $\alpha$ ade2-1 his3-11,15 ura3-52 leu2-3,-112 trp1-1	(151)
<b>BY Ole1-GFP</b>	BY4741 with GFP after OLE1	(36)
<b>BY Ole1-STOP-GFP</b>	BY4741 stop-GFP	This study
<b>BY <math>\Delta</math>ole1</b>	BY4741 YGL055W $\Delta$ ::KANMX4	Euroscarf
<b>BY <math>\Delta</math>mga2</b>	BY4741 YIR033W $\Delta$ ::KANMX4	Euroscarf
<b>BY <math>\Delta</math>spt23</b>	BY4741 YKL020C $\Delta$ ::KANMX4	Euroscarf
<b>BY <math>\Delta</math>ubx2</b>	BY4741 YML013W $\Delta$ ::KANMX4	Euroscarf
<b>BY <math>\Delta</math>sct1</b>	BY4741 YBL011W $\Delta$ ::KANMX4	Euroscarf
<b>BY <math>\Delta</math>erg6</b>	BY4741 YML008C $\Delta$ ::KANMX4	Euroscarf



<b>BY <math>\Delta</math>vac4</b>	BY4741 YBR097W $\Delta$ ::KANMX4	Euroscarf
<b>BY <math>\Delta</math>atg1</b>	BY4741 YGL180W $\Delta$ ::KANMX4	Euroscarf
<b>BY RFP-ERG6</b>	BY4742 RFP-KanMX6	Euroscarf
<b>BY RFP-TMD</b>	RS453B with pRS405 RFP-TMD	(152)
<b>BY RFP-TOM6</b>	RS453B with pRS405 RFP-TOM6	(153)
<b>OLE1-GFP - ERG6-RFP</b>	Mating of OLE1-GFP and RFP-ERG6	This study
<b>BY mCherry-Ole1</b>	BY4741 TEF2 mCherry-OLE1 N'-SWAT library	Maya Schuldiner
<b>BY mCherry-Sct1</b>	BY4741 TEF2 mCherry-SCT1 N'-SWAT library	Maya Schuldiner
<b>BY Ubx2-GFP</b>	BY4741 with GFP after UBX2	(36)
<b>BY Sct1-GFP</b>	BY4741 with GFP after SCT1	(36)
<b>BY Sec63-GFP</b>	BY4741 with GFP after SEC63	(36)
<b>BY Scs2-GFP</b>	BY4741 with GFP after SCS2	(36)
<b>BY Mnn9-GFP</b>	BY4741 with GFP after MNN9	(36)
<b>BY NmaIII-GFP</b>	BY4741 with GFP after NMAIII	(36)
<b>BY Pex3-GFP</b>	BY4741 with GFP after PEX3	(36)
<b>BY Sac6-GFP</b>	BY4741 with GFP after SAC6	(36)
<b>BY Vac4-GFP</b>	BY4741 with GFP after VAC4	(36)
<b>BY <math>\Delta</math>ole1 SCD 1</b>	BY $\Delta$ ole1 with pAG415-GPD Flag-hsSCD1	Robert Ernst
<b>BY4741-RFP-HDEL</b>	BY4741 with RFP-HDEL	This study
<b>BY Ole1-GFP-RFP-HDEL</b>	BY Ole1-GFP with RFP-HDEL	This study
<b>BY <math>\Delta</math>spt23-RFP-HDEL</b>	$\Delta$ spt23 with RFP-HDEL	This study
<b>BY <math>\Delta</math>mga2-RFP-HDEL</b>	$\Delta$ mga2 with RFP-HDEL	This study
<b>BY <math>\Delta</math>ubx2-RFP-HDEL</b>	$\Delta$ ubx2 with RFP-HDEL	This study
<b>BY <math>\Delta</math>ole1-RFP-HDEL</b>	$\Delta$ ole1 with RFP-HDEL	This study
<b><i>Schizosaccharomyces pombe</i></b>	<i>h+ ura4-<math>\Delta</math>18 leu1-32 ade6</i>	Snezhka Oliferenko
<b><i>Schizosaccharomyces japonicus</i></b>	<i>ura4sj- D3 ade6sj-domE</i>	Snezhka Oliferenko
<b><i>Candida albicans</i></b>	Strain F/6862	F2G
<b><i>Candida krusei</i></b>	Strain ATCC 6258	F2G

<b><i>Aspergillus fumigatus</i></b>	Strain AF210	F2G
<b><i>Aspergillus terreus</i></b>	Strain AT4	F2G

**Table 3.1. Yeast strains used in this study.** This table lists all strains used during this study. Sources of strains are: Euroscarf and kind gifts from Snezhka Oliferenko and Robert Ernst.

## 2. Plasmids

The plasmids used in this study are listed in Tables 3.2, 3.3, and 3.4. Yeast plasmids were based on the pRS4xx series (154).

<b>Plasmid name</b>	<b>Description</b>	<b>Source</b>
<b>Pho5 &gt; GFP-GFP</b>	pRS416 (URA3): GFP-GFP (PHO5 promoter)	Tim Levine
<b>RFP-Tom6p</b>	pRS405 (LEU2): RFPx2-Tom6p (PHO5 promoter)	Tim Levine
<b>GAL &gt; OLE1 (5'/3' ends)</b>	pRS416 OLE1: 5' 84bp – NotI – MluI – 3' 81bp - GFP (GAL1/10 promoter)	This study
<b>RFP-TMD</b>	pRS405 (LEU2): RFPx2-C-term of Scs2p (PHO5 promoter)	Tim Levine
<b>RFP-HDEL</b>	RFP-HDEL :: NAT (Related to RFP-HDEL plasmid (PMID: 22250200))	Alexandre Toulmay

**Table 3.2. Yeast expression plasmids used in this study.** All plasmids were based on the pRS4 vector series. pRS416 = CEN-URA3, pRS405 = integrating LEU2.

Plasmid name	Description	Source
<b>Mutagenic plasmid library</b>	pRS416 (URA3): mutagenized OLE1 – GFP (PHO5 promoter)	Genscript
<b>BG1805</b>	2 $\mu$ (URA3): OLE1-HA-ZZ (GAL1/10 promoter)	Dharmacon

**Table 3.3. Purchased yeast expression plasmids.** A library of mutagenic plasmids that contain between 3-10 mutations per kb throughout the OLE1 ORF was obtained from Genscript. BG1805 contains the OLE1 ORF followed by a tandem affinity tag was purchased from Dharmacon.

The homosapien ORF of the  $\Delta 9$  desaturase SCD1 was obtained through purchase of I.M.A.G.E. fully sequenced cDNA clones.

Gene name	I.M.A.G.E source	Clone ID	Unigene ID
SCD1	Source Bioscience	IRAU969E0731D	Hs.558396

**Table 3.4. SCD1 IMAGE clone.** The SCD1 IMAGE clone was used as the source for the mammalian  $\Delta 9$  desaturase and homologue of Ole1p, SCD.

### 3. MC1061 bacteria

#### 3.1. Competent MC1061

5 MC1061 *Escherichia coli* colonies were picked from a fresh LB agar plate and were grown over night at 30 °C in LB broth at 300 rpm. Cultures were diluted 1 in 200 into 250 ml of LB broth and grown for a further 4 hours at 37 °C until an OD 600 of 0.5 was reached. The culture was placed on ice for 5 minutes. Cells were collected by centrifugation. The pellet was resuspended in 62.5 ml of ice-cold 0.1 M MgCl<sub>2</sub> and incubated on ice for 10 minutes. Cells were centrifuged, and the pellet resuspended in 31 ml of 0.1 M CaCl<sub>2</sub> and incubated on ice for a further 30 minutes. The sample was centrifuged and the pellet resuspended in 12.5 ml 0.1 M CaCl<sub>2</sub> and 13% glycerol. This final suspension was distributed as 120  $\mu$ l aliquots and immediately stored at -80 °C.

### **3.2. MC1061 transformation**

MC1061 *E. coli* were transformed by gently mixing 15 µl of cells with 5 µl of DNA on ice for 30 minutes. The mixture was then incubated at 42 °C for 60 seconds before 90 µl of LB broth was added and the sample incubated at 37 °C for a further 30 minutes. Cells were plated on to the appropriate antibiotic containing plate and left at 30 °C overnight.

### **4. Plasmid miniprep**

Transformed bacteria were selected for by the appropriate antibiotic. Single colonies were selected and grown at 37 °C in sterile liquid culture containing 2 ml of LB broth and antibiotic for 6 hours. Qiagen's Plasmid Miniprep Kit was used to extract DNA according to the manufacturer's instructions.

### **5. Digests**

To ensure plasmids were correct, specific restriction enzymes were selected to digest the vector DNA into uniquely identifying patterns. Digests were done in a total volume of 10 µl and contained approximately 0.75 µg of DNA, 1 - 10 units of enzyme and 1x of appropriate buffer. The digest mixture was incubated at 37 °C for 1 hour. DNA was separated by electrophoresis on an agarose gel.

### **6. Agarose gel electrophoresis**

Gel electrophoresis was used to separate DNA fragments by size. Gels most often contained 1% (w/v) agarose, 1x TAE buffer, and 1x SafeView Nucleic Acid Stain. The gels were loaded with approximately 10 µl of sample and DNA ladder, both of which were mixed with 5x loading buffer. Gels were run in 1x TAE buffer at 100 V for 20 minutes. DNA was visualised by UV.

### **7. Gel purification of DNA**

Following DNA band separation, required fragments were cut out of the gel and DNA was recovered using Qiagen's QiaQuick Gel Extraction Kit per manufacturer's instructions.

## 8. Yeast transformation

Yeast were grown over night at 30 °C in YPD broth. The following morning, they were diluted 1:100 into 5ml of YPD broth and grown for a further 5 hours at 30 °C at 300 rpm. The cells were collected by centrifugation and washed in LATE (0.1 M LiAc, 1mM EDTA, and 10 mM Tris-HCl (pH 7.5)). The pellet was resuspended in residual liquid. Cells were incubated for an hour at room temperature with 5 µg of plasmid, 5 µl of single-stranded salmon sperm DNA (10 mg/ml) and 300 µl of PLATE (40% polyethylene glycol 3350 in LATE). 40 µl of DMSO was added and the mixture incubated at 42 °C for 15 minutes. Cells were then pelleted by centrifugation and resuspended in 100 µl of water and plated on to the required selective media. Transformations were grown at 30 °C for at least 48 hours.

### 8.1. RFP-HDEL

The RFP-HDEL plasmid was digested as described above (point 5) with the enzyme EcoRV for 1 hour at 37 °C. The enzyme was inactivated at 80 °C for 20 minutes. The digest mixture was then used to transform *S. cerevisiae* strains as describe above in point 8. The linearised RFP-HDEL marker inserted into the *trp* locus. The transformation was grown on YPD agar containing 50 µg/ml of nourseothricin (NAT) for 48 hours. Colonies were screened for RFP-HDEL integration by confocal microscopy.

## 9. Yeast plasmid isolation

Yeast plasmids were isolated using the Qiagen Plasmid Miniprep Kit per a modified method by Madhu et al (155). 100 ml of yeast were grown over night at 30 °C in selective liquid media. Cells were collected by centrifugation and resuspended in 500 µl of high salt solution in Buffer P1. The cell wall was digested using 1.2 M sorbitol, 0.1 M NaPO<sub>4</sub>, and 0.5 mg/ml 100T Zymolyase and incubated at 37 °C for 45 minutes. Cells were alkaline lysed by 1 ml of Qiagen Buffer 2 and incubated at 22 °C for 10 minutes. 1.4 ml of Buffer N3 was added and the mixture was incubated on ice for 30 minutes. The mixture was separated by centrifugation such that the cell debris pelleted, and the supernatant contained the plasmid. The supernatant was collected and added to a miniprep column. The purification of the DNA was performed as described in (155).

## **10. Yeast DNA isolation**

### **10.1. DNA isolation through zymolyase**

Zymolyase DNA preparations were used as template DNA for PCR products less than 700 base pairs. Yeast DNA was isolated using 100T zymolyase. A 3 mg/ml stock of 100T zymolyase was prepared and stored at -20 °C. The stock was diluted 1:10 in 1x PBS and a single yeast colony was added to 20 µl zymolyase and incubated at 30 °C for 20 minutes immediately followed by a heat shock at 99 °C for 20 minutes.

### **10.2. DNA isolation through genomic preparation**

Genomic DNA preparations were used as template DNA for PCR products greater than 700 base pairs. 5 ml of yeast culture were grown over night in appropriate media at 30 °C. Cells were collected by centrifugation and resuspended in residual liquid. 100 µl of a 2% Triton X-100, 1% SDS, 100 mM NaCl, 10 mM Tris HCl (pH 8.0), 1mM Na<sub>2</sub>EDTA solution was added to the pellet, along with 100 µl of phenol:chloroform:isoamyl alcohol (25:24:1) and 150 mg of acid-washed glass beads. Cells were vortexed for 3 minutes. 200 µl of TE (pH 8.0) was added and the sample was centrifuged for 5 minutes at 13000 rpm. The aqueous layer was decanted into a fresh tube, 500 µl of ethanol was added, and the sample was centrifuged for 2 minutes. The supernatant was discarded, and the pellet was resuspended in 200 µl TE and 2.5 µl of a 6 mg/ml stock of RNAase A. The sample was incubated at 37 °C for 5 minutes. 7µl of a 6 M ammonium acetate solution and 500 µl of ethanol was added. The sample was centrifuged for 2 minutes. The liquid was decanted, and the pellet air-dried. The pellet was resuspended in 50 µl of TE and stored at -80 °C.

## **11. HeLa cell transfection and staining**

HeLa transfection and staining procedures were done under the guidance of Dr Emily Eden. All reagents used were a gift from Dr Eden. Cells were grown to 50% confluency and treated with 500 µg/ml F900742 for 4 hours. The following day, cells were transfected with the plasmid mCherry-Sec61. 0.3 µg of DNA was added to 100 µl of optimen, this mix was added to lipofectamine-optimen and incubated at room temperature for 20 minutes. The plasmid mixture was added to the HeLa cells and incubated overnight. The following day, the lipid droplet dye LD540 was added to the

wells and incubated for 1 hours at room temperature. Cells were fixed for 20 minutes in 4% PFA and 0.1% glutaraldehyde in PBS. Cells were mounted on to microscope cover slips with a DAPI-incorporated mount (Invitrogen, catalogue number P36935).

### **12. Primers**

Primers were used for cloning in a stop codon into BY Ole1-GFP (p67), gap repair of the plasmid GAL > OLE1 (5'/3' ends) (p128), as well as for sequencing the OLE1 ORF (p129 – p140). All primers are listed in Table 3.5.

### **13. Polymerase Chain Reaction (PCR)**

The OLE1 ORF was amplified by PCR using OLE1 F1 and OLE1 R1 which yielded a ~1500 bp product. Each reaction was in a total volume of 12.5 µl and contained 200 µM dNTPs, 0.4 µM of forward and reverse primers, 0.3 units of GoTaq polymerase, and GoTaq reaction buffer. The proofreading polymerase Velocity was also added to the Ole1-stop-GFP PCR. PCR cycles were carried out at 5 minutes at 90 °C, 40 x (94 °C 15 seconds, 58 °C 1 second, 52.5 °C 20 seconds, 60 seconds per kb at 72 °C), 7 minutes at 72°C. PCR products were separated on an agarose gel and DNA was purified as described above.

Primer name	Description (5' -> 3')
<b>Primers used for cloning</b>	
OLE1 Stop F	taaaggagaagaacttttactggagttggttatcaaggaaagtaagaactctgctattagaa tggctagtaagagaggtgaaatctacgaaactggtaagtcttt
OLE1 R	gatactccgaggactagtttaaagaacttaccagtttc
OLE1 ORF F1	cctctacgagctcatgccaacttctggaactac
OLE1 ORF R3	gtcctaagctcgagaaaagaacttaccagtttcgtag
<b>Primers used for sequencing</b>	
OLE1 Prom F	ccctctgaagcttgacacatggaaataagtcaagg
OLE1 Prom R	aggattggatcctttgttgaatgttttagtgc
OLE1 ORF F1	cctctacgagctcatgccaacttctggaactac
OLE1 ORF F2	ggggccactctcacagaattcac
OLE1 ORF F3	ctgggtccagtttgactg
OLE1 ORF R1	ccagtgagcggagtaagatctg
OLE1 ORF R2	cagtcaaaactggaccccag
OLE1 ORF R3	gtcctaagctcgagaaaagaacttaccagtttcgtag
GFP R1	catctaattcaacaagaattggg
GFP R2	ggtagtttccagtagtgc
SCD ORF F	attacaacaagaagtgatcccggcatccga
SCD ORF R	gtaccgggccccccagtttccatctccggttcttttaactctgg

**Table 3.5. Primers used in this study.** Ole1 stop F and Ole1 R were used to insert a stop codon directly after the Ole1 ORF, but prior to the GFP tag in the strain BY Ole1-GFP. OLE1 Prom F and Ole1 Prom R were used to sequence the OLE1 promoter. To ensure a clear signal was obtained for the entire ORF, 3 forward strand primers and 3 reverse strand primers were used to sequence the OLE1 ORF. The forward primers and the reverse primers were complementary to sequence that was approximately 600 base pairs apart. OLE1 ORF F1, OLE1 ORF F2, and OLE1 ORF F3 were used to sequence the forward strand of OLE1 in the 5' to 3' direction. OLE1 ORF R1, OLE1 ORF R2, and OLE1 ORF R3 were used to sequence the OLE1 reverse strand in the 5' to 3' direction. GFP R1 and GFP R2 were used to sequence the reverse strand of GFP in the 5' to 3' direction. SCD ORF F and SCD ORF R were used to sequence the SCD ORF in the SCD1 IMAGE clone and BY *Δole1* SCD 1.



#### **14. Passaging**

A YPD agar plate had a hole made in the middle using the wide end of a blue 1 ml pipette tip. 100 µl of a 4 mg/ml solution of F900742 was added to the well and left at room temperature for 6 hours to allow the drug to disperse throughout the agar thus leaving a concentration gradient of drug from the centre to the outside of the plate. Log phase cells were spread evenly across the entirety of the plate and grown at 30 °C for 48 hours. After this incubation, a fresh plate was prepared as described above, but cells were taken from the zone of low growth, diluted in deionised water and spread across the fresh plate. The minimum inhibitory concentration of every 5<sup>th</sup> passage was determined. The OLE1 ORF of every 5<sup>th</sup> passage was sequenced.

#### **15. Minimum inhibitory concentration (MIC)**

##### **15.1. *Saccharomyces cerevisiae***

Yeast were grown in 2 ml of YPD broth overnight at 30 °C. The following morning samples were diluted 1:200 into 2 ml of YPD broth and grown to mid log phase at 30 °C. At OD<sub>600</sub> of 0.5, cells were re-diluted to OD 0.1 in 5 ml of YPD broth and inoculated with F900742. F900742 was prepared as a series of two-fold serial dilutions such that the highest concentration used was 100 µg/ml and the lowest 0.2 µg/ml. Samples were grown for 24 hours at 30 °C. The MIC was identified by the concentration of drug where there was no yeast growth, IC<sub>90</sub> as the concentration of drug where there was 90% less growth, and the IC<sub>50</sub> as the concentration of drug where there was 50% reduced growth relative to untreated cells. Due to the inherent differences between BY  $\Delta ole1$  and all other strains, BY  $\Delta ole1$  grown in YPD supplemented with 1 mM oleic and was treated with F900742 at a maximum concentration of 1000 µg/ml. The MIC, IC<sub>90</sub>, and IC<sub>50</sub> were assessed by OD 600 measurement.

##### **15.2. *Schizosaccharomyces japonicus* and *Schizosaccharomyces pombe***

*S. japonicus* and *S. pombe* were grown in YES media. The MIC of *S. japonicus* and *S. pombe* was determined as described in 15.1.

### **15.3. *Aspergillus and Candida species***

Plates for MIC readings of *Candida* and *Aspergillus* species were prepared as follows: Stock solutions were prepared at 5 mg/ml of F900742, F902921, F902947, F902973, and F902988, voriconazole at 0.8 mg/ml, amphotericin B at 0.2 mg/ml, and olorofim at 0.4 mg/ml in DMSO. Test drug concentrations were prepared in a 96 well plate by doubling dilution such that the final concentrations of F900742, F902921, F902947, F02973, and F902988 ranged from 50 µg/ml to 0.05 µg/ml, voriconazole between 8 µg/ml to 0.008 µg/ml, amphotericin B between 2 µg/ml to 0.002 µg/ml, and olorofim between 4 µg/ml to 0.004 µg/ml in a total volume of 400 µl. 20 µl of drug dilution was then robotically added to four replica 96 well plates. RPMI media was added such that the final concentration was 1x in 100 µl. The pathogenic fungi chosen to test were *Candida albicans*, *Candida krusei*, *Aspergillus fumigatus*, and *Aspergillus terreus*. Suspensions of fungi were added to each plate such that *Aspergillus* strains were at a final concentration of  $1 \times 10^4$  CFU/ml and *Candida* strains at  $1 \times 10^3$  CFU/ml. Plates were grown for 48 hours at 35 °C. Strains were also grown in parallel on untreated complete media plates. The MIC was identified as the first well with no growth as determined by visual examination.

### **15.4. HeLa**

HeLa cells were gifted from Dr Louise Wong and Dr Emily Eden. HeLa cells were grown until they were 50% confluent in a 24 well plate. A stock solution of 5 mg/ml F900742 in water was prepared. F900742 was serially diluted such that the final concentration of drug ranged between 1 mg/ml and 3.9 µg/ml. HeLa growth was visually estimated by percentage of plate coverage.

## **16. Colony growth assay**

### **16.1. Using colony number to determine cell growth**

Yeast strains were grown overnight in 2 ml of YPD broth at 30 °C and diluted 1:200 into 5 ml of fresh YPD broth the following morning. Cells were grown to log phase (approximately 6 hours). To enable determination of colony number, strains were serially diluted so that there were approximately 4000, 200, and 10 cells in 1.5 µl of

liquid. A 48 pin replicator was used to evenly add approximately 1.5  $\mu$ l of cells to YPD only plates or plates containing F900742. Plates were incubated for 48 hours at appropriate temperature (most often 30 °C).

### **16.2. Using OD 600 to determine cell growth**

Yeast were grown over night in 2 ml of liquid YPD at 30 °C and 300 rpm. The following morning, cultures were diluted 1 in 200 into fresh YPD broth and grown at 30 °C until the OD 600 was 0.5 (approximately 6 hours). Samples were further diluted to OD 0.1 in 2 ml of YPD. F900742 or other chemicals were added at the desired final concentration. 24 hours after drug addition, the OD 600 was measured for both the treated and untreated samples.

### **17. Growth curve**

A single colony of BY4741 was suspended into 2 ml of YPD broth and serially diluted 1:100 three times in liquid YPD such that following growth over night at 30 °C and 300 rpm the OD 600 was at OD 0.5 in the morning. BY4741 was diluted to OD 0.1 in YPD broth. 50  $\mu$ g/ml F900742 was added to 5 ml of the cell suspension. A 5 ml cell suspension at OD 0.1 was used as the untreated control group. The OD 600 of the treated and untreated samples was measured every 2 hours for the first 12 hours and then at 24 hours.

### **18. Microscopy**

#### **18.1. Confocal microscopy**

Yeast containing a fluorescently tagged gene or expressing a fluorescent plasmid were grown over night in 2 ml of complete or selective media at 30 °C and 300 rpm, diluted 1:100 in the morning and grown until mid-log phase (OD 0.5) before treatment.

Following treatment, cells were pelleted by gentle centrifugation and immobilised between a cover slip and a glass slide. HeLa cells were fixed onto a slide. Yeast and HeLa were examined using a Leica SP8 Confocal Microscope with a 63x/NA1.4 objective lens at room temperature using LCS software. Line averaging of 16 was used. Images were processed with Image J.

### **18.2. Total cellular fluorescence**

The quantification of protein amounts was determined by using the corrected cellular fluorescence per cell. Entire, unprocessed confocal images were used for this: Three random equal areas of the image containing no cells were measured and averaged to determine background fluorescence. The total fluorescence of the image was also measure and the number of cells manually counted. All values were exported into Microsoft Excel and data was processed using the following equation:

$$\text{Average cellular fluorescence} = \frac{(\text{total fluorescence} - \text{average background})}{\text{number of cells}}$$

Prism 6 (Graphpad) was used to generate graphs and statistics.

### **18.3. ROS Visualisation**

Dichlorofluorescein diacetate (H<sub>2</sub>DCF-DA) can permeate cells where it is oxidised in the presence of ROS rendering it the impermeable, highly fluorescent dichlorofluorescein. This can be used to indirectly quantify mitochondrial ROS production. Mid log phase cells were treated with 100 µg/ml F900742 in liquid for 2 hours at 30 °C. Half of the samples were treated with a final concentration of 150 mM of the antioxidant N-acetylcysteine for 1 hour. All samples were treated with a final concentration of 50 µM of H<sub>2</sub>DCF-DA for 30 minutes. Cells were then spun and washed twice in water before visualisation at excitation/emission 492–495/517–527 nm.

### **18.4. Electron microscopy**

A single colony of BY Ole1-GFP was suspended into 2 ml of YPD broth and serially diluted 1:100 three times into 2 ml liquid YPD such that following growth over night at 30 °C and 300 rpm the OD 600 was at OD 0.5 in the morning. In the morning, cells were diluted in YPD liquid media to OD 0.1 in 15 ml of fresh YPD. At OD 0.5, cells were treated with 100 µg/ml F900742. Following 2 or 4 hours of treatment, cells were pelleted, washed in water, resuspended in 1.5% KMnO<sub>4</sub> and incubated at 4 °C for 30 minutes. KMnO<sub>4</sub> was replaced with fresh solution and incubated at 4 °C for a further 30 minutes. Cells were washed five times in water before being dehydrated by incubations in increasing amounts of acetone at room temperature with gentle agitation. Dr. Matt Hayes (UCL) then proceeded with the embedding in Spurr's resin

and sectioning. Dr. Hayes also imaged the *S. cerevisiae* samples. A transmission electron microscope Jeol 1400 was used to image samples.

### **19. Immunoblot**

BY Ole1-GFP was grown over night in liquid YPD at 30 °C and 300 rpm. Cells were diluted 200 fold into fresh YPD in the morning and grown for 8 hours at 30 °C and 300 rpm. Cells were diluted 1 in 2000 into 2 ml of YPD and grown over night at 30 °C and 300 rpm. The OD 600 was 0.5 in the morning. Samples were treated with 100 µg/ml F900742 with or without 1 mM oleic acid supplementation for 2 hours. Cells were mechanically lysed as follows: cells were collected by centrifugation and resuspended in residual liquid. 0.1 g of acid-washed glass beads and 200 µl of ice cold TEPI (50 mM Tris HCl pH 7.5, 5mM EDTA pH 8, the protease inhibitors AEBSF (Sigma Aldrich, catalogue number 76307) and protease inhibitor cocktail III (Calbiochem, catalogue number 539134) were added at 100 µM). Samples were vortexed 5 times at 13000 rpm for 30 seconds. 200 µl of 2 x sample buffer (0.12 M Tris HCl pH 6.8, 100 mM DTT, 20% glycerol, 5% SDS, 0.025% bromophenol blue) was added and samples were immediately incubated at 80 °C for 10 minutes. Samples were centrifuged and the supernatant removed into a fresh tube. Lysed samples were immediately loaded into a 10% SDS gel. The gel was run at 100 V for 10 minutes followed by an hour at 150 V. A nitrocellulose membrane was placed over the gel and proteins were transferred using 100 V for 2 hours. The membrane was blocked in 1 x PBS, 0.1% tween 20 in 5% milk for 30 minutes. The membrane was incubated with the primary antibody (Anti-GFP) for 1 hour. The membrane was washed 3 time in PBS-tween and then incubated for a further hour in PBS-tween-milk block containing secondary antibody (polyclonal goat anti-rabbit). The membrane was washed in PBS-tween. ECL reagent 1 and reagent 2 (GE Healthcare Life Science, catalogue number RPN2106) were added so they just covered the membrane. Antibodies used listed in table 3.6.

### 19.1. Antibodies for immunoblot

Name	Supplier	Species	ID
Anti-GFP	Abcam	Rabbit	AB6556
Polyclonal goat anti-rabbit	Dako	Goat	PO448

**Table 3.6. Antibodies used in this study.**

### 20. PBS and BSA reversal assay

A single colony of BY4741 and BY Ole1-GFP were grown over night in liquid YPD at 30 °C and 300 rpm. Both samples were diluted 1:100 in the morning and grown at 30 °C and 300 rpm. At OD 0.5, cells were further diluted in fresh YPD to OD 0.1. 100 µl of cell suspension was added to a 96 well, flat bottomed, clear plate. F900742 was added such that wells containing BY4741 contained a final concentration of 50 µg/ml F900742 and BY Ole1-GFP was supplemented with a final concentration of 25 µg/ml of drug. PBS and/or BSA was added to liquid YPD media such that the final amount was 10% PBS or 0.5% BSA. Samples were grown in a 96 well plate for 24 hours at 30 °C and were not shaken. The amount of growth was measured using absorbance at wavelength 600 nm by a plate reader. Prior to OD measurement, the plate was manually shaken to disrupt cells that had settled at the bottom of the wells.

### 21. Chemicals

#### 21.1. F900742

F900742 was gifted by F2G (Eccles, UK). A stock solution was made of 5 mg/ml in DMSO (colony growth assay in figure 4.3 and all experiments in chapter 6) or water (all other experiments). The concentration used in experiments ranged from 6 µg/ml to 1000 µg/ml. Cells were grown over night, diluted in the morning, and re-grown to OD 0.5. Cells were further diluted to approximately OD<sub>600</sub> 0.1 for determining the MIC and treated at OD<sub>600</sub> 0.5 for microscopy experiments.

### **21.2. F902921, F902947, F902973, F902988**

F902921, F902947, F902973, and F902988 were gifted from F2G. A stock solution was made of 5 mg/ml in DMSO. The stock was serially, two-fold diluted such that the working concentration ranged between 50 µg/ml and 0.05 µg/ml.

### **21.3. Amphotericin B**

For *S. cerevisiae* studies, amphotericin B was obtained from Sigma Aldrich (catalogue number A2942). A stock solution of 250 µg/ml in DMSO was made. Cells were grown over night and diluted in the morning. At an OD 600 of 0.5, cells were treated with 250 ng/ml of amphotericin B.

For *Candida* and *Aspergillus* studies, amphotericin B was gifted by F2G. Amphotericin B was made as a stock at 0.2 mg/ml in DMSO which was serially diluted to working concentrations ranging between 2 and 0.002 µg/ml.

### **21.4. Voriconazole**

Voriconazole was gifted by F2G. Voriconazole was made as a stock solution at 0.8 mg/ml in DMSO. Voriconazole was added to *Aspergillus* or *Candida* liquid media at concentrations between 8 and 0.008 µg/ml.

### **21.5. Olorofim**

Olorofim (F901318) was gifted by F2G. Olorofim was made as a stock solution at 0.4 mg/ml in DMSO. Olorofim was added to *Aspergillus* liquid media at concentrations between 4 and 0.004 µg/ml. Of note, olorofim was only used as a control for *Aspergillus* studies as it has been previously shown to have no activity against *Candida* species (77).

### **21.6. Oleic acid, palmitoleic acid, and stearic acid**

Unsaturated fatty acids were all purchased from Sigma Aldrich (catalogue number O1008 oleic acid; P9417 palmitoleic acid; S4751 stearic acid). Stocks solutions of 1 M oleic acid, palmitoleic acid and stearic acid were made in DMSO. Oleic acid and

palmitoleic acid were both added individually to liquid media or agar plates such that the final concentration of each was 1 mM and 0.5 mM when added together. Stearic acid was added to liquid media at a final concentration of 1 mM.

For experiments where oleic acid and/ or palmitoleic acid reversed F900742 action, log phase cells were treated with F900742 for 2 hours, washed and resuspended in fresh YPD supplemented with the appropriate amount of unsaturated fatty acid and grown for a further 2 hours at 30 °C and 300 rpm.

### **21.7. Cycloheximide**

Cycloheximide was purchased from Sigma Aldrich (catalogue number 7698). A stock was made at 10 mg/ml in DMSO. BY Ole1-GFP was grown to mid log phase (approximately OD 0.5). Cycloheximide was added to liquid media at 10 µg/ml either alone or in conjunction with F900742. Cells were incubated at 30 °C for up to 4 hours.

### **21.8. MG132**

MG132 was purchased from Sigma Aldrich (catalogue number 8699). BY Ole1-GFP was grown to mid log phase (approximately OD 0.5). MG132 was added to liquid media at an indicated final concentration of either 50 µM or 150 µM either alone or in conjunction with F900742 and/ or oleic acid. Cells were incubated at 30 °C for up to 4 hours

## **22. *Galleria mellonella* infection model**

*Galleria mellonella* larvae were used as an *in vivo* model for candidiasis. *G. mellonella* were obtained from Livefoods Direct Ltd, Sheffield. Larvae were left in the dark at room temperature until use. *G. mellonella* were all in the final instar larval stage of development. Larvae were of a similar size and weight, approximately 2 cm and 330 +- 25 mg. *G. mellonella* health was determined by flesh colour and movement in response to physical stimuli and light. *G. mellonella* were classified as dead when they were a grey-black colour and did not respond to physical stimuli. A Hamilton syringe was used to inject 10 µl into the hemocoel via the prolegs. The syringe was cleaned with 70% ethanol and washed in PBS after each use.



### **22.1. *C. albicans* inoculum testing**

A pilot study to determine optimum *C. albicans* inoculum size was performed as follows: *C. albicans* were grown on SAB agar overnight at 35 °C. A colony was picked the following day and diluted into sterile PBS such that the final concentrations of *C. albicans* were  $5 \times 10^4$ ,  $1 \times 10^4$ , or  $5 \times 10^3$  CFU/ml. Each inoculum concentration represented a test group. There were five, healthy looking larvae in each group. 10 µl of inoculum was injected into the bottom left prolag. Two control groups were used; one was untreated, the other was injected with 10 µl of PBS. *G. mellonella* were put into a dark, 35 °C incubator. The number of alive, dead, and sick larvae were noted at 24 hour intervals.

### **22.2. F900742 tolerance testing**

The MIC of F900742 in *C. albicans* was determined as 0.8 µg/ml by F2G. Fresh F900742 was prepared in water such that the final concentration was 0.8 µg/ml or 1.6 µg/ml. *G. mellonella* were injected with 10 µl of either concentration of F900742 or PBS into the bottom left prolag with a total of five larvae in each group. A further five were untreated. Larvae were put into a dark, 35 °C incubator. The number of alive, dead, and sick larvae were noted 24 hour intervals.

### **22.3. *Galleria mellonella* survival assay single F900742 dose**

Three groups of larvae were injected with 10 µl of  $5 \times 10^4$  CFU/ml of *C. albicans* via the last left prolag. One control group was injected with 10 µl PBS; the other was untreated. Following 1 hour of incubation at 35 °C, each of the inoculated groups received a second injection of either 0.8 µg/ml or 1.6 µg/ml F900742 or PBS via the last right prolag. The control group received a second PBS injection via the last right prolag. Larvae were put into a dark, 35 °C incubator. The number of alive, dead, and sick larvae were noted at 24 hour intervals. 10 larvae were used per group. This experiment was repeated four times.

#### **22.4. *Galleria mellonella* survival assay double F900742 dose**

*G. mellonella* were treated as described above in 20.3. 24 hours after *C. albicans* inoculation, *G. mellonella* were treated with an additional injection of either 0.8 µg/ml F900742 or PBS via the penultimate left proleg. The number of alive, dead, and sick larvae were noted at 24 hour intervals.

#### **22.5. Fungal burden analysis**

To evaluate the effect of F900742 on larvae infected with *C. albicans*, total fungal burden was evaluated 72 hours post treatment. Three groups of larvae were injected with the yeast and either 0.8 µg/ml or 1.6 µg/ml F900742 or PBS as described above (22.3 and 22.4) and incubated at 35 °C for 3 days. Three larvae from each group were randomly chosen to be frozen prior to homogenisation using a pestle and mortar. 100 µl of PBS was added to each homogenate, mixed and transferred into a 96 well plate containing 100 µl PBS. Homogenates were serially diluted 1/20 into PBS. 1.5 µl of each dilutant was added to a SAB agar plate. Colony growth analysis was performed after 24 hours at 35 °C.

# Results

# CHAPTER 4

## F900742 induced Ole1p mislocalisation

### 4.1 Introduction

Studies by F2G, Manchester UK, demonstrated that a novel compound, F900742, elicits broad-spectrum antifungal activity (Table 4.1), including good efficacy against multiple *Aspergillus* and *Candida* strains. In addition, F900742 demonstrates potent antifungal activity against fluconazole and amphotericin B clinically resistant patient isolates, such as *C. albicans*, *C. tropicalis*, and *C. krusei*, as well as other moulds and dermatophytes. Early target identification studies at F2G identified Ole1p as a hit in a haploinsufficiency screen in yeast and that the addition of either of the monounsaturated fatty acids, oleic acid or palmitoleic acid, rendered F900742 ineffective in fungi suggesting that Ole1p, or at least the OLE1 pathway, is the target of this drug. In an era where overcoming drug resistance is of paramount importance, compounds that target  $\Delta 9$  desaturase represent a novel and promising antifungal drug class.

Minimum inhibitory concentration ( $\mu\text{g/ml}$ )																
RPMI											ISO		RPMI			
<i>C. albicans</i>	<i>C. parapsilosis</i>	<i>C. tropicalis</i>	<i>C. glabrata</i>	<i>C. krusei</i>	<i>A. niger</i>	<i>A. fumigatus</i>	<i>A. terreus</i>	<i>A. flavus</i>	<i>A. terreus 49</i>	<i>A. fumigatus 210</i>	<i>E. Coli</i>	<i>S. Aureus</i>	<i>R. arrhizus RA2</i>	<i>F. solani FS1</i>	<i>Scedosporium 5890</i>	<i>T. rubrum</i>
0.8	0.2	1.6	25	0.1	0.8	0.8	0.8	0.8	0.8	0.8	50	50	0.8	6.2	3.1	0.2

**Table 4.1. Table of minimum inhibitory concentrations of selected yeast, bacteria, dermatophytes and moulds.** Data from experiments performed by F2G. Strains were grown in appropriate liquid culture supplemented with F900742 for 24 hours. MICs were identified by the point that no growth was observed.

The yeast  $\Delta 9$  desaturase, Ole1p, is an ER integral membrane protein. Previous studies have identified residues required for enzyme function; mutations at these sites render the cell auxotrophic for unsaturated fatty acids (156). More recently, Tatzer et al investigated the early responses to inhibition of fatty acid desaturation using conditional desaturase mutants (157). The expression of Ole1p fluctuates in response to various stimuli, for example temperature. Tatzer et al identified that Ole1p relocates to aberrant cellular compartments in two temperature sensitive strains (Ole1<sup>ts</sup>) grown at non-permissive conditions (37 °C). Each strain contained a single OLE1 allele with one amino acid substitution: one contained a cytosine to thymine swap in an evolutionarily non-conserved residue at the C-terminal cytochrome b<sub>5</sub> domain which conferred an alanine to valine substitution (A484V), and the other contained a serine to phenylalanine mutation in an evolutionarily conserved position (S303F) at the C-terminus of the fourth transmembrane domain. Both alleles induced the same phenotypes. After just 7 minutes at the non-permissive temperature, Tatzer noted that a GFP-tagged version of the mutant desaturases relocates from the ER to a punctate pattern throughout the cytosol, but not the wild type protein. Incubation for 30 minutes at this temperature reduced the number of puncta, however the remaining spots increased in size and intensity which is accompanied by the puncta appearing more often at the cell periphery. Tatzer observed the relocation of the mutant enzymes in greater than 80% of cells examined. They determined that the relocation event is lipid dependent as no relocation of either Ole1<sup>ts</sup>-GFP was observed in cells cultivated with unsaturated fatty acids, but did occur in the presence of saturated fatty acids. Furthermore, a shift from non-permissive conditions back to permissive conditions (30 °C) for 20 minutes was sufficient to completely restore wild type ER localisation and desaturase activity.

Studies have shown that cyanides and azides can inhibit  $\Delta 9$  desaturase activity through inhibition of activity at the di-iron centre of Ole1p (158). Tatzer investigated whether either sodium azide or potassium cyanide was sufficient to induce relocation in the GFP-tagged version of both wild type and temperature sensitive Ole1p. Relocation was observed in both OLE1 mutant alleles treated with either the cyanide or azide inhibitor even at permissive conditions suggesting that the

enzyme relocalisation was not a specific response for the Ole1<sup>ts</sup> mutants, instead it was a consequence of the inhibition of Ole1p activity irrespective of mechanism.

Tatzer next investigated the subcellular region(s) where Ole1p<sup>ts</sup> relocalised to. Fractional centrifugation and equilibrium density gradient centrifugation analysis revealed no significant difference between the fraction properties of wild type Ole1p and Ole1p<sup>ts</sup>. It was therefore determined that Ole1p<sup>ts</sup> most likely relocalises to compartments that are ER-like and are derived from the ER. Tatzer also noted significant alterations in lipid biosynthesis such that saturated C16 and C18 (palmitic acid and stearic acid) were incorporated into lipids at the expense of the unsaturated counterparts, palmitoleic acid and oleic acid, in cells expressing either of the mutant desaturases at non-permissive temperature. The level of desaturation of palmitic acid and stearic acid was reduced to less than 1% of the wild type after 30 minutes at non-permissive conditions. Tatzer et al also observed that the relocalisation of mutant desaturase is selective as the localisation of the ER resident protein Sec63p-GFP was unaffected under conditions where Ole1p<sup>ts</sup>-GFP exhibited significant relocalisation. Tatzer examined the subcellular morphology of cells grown at nonpermissive conditions by EM. They observed aberrant, membranous structures that could not be assigned to any currently known organelle both in the cytosol and in close proximity to the nucleus, as well as a large membrane enclosed compartment at the cell periphery where it is likely Ole1p<sup>ts</sup> relocalised. Overall, Tatzer reported the selective, non-allele specific, and conditional relocalisation of Ole1p<sup>ts</sup>-GFP when grown in non-permissive conditions. Furthermore, this is not a temperature-dependent response as it can be induced by treatment with desaturase inhibitors suggesting that a reduction in desaturase function (chemical or genetic) is coupled with relocalisation as a result of an altered lipid profile (157).

Linking the data presented by Tatzer that identified the subcellular relocalisation of Ole1<sup>ts</sup>-GFP at non-permissive temperatures in a lipid dependent manner to the early data from F2G suggesting that Ole1p was the target of F900742, the localisation of an endogenously GFP tagged version of Ole1p (Figure 4.1) in response to F900742 was

investigated. It was expected that if Ole1p, or indeed a regulator of this protein, was the target of F900742 then a similar localisation pattern would be observed to Tatzer.

This chapter investigated Aim 1 of this study: test the activity of F900742 in the yeast *S. cerevisiae*.

## 4.2 Results

### 4.2.1 *S. cerevisiae* was sensitive to F900742

The majority of studies were performed in *S. cerevisiae*, therefore initial experiments investigated the sensitivity of this strain to F900742. *S. cerevisiae* is a budding yeast that can reproduce as either a mating-type (MAT) MAT $\alpha$  or MAT $\alpha$  haploid or as a MAT $\alpha$ -MAT $\alpha$  diploid. BY4741 and BY4742 are wild type haploid *S. cerevisiae* derived from the S288C parent strain (159). BY4741 contains a MAT $\alpha$  locus and BY4742 a MAT $\alpha$ , and this is the only locus where these two strains vary. The *S. cerevisiae* lifecycle involves intervals of logarithmic growth and stationary phases. During stationary phase, yeast have a relatively low metabolic activity with limited *de novo* lipid synthesis. In contrast, logarithmic (log) growth is associated with rapid cell division, approximately once every 90 minutes under optimum growth conditions, through a process whereby the daughter cell buds off the mother. During log phase, there is a high level of *de novo* lipid synthesis and an increase in the expression of enzymes required for these processes, including Ole1p. Therefore, all experiments were performed with cells that were in a mid-logarithmic growth phase.

The minimum inhibitory concentration (MIC) of *S. cerevisiae* was investigated in the wild type haploid *S. cerevisiae* strain BY4741. Data from F2G suggested that Ole1p is the target of F900742, therefore the MIC of a GFP-tagged OLE1 haploid BY4741 strain also investigated. This strain was constructed by Huh et al (36). Huh designed a strategy to utilise the yeast homologous recombination mechanism to generate a strain containing a genomic GFP tag that is in-frame with and immediately following the OLE1 ORF, but before the OLE1 terminator (Figure 4.1) (strain referred to as BY Ole1-GFP hereon).

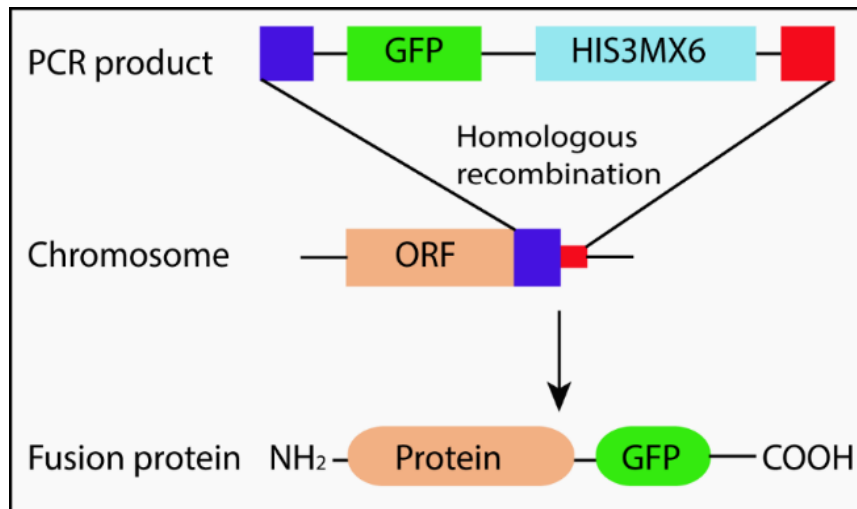


**Figure 4.1. BY Ole1-GFP construct.** BY Ole1-GFP was taken from a collection constructed by Huh et al. A GFP tag directly follows the OLE1 ORF and is in frame before the OLE1 stop codon. The OLE1 chromosome was tagged through oligonucleotide-directed homologous recombination using a pair of primers that were homologous to the chromosomal insertion at the 5' end and the insert containing the GFP tag at the 3' end of each primer. The GFP tag was amplified by PCR and transformed into haploid wild type yeast. Figure adapted from (36).

The EUCAST method for determining the minimum inhibitory concentration (MIC) of novel antifungal agents in pathogenic yeast and moulds recommends that RPMI 1640 media is used (160,161). *S. cerevisiae* were grown in RPMI 1640 for 24 hours in serial two-fold dilutions of F900742. However, *S. cerevisiae* grew poorly in this media with an average optical density (OD 600) in the untreated sample of 0.7 after 24 hours of growth (starting OD 600 of 0.1) (Figure 4.2A). The minimal growth observed in RPMI 1640 was deemed insufficient for future experiments, therefore MICs were re-evaluated in the complete media YPD. Poor *S. cerevisiae* growth in RPMI has also been noted in previous studies (162).

The MICs of BY4741 and BY Ole1-GFP were determined by growing cells in YPD liquid culture for 24 hours in the presence of F900742. Serial two-fold dilutions of F900742 was used to create a 16-fold concentration range. The MIC was identified by the point that there was no growth, the IC90 where there was less than 90% growth, and the IC50 where there was less than 50% growth relative to the untreated sample after 24 hours observed by a reduction in OD 600. BY Ole1-GFP was more sensitive to F900742



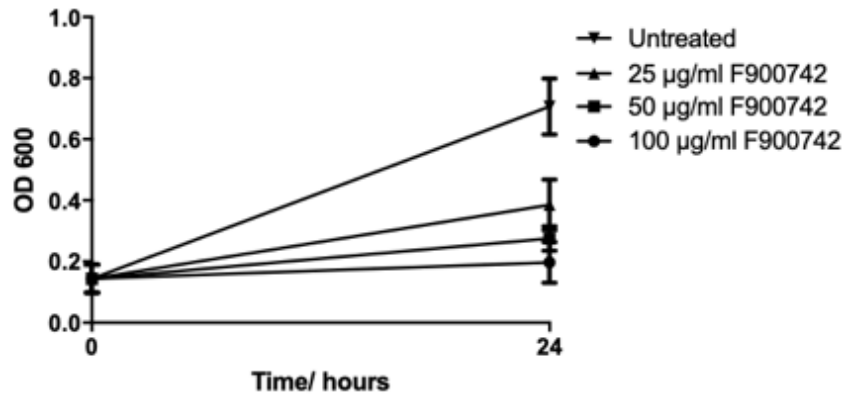
than BY4741 (Figure 4.2B and Figure 4.2C), the MICs of these strains were 25 µg/ml and 50 µg/ml, respectively. *S. cerevisiae* was less sensitive than any of the pathogenic fungi listed in (Table 4.1). The MIC of BY Ole1-GFP was one-fold lower than wild type which could possibly be due to alterations to protein folding induced by the C terminal GFP tag. To confirm whether the GFP tag influenced the sensitivity of BY Ole1-GFP, the primers Ole1 Stop F and Ole1 R were used to insert a stop codon in-frame and directly after the OLE1 ORF (method described on page 59), but before the GFP tag so that this strain would no longer express the fluorescent protein. The correct insertion of the stop codon was confirmed by Sanger sequencing and a lack of fluorescence by confocal microscopy. The MIC of BY OLE1-stop-GFP was the 50 µg/ml, the same as wild type BY4741 (Figure 4.2B and Figure 4.2C). It was concluded that the GFP tag did affect the sensitivity of this strain to F900742 due to slight alterations to the structure of Ole1p.

The fission yeast *Schizosaccharomyces pombe* and *Schizosaccharomyces japonicus* are evolutionarily distinct from budding yeast. Although all termed “yeast”, differences between *S. pombe*, *S. japonicus*, and *S. cerevisiae* make them useful complementary systems when studying a variety of processes, for example cell growth under various conditions and response to DNA damage. The genomes between the budding and fission yeast are significantly different, highlighted by haploid *S. cerevisiae* having 16 chromosomes and 6000 genes whilst haploid *S. pombe* have just 3 chromosomes and approximately 4800 genes, and display a lack of synteny. In addition, *S. pombe* has more genes conserved with metazoans than *S. cerevisiae*, however both species share genes with metazoans that the other lacks (163). Even where functions are seemingly similar, study in more than one yeast provides complimentary information. The genomes of *S. pombe* and *S. japonicus* encode  $\Delta 9$  desaturase, OLE1, as such the sensitivity of these strains to F900742 was also assessed.

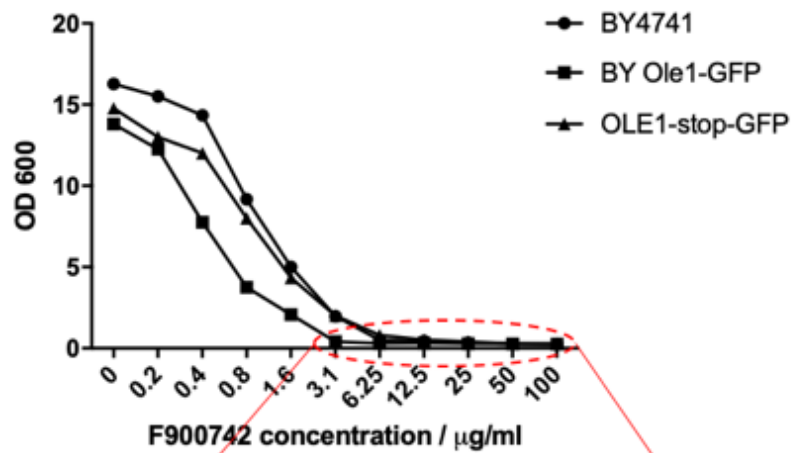
*S. pombe* and *S. japonicus* were grown in appropriate media supplemented with F900742 for 24 hours. *S. pombe* was more resistant to F900742 than either *S. japonicus* or *S. cerevisiae* with a MIC greater than the highest concentration of drug tested (200 µg/ml). *S. japonicus* was as sensitive as BY4741 wild type (Figure 4.2D).

These results add to the broad-spectrum activity of F900742. The MIC, IC90, and IC50 for all tested strains are summarised in figure 4.2E.

**A)**



**B)**



**C)**

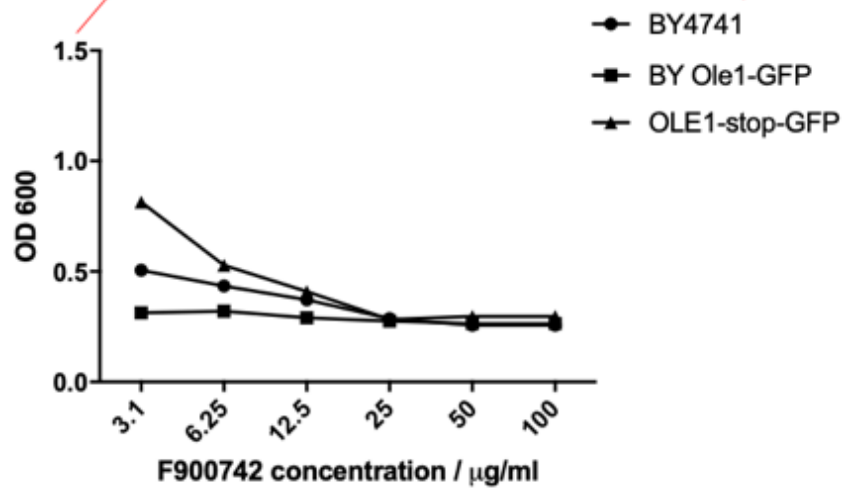
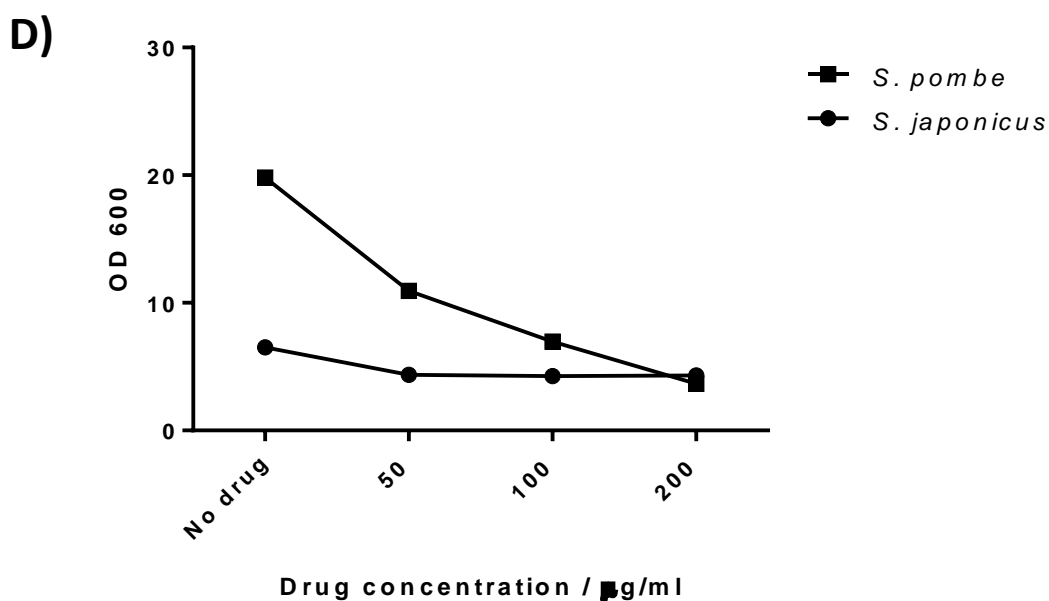


Figure 4.2 continues over page



E)

Strain	IC50 µg/ml	IC90 µg/ml	MIC µg/ml
BY4741	1.0	4.5	50
BY Ole1-GFP	0.5	2.5	25
OLE1-Stop-GFP	0.9	4.5	50
<i>S. japonicus</i>	25	50	100
<i>S. pombe</i>	N/a	N/a	>200

**Figure 4.2. MICs of *S. cerevisiae*, *S. japonicus*, and *S. pombe*.** The MICs of *S. cerevisiae*, *S. pombe*, and *S. japonicus* to F900742 was assessed by preparing two-fold dilutions of drug and determining growth of the yeast after 24 hours at 30 °C relative to the untreated control. Growth was measured by OD 600. (A) *S. cerevisiae* wild type BY4741 grew minimally in RPMI after 24 hours in media containing no drug. (B) and (C) The MIC of strains was determined by growing cells in complete liquid YPD media containing F900742 for 24 hours. The OD 600 was measured and the MIC, IC90, and IC50 were identified. The activity of F900742 was assessed in the *S. cerevisiae* strains BY4741, BY Ole1-GFP and OLE1-stop-GFP. BY Ole1-GFP was more sensitive to F900742 than BY4741 as noted by their respective MICs of 25 and 50 µg/ml. The MIC of OLE1-stop-GFP was 50 µg/ml. (A-C) N = 3. (D) The *Schizosaccharomyces* strains *S. pombe* and *S. japonicus* were grown in YES media treated with F900742. The MIC in *S. japonicus* was identified as 50 µg/ml, the same as BY4741, whereas *S. pombe* was substantially less sensitive with an MIC greater than 200 µg/ml. IC50 and IC90 could not be determined for *S. pombe*. N = 3. (E) Summary of all MIC, IC90, and IC50 of all tested strains.

The sensitivity of *S. cerevisiae* to F900742 was also determined through identifying growth phenotypes on complete media agar supplemented with drug by the colony growth assay. Fresh cells were grown until there were approximately  $4 \times 10^6$  per 100  $\mu$ l. Cells were serially diluted 1:20 fold into 100  $\mu$ l and 1.5  $\mu$ l was added to complete media agar plates containing F900742 using a 48 pin replicator (Figure 4.3). The wild type haploid *S. cerevisiae* strains BY4741, BY4742 and R453C demonstrated sensitivity to F900742. 15  $\mu$ g/ml of F900742 was sufficient to completely inhibit the growth of BY4742 at the most dilute number of cells (Figure 4.3 row 4) and substantially reduce the growth of BY4741 and R453C at the corresponding cell number relative to the YPD only plate. BY4741 and BY4742 only differ at the MAT a and MAT  $\alpha$  locus, therefore the growth in BY4741 in row 4 of the 15  $\mu$ g/ml plate was assumed to be a contaminant or artefact. BY4741 and BY4742 demonstrated similar sensitivity at all cell dilutions when grown on 5 and 10  $\mu$ g/ml of F900742 with both strains growing better at the lower drug concentration. 10  $\mu$ g/ml of F900742 was sufficient to induce a reduced growth phenotype relative to plates not containing drug in all three wild type strains. Of note, R453C is a wild type yeast that is unrelated to the S288c parent for all other strains in this experiment. R453C was the most resistant to F900742 as denoted by the greatest amount of growth on the 15  $\mu$ g/ml plate. F900742 was solubilised in DMSO. A control plate containing DMSO only was used to confirm that the DMSO concentration used was non-toxic. There was no difference in growth of any strain between the DMSO supplemented plate and YPD only.

BY Ole1-GFP exhibited considerable sensitivity at just 5  $\mu$ g/ml of F900742 with minimal growth in the largest cell dilution (Figure 4.3 row 4) and substantially reduced growth in the previous two dilutes at this concentration (row 2 and 3) relative to the YPD only plate. 15  $\mu$ g/ml of F900742 was sufficient to inhibit all BY Ole1-GFP growth at the most dilute cell concentration (Figure 4.3 row 4) and only permit minimal growth in row 3. There was less growth in each of the lowest three cell concentrations (Figure 4.3 rows 2, 3, 4) at 10  $\mu$ g/ml than the respective row at 5  $\mu$ g/ml. Similar growth was observed in the highest two cell concentrations (Figure 4.3 rows 1 and 2) on both the 10  $\mu$ g/ml and 15  $\mu$ g/ml plates. There was less growth at the lowest two cell concentrations (Figure

4.3 rows 3 and 4) at 15  $\mu\text{g}/\text{ml}$  than 10  $\mu\text{g}/\text{ml}$ . BY Ole1-GFP was more sensitive to F900742 than any of the three wild type strains.

To investigate the sensitivity of mutants of the OLE1 pathway to F900742, strains that were null for the Ole1p regulator Ubx2p and the Ole1p competitor Sct1p were grown on F900742. Previous studies have suggested that Ubx2p is required to guide ubiquitinated Mga2p and Spt23p to Cdc48 which is responsible for the release of the soluble P90 fragments and their subsequent translocation into the nucleus for activation of OLE1 transcription (91). Following the observation by Surma that P120 Mga2p increases in BY  $\Delta\text{ubx2}$  cells and this is associated with a decrease in amount of Ole1p, the sensitivity of this strain to F900742 was tested. It was expected that BY  $\Delta\text{ubx2}$  would demonstrate greater sensitivity to F900742 than wild type strains due to inherently low levels of Ole1p. BY  $\Delta\text{ubx2}$  A cells were grown on agar plates containing F900742 as described above. BY  $\Delta\text{ubx2}$  demonstrated the greatest sensitivity to F90042 with no growth after 48 hours at any F900742 concentration (lowest concentration tested was 5  $\mu\text{g}/\text{ml}$ ). For comparison, all other tested strains demonstrated some growth at the highest number of cells at all drug concentrations (Figure 4.3). Kolawa et al showed that the ubiquitinated forms of Mga2p and Spt23 accumulate in BY  $\text{ubx2}$  null cells. BY  $\Delta\text{ubx2}$  cells are functionally viable, however display a reduction in growth phenotype when grown at either 30 °C and 37 °C on complete media which can be rescued by supplementation with 0.2% oleic acid. Furthermore, they showed that OLE1 mRNA is substantially decreased in BY  $\Delta\text{ubx2}$  (144). Therefore, the increased sensitivity of this strain is speculated to be due to a lower content of Ole1p as a result of a reduction in *de novo* protein synthesis of the desaturase.

The activity of Ole1p is also regulated by the glycerol-3-phosphate acyltransferase, Sct1p. Studies by De Smet et al identified Sct1p as a competitor of Ole1p for the common substrates C16:0 CoA and C18:0 CoA. Deletion of SCT1 results in an increase in desaturation of fatty acids (147). Although this has not been confirmed, the increase in fatty acid desaturation noted by De Smet is likely to a result of an increase in expression of Ole1p to avoid lipotoxicity due to the build-up of saturated fatty acids.

Therefore, it is expected that BY  $\Delta sct1$  has the greatest Ole1p content and would be the least sensitive to the drug. Counter to BY  $\Delta ubx2$  A, BY  $\Delta sct1$  A was the least sensitive to F900742 (Figure 4.3). There was a very slight reduction in growth of BY  $\Delta sct1$  A at 15  $\mu\text{g}/\text{ml}$  relative to the untreated plate. Lower drug concentrations induced only a very slightly reduced growth phenotype in this strain at the lowest concentration of cells (row 4).

Overall, strains that were predicted to have a greater Ole1p concentration (BY  $\Delta sct1$ ) demonstrated the lowest sensitivity to F900742, and F900742 displayed the highest growth inhibitory activity in strains with the lowest expected desaturase content (BY  $\Delta ubx2$ ). BY Ole1-GFP was more sensitive to F900742 than the wild type strains. R453C was more resistant than either BY4741 or BY4742.

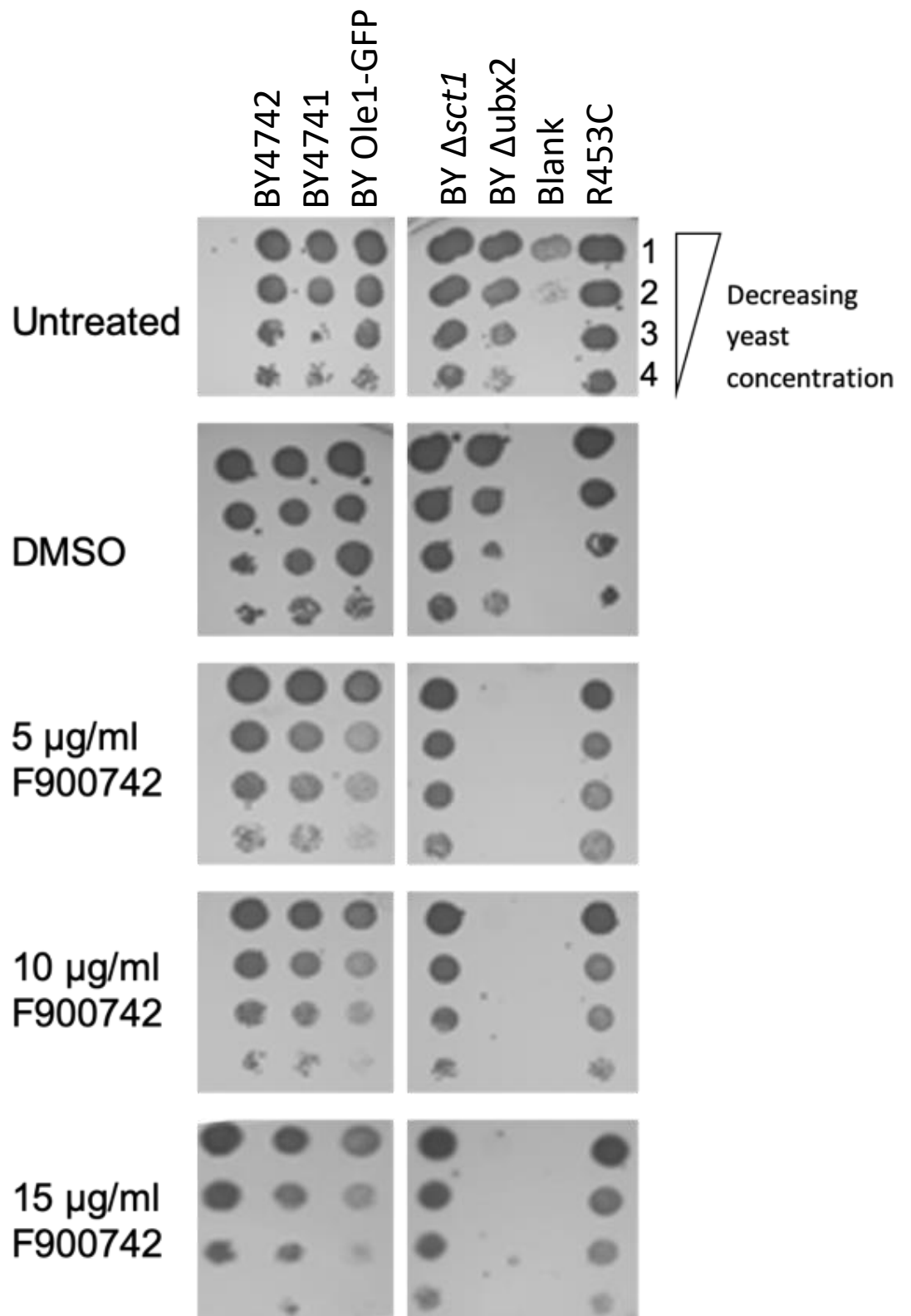


**Figure 4.3. OLE1 pathway mutants altered the sensitivity to F900742.** Growth assay of wild type yeast as well as delete and GFP-tagged strains of components of the OLE1 pathway demonstrated sensitivity to F900742 on complete media plates supplemented with either 5, 10, or 15  $\mu\text{g/ml}$  of F900742. BY  $\Delta\text{ubx2}$  was the most sensitive strain, followed by BY Ole1-GFP. BY  $\Delta\text{sct1}$  was the least sensitive and showed a similar growth phenotype to the wild type R453C. Wild type BY4742 was more sensitive than BY4741, both of which were more sensitive than the alternative wild type strain R453C. Plates without any F900742 or plates supplemented with 2% DMSO only were used as controls. Plates were grown at 30 °C for 48 hours. N = 3. Row labelling of yeast dilution same for all plates.



### 4.2.3 Higher temperatures reduced the activity of F900742

*S. cerevisiae* are poikilothermic organisms, that is their temperature varies considerably in response to the environmental temperature. To maintain proper cell function at extreme temperatures, yeast activate processes to ensure normal homeostasis, for example altering the degree of membrane lipid saturation via the induction or inhibition of the  $\Delta 9$  fatty acid desaturase. Lower temperatures (15 °C) are associated with a more rigid membrane and require an increase in acyl chain desaturation and Ole1p expression to maintain proper membrane fluidity. In contrast, there is a large reduction in Ole1p expression and acyl chain desaturation at higher temperatures (37 °C) (98). Therefore, the inhibition of the OLE1 pathway at lower temperatures was expected to have a more profound effect. The sensitivity of *Saccharomyces cerevisiae* to F900742 was also tested at temperatures lower (25 °C) and higher (37 °C) than 30 °C.

Serial dilutions of cells were prepared and grown on agar plates as previously described. Plates either contained YPD only or YPD supplemented with 15 µg/ml of F900742. Plates were incubated at 25 °C, 30 °C, or 37 °C for 48 hours (Figure 4.4). Consistent with published data, all untreated strains grew best on YPD only at 30 °C. All strains demonstrated a reduction in growth when plated on to F900742 compared to YPD only at all comparative temperatures. All strains grew better at 37 °C than 25 °C on F900742 which is likely to be due to a greater requirement for the desaturase at lower temperatures. Consistent with above data showing that BY  $\Delta sct1$  was the least sensitive to F900742 at 30 °C (Figure 4.3), this strain also was the least sensitive to the drug at both 25 °C and 37 °C (Figure 4.4). Although BY  $\Delta ubx2$  was demonstrably the most sensitive to F900742 at 30 °C (Figure 4.3), BY Ole1-GFP was the most sensitive strain at both 25 °C and 37 °C (Figure 4.4). It has been previously shown that BY Ole1-GFP has a lower MIC than wild type BY4741, and that this difference is likely due to structural changes in the desaturase conferred by the GFP tag (Figure 4.2B). The increased requirement for fatty acid desaturation at lower temperatures coupled with a greater degree of desaturase inhibition in BY Ole1-GFP resulted in a lower growth phenotype of this strain than wild type at 25 °C. R453C was less sensitive than either of

the BY wild type strains on F900742 at both 25 °C and 37 °C, and on YPD only plates at respective temperatures (Figure 4.4).

Overall, F900742 was more active against all tested strains at 25 °C than at 30 °C or 37 °C likely due to a greater requirement for  $\Delta 9$  desaturase activity at lower temperatures. BY Ole1-GFP was most sensitive to F900742 at 25 °C, whilst BY  $\Delta ubx2$  was the most sensitive at 30 °C. F900742 was least active in BY  $\Delta sct1$  at all temperatures. It is important to note, that this was only performed once, therefore more repeats would be needed for a more robust conclusion.

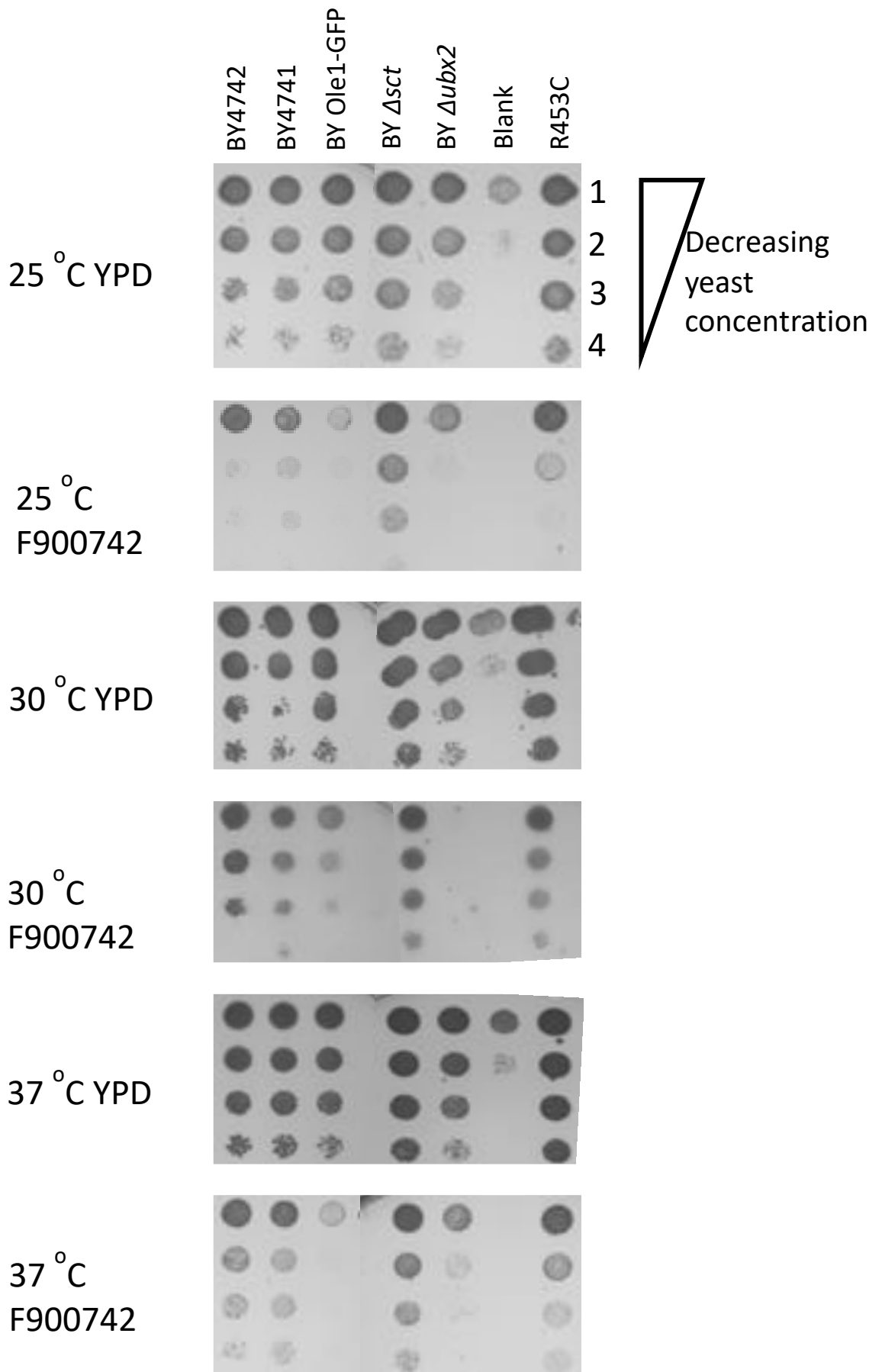


**Figure 4.4. F900742 displayed temperature sensitive activity.** All strains were most sensitive to F900742 at lower temperatures. All strains grew better on YPD only than in the presence of F900742 at all temperatures. All untreated strains grew best at 30 °C and 37 °C than 25 °C. BY Ole1-GFP was the most sensitive to F900742 at 25 °C and 37 °C, whereas BY  $\Delta ubx2$  was the most sensitive at 30 °C. BY  $\Delta sct1$  was the least sensitive at all temperatures tested. BY4741 and BY4742 were more sensitive than R453C. N = 3. F900742 containing plates were supplemented with 15  $\mu\text{g/ml}$  of drug and grown at the relevant temperature for 48 hours.

#### **4.2.4 F900742 induced a redistribution of Ole1p**

Ole1p has been previously shown to localise to the peripheral and nuclear ER membrane (164). In yeast, the ER can be classified as nuclear ER, peripheral ER, or ER strands that link the nuclear and peripheral (Figure 4.5A). The strain BY Ole1-GFP was used to determine Ole1p localisation using confocal microscopy. Ole1p-GFP was seen in patterns consistent with its localisation on the nuclear ER, peripheral ER, and ER strands linking the two (Figure 4.5B and 4.5C).

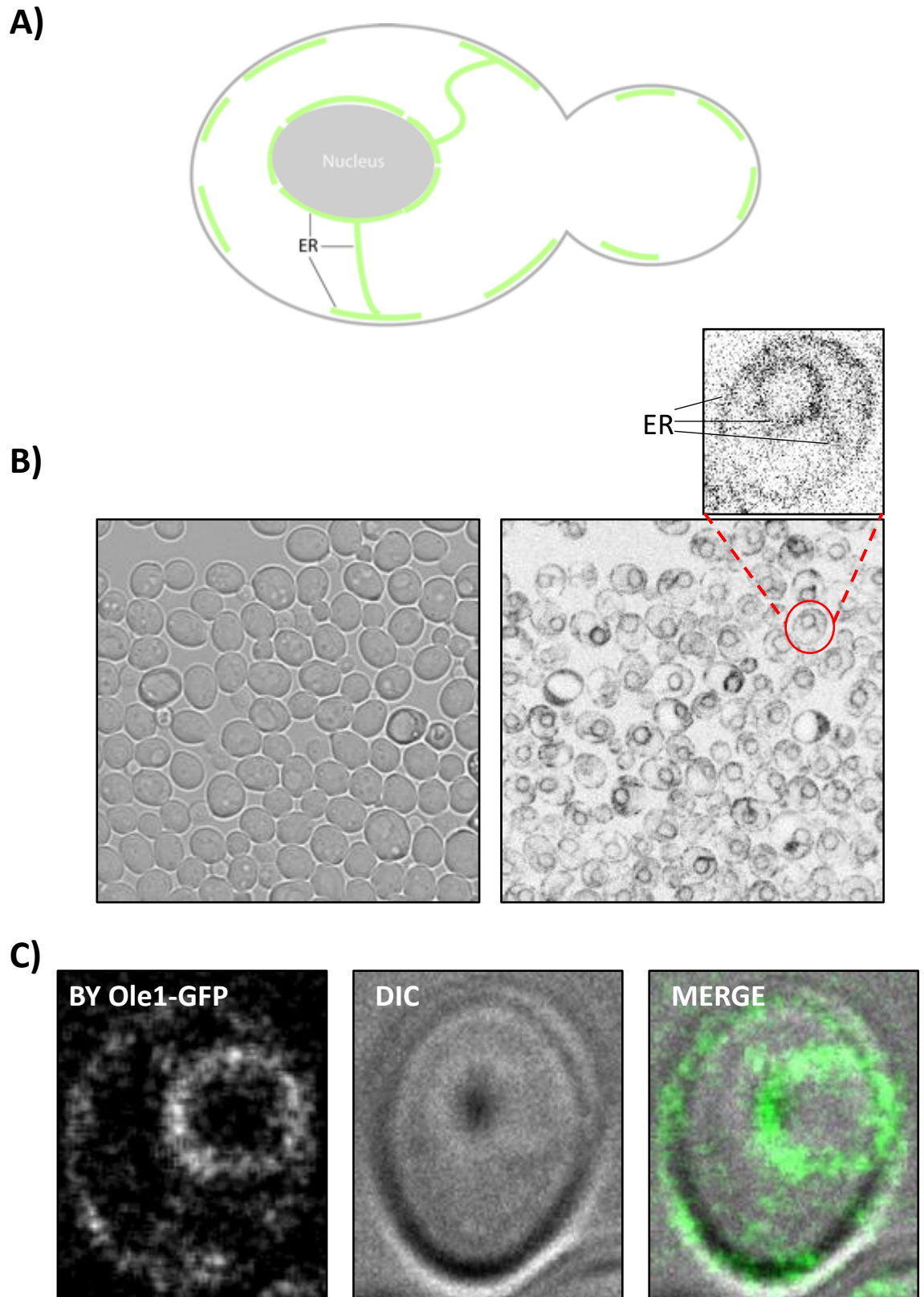


**Figure 4.5. Ole1p-GFP localised to the peripheral and nuclear ER.** (A) Cartoon illustrating the ER distribution in *Saccharomyces cerevisiae*. There are three classes of ER: the nuclear ER, the peripheral ER and strands of ER that link the peripheral and nuclear ER. (B and C) Confocal microscopy image of the strain BY Ole1-GFP in log phase. Ole1p-GFP did localise to the nuclear and peripheral ER and the linking strands.

F2G have previously shown that unsaturated fatty acids, but not saturated fatty acids inhibited the action of F900742 suggesting that the activity of F900742 was lipid dependent (Figure 1.3). Taken together with data presented by Tatzer et al (157), it was expected that the drug would induce a mislocalisation of Ole1p. To investigate this, BY Ole1-GFP was treated with F900742 and examined at time intervals of 30 minutes, 60 minutes, 120 minutes, and 240 minutes (Figure 4.6). Treatment with F900742 induced Ole1p-GFP to redistribute to dense puncta that appeared consistent with the nuclear and peripheral ER (red arrow Figure 4.6F) or tubes that span the length of the cell (blue arrow Figure 4.6F). The aberrant localisation of Ole1p-GFP was first observed after 60 minutes of treatment, however puncta were faint and only in a minority of cells (one puncta was observed in approximately 20% of imaged cells and less than 5% contained two or more puncta) (Figure 4.6D). Appearance of puncta and tubes was at the expense of Ole1p localisation on the ER. Greater than 80% of cells contained three or more puncta or tubes following 120 minutes of treatment which was associated with an increase in the brightness and size of each relative to the 60 minute sample (Figure 4.6F). There was a further increase in brightness and size by 240 minutes, but this was associated with a reduction in the number of puncta per cell with greater than 80% of observed cells containing either 1 or 2 puncta and only a minority of cells containing tubes (Figure 4.6H). A single, very large puncta, but not tubes, was observed in all cells imaged that were treated for 24 hours with F900742 (Figure 4.6J). The expression of Ole1p in the untreated sampled visibly decreased between 2 and 4 hours, and further at 24 hours. The reduction in Ole1p-GFP expression can be explained by the fact that cells would be starting to exit logarithmic growth phase 4 hours into this experiment as more are entering into a stationary growth phase. By 24 hours, all cells would be expected to be in stationary phase. Stationary phase cells require very little desaturase, therefore are associated with a lower Ole1p expression. To account for the variations in Ole1p requirements, the desaturase is naturally a short-lived protein with a half-life of approximately 30 minutes (165). Of note, there was no mention in Tatzer et al of Ole1p<sup>ts</sup>-GFP redistributing to tubes at non-permissive temperatures.

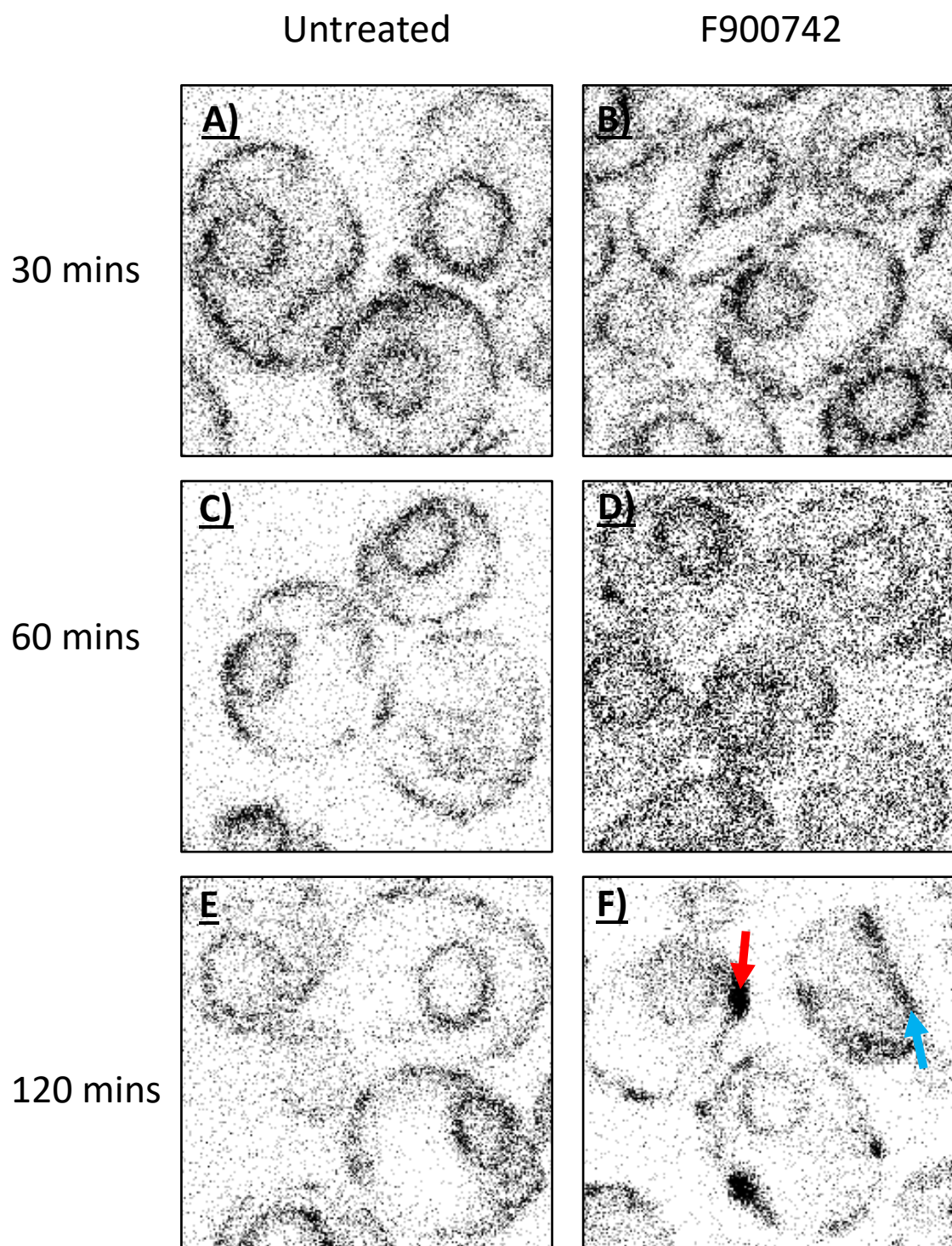
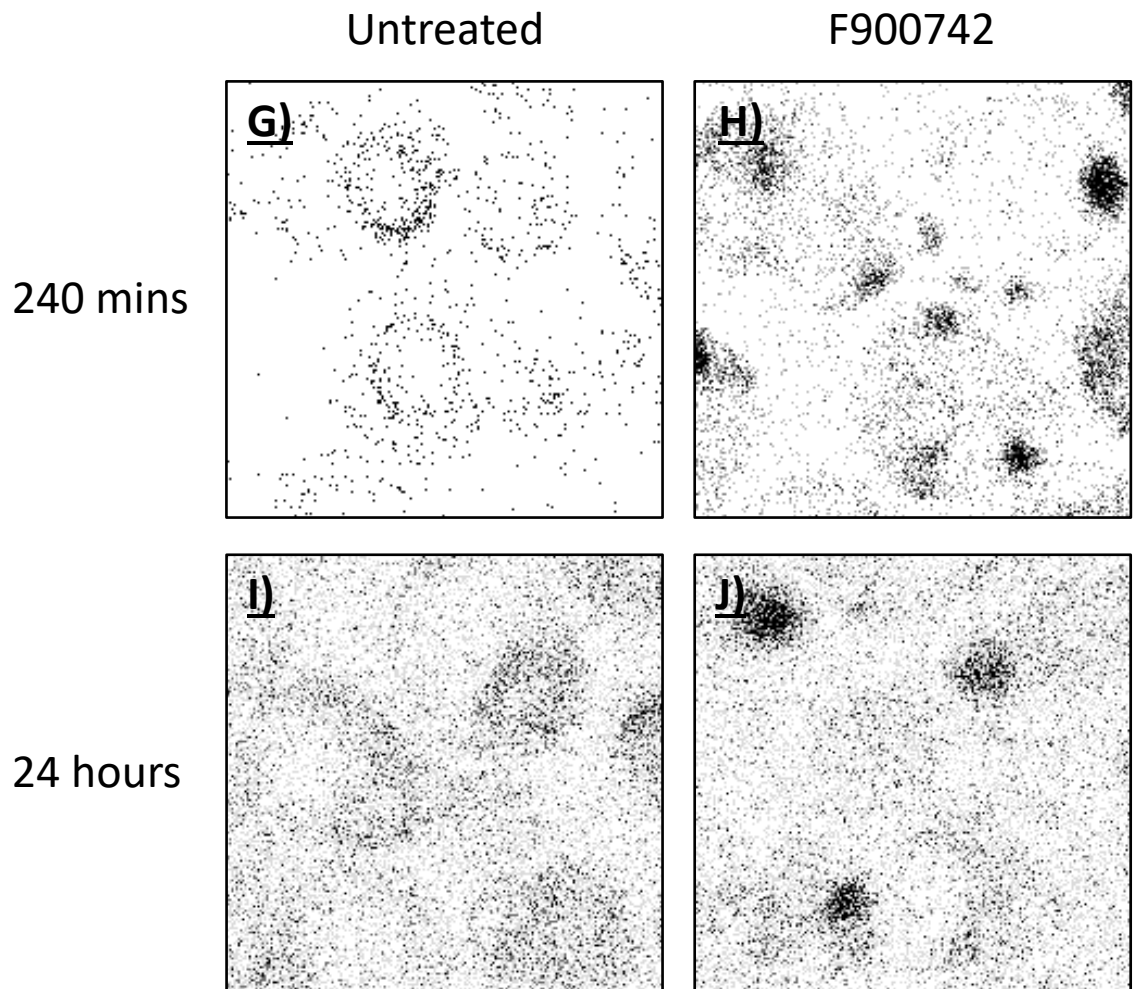


Figure 4.6 continues over page





**Figure 4.6. F900742 induced the relocalisation of Ole1p-GFP.** Log phase BY Ole1-GFP cells were treated with 50  $\mu\text{g/ml}$  F900742 for up to 24 hours and grown at 30  $^{\circ}\text{C}$ . Samples were taken at 30 minutes, 1 hour, 2 hours, 4 hours, and 24 hours for confocal microscopy. Incubation times 2 hours and longer with F900742 induced a relocalisation of Ole1p-GFP to dense puncta (F, red arrow) and to tubes (F, blue arrow) that spanned the length of the cell (F, H, J). The relocalisation of Ole1p-GFP was at the expense of normal ER distribution. The puncta and tubes first appeared in a minority of cells and were only very faint after 60 minutes of treatment (D), however following 120 minutes there was an increase in puncta size and brightness (F). A 240 minute incubation induced the formation of puncta that were brighter and bigger in size, however this was associated with a reduction in the number of puncta per cell (H). (J) 24 hour incubation with F900742 induced the formation of a single, large puncta only at the periphery in every cell and very limited Ole1p-GFP localisation to the ER. (B) There were not obvious differences to Ole1p-GFP distribution after 30 minutes to the untreated. (A,C,E,G,I) Ole1p-GFP was localised to the ER in all untreated samples. There was a large reduction in amount of Ole1p-GFP by 240 minutes (G) which was also observed after 24 hours (I). N = 4

#### 4.2.5 F900742 induced an increase in expression of Ole1p-GFP

The average amount of fluorescence per cell (termed arbitrary fluorescence) was quantified as described in the methods. Briefly, the total, unprocessed image fluorescence was measured, and average background subtracted. The total number of cells was manually counted. Values were put into the equation:

$$\text{Arbitrary fluorescence} = \frac{(\text{total fluorescence} - \text{average background})}{\text{number of cells}}$$

Cells were in the same phase of growth, there was a surplus of drug relative to desaturase, and the same microscope was used to measure samples to ensure equivalent exposure of all cells for all images taken. Microscope settings were identical for all like experiments.

The relocalisation of Ole1p-GFP following treatment with F900742 was accompanied by an increase in total cellular fluorescence (Figure 4.7). Interestingly, despite the lack of obvious Ole1p-GFP puncta, F900742 induced a large and significant increase in fluorescence after just 60 minutes which increased further by 120 minutes followed by a slight decrease in fluorescence by 240 minutes (Figure 4.7A). This reduction was also noted in the untreated sample and is assumed to be due to the natural turnover of Ole1p as cells exit log phase described above.

Calculating arbitrary fluorescence is an indirect method to determine the amount of Ole1p-GFP. To corroborate the increase in Ole1p-GFP expression in response to F900742, the protein amount was determined by western blot with an anti-GFP antibody. The molecular weight of Ole1p-GFP was calculated to be 85.4 kDa (molecular weight of Ole1p is 58.4 kDa; molecular weight of GFP is 27 kDa). There was a substantial increase in the amount of protein following 2 hours of treatment with F900742. A Ponceau stain of the membrane was used to confirm equal loading of samples (Figure 4.7B).

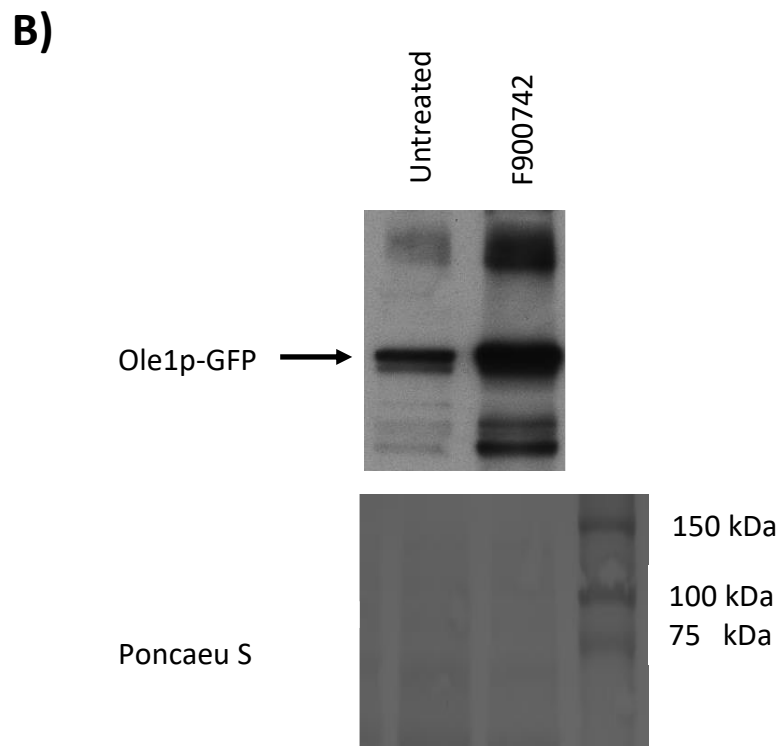
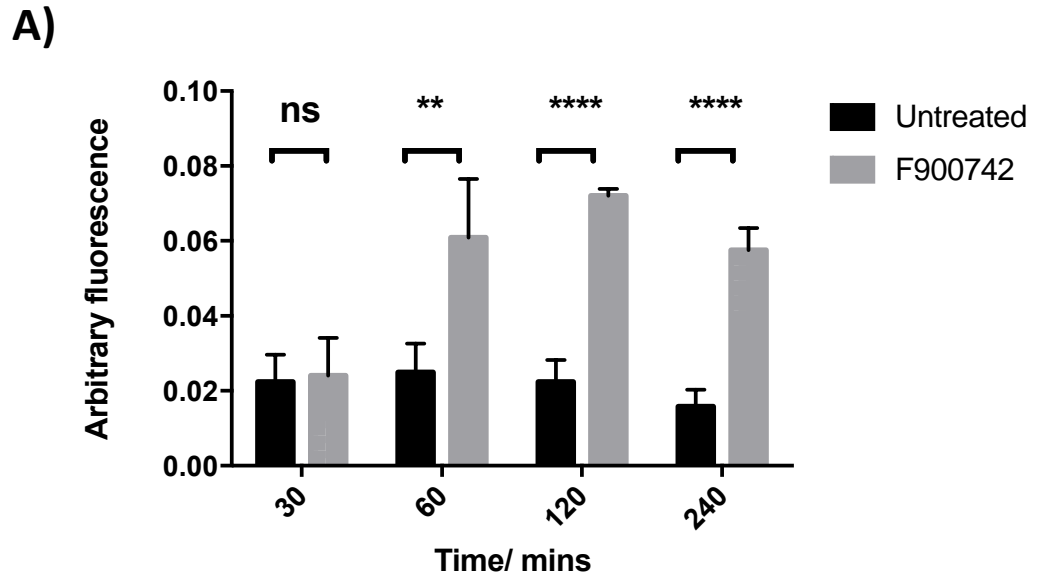


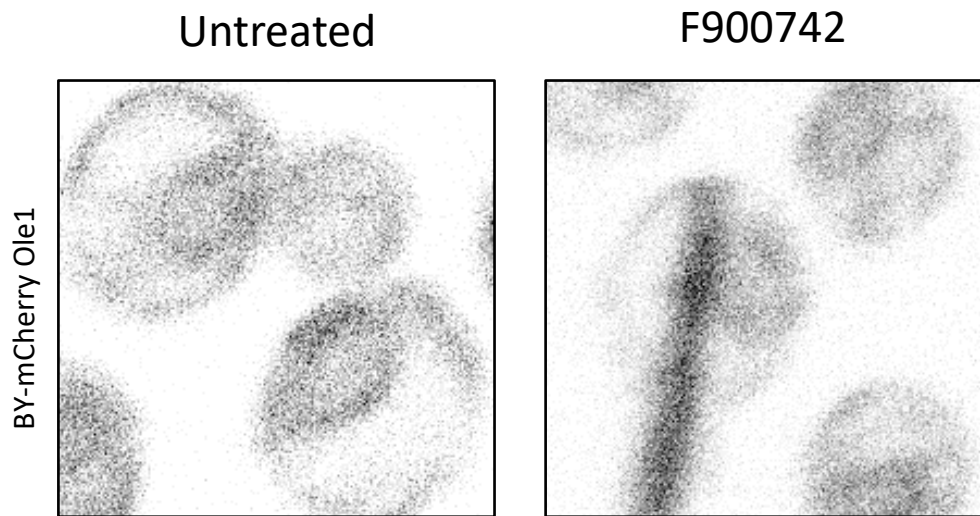
**Figure 4.7. F900742 induced an increase in expression of Ole1p-GFP.** (A) 60 minute incubation with F900742 was sufficient to induce a significant increase in fluorescence relative to untreated cells. Maximum fluorescence was observed after 120 minutes of treatment. There was a slight decrease in fluorescence at 240 minutes. The expression of Ole1p-GFP in untreated untreated samples slightly increased over the first 120 minutes and was followed by a slight decrease by 240 minutes. N = 5. (B) Immunoblot with anti-GFP antibody to detect Ole1p-GFP. F900742 induced an increase in amount Ole1p-GFP. A ponceau stain was used to determine equal protein loading at the 85 kDa region. BY Ole1-GFP was treated for 2 hours with 100  $\mu$ g/ml F900742. Samples were incubated at 30  $^{\circ}$ C. N = 2.

#### 4.2.6 Ole1p relocalisation was specific to F900742

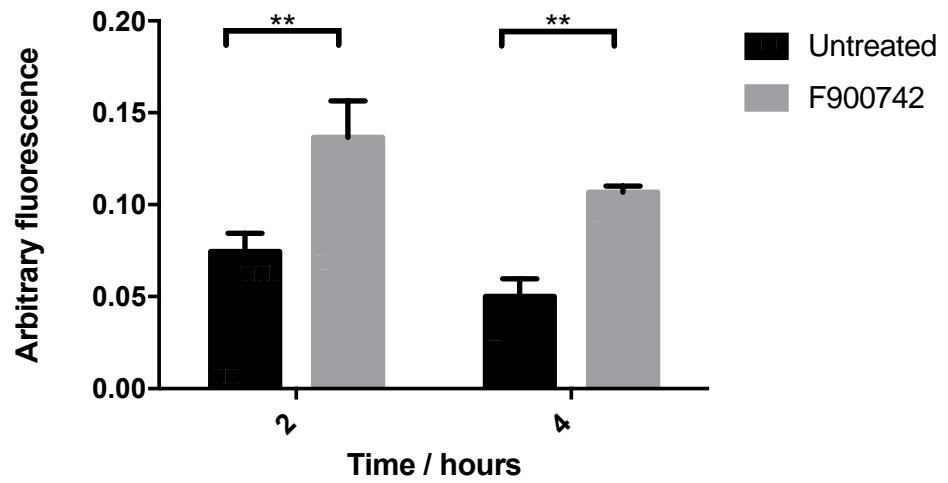
The MIC of BY Ole1-GFP was one-fold higher than both BY4741 and OLE1-stop-GFP suggesting that the C-terminal GFP tag is interfering with the structure of Ole1p, but not in a manner that sufficiently affects the function of the desaturase (Figure 4.2). To assess whether the GFP tag was enhancing the mislocalisation of Ole1p-GFP, the localisation of Ole1p was investigated in an alternative strain of *S. cerevisiae* that contains an mCherry tag at the N-terminus of the OLE1 ORF and before a TEF1 promoter. As with BY Ole1-GFP, there was a redistribution of BY mCherry-Ole1 to dense tubes and puncta, which was associated with a significant increase in arbitrary fluorescence following 2 and 4 hours of treatment with F900742 (Figure 4.8A and 4.8B). The expression of OLE1 is regulated by the TEF1 promoter in the strain BY mCherry-Ole1. The TEF1 promoter is a more powerful promoter than OLE1, therefore it was expected that the desaturase would be more highly expressed in this strain than wild type. This strain was associated with an MIC greater than 100  $\mu\text{g/ml}$  (data not shown). Consistent with a higher MIC, mCherry-Ole1 relocalisation was noted in just 30% of cells after 2 hours and 70% of cells after 4 hours of incubation with F900742, substantially lower than observed in BY Ole1-GFP.

To confirm that the relocalisation of Ole1p-GFP was a specific response to F900742 and the inhibition of the OLE1 pathway rather than a general response to antifungal compounds, BY Ole1-GFP was treated with amphotericin B for 2 hours. Amphotericin B is polyene that exerts antifungal activity through a mechanism that is independent of the OLE1 pathway. Amphotericin B did not induce the relocalisation of Ole1p-GFP in any cells observed (Figure 4.8C).

A)



B)



C)

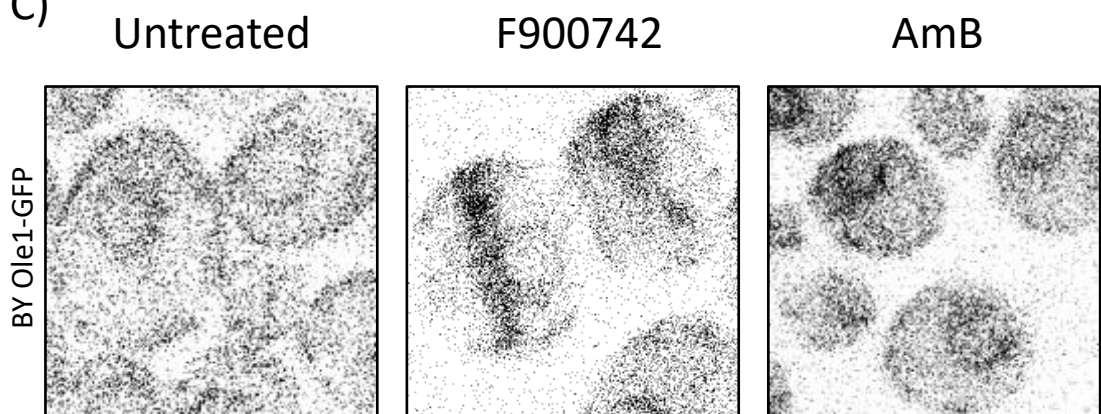


**Figure 4.8. Relocalisation events were specific between Ole1p and F900742.** (A) BY mCherry-Ole1 was incubated with F900742. F900742 induced the formation of aberrant tubes and puncta that were not observed in any of the untreated cells that were imaged. Mislocalisation of Ole1p was noted in 30% of cells at 2 hours and 70% of cells by 4 hours. N = 3. (B) The relocalisation of mCherry-Ole1 was associated with a significant increase in fluorescence at both 2 and 4 hours relative to the untreated counter sample. N = 3. (C) The redistribution of Ole1p was a response specific to F900742. BY Ole1-GFP was treated with F900742 or amphotericin B for 2 hours. Amphotericin B did not induce redistribution of Ole1p-GFP in any of the cells imaged. F900742 was added at 100 µg/ml. Amphotericin B was added at 250 ng/ml. Samples were grown at 30 °C. N = 2.

#### **4.2.7 Unsaturated fatty acids inhibited the redistribution of Ole1p-GFP**

Throughout eukaryotes,  $\Delta 9$  desaturases catalyse the desaturation of palmitoleic acid (C16:0) and stearic acid (C18:0) to palmitoleic acid (C16:1) and oleic acid (C18:1). Early target identification experiments at F2G identified oleic acid, but not saturated fatty acids as an inhibitor of the antifungal properties of F900742 in pathogenic fungi.

##### **4.2.7.1. Oleic acid**

To examine whether oleic acid was sufficient to inhibit the relocalisation of Ole1p-GFP in *S. cerevisiae*, 1mM of oleic acid was added at the same time as F900742. No imaged cells expressed mislocalised Ole1p-GFP when oleic acid was added in conjunction with F900742 (Figure 4.9A). Furthermore, there was a visual reduction in the amount of Ole1p-GFP as determined by a reduction in brightness in cells treated with oleic acid irrespective of F900742 addition. The visual observations were corroborated by quantification of fluorescence and calculating the arbitrary fluorescence as previously described (Figure 4.9B). Oleic acid was sufficient to inhibit an increase in Ole1p-GFP expression. Consistent with published data (135), oleic acid only was sufficient to induce a reduction in the amount of Ole1p-GFP - a significant effect was observed after 2 hours relative to the untreated sample (Figure 4.9B). The reduction in Ole1p-GFP irrespective of F900742 addition. There was a significant difference between the sample treated with F900742 only and F900742 plus oleic acid after just 60 minutes. The amount of fluorescence decreased further in both samples treated with oleic acid throughout the remaining 3 hours of the experiment. The reduction in arbitrary fluorescence in the presence of oleic acid was corroborated by immunoblotting samples treated for 2 hours. There was a decrease in band intensity in samples treated with oleic acid or oleic acid and F900742 relative to both the untreated and the F900742 treated samples (Figure 4.9C).

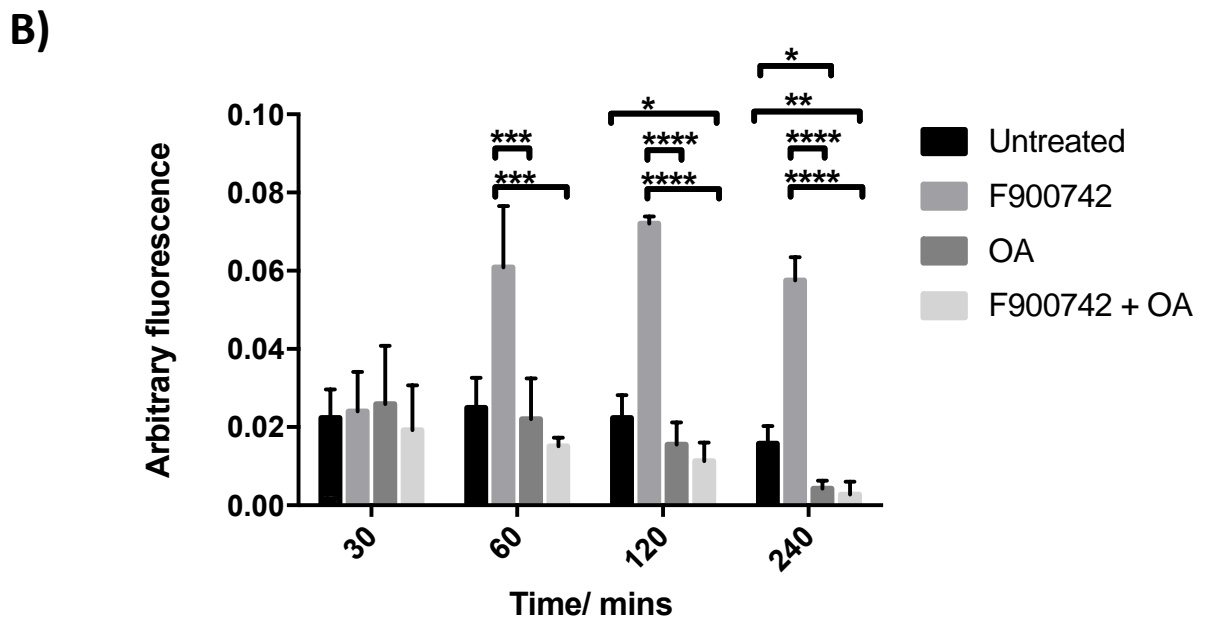
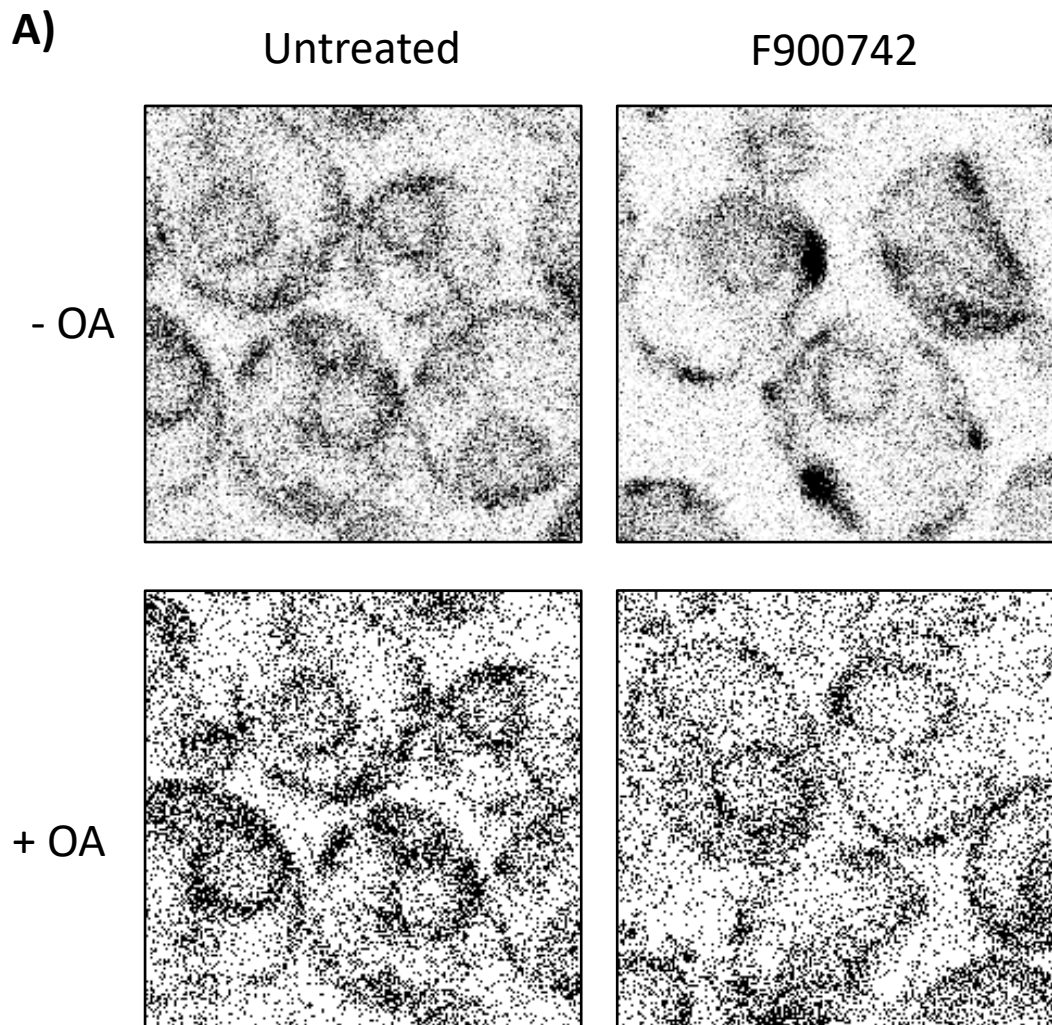
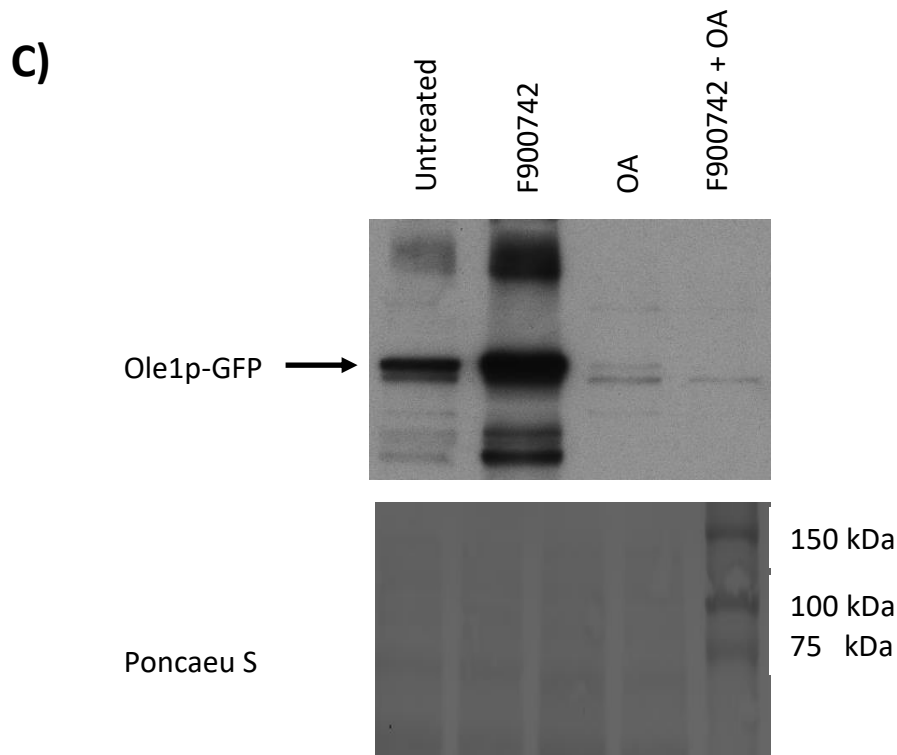


Figure 4.9 continues over page





**Figure 4.9. Oleic acid rescued the activity of F900742.** 1 mM oleic acid was supplemented to YPD either alone or at the same time as 100  $\mu\text{g/ml}$  F900742. Samples were incubated at 30  $^{\circ}\text{C}$  for up to 4 hours. (A) Samples were taken at 30, 60, 120, and 240 minutes. Oleic acid prevented the F900742-induced redistribution of Ole1p-GFP to puncta and tubes in all samples. Oleic acid alone was sufficient to visually reduce the amount of Ole1p-GFP. (B) Confocal images were quantified. Oleic acid induced a reduction in Ole1p-GFP expression in both samples treated with the unsaturated fatty acid relative to the untreated sample. The oleic acid reduction in Ole1p-GFP expression was irrespective of F900742 supplementation. There was a significant difference in fluorescence between samples treated with F900742 only or F900742 and oleic acid after 60 minutes. A significant difference between the sample treated with oleic acid and the untreated control was observed after 120 minutes, and between the untreated and oleic and F900742 after 240 minutes. There was no significant difference between the oleic acid only and F900742 and oleic acid samples at any time point. (A and B)  $N = 4$ . (C) Ole1p-GFP expression was also determined by immunoblot using an anti-GFP antibody. Samples were treated with F900742 only, oleic acid only, or F900742 and oleic acid only for 2 hours. Oleic acid induced a large reduction in the amount of protein detected irrespective of F900742. A ponceau stain confirmed equal sample size was loaded. 85.4 kDa region shown.  $N = 2$ .

The finding that oleic acid inhibited F900742-induced relocalisation of Ole1p-GFP and reduced the expression of Ole1p-GFP is in line with previous work confirming that the expression of Ole1p is repressed by multiple factors including the presence of its products, for example oleic acid (135). Furthermore, Tatzer also noted that the addition of unsaturated fatty acids prevented puncta formation in both temperature sensitive strains, whereas saturated fatty acids did not affect the cellular distribution of Ole1p (157). Therefore, the inhibition of Ole1p-GFP relocalisation by oleic acid is indicative that the Ole1p pathway is the likely target of F900742.

Oleic acid not only prevented an increase in fluorescence and Ole1p-GFP redistribution, but it was sufficient to almost fully reverse this phenotype (Figure 4.10A). Cells were treated with F900742 for 2 hours before they were washed in water and resuspended in fresh YPD containing oleic acid. Samples were taken at 30, 60 and 120 minutes after oleic acid addition. Images were also taken of cells that were treated with F900742 just before oleic acid was added, and of cells that were treated with F900742 only. Thus far, data demonstrated that F900742 induced a significant increase in total cell fluorescence after 60 minutes which increased further by 120 minutes (Figure 4.7). 30 minutes of treatment with oleic acid was sufficient to reduce the amount of fluorescence induced by F900742 such that there was no significant difference to the untreated cells, as well as induced a significant difference compared to F900742 only treated cells (Figure 4.10B). The reduction in cellular fluorescence was accompanied by an elongation of the puncta after 30 and 60 minutes with a complete redistribution to wild type ER morphology after a 2 hour incubation with oleic acid (Figure 4.10A). Furthermore, a 30 minute incubation with oleic acid was sufficient to noticeably reduce the number of cells containing relocalised Ole1p-GFP puncta and the number of puncta within each cell. There was a wild type distribution of Ole1p-GFP to the ER in cells treated with oleic acid for 120 minutes. These results were also observed when oleic acid was supplemented to media containing F900742 after 2 hours of incubation with the drug.

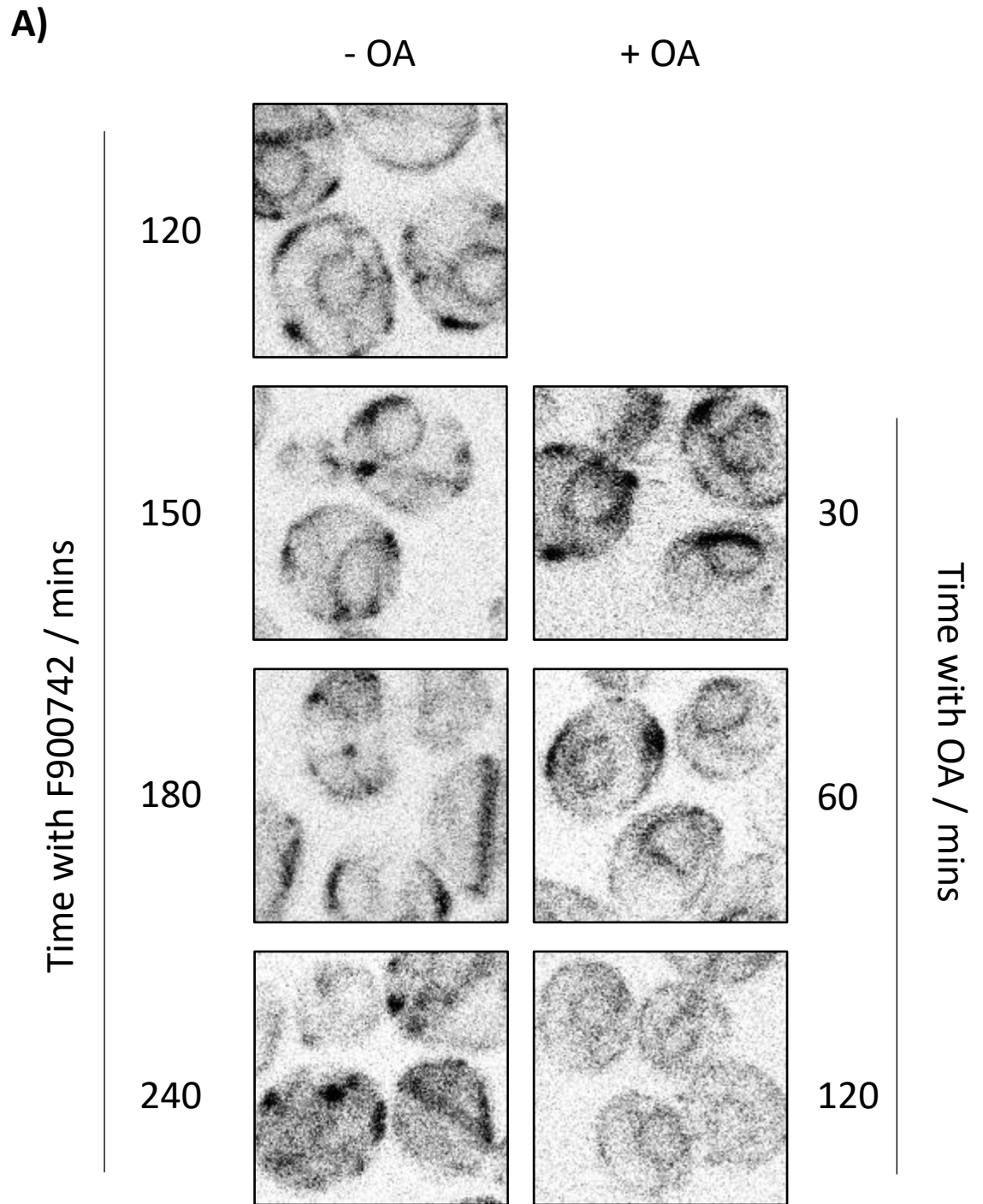
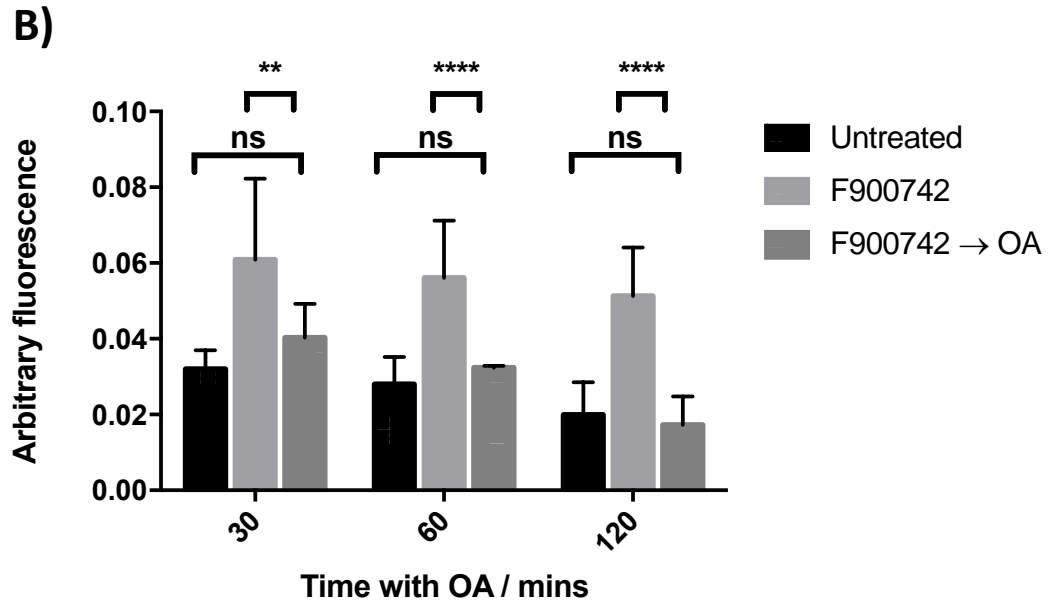


Figure 4.10 continues over page



**Figure 4.10. Oleic acid reversed the relocalisation of Ole1p-GFP and the associated increase in expression.** Cells were treated with 100  $\mu\text{g}/\text{ml}$  F900742 for 120 minutes, washed, and treated with 1mM oleic acid in fresh media for a further 120 minutes. Cells were incubated at 30  $^{\circ}\text{C}$ . A) 30 minutes after oleic acid addition, Ole1p-GFP puncta appeared elongated. Fewer cells contained puncta by 60 minutes. Remaining puncta were less bright and there were fewer per cell. Oleic acid completely redistributed Ole1p-GFP to a wild type ER localisation after 120 minutes. N = 4. B) Quantification of fluorescence. Although puncta were still observed in the majority of cells, a 30 minute incubation with oleic acid was sufficient to reduce the total cell fluorescence such that there was a non-significant difference to untreated cells, and there was a significant difference to F900742 treated cells.

#### 4.2.7.2 Palmitoleic acid

Ole1p can insert a cis-double bond between carbon 9 and 10 of both palmitoyl CoA and stearoyl CoA to produce the monounsaturated C16 and C18 products palmitoleic acid and oleic acid, respectively. Like oleic acid, it has been previously identified that palmitoleic acid can rescue the growth of both *S. cerevisiae* and *C. albicans* mutants for various components of the OLE1 pathway (154,166,167). Figure 4.9 identified that oleic acid was sufficient to inhibit the relocalisation of Ole1p-GFP and the concurrent increased fluorescence. 1 mM of palmitoleic acid was also sufficient to inhibit the formation of Ole1p-GFP puncta in cells treated with F900742 (Figure 4.11A). No puncta or tubes were observed in any of the imaged cells treated with F900742 and palmitoleic acid. Furthermore, palmitoleic acid induced a reduction in the amount of Ole1p-GFP irrespective of F900742 supplementation. 60 minutes of co-treatment with palmitoleic acid and F900742 was sufficient to induce a significant difference between Ole1p-GFP compared to F900742 only. There was a continual decrease in the amount of Ole1p-GFP in both samples treated with palmitoleic acid throughout the experiment. There was no significant difference in Ole1p-GFP expression between either sample treated with palmitoleic acid at any time point (Figure 4.11B).

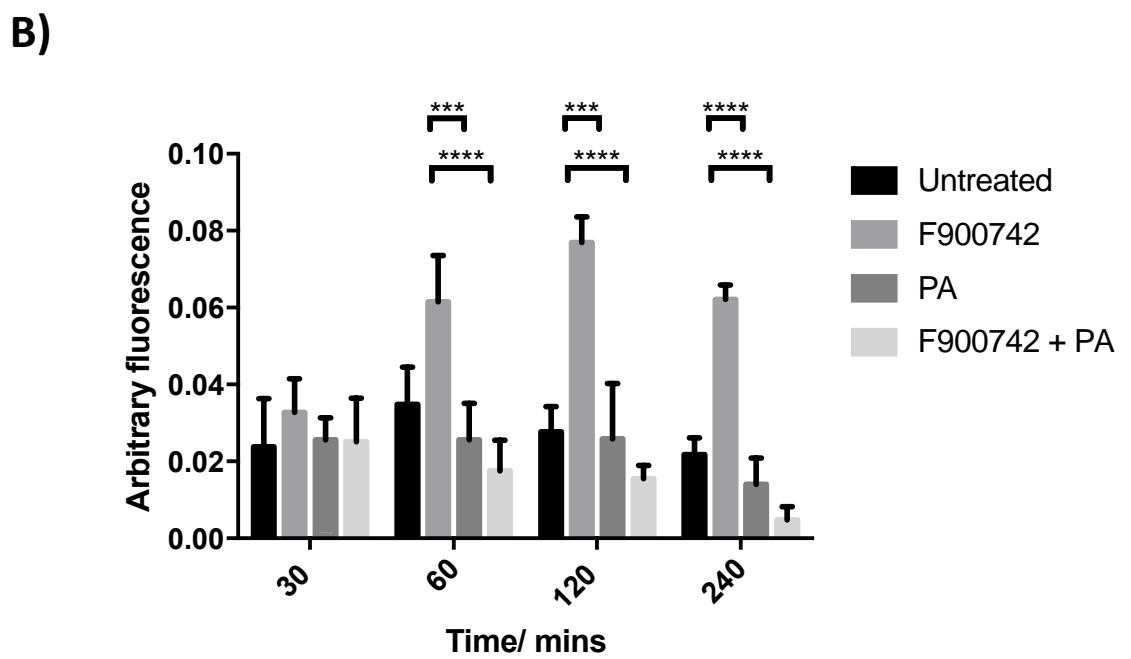
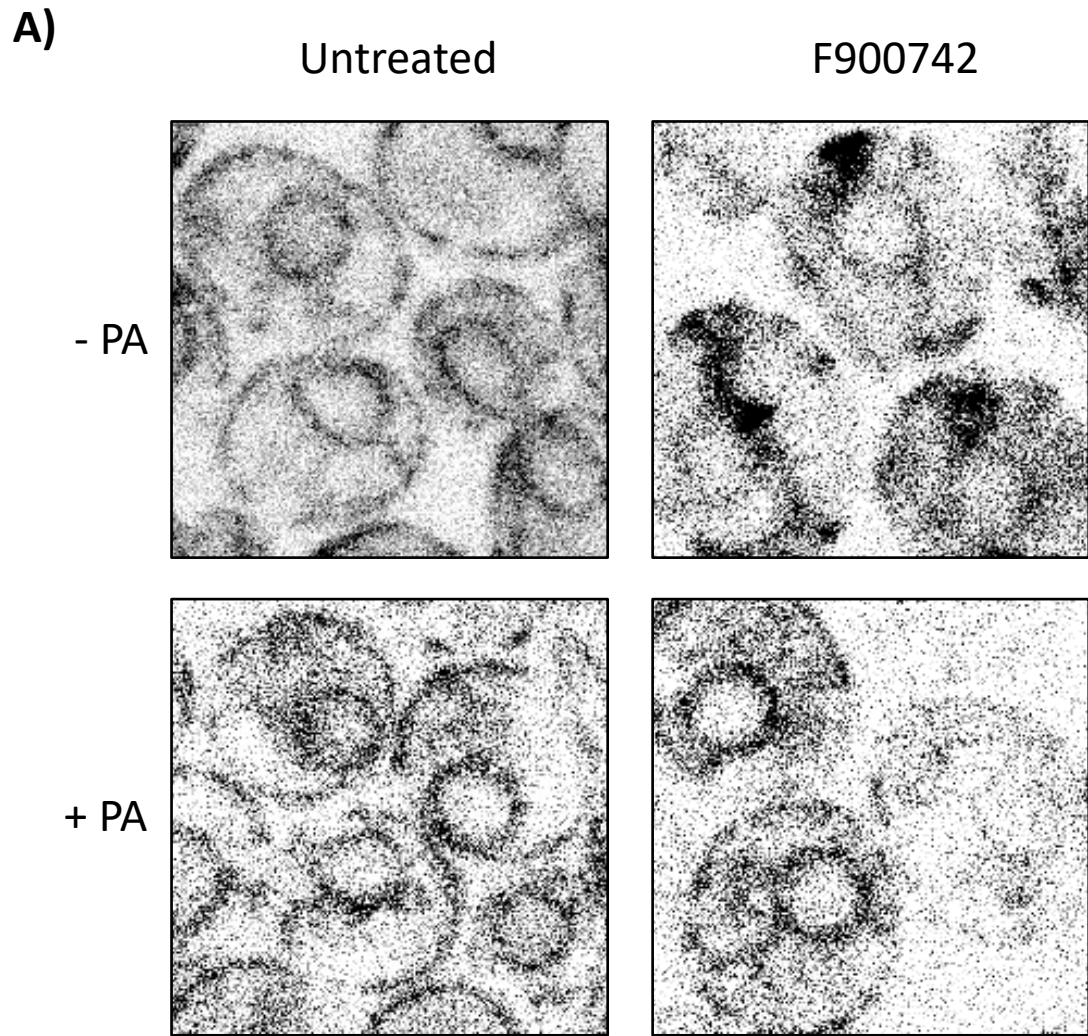


**Figure 4.11. Palmitoleic acid inhibited the activity of F900742.** (A) 1mM Palmitoleic acid inhibited the F900742-induced relocalisation of Ole1p-GFP to puncta and tubes. No redistribution was observed in any cell treated with F900742 and palmitoleic acid. Irrespective of F900742 supplementation, palmitoleic acid induced a visual decrease in the amount of Ole1p-GFP relative to the untreated sample. (B) Palmitoleic acid prevented the increase in fluorescence as a result of F900742 treatment. There was a significant difference in Ole1p-GFP expression after 60 minutes between samples treated with F900742 only or F900742 and palmitoleic acid. There was no significant difference between the two samples treated with palmitoleic acid at any time point. F900742 was added at 100 µg/ml. Samples were grown at 30 °C. N = 4.

Earlier data confirmed that oleic acid reversed the redistribution of Ole1p-GFP and reduced the average cellular fluorescence to that of untreated samples (Figure 4.10). To investigate whether palmitoleic acid had the same reversal effects as oleic acid, 1 mM palmitoleic acid was added to cells that had been pre-treated with F900742 for 2 hours. Cells were washed and resuspended in fresh YPD prior to palmitoleic acid addition. Palmitoleic acid induced the complete redistribution of Ole1p-GFP to wild type ER localisation by 120 minutes. Ole1p-GFP relocated by forming elongated puncta most often at the periphery of the cell following after a 30 minute incubation with palmitoleic acid which further elongated, and reduced in number, by 60 minutes (Figure 4.12A). Palmitoleic acid reduced the amount of Ole1p-GFP to a level that was not significantly different from the untreated sample after 30 minutes (Figure 4.12B). This was associated with a significant difference to the drugged sample. The amount of Ole1p-GFP continued to decrease in response to palmitoleic acid exposure throughout the duration of the experiment.



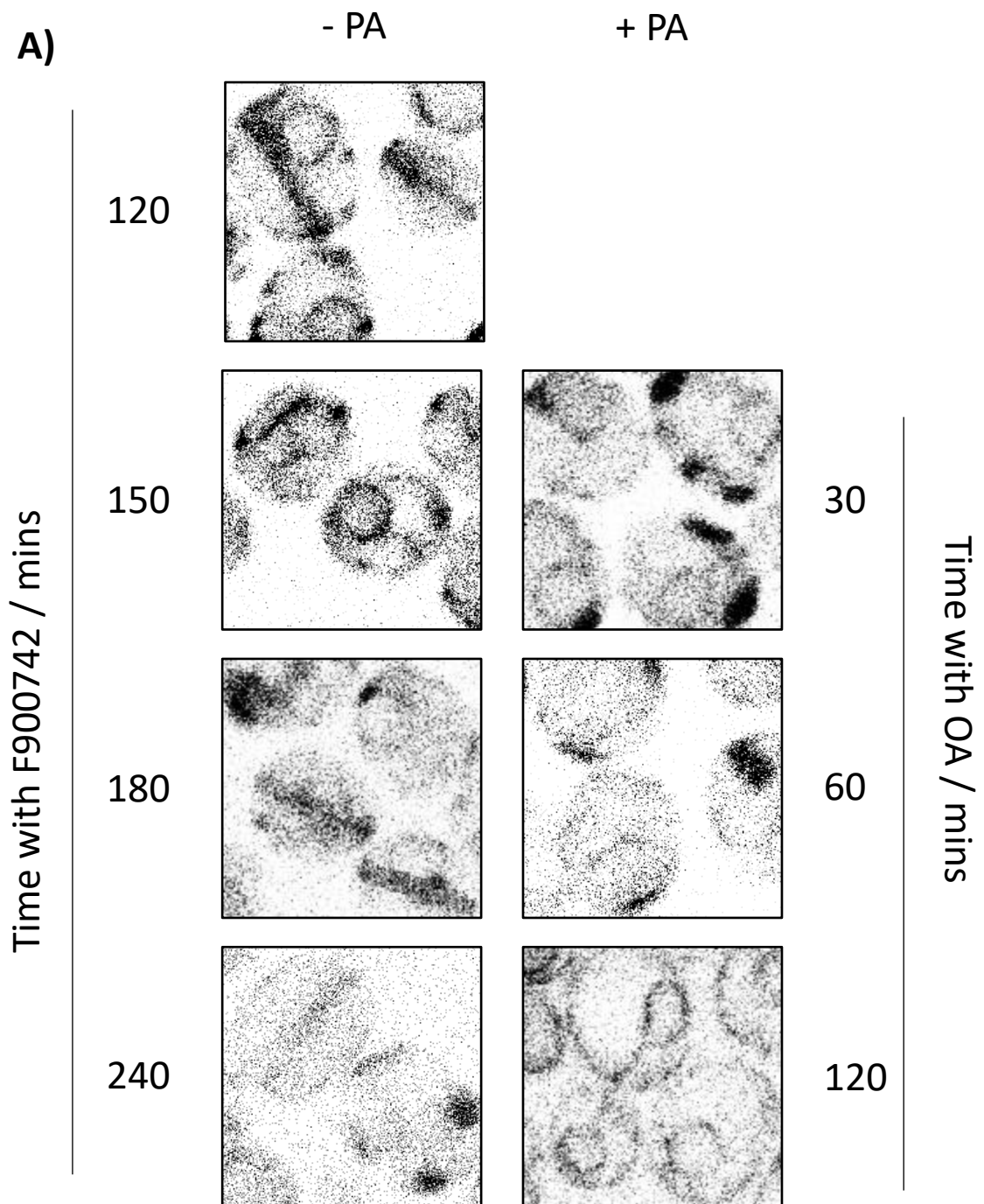
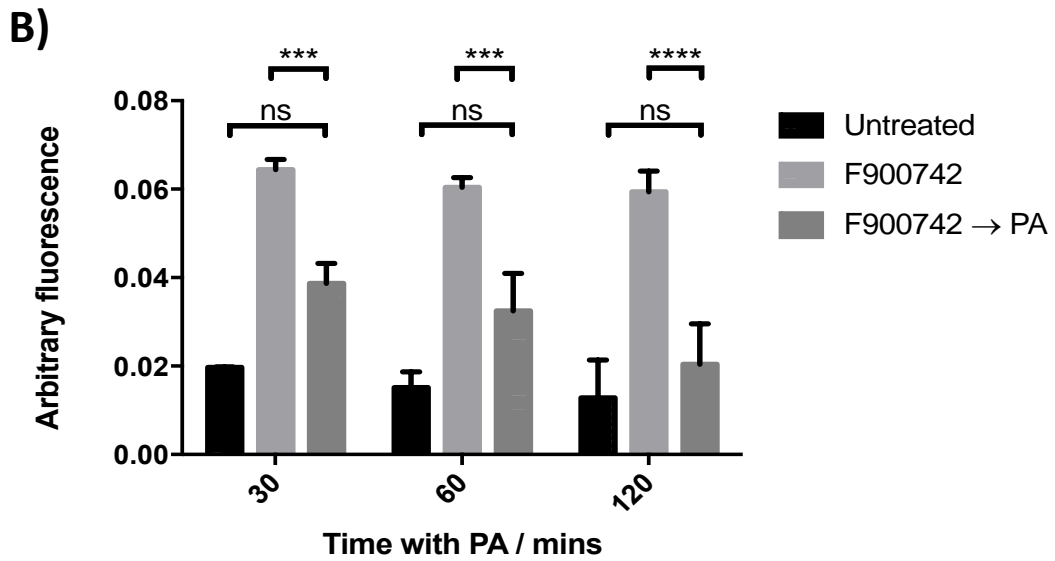


Figure 4.12 continues over page



**Figure 4.12. Palmitoleic acid reversed the relocalisation and increased expression of Ole1p.** (A) 1 mM Palmitoleic acid induced elongation of F900742-induced Ole1p-GFP puncta after 30 minutes. The number of puncta per cell reduced by 60 minutes, and Ole1p-GFP was observed to have a normal ER localisation with no puncta after 120 minutes. (B) 30 minutes with palmitoleic acid was sufficient to reduce the amount of Ole1p-GFP such that there was not a significant difference to the untreated sample and there was a significant difference with F900742. F900742 added at 100  $\mu$ g/ml. N = 3.

*In vivo*, cells adjust the expression of OLE1 in response to exogenous palmitoleic acid and oleic acid. Both monounsaturated fatty acids are present simultaneously at physiologically relevant levels and both modulate the expression of OLE1. Palmitoleic acid or oleic acid individually did significantly reduce the amount of Ole1p-GFP and reversed the punctate relocalisations induced by F900742. Next it was investigated whether together oleic acid and palmitoleic acid had a more profound effect on inhibiting the activity of F900742 (Figure 4.13). As noted in both reversal experiments with a single unsaturated fatty acid, together oleic acid and palmitoleic acid were able to induce a reduction in amount of Ole1p-GFP after 30 minutes of treatment. There was a greater reduction in the number of remaining Ole1p-GFP puncta by 60 minutes when both unsaturated fatty acids were added compared to just either one (Figure 4.13A). Furthermore, following 120 minutes with both unsaturated fatty acids, Ole1p-GFP appeared to have a more even distribution throughout the cytosol, with only a slight enrichment at the ER. This was not observed in the recovery of Ole1p-GFP relocalisation when either of the unsaturated fatty acids were added alone (Figure 4.10 and Figure 4.12).

Overall, there was a greater reduction in the amount of Ole1p-GFP expression when both oleic and palmitoleic acid were added together, however either alone is sufficient to induce significant reductions in the amount of protein

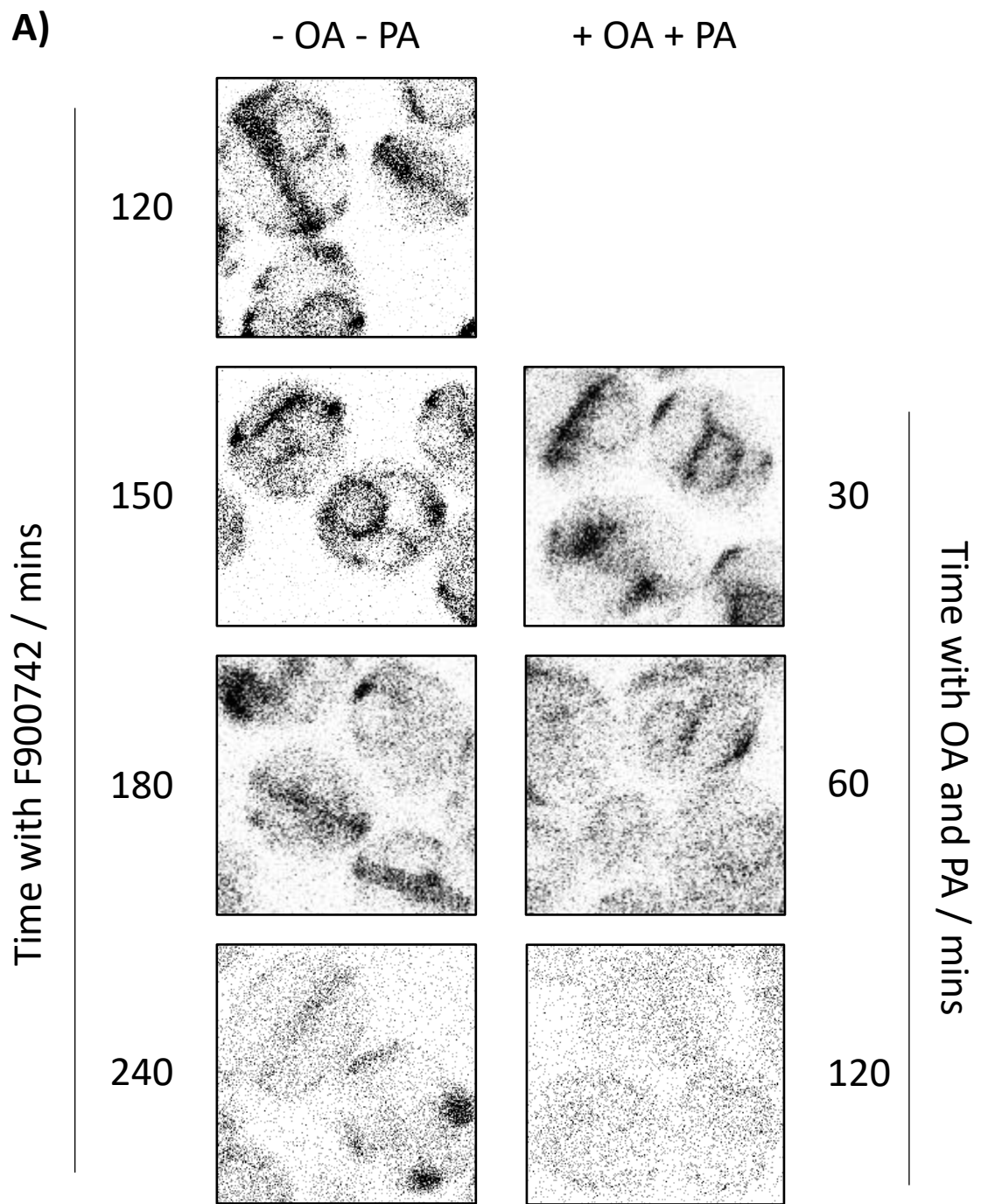
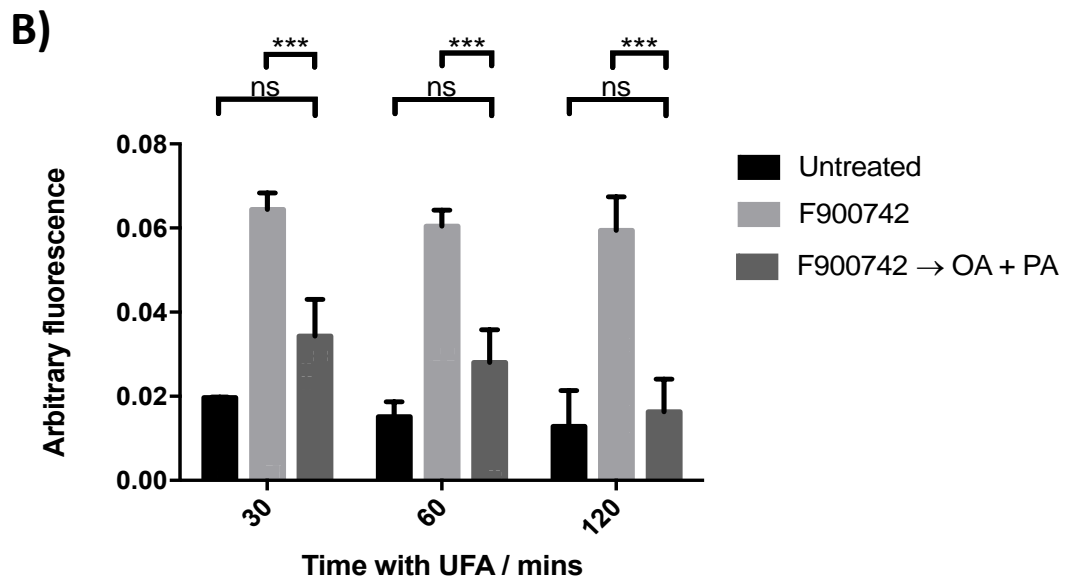


Figure 4.13 continues over page

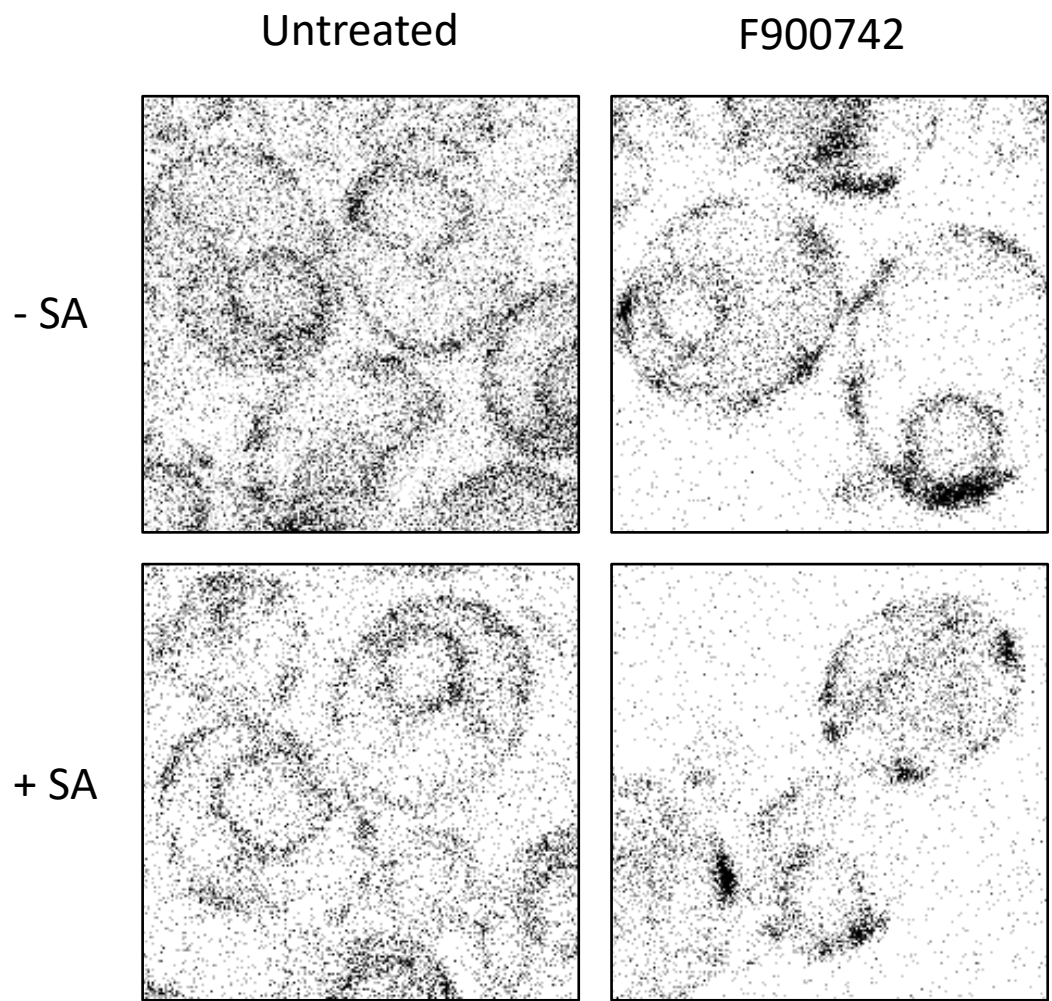


**Figure 4.13. Oleic acid and palmitoleic acid inhibited and reversed F900742 activity.** (A) Unsaturated fatty acid supplementation induced the elongation of Ole1p-GFP puncta after 30 minutes of incubation. There was a substantial reduction in the number of cells containing relocated Ole1p-GFP by 60 minutes. No observed cell contained redistributed Ole1p-GFP after 120 minutes of incubation with oleic acid and palmitoleic acid. The addition of the unsaturated fatty acids was also associated with a reduction in Ole1p-GFP expression. (B) The addition of oleic acid and palmitoleic acid induced a reduction in Ole1p-GFP expression after 30 minutes such that there was not a significant difference to the untreated sample and there was a significant difference to the F900742 treated cells. F900742 was added at 100  $\mu\text{g}/\text{ml}$ . Oleic acid and palmitoleic acid were both added at 0.5 mM. 0.5 mM of oleic acid and palmitoleic acid was added to samples. 100  $\mu\text{g}/\text{ml}$  F900742 was used. Samples were incubated at 30  $^{\circ}\text{C}$ . N = 3.

#### 4.2.7.3 Stearic acid

Stearic acid is a saturated C18 fatty acid that is essential in the human diet and, unlike other saturated fatty acids, circulating levels have been linked to some health benefits (168). Stearic acid can be synthesised through the elongation of palmitic acid (C16:0) by elongases or can be obtained in the diet through meats and butters. Stearic acid is the precursor for its unsaturated counterpart, oleic acid (C18:1), that is synthesised by a desaturation reaction catalysed by Ole1p. To investigate the saturated fatty acid effects on F900742, 1mM of stearic acid was added at the same time as F900742. Unlike either of the unsaturated fatty acids, stearic acid did not inhibit Ole1p-GFP relocalisation (Figure 4.14A), nor did it inhibit the associated increase in amount of Ole1p-GFP fluorescence (Figure 4.14B). Stearic acid alone did not affect the expression of Ole1p-GFP relative to the untreated sample. During the initial screening phase, F2G showed that F900742 was inhibited by unsaturated fatty acids, but not saturated fatty acids. Here, I have shown that F900742 induced Ole1p-GFP to relocalise to puncta or tubes within BY Ole1-GFP cells and that this event is lipid-dependent. The relocalisation of Ole1p is prevented by the unsaturated fatty acids oleic acid and palmitoleic acid, but not the saturated fatty acid stearic acid.

A)



B)

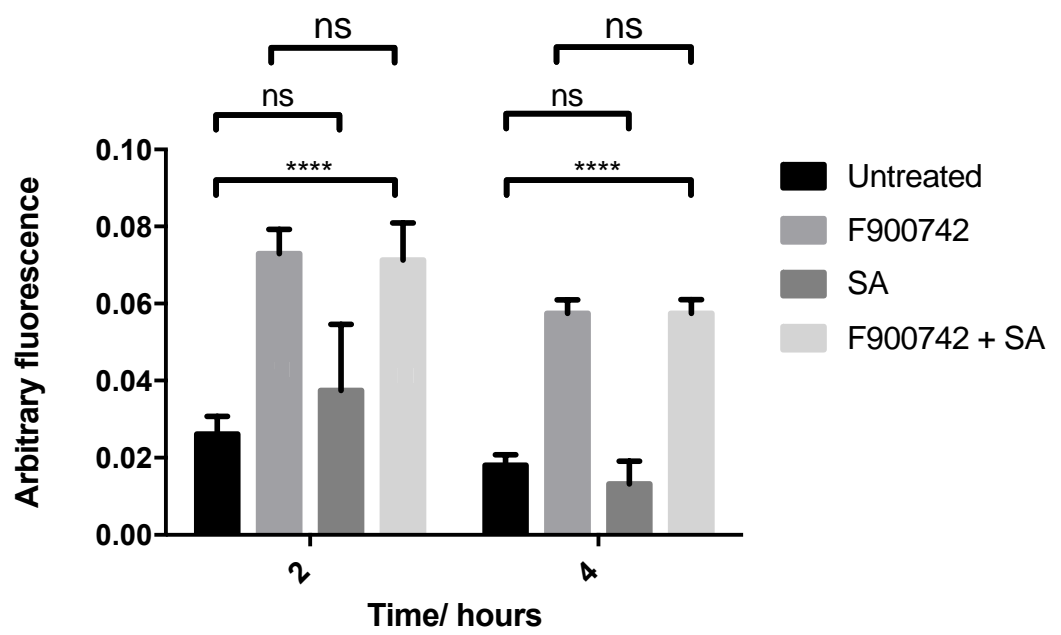


**Figure 4.14. Stearic acid did not reverse F900742 activity.** (A) 1 mM Stearic acid did not reverse the redistribution of Ole1p-GFP when added with F900742. Stearic acid addition did not interfere with Ole1p-GFP localisation nor the amount of protein at the ER. (B) Quantification of fluorescence confirmed that there was no significant difference in amount of Ole1p-GFP between samples treated with F900742 supplemented with stearic acid compared to drug alone after either 2 or 4 hours. There was a significant difference in fluorescence between the untreated sample and both samples treated with F900742, irrespective of stearic acid supplementation (significance between untreated and F900742 unlabeled here, but shown in figure 4.12). Stearic acid alone did not induce any significant growth effects relative to the untreated sample. F900742 added at 100 µg/ml. Samples were incubated at 30 °C. N = 3.



Thus far it has been demonstrated that the endogenous products of  $\Delta 9$  desaturases, the unsaturated fatty acids oleic acid and palmitoleic acid, can reverse the activity of F900742. Either of the unsaturated fatty alone or in combination were sufficient to reverse the antifungal growth phenotype induced by F900742 and the relocalisation of Ole1p. In contrast, the substrate of this enzyme, stearic acid, was insufficient to reverse the activity of F900742.

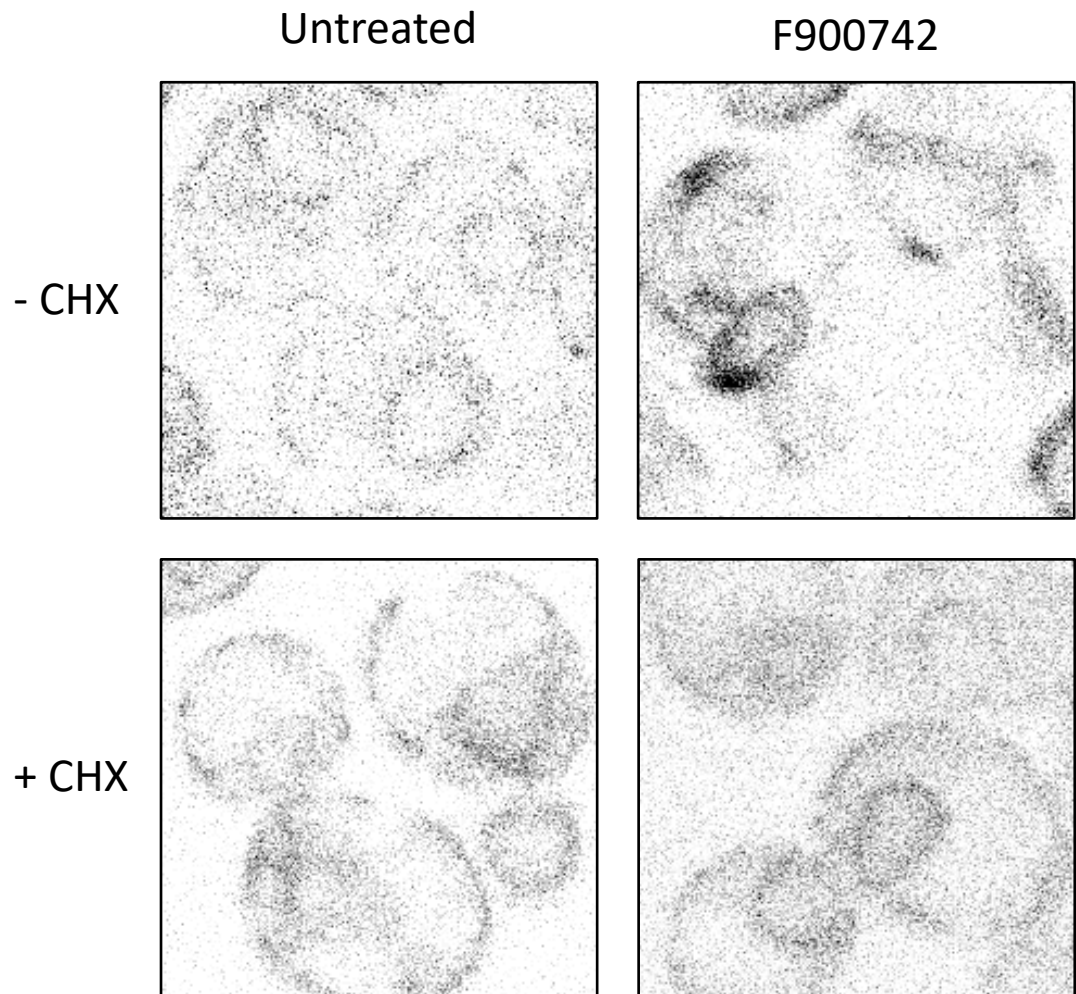
#### **4.2.8 F900742 initiated an increase in Ole1p-GFP protein synthesis**

As discussed in more detail in the introduction, it is essential that Ole1p is tightly regulated. Mechanisms to alter the expression of Ole1p at the level of transcription and mRNA stability in response to various stimuli, including diet, temperature and hypoxia are conserved throughout eukaryotes (131,138,139).

So far, data has shown that F900742 initiated a redistribution of Ole1p and induced an increase in Ole1p-GFP fluorescence. Cycloheximide (CHX) exerts its effects as a pan-inhibitor of the translational elongation steps in protein synthesis by interfering with the movement of tRNA and mRNA in relation to the ribosomes (169). To investigate the increase in fluorescence of Ole1p-GFP as determined by measuring the arbitrary fluorescence of confocal images, cells were grown to log phase and were treated with F900742 and cycloheximide simultaneously. Cycloheximide was sufficient to inhibit the redistribution of Ole1p-GFP in any cells treated with both the protein synthesis inhibitor and F900742 (Figure 4.15A). Importantly, although cycloheximide is a non-specific protein synthesis inhibitor, it did not interfere with the localisation of Ole1p-GFP to the ER, nor the morphology of the ER. Furthermore, cycloheximide inhibited the increase in average cellular fluorescence induced by F900742 such that there was no significant difference between the untreated sample and F900742 + cycloheximide after 2 or 4 hours of treatment (Figure 4.15B). Cycloheximide induced a significant difference between F900742 only and with the addition of cycloheximide. This data suggested that the increase in Ole1p-GFP fluorescence was due to an increase in *de*

*novo* protein synthesis of the desaturase. It is likely that the newly synthesised proteins were redistributing to the puncta or tubes.

A)



B)

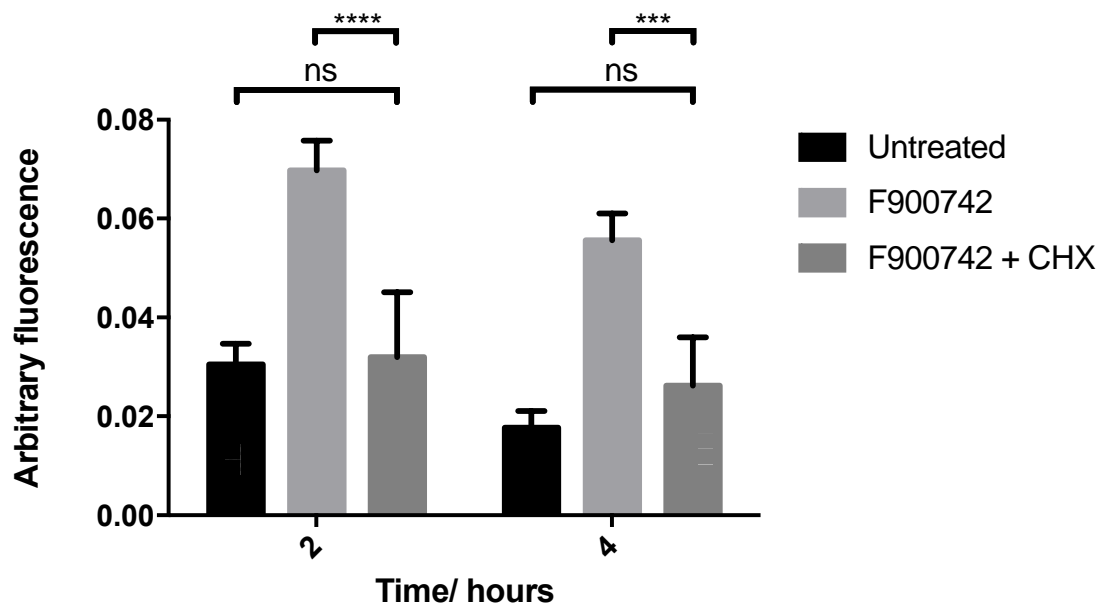


**Figure 4.15. F900742 induced an increase in OLE1 transcription.** (A) BY Ole1-GFP were treated with F900742 and cycloheximide for 4 hours. Cycloheximide was sufficient to inhibit the relocalisation of Ole1p-GFP. None of the imaged cells contained Ole1p-GFP puncta or tubes after treatment with cycloheximide and F900742. (B) Quantification of fluorescence. Treatment with cycloheximide inhibited the de novo synthesis of Ole1p-GFP. Samples treated with F900742 and cycloheximide were associated with a non-significant difference in fluorescence to the untreated sample, whereas there was a significant difference between F900742 and F900742 with cycloheximide samples. F900742 was added at 100  $\mu\text{g}/\text{ml}$ . Cycloheximide was added at 10  $\mu\text{g}/\text{ml}$ . Samples were incubated at 30  $^{\circ}\text{C}$  for 4 hours. N = 3.

#### 4.2.9 F900742 altered the expression of Ubx2p and Sct1p

The precise mechanism(s) by which OLE1 is transcriptionally activated remain to be determined, however it requires the processing of the transcriptional activators Mga2p and Spt23p via a series of ubiquitination reactions involving Ubx2p as a tethering complex to the activation machinery and subsequent cleavage into their active forms (136). *Δubx2* cells exhibit a reduction in OLE1 mRNA and a 40% reduction in Ole1 enzyme level relative to wild type, and is associated with a shift in the lipidome to more saturated lipid species (91). To investigate whether there was also an increase in the transcriptional regulators of OLE1, the expression and localisation of Ubx2p-GFP was assessed. BY Ubx2-GFP cells were treated with F900742 for 4 hours. Ubx2p-GFP is an ER transmembrane protein that localised to similar puncta and tubular structures that were observed in BY Ole1p-GFP (Figure 4.16A). Furthermore, F900742 induced an increase in Ubx2p-GFP expression which was not unexpected given Ubx2p regulates the expression of Ole1p and F900742 has been shown to induce the protein synthesis of Ole1p (Figure 4.16B). There was an increase in Ubx2p-GFP expression after 30 minutes which increased further by 60 and again at 120 minutes. As with Ole1p-GFP, there was a slight reduction in Ubx2p-GFP expression by 240 minutes.

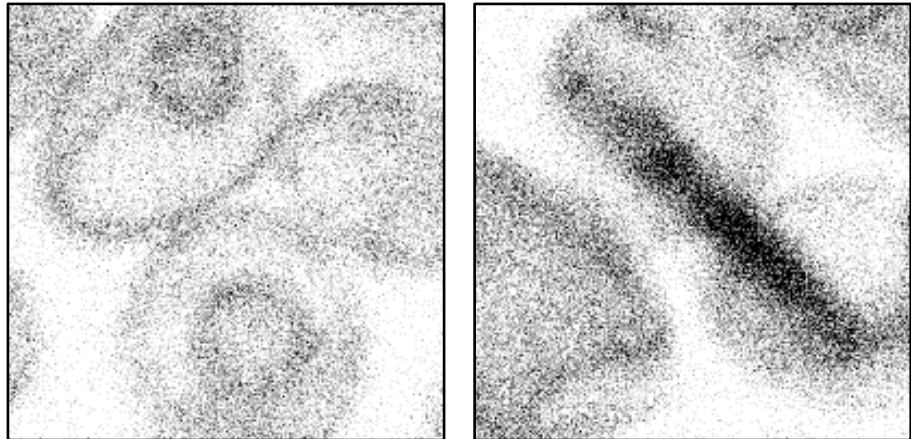
The activity of Ole1p is negatively regulated through competition with Sct1p for the substrates C16 and C18 saturated CoA (147). Sct1p binds to saturated CoA and sequesters them into saturated lipids, whereas Ole1p desaturates acyl chains to generate unsaturated lipids. Therefore, there is a seesaw balancing act between the expressions of Ole1p and Sct1p to ensure that correct membrane lipid content is maintained. Excess saturated or unsaturated fatty acids can induce lipotoxicity, therefore cellular protective mechanisms ensure that excess saturated fatty acids are either stored in lipid droplets or sequestered by Sct1p into saturated lipids. F900742 induced the relocalisation of Sct1p-GFP to tubes and puncta in greater than 80% of observed cells at 4 hours (Figure 4.16C), however this was associated with an overall decrease in amount of Sct1p-GFP at 2 hours and further at 4 hours (Figure 4.16D). There was a significant difference in expression of the untreated and treated at both 2 and 4 hours.

A)

BY Ubx2-GFP

Untreated

F900742



B)

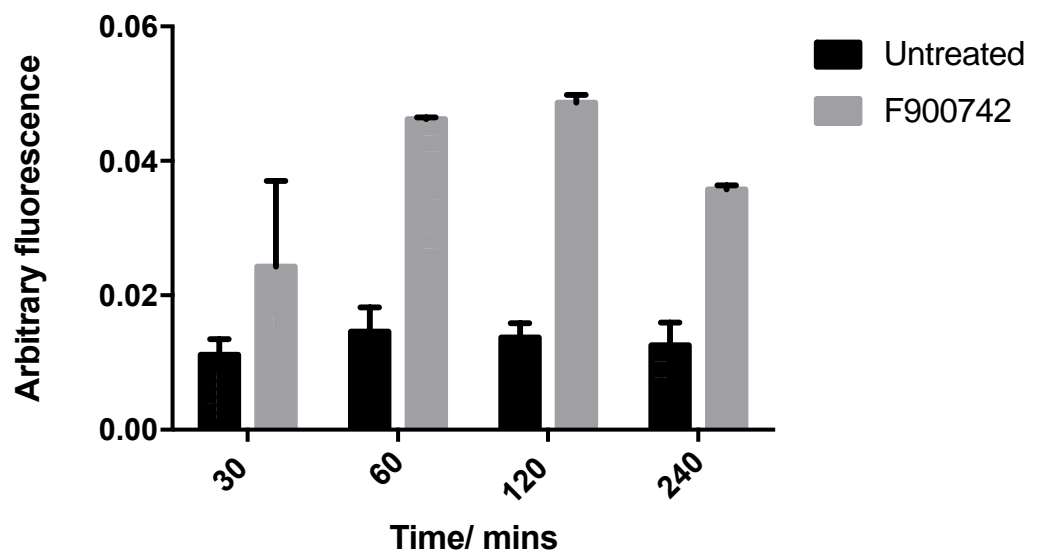
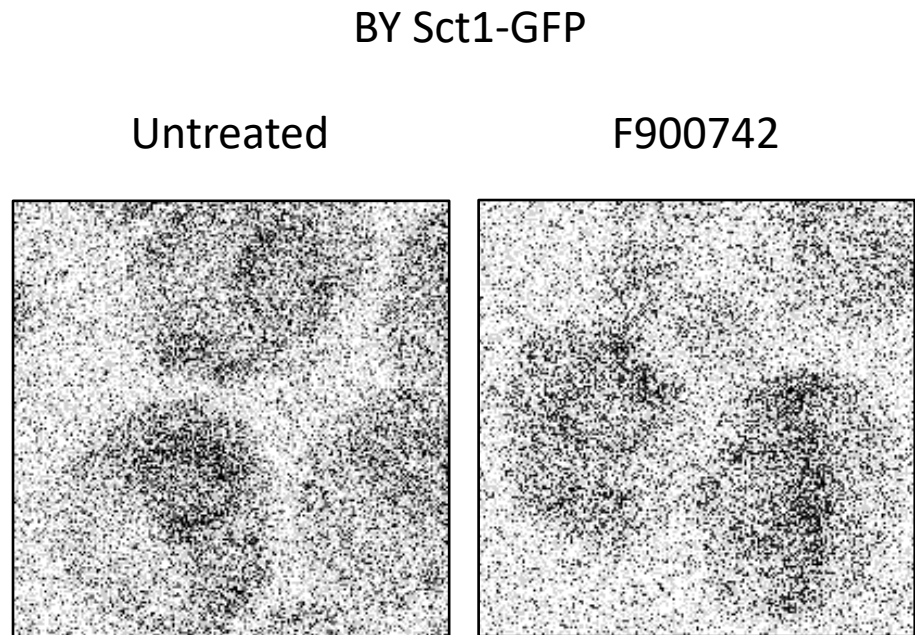
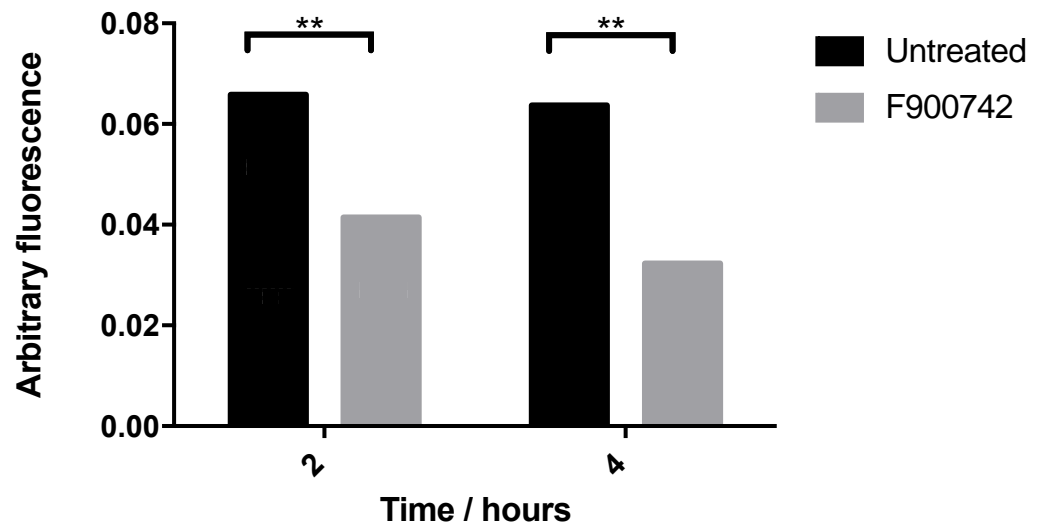


Figure 4.16 continues over page

C)



D)



**Figure 4.16. F900742 induced the relocalisation of Ubx2p-GFP and Sct1p-GFP.** (A) A 2 hour incubation with 100  $\mu\text{g/ml}$  F900742 was sufficient to induce the redistribution of Ubx2p-GFP to tubes and puncta in 80% of cells observed. (B) There was an increase in Ubx2p-GFP expression after a 30 minute incubation with F900742. The amount of fluorescence further increase at both the 60 and 120 minute readings, but decreased slightly after 240 minutes. (A and B)  $N = 2$ . (C) F900742 induced a redistribution of Sct1p-GFP to puncta and tubes in 40% of cells. The overall expression of Sct1p-GFP visually decreased after 2 hours with the drug. (D) There was a significant decrease in the expression of Sct1p-GFP after 2 hours in samples treated with F900742 relative to the untreated control. There was a further decrease in Sct1p-GFP expression after 4 hours. Samples were incubated at 30  $^{\circ}\text{C}$ .  $N = 3$ .

### 4.3 Discussion

The experiments presented in this chapter used confocal microscopy to identify the localisation of a GFP tagged version of Ole1p in *S. cerevisiae*. Experiments confirmed that:

- 1) F900742 induced unsaturated lipid-dependent relocalisation of Ole1p
- 2) F900742 induced an increase in Ole1p expression at the transcriptional level
- 3) The relocalisation of Ole1p-GFP was rapid and reversible

The data presented in this chapter extended the pan antifungal activity of F900742 to include *S. cerevisiae*. The MIC of F900742 in *S. cerevisiae* was approximately 100 times greater than the MICs of pathogenic fungi identified by F2G in table 4.1. This could be due to inherent difference between fungal species or could be due to difference in the media that the *S. cerevisiae* and the pathogenic fungi MIC testing was performed in. Per the EUCAST and CLSI recommendations, F2G performed the MICs in RPMI media. This media contains a low level of lipid. However, *S. cerevisiae* are unable to grow sufficiently in RPMI so these strains were grown in YPD – a nutrient rich media that does contain lipids. The expression level of Ole1p has been previously shown to be negatively regulated by supplementation of external unsaturated fatty acids and therefore it is possible that the requirement of *S. cerevisiae* for Ole1p is much less when grown in YPD than the requirements of the pathogenic fungi for this enzyme in RPMI.

F900742 induced the relocalisation of Ole1p-GFP, mCherry-Ole1p, Ubx2p-GFP, and Sct1p-GFP. All proteins relocalised to dense puncta that appeared at the cell periphery and cytosolic compartments, as well as to long tubes that stretched the length of the cell. The puncta increased in size, but decreased in number with longer treatments. Concurrent with the relocalisation of these proteins was an increase in amount of Ole1p and Ubx2p, but a decrease in the amount of Sct1p. The increase in expression of Ole1p-GFP was due to an increase in transcription of OLE1. Furthermore, the relocalisation of Ole1p, as well as the increase in expression of this protein, was shown



to be lipid dependent: either of the products of Ole1p (oleic acid and palmitoleic acid), but not the saturated substrate (stearic acid), were sufficient to prevent the punctate distribution of Ole1p-GFP and the associated increase in protein expression induced by F900742, and were sufficient to induce a redistribution of Ole1p-GFP to that of wild type within 30 minutes. Importantly, the possibility that Ole1p relocates upon exposure to antifungals that act independently of the OLE1 pathway was eliminated as no Ole1p redistribution was noted when cells were exposed to the polyene amphotericin B.

Previous studies have demonstrated that chemical or genetic inhibition of Ole1p activity results in a lipid profile that has an increase in the amount saturated lipid species at the expense of the unsaturated counterparts (91,147,157). Alterations to the lipid balance via disruption to the OLE1 pathway requires the induction of Ole1p expression or the supplementation of unsaturated fatty acids for cells to remain viable (116). It was predicted that F900742 inhibited Ole1p that rendered cells with an aberrant lipid profile that was skewed towards a more saturated lipidome thereby activating processes to induce the expression of the desaturase. The data presented in this chapter suggested a feedback mechanism whereby a 60 minute treatment with F900742 was sufficient to inhibit the activity of Ole1p which the yeast responded to by increasing the transcription of OLE1 and localising Ole1p-GFP to puncta and tubes. Inferring from previous studies, it is likely that the inhibition of Ole1p activity by F900742 reduced the desaturation content of free fatty acid pools and membrane lipids to potentially lipotoxic levels. This would induce a reduction in membrane fluidity. Mga2p, and possibly Spt23p, would sense the alterations in membrane physicochemical properties. In a bid to increase the cell's desaturated lipid content, Mga2p would dimerise and rotate within the ER membrane with subsequent recruitment of the proteasome and ultimately driving the activation of OLE1 transcription. This would increase the amount of Ole1p available for fatty acid desaturation. Concurrent with the increase in OLE1 transcription, there was a decrease in the competitor of Ole1p, Sct1p, which is likely to ensure the availability of the maximum number of saturated acyl chains for Ole1p. Despite the increase in Ole1p expression after 60 minutes, it is likely that the amount of drug overwhelmed the

desaturase resulting in no desaturase activity and a further build-up of saturated lipids and an additional increase in the amount of Ole1p by 120 minutes. There was a slight reduction in amount of Ole1p-GFP between 120 minutes (2 hours) and 240 minutes (4 hours) after drug addition. This could be explained either by the natural metabolic shifts that occur within *S. cerevisiae* over a 4 hour period requiring less Ole1p as the yeast are exiting from a rapid growth (logarithmic) phase and entering into a more stationary, slower growth phase, or it could be due to some populations of cells dying due to lipotoxicity. The mechanism of drug action is investigated further in chapter 6. However, it is important to note that although data identified unsaturated fatty acids, but not saturated fatty acids prevent and reverse phenotypes induced by F900742, this does not confirm that Ole1p is the target of F900742. Further to studies to investigate the target of F900742 were performed in chapter 5.

Additional studies would help to cement the positive feedback loop suggested above. Understanding whether F900742 does indeed induce an alteration in the lipidome after 60 minutes and whether this is sufficient to induce lipotoxic protective responses remain to be established. Whole cell lipidomic approaches, such as thin layer chromatography or mass spectroscopy, could be utilised to investigate the lipidome at various time points after F900742. Potential alterations in the lipidome could then be married to changes in membrane fluidity using the fluorescent dye laurdan and alterations in the expression of Ole1p via real time-PCR. Furthermore, as with the temperature sensitive mutants used in Tatzler et al (157), the physiological purpose, if any, of Ole1p relocalisation remains to be determined. Aberrant ultrastructural features of *S. cerevisiae* induced by F900742 was investigated in chapter 6.

# CHAPTER 5

## F900742 target verification

### 5.1 Introduction

Data presented in chapter 4 identified the mislocalisation of Ole1p and its regulators as a consequence of F900742 exposure in *S. cerevisiae*. Alongside the relocalisation of the desaturase, C16 and C18 unsaturated fatty acids, but not saturated fatty acids, reversed the action of F900742 suggesting that inhibition of the Ole1p pathway is essential for drug activity. However, difficulties in confirming that F900742 inhibits Ole1p stem from the challenges in purifying membrane proteins: Ole1p has four transmembrane domains that anchor it to the ER. To date, no group has reported the successful purification of Ole1p, therefore it is not currently possible to develop an *in vitro* assay utilising purified Ole1p, nor is it possible to obtain a drug-protein crystal structure. To confirm the target of F900742 was Ole1p, a series of mutagenesis experiments were (Aim 2, 3, 4). This approach is also not without limitations. OLE1 is an essential gene; its deletion renders cells non-viable unless grown in the presence of C16 or C18 unsaturated fatty acids (165), therefore the mutagenesis experiments must not interfere with the functional viability of the desaturase or risk lipotoxicity and cell death.

The structure of Ole1p has not been resolved, which makes the design of fungi-specific inhibitors challenging. The majority of structural information about the *S. cerevisiae* desaturase has been inferred from crystal structures of the mouse and human Scd1 isoforms (125,128). Assuming F900742 targets Ole1p, this protein is conserved throughout eukaryotes and could risk severe adverse and intolerable effects to patients through non-selective inhibition of both the human and the yeast  $\Delta 9$  desaturase. To overcome this potential barrier to clinical use, it is possible to design the drug such that it targets sequence differences at the active site between the human and fungal (for example *Aspergillus* and *Candida*) enzymes. F2G employed a rational, activity-function structural design process that aimed to ensure F900742

targeted sequence differences between the human and fungal active sites. Much of the structural information on Ole1p is based on inferences from the mammalian isoforms and conservations between residues throughout eukaryotic species. Truncated forms of the human and mouse Ole1p isoform, Scd1, have been crystallised. The development of techniques to isolate and purify Ole1p will prove invaluable for understanding the OLE1 pathway and provide rational design of Ole1p inhibitors that do not target Scd1.

This chapter aimed to confirm that Ole1p was the target of F900742 through a series of mutagenesis experiments (Aims 2, 3, 4).

## 5.2 Results

### 5.2.1 Deletion of OLE1 reduced the sensitivity of *S. cerevisiae* to F900742

Oleic acid is the C18 monounsaturated product of Ole1p. Uptake of oleic acid from the surrounding environment results in the rapid degradation of Ole1p and its mRNA. In addition, 1mM of oleic acid has been previously shown to be sufficient to sustain growth of cells containing temperature-induced or genetically knocked out reduced levels of Ole1p (157,165). To confirm the dependence of *ole1* null strains for oleic acid, the strain BY  $\Delta ole1$  was taken from a widely available gene deletion collection and grown on YPD agar or YPD supplemented with 1mM oleic acid. BY4741 wild type was used as a control. BY  $\Delta ole1$  was able to grow slowly on the plate supplemented with oleic acid, however there was very minimal growth noted on the YPD only plate (Figure 5.1). There was more BY4741 growth on the plate supplemented with oleic acid than BY  $\Delta ole1$ , and significantly more growth than on the oleic acid null plate

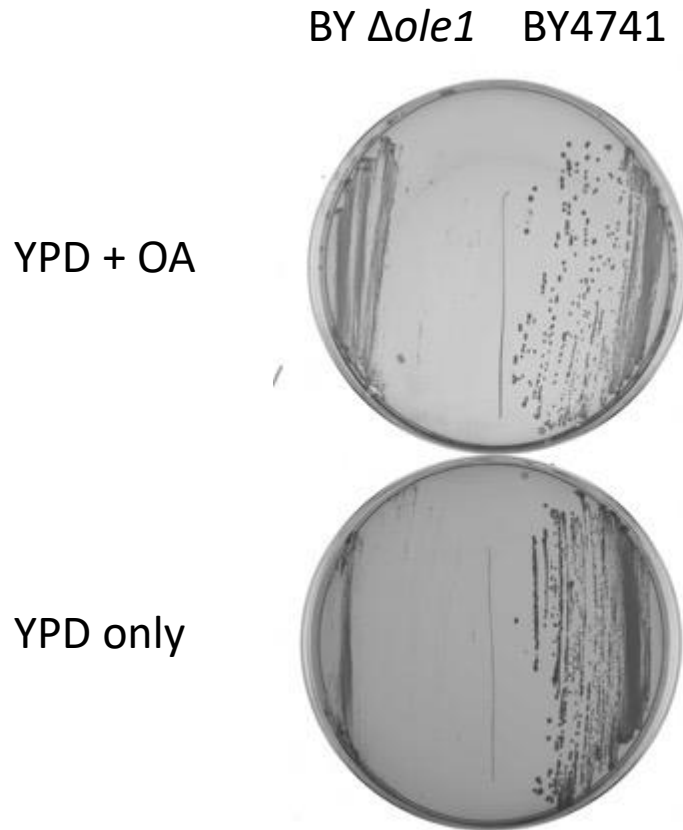


**Figure 5.1. Deletion of OLE1 generated an unsaturated fatty acid auxotroph.** BY4741 wild type and BY  $\Delta ole1$  were grown on either YPD agar or YPD agar that had been supplemented with 1mM oleic acid for 48 hours at 30 °C. Both strains grew on the oleic acid-containing plate. BY  $\Delta ole1$  was unable to grow in the absence of exogenous unsaturated fatty acids. Oleic acid had minimal effects on the growth of BY4741 wild type. N = 1.

Ole1p is the sole  $\Delta 9$  desaturase in *S. cerevisiae*. To validate that Ole1p is the target of F900742, BY  $\Delta ole1$  were grown in liquid media supplemented with drug. The theory was that in the absence of target, the drug would have no effect on cell growth. However, *ole1* null cells require the supplementation of unsaturated fatty acids to remain viable (Figure 5.1) which caused several caveats to this experiment which are discussed in more detail below (130). The growth of BY  $\Delta ole1$  was assessed through measuring the OD 600. BY4741 and BY Ole1-GFP were grown in parallel. As previously demonstrated, BY  $\Delta ole1$  did not grow when the media was not supplemented with

oleic acid, therefore no growth was noted in the untreated or F900742 only samples (Figure 5.2A). In contrast, there was substantial growth of this strain when the media was supplemented with oleic acid. There was also a considerably greater OD 600 in both wild type and BY Ole1-GFP in the presence of the unsaturated fatty acid than YPD only (untreated). Interestingly, the OD 600 was approximately a third less in all three strains when oleic acid together with F900742 was supplemented to the media relative to oleic acid only. Oleic acid and F900742 addition slightly reduced the OD 600 of BY4741 and BY Ole1-GFP compared to the readings of the untreated samples.

It is important to note that there are several major flaws to this experiment due to the requirement for oleic acid supplementation to maintain  $\Delta ole1$  strain viability. Firstly, the addition of oleic acid resulted in the formation of intracellular, cytosolic black dots in all cells. These are assumed to be lipid droplets as a result of excess oleic acid. These are large in size and there were multiple per cell. It was expected that an increase in the number and size of lipid droplets would be sufficient to distort the light path of the spectrophotometer making OD 600 measurement an unreliable method to assess cell growth (135). An increase in the number of lipid droplets observed as black intracellular dots were noted in DIC images taken of samples treated with oleic acid irrespective of F900742 addition (Figure 5.2B. Data not shown for DIC image of F900742 treated cells). Secondly, unsaturated fatty acids negatively regulate the expression of OLE1 suggesting that the expression and function of the desaturase is mostly redundant under these conditions in BY4741 and BY Ole1-GFP. It was predicted that the expression of Ole1p in BY4741 and BY Ole1-GFP grown in media supplemented with oleic acid was lower than is physiologically relevant for desaturase activity as such F900742 was not expected to initiate any cytotoxic effects. However, it is interesting to note that all three strains did demonstrate a reduction in OD when treated with F900742 and oleic acid compared to the fatty acid alone. A possible explanation for this could be an alternative target to Ole1p. This experiment was only repeated twice, therefore statistically significant conclusions cannot be drawn.

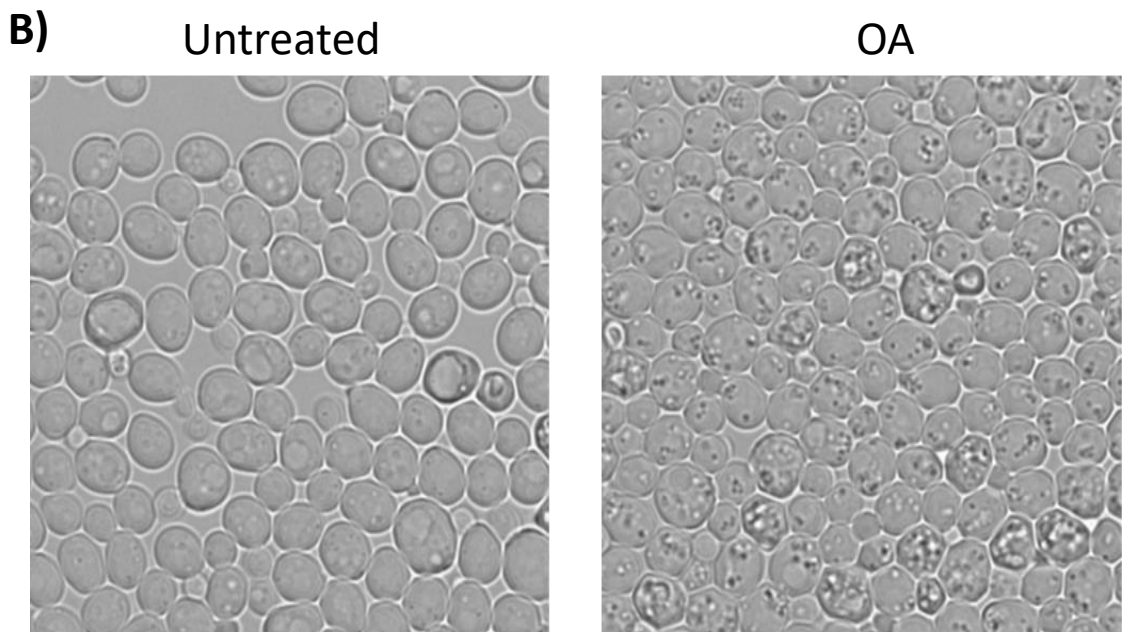
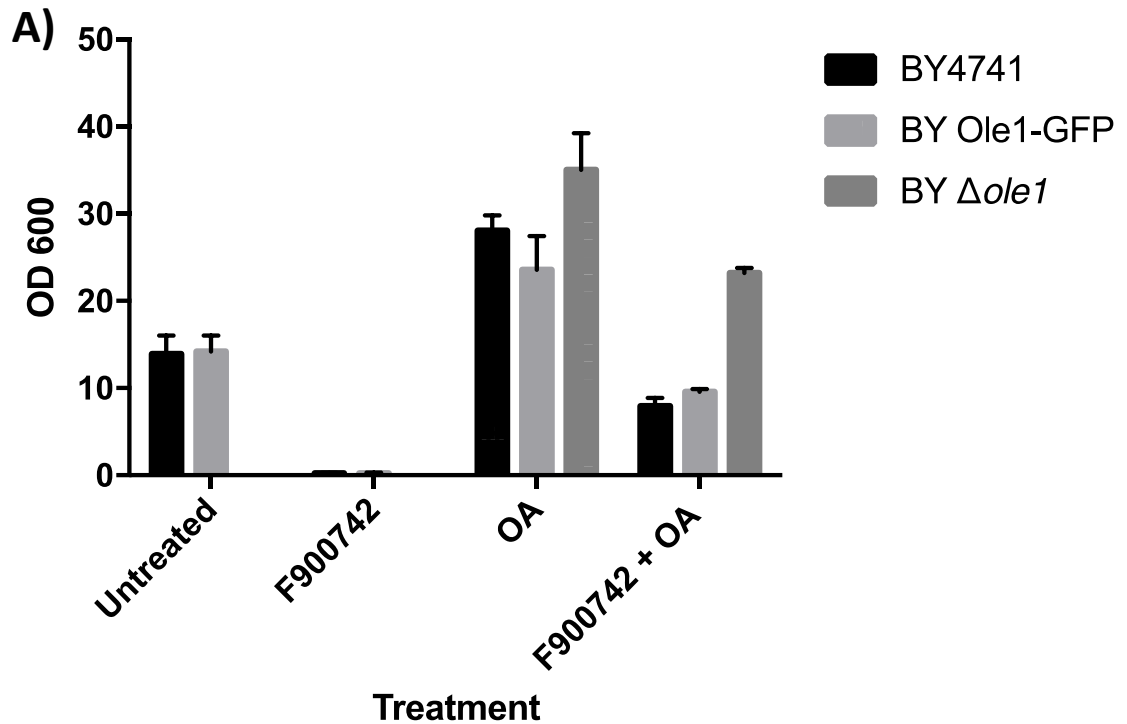


**Figure 5.2. Deletion of OLE1 altered the sensitivity of F900742.** BY4741, BY Ole1-GFP, and BY  $\Delta ole1$  were grown in YPD supplemented with F900742, oleic acid, or F900742 and oleic acid for 24 hours at 30 °C. (A) BY  $\Delta ole1$  did not grow in the absence of exogenous unsaturated fatty acid supplementation. Oleic acid induced a substantially greater OD 600 in BY4741, BY Ole1-GFP, and BY  $\Delta ole1$ . F900742 and oleic acid co-addition reduced the OD 600 in all strains relative to oleic acid only, but was increased relative to F900742 alone or the untreated samples. F900742 was added at 50  $\mu\text{g}/\text{ml}$ . Oleic acid was added at 1mM. N = 2. (B) Supplementation of external oleic acid induced the formation of lipid droplets. Oleic acid, irrespective of F900742 addition, induced an increase in the number and size of lipid droplets as denoted by black dots within cells in DIC field in all cells imaged. In contrast, untreated cells or F900742 treatment only did not induce the accumulation of lipid droplets. Data not shown for DIC image of F900742 treated cells. F900742 added at 100  $\mu\text{g}/\text{ml}$ . Oleic acid added at 1 mM.

To further investigate the possibility of an alternative target to Ole1p, the growth of BY  $\Delta ole1$  was assessed across a ten-fold range of F900742. As before, the media was supplemented with oleic acid to ensure strain viability. There was no significant reduction in cell growth of BY  $\Delta ole1$  after 24 hours of treatment with either 100 or 250  $\mu\text{g/ml}$  F900742 relative to the untreated sample (Figure 5.3). This suggested that it is likely that the reduction noted in OD 600 between samples treated with oleic acid only and oleic acid with F900742 were also non-significant (Figure 5.2A). In comparison, F900742 was active against all other tested *S. cerevisiae* strains containing Ole1p at concentrations lower than 100  $\mu\text{g/ml}$  (Figure 4.2). Both 500 and 1000  $\mu\text{g/ml}$  of F900742 were sufficient for significant growth inhibitory activity (Figure 5.3). This suggested that at very high concentrations of F900742, far higher than is required for antifungal activity in strains containing Ole1p, the drug may have induced growth inhibition by binding to alternative targets. Alternatively, at very high concentrations, the drug could have non-specifically inhibited proteins inducing general cytotoxic mechanisms that inhibited cell growth. As discussed above, there are large caveats with this experiment that stem from the requirement to add oleic acid to the media.



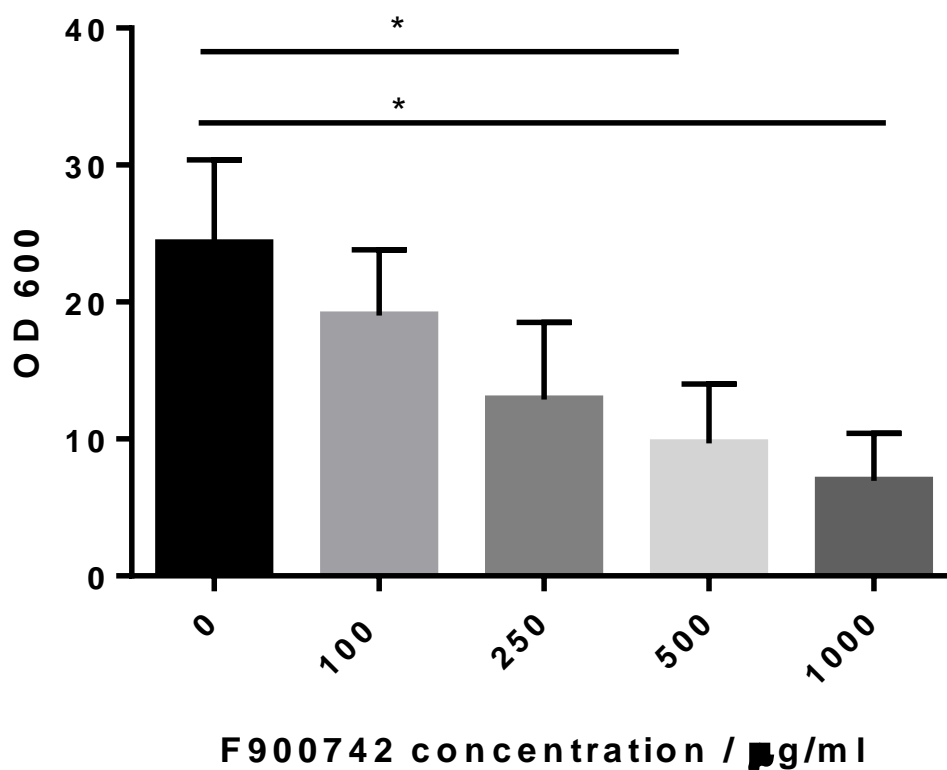


**Figure 5.3. BY  $\Delta ole1$  was sensitive to F900742 at high concentrations.** The OD 600 was used to assess cell growth of BY  $\Delta ole1$  after 24 hours of incubation at 30 °C with F900742 at 100, 250, 500, or 1000  $\mu\text{g/ml}$ . 1 mM of oleic acid was supplemented to the media of all samples to maintain cell viability. F900742 induced a significant reduction in OD 600 at concentrations greater than 500  $\mu\text{g/ml}$ . No significant difference in optical density was noted in samples treated with either 100 or 250  $\mu\text{g/ml}$  F900742, however a significantly reduction was noted in samples treated with 500 or 1000  $\mu\text{g/ml}$ . N = 3.

### 5.2.2 OLE1 overexpression reduced the inhibitory capacity of F900742

Experiments with *ole1* null yeast are hampered by the fact that these cells require the supplementation of oleic acid. An alternative approach to manipulate the expression of Ole1p is to express the protein off exogenous promoters. BY4741 and BY Ole1-GFP both express Ole1p off the endogenous OLE1 promoter, whereas BY mCherry-Ole1 and BY mCherry-Sct1 both contain an mCherry tag at the N terminus of the OLE1 ORF and are expressed off the TEF1 promoter. TEF1 is a highly expressing promoter relative to the endogenous promoters, therefore it would be expected that both Ole1p and Sct1p levels in these strains would be greater than in the wild type. Although this was not

done, the amount of Ole1p and Sct1p in all strains could have been measured by real time PCR. Further to this, De Smet et al have previously shown that an increase in Ole1p or Sct1p expression would skew the lipid profile in favour of desaturated or saturated lipids, respectively (147). To compensate for this imbalance, it is likely that a concurrent increase in expression of the saturated CoA competitor would be observed rendering both strains with substantially increased Ole1p and Sct1p, but a normal lipid profile. Thin layer chromatography could be used to confirm the degree of lipid desaturation in cells treated with F900742, however this was not performed due to equipment restrictions. Based on inferences from previous studies (147) and the known strengths of promoters, it was predicted that that BY mCherry-Sct1 and BY mCherry-Ole1 have a higher expression of Ole1p than either BY4741 or BY Ole1-GFP. In addition, the expression of Ole1p was exogenously increased by the transformation of BY  $\Delta ole1$  with the plasmid pOLE1<sup>wt</sup>. The plasmid contains the complete wild type OLE1 ORF which is followed immediately by a GFP tag and is expressed off the promoter PHO5. The PHO5 promoter is a stronger promoter than OLE1, as such it was expected that Ole1p would be more highly expressed in this strain than wild type. Of note, the activity of Ole1p was not assessed in any strains, however this would be an interesting investigation for future studies. In summary, Ole1p is expressed at wild type level in BY4741 and BY Ole1-GFP, expression of the desaturase is expected to be higher than either of wild type strains in BY mCherry-Ole1, BY mCherry-Sct1 and BY  $\Delta ole1$  + pOLE1<sup>wt</sup>.

All 5 of the abovementioned strains were grown to log phase and treated with 50  $\mu\text{g/ml}$  of F900742 for 24 hours. Cell growth was inferred by measuring the OD 600. After 24 hours of incubation, there was no significant difference in OD between any of the untreated strains (Fig 5.4). F900742 induced a significant reduction in growth of BY4741, BY Ole1-GFP, BY mCherry-Ole1, and BY  $\Delta ole1$  + pOLE1<sup>wt</sup> relative to their untreated counterparts. F900742 did not induce a significant reduction in growth of BY mCherry-Sct1 compared to the untreated sample. There was a significant difference in growth between BY4741, that expressed Ole1p at the wild type level, and BY mCherry-SCT1, that is predicted to have the highest level of Ole1p, after 24 hours of incubation

with F900742 with BY mCherry-Sct1 having a significantly higher OD. There were no significant differences in growth between any of the other treated samples and wild type. The decreased sensitivity of BY mCherry-Sct1 to F900742 was predicted to be due to a high level of Ole1p that overwhelms the inhibitory capacity of the drug.

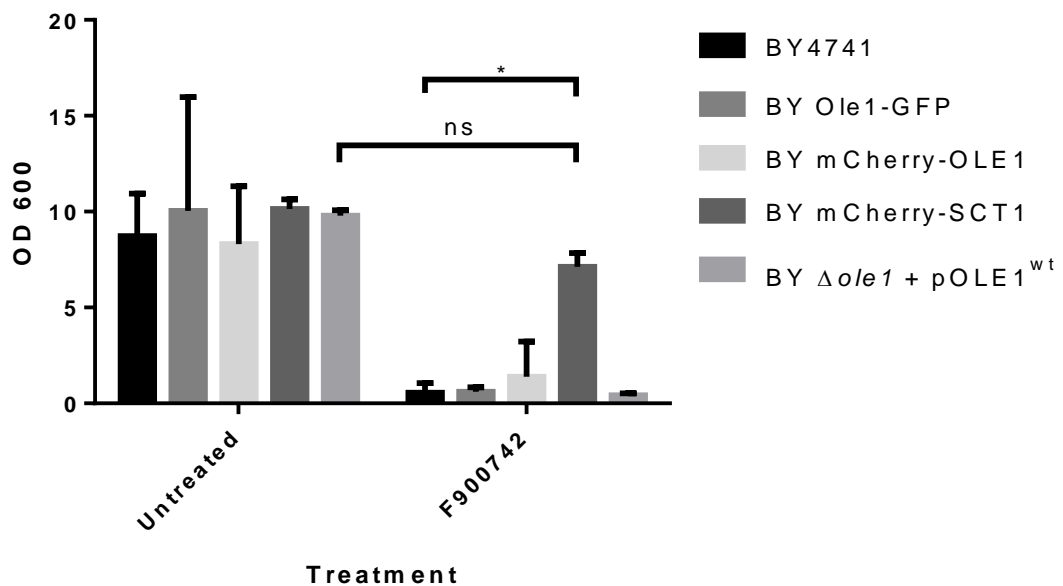


**Figure 5.4. Overexpression of Ole1p reduced the inhibitory capacity of F900742.** Strains expressing OLE1 from exogenous promoters were used to vary the expression of Ole1p. Strains were grown in YPD for 24 hours at 30 °C with 50  $\mu$ g/ ml F900742. F900742 did not significantly reduce the growth of BY mCherry-Sct1 relative to the untreated counterpart. F900742 induced a significant reduction in optical density in all other strains. There was a significant difference in growth between the wild type strain BY4741 and the OLE1 overexpressing strain BY mCherry Sct1 treated with F900742. No significant differences were observed between BY4741 and other strains treated with F900742. There was no significant difference in growth between any of the untreated strains. N = 4

### **5.2.3 F900742 was not active in HeLa cells at concentrations relevant for antifungal activity**

Many of the current clinical antifungal treatments are hampered by the fact that they display significant adverse toxicity and sufficiently undesirable side effects, for example nephrotoxicity, that often make completion of treatment programmes impossible. This is frequently associated with a fatal patient outcome. As previously discussed, antifungal drugs are required to target the pathogenic fungi, but not host cells. However, like humans, fungi are eukaryotes thereby limiting the availability of unique drug targets.

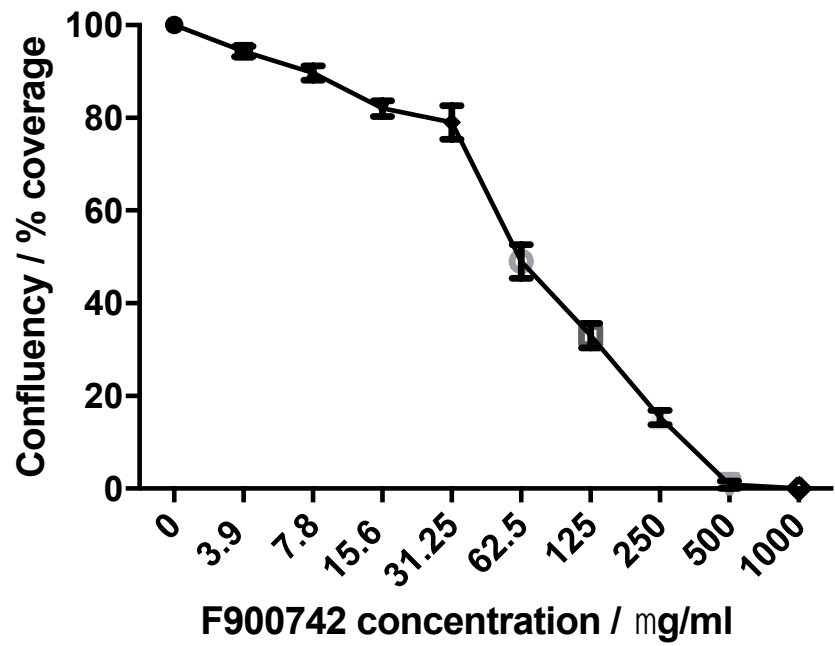
There is just 36% primary sequence similarity between the *S. cerevisiae* and human  $\Delta 9$  desaturase isoforms, Ole1p and Scd1 respectively, however there is greater than 70% sequence homology at the active site. To avoid adverse toxicity through F900742 also targeting the human isoforms, the drug was designed by F2G to target primary sequence differences between fungi and human desaturases at the active site. The structure of Ole1p has not been resolved which makes the design of specific inhibitors more challenging. The majority of structural information about the *S. cerevisiae* desaturase has been inferred from crystal structures of the mouse and human Scd1 isoforms (125,128). The purification and structural resolution of Ole1p will undoubtedly aid the design of future fungi-specific desaturase inhibitors. *S. cerevisiae* contain just one  $\Delta 9$  desaturase, humans contain two (Scd1 and Scd5). Scd1 is ubiquitously expressed, but particularly high expressions are noted in adipose tissues and the liver. SCD5 was more recently identified (170). Current data has only identified Scd5 expression in the human brain and pancreas.

To assess the efficacy of F900742 in a mammalian cell line, HeLa cells were grown until they were 50% confluent and treated with F900742 over a 250-fold range for 24 hours. It was expected that F900742 would have a higher MIC than any of the fungal strains tested. The MIC was determined as 500  $\mu\text{g}/\text{ml}$ , the IC90 at 275  $\mu\text{g}/\text{ml}$ , and the IC50 at 62.5  $\mu\text{g}/\text{ml}$  (Figure 5.5A and Figure 5.5B). Therefore, the MIC of F900742 in HeLa cells

was over 10 times greater than *S. cerevisiae* and over 500 times greater than any of the pathogenic fungal strains tested by F2G (Table 4.1), as such it would be expected that at clinically relevant doses there would be limited F900742 adverse toxicity to the patient through Scd1 inhibition. Additional human cell lines, including from the pancreas and brain, an *in vivo* mammalian studies would be required to provide a greater representation of the effects of F900742 to human tissues.

Next it was investigated whether F900742 induced morphological changes to HeLa cells. Cells were transfected with Sec61 to visualise the ER and stained with LD540 and DAPI to visualise the lipid droplets and nucleus. Dr Emily Eden kindly helped with the staining and slide preparation. HeLa cells were treated with 500 µg/ml for 4 hours (Figure 5.5C). Untreated cells appeared to have continuous ER and also contained many small lipid droplets distributed throughout the cytoplasm (white arrowhead). F900742 induced large holes scattered throughout the ER (orange arrowhead) and an increase in amount of ER denoted by the brightness of the stain. There was also an increase in lipid droplet size, but a decrease in number (white arrow). No differences were observed in nucleus size or shape. Although this experiment was performed at a concentration of F900742 that was far greater than required for antifungal activity, F900742 did induce large morphological changes and significant cytotoxic effects in the HeLa cell line. It would be interesting to investigate the early morphological changes induced by F900742 in organelles that are directly regulated by Scd1 such as the ER, lipid droplets and mitochondria.

A)



B)

IC	F900742 concentration $\mu\text{g/ml}$
IC50	62.5
IC90	275
MIC	500

C)

Untreated

F900742

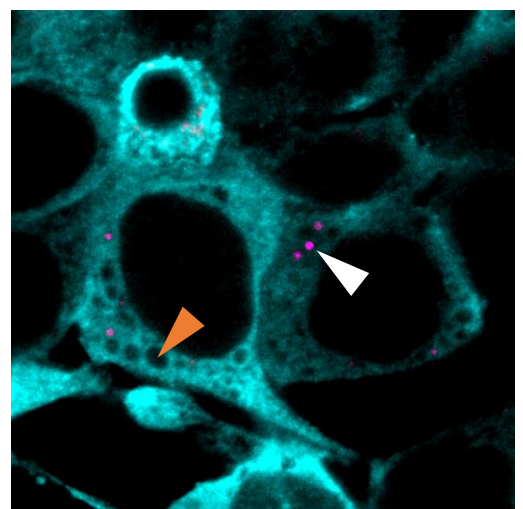
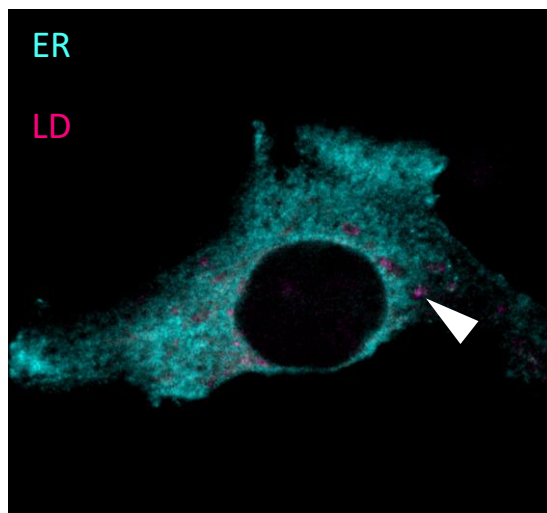


**Figure 5.5. F900742 was not active in HeLa cells at concentrations relevant for antifungal activity.** HeLa cells were cultured until 50% confluent before treatment with F900742. (A) and (B) Confluency was visually assessed after 24 hours. The MIC was determined as 500  $\mu\text{g/ml}$ , IC90 as 275  $\mu\text{g/ml}$ , IC50 as 62.5  $\mu\text{g/ml}$ . N = 3. (C) HeLa cells were treated with 500  $\mu\text{g/ml}$  F900742 for 4 hours prior to ER and lipid droplets analysis. F900742 induced multiple holes in the ER (orange arrowhead) and an increase in size, but a decrease in number of lipid droplets (white arrowhead). Images taken by Emily Eden.

#### 5.2.4 F900742 inhibited Scd1 function in *ole1* null yeast

Stukey et al described an *ole1* null *S. cerevisiae* strain that was functionally viable through the expression of the rat  $\Delta 9$  desaturase Scd1 in the absence of unsaturated fatty acids (116). It would, therefore, be expected that other mammalian Scd1 isoforms, for example human Scd1, would also render an *ole1* null strain viable. The F900742 inhibitory concentration in HeLa cells was substantially higher than any of the fungal strains tested so it was hypothesised that replacement of OLE1 for SCD1 would render a strain that is functional, but resistant to F900742. This would confirm that Ole1p was the target of F900742.

The strategy to construct a strain of yeast that expressed Scd1 as the sole  $\Delta 9$  desaturase was to utilise the yeast homologous recombination system to insert the SCD ORF into an *ole1* null strain. Early into the cloning it was discovered that Professor Robert Ernst's group had a strain of *S. cerevisiae* that expressed SCD1 in an *ole1* null background. Professor Ernst kindly agreed to share this strain (referred to as humanised Ole1p). The humanised strain was created using a BY4741  $\Delta ole1$  background that was transformed with a plasmid containing SCD regulated by the GDP promoter. It was confirmed that the human  $\Delta 9$  desaturase substitution was sufficient to rescue the growth of *ole1p* null cells in the absence of unsaturated fatty acid supplementation and that the humanised strain contained SCD1 in place of Ole1p by PCR (data not shown).

BY4741 wild type and the humanised strain were grown to log phase and treated at the BY4741 MIC (50  $\mu\text{g}/\text{ml}$ ) for 24 hours with F900742. OD 600 was used to determine the amount of cell growth and, therefore infer the degree of F900742 growth inhibition. Contrary to original expectations, the humanised strain was as sensitive to F900742 as the wild type (Figure 5.6). There was no significant difference in growth between BY4741 and the humanised strain following a 24 hour incubation with F900742. There was a significant decrease in growth between the treated and untreated humanised strain. These results were repeatable (N = 5).



For an antifungal to be an effective clinical treatment, it must target only the fungal enzyme at therapeutic doses or adverse side effects could prove intolerable for the patient. The design of the drug was such that it would target residue differences between the Ole1p and Scd1 active sites, therefore it was initially hypothesised that F900742 would not inhibit growth in the humanised strain as it would not target Scd1 function. However, figure 5.6 demonstrated that irrespective of whether the human or the *S. cerevisiae*  $\Delta 9$  desaturase is expressed, F900742 induced a not significantly different amount of antifungal activity. Although the result of this experiment was contrary to original expectations, it did prove incredibly valuable and, when taken alongside other data, it does affirm that the target of F900742 is Ole1p through the elimination of alternative possibilities. This is discussed further in the discussion in section 5.3. Furthermore, and of significant concern for the development of this drug and its use in patients, F900742 displayed significant activity against Scd1 at antifungal relevant concentrations in the humanised strain. Although there are predicted to be sufficient residue differences between the active sites of Ole1p and Scd1, a high degree of structural similarity is to be expected as they share common substrates and mechanisms.

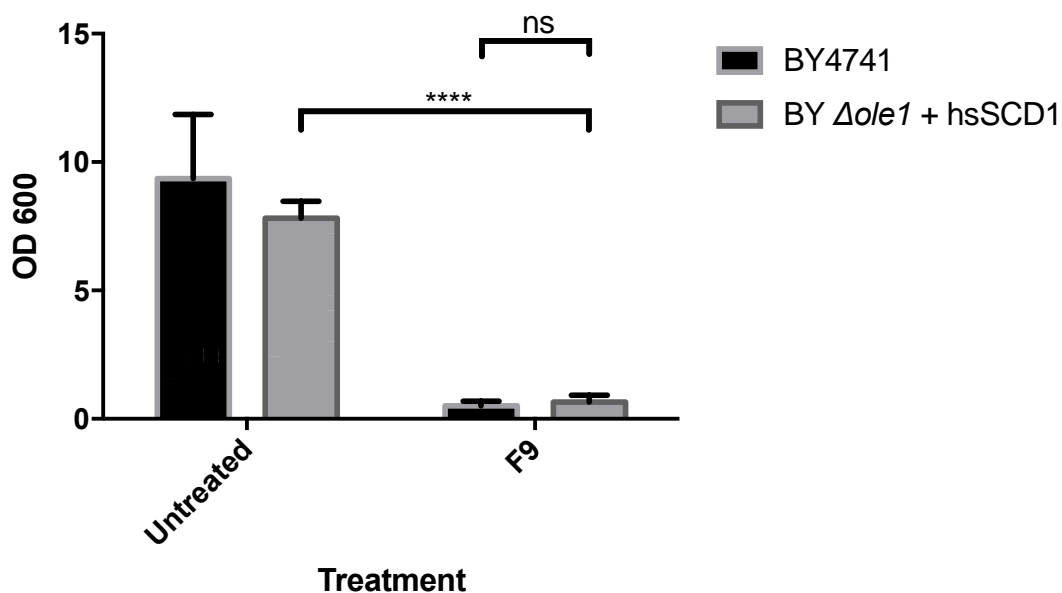


**Figure 5.6. F900742 inhibited Scd1 function in *ole1* null yeast.** Growth of *S. cerevisiae* containing the human  $\Delta$ 9 desaturase SCD1 was significantly reduced by F900742 compared to the untreated sample. There was no significant difference in F900742-inhibited growth between the wild type *S. cerevisiae* and the humanised strain. F900742 was added at 50  $\mu$ g/ml. OD 600 was measured after 24 hours. Samples were grown at 30 °C. N = 5.

### 5.2.5 Identification of residues essential for F900742

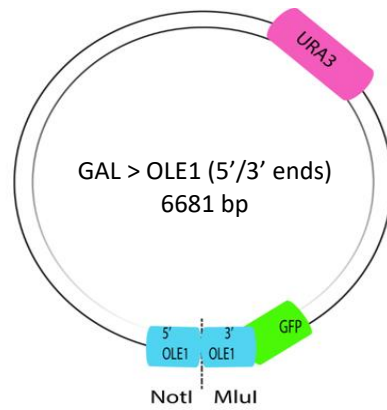
It is not currently possible to obtain a crystal structure of the Ole1p-F900742 complex. Although this would be useful to determine the stoichiometry of drug binding, mutagenesis methods can also be used to ascertain residues essential for complex formation. However, it is important to note that this is not without difficulties. OLE1 is an essential gene, as such mutations must maintain the protein's functionality or would induce lipotoxic cell death. Equally, mutations that enhance F900742 binding would exacerbate the antifungal activity of the drug: only mutations that render *S. cerevisiae* more resistant to and result in a hypergrowth phenotype to the drug would be identified. Several mutagenic strategies were employed to further investigate the

binding of F900742 to Ole1p. The first induced random mutations throughout the OLE1 ORF to investigate residues essential for drug binding through hyper-growth assays. Secondly, *S. cerevisiae* were repeatedly exposed to F900742 through repeat passaging to induce mutations that make the yeast resistant or tolerant.

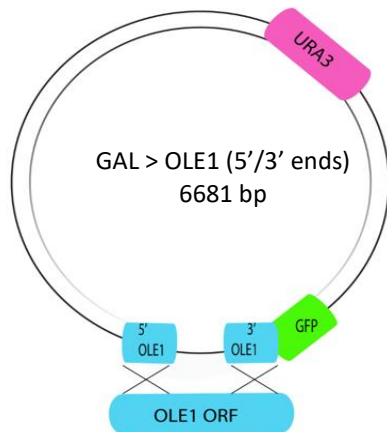
The initial strategy was to identify hyper-growth mutants that displayed differing resistance to F900742 through the generation of a library that contained random mutations throughout the OLE1 ORF. Mutant strains were to be grown on YPD and transferred to a YPD plate supplemented with a concentration of F900742 that enabled only minimal growth in OLE1 wild type. The OLE1 ORF would be sequenced from colonies that demonstrated an increased growth phenotype, thereby identifying residues that are essential for inhibiting drug binding. This strategy required the substitution of the native OLE1 ORF for a mutant copy through utilising the yeast innate homologous recombination system. The initial step of this strategy was to generate a plasmid containing the wild type OLE1 ORF and subsequent steps would be to generate a library of mutants throughout the ORF that would be cloned into the empty plasmid. Professor Tim Levine made a plasmid (GAL > OLE1 (5'/3' ends)) containing the first and last 80 bases of OLE1 with a GFP tag immediately following the end of the ORF (Figure 5.7). This plasmid was linearised and simultaneously transfected into  $\Delta ole1$  yeast with the PCR product of the entire, wild type ORF. Yeast were grown on selective media and after 72 hours there were small colonies. 10 of these colonies were tested and all were shown to have successfully cloned the wild type ORF into the plasmid by PCR (data not shown). However, although cloning was seemingly successful, Ole1p appeared mislocalised in both lag and log phase cells (data not shown). This method was repeated multiple times, but Ole1p was distributed throughout the cytoplasm or localised to puncta at the periphery in all cells imaged. As this initial phase was unsuccessful, the assessment of F900742 binding to Ole1p was not pursued by the recovery of mutant OLE1 DNA.

To overcome the failure in the homologous recombination of mutant OLE1 approach, a library of plasmids containing random mutations in the OLE1 ORF at a frequency of 3 - 10 substitutions per kb was purchased from Genscript (Ole1<sup>mut</sup>-GFP). It was confirmed

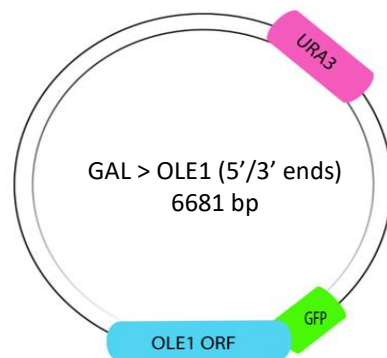
that both the promoter and GFP tag were in-frame with the OLE1 ORF. Part of the library was transformed into bacteria and selected for on ampicillin. The plasmids were purified and the entire OLE1 ORF of 15 plasmids was sequenced. A summary of amino acid substitutions and their position within the OLE1 ORF are summarised in figure 5.8. 30 amino acid substitutions were noted, as such it was estimated that each plasmid contained two amino acid substitutions. One plasmid contained wild type OLE1. This was plasmid was used in all preliminary experiments and as a control plasmid in subsequent experiments.



Plasmid containing 5' and 3' ends of OLE1



Homologous recombination to insert the OLE1 ORF in  $\Delta ole1$



Final plasmid product containing wild type OLE1

**Figure 5.7. OLE1 homologous combination mutagenic cloning strategy.** The strategy to generate a library of OLE1 mutants using homologous recombination was tested with wild type OLE1. OLE1 successfully integrated into the plasmid as determined by colony growth on selective media.

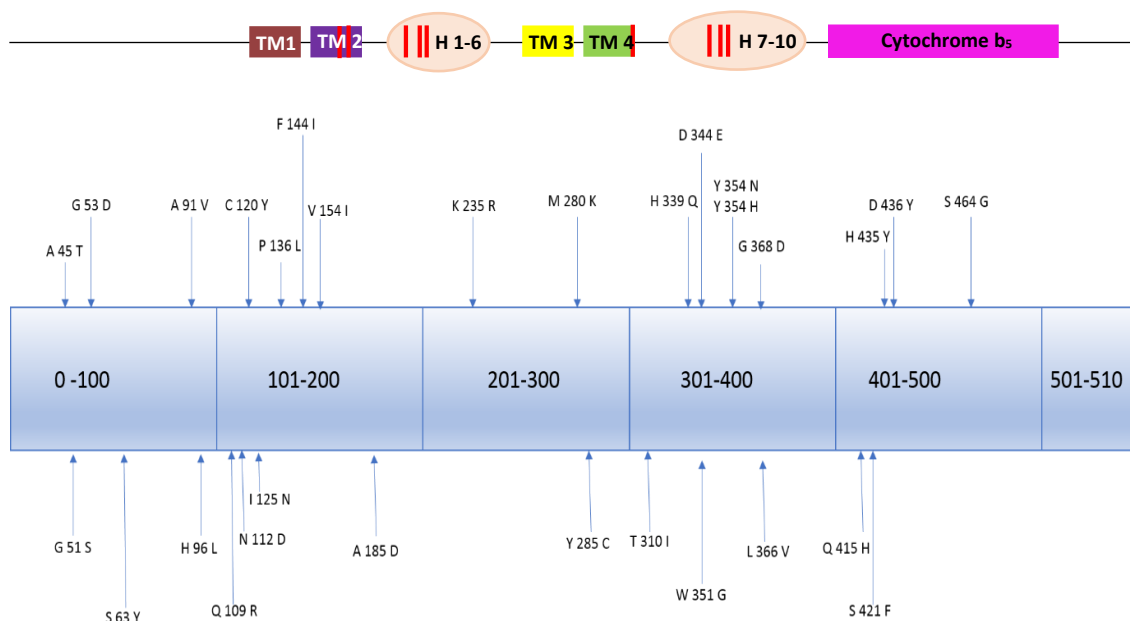


**Figure 5.8. Summary of amino acid substitutions within the OLE1 ORF.** 15 plasmids from the OLE1 mutagenic library were sequenced. 30 base substitutions that resulted in amino acid substitutions were observed and are summarized here. Additional redundant base substitutions were also noted (data not shown). Top figure provides a reference for the location of the four transmembrane domains and the ten cytosolic helices relative to the amino acid substitutions. TM 1-4 represents the four transmembrane domains. H 1-10 represents the ten cytosolic helices which are clustered in to two groups with H 1-6 in cluster 1 between TM 2 and TM 3, and H 7-10 in cluster 2 after TM 4. The red bars indicate the 9 conserved histidine residues. Two are within TM 2, three are in H 2, one is in TM 4, and three are in H 8. The region after amino acid 396 contains the cytochrome  $b_5$  reductase domain.

Prior to transformation with the mutant library, the concentration of F900742 that only just allowed growth of BY  $\Delta ole1$  containing pOLE1<sup>wt</sup> was determined. Sterile glass beads were used to evenly distribute the transformation mix across the plate. Plates were supplemented with F900742 at a concentration between 100 and 0.1  $\mu\text{g}/\text{ml}$ . 6.25  $\mu\text{g}/\text{ml}$  of F900742 was sufficient to just allow the growth of yeast colonies in an evenly distributed manner without overcrowding (Figure 5.9). This would ensure that single colonies that demonstrated hyper-growth could be easily isolated for sequencing. The mutant library was transformed in BY  $\Delta ole1$  and grown on YPD supplemented with F900742. Colonies that displayed a hyper-growth phenotype were sequenced to identify base substitutions that rendered the yeast more resistant to F900742.



**Figure 5.9. Pilot study to determine F900742 concentration for minimal growth of yeast.** *BY Δole1* were transformed with *pOLE1<sup>wt</sup>*, diluted 100 fold, and plated onto YPD agar containing F900742. Colonies were grown at 30 °C for 48 hours. Sufficient growth of colonies, but sparsely distributed across the plate was noted when 6.25 µg/ml of F900742 was supplemented.

There are several limitations to this strategy. Firstly, only mutations that rendered yeast more resistant to the drug were observed; mutations that rendered a more sensitive strain displayed a hypo-growth phenotype and were unable to grow. Furthermore, the mutagenic library is expressed off a PHO5 promoter which overexpressed OLE1 relative to wild type levels. It was confirmed that BY  $\Delta ole1$  transformed with pOLE1<sup>wt</sup> displayed correct desaturase localisation, however F900742 induced minimal relocalisation of Ole1p-GFP likely due to overexpression of the protein overwhelming the inhibitory capacity of the drug (Figure 5.10A). Therefore, it was decided that the library would be transformed into the Sct1p overexpressing strain BY mCherry-Sct1. Under normal conditions, overexpression of either Sct1p or Ole1p is paralleled by an increase in the other to maintain the balance of lipid acyl chain saturation. It was expected that the overexpression of Sct1p in BY mCherry-Sct1 would balance the increase in Ole1p expression from the plasmid. A caveat to this is BY mCherry-Sct1 contains a copy of OLE1 which is already likely to be overexpressed and, therefore, Ole1p expression from the plasmid would further increase the Ole1p content. F900742 did induce Ole1p-GFP relocalisation in BY mCherry-Sct1p (Figure 5.10B).

BY mCherry-Sct1 was transformed with pOLE1<sup>mut</sup> and grown on YPD supplemented with 6.25  $\mu\text{g/ml}$  F900742. Hyper growth, characterised by a larger colony size relative to the wild type control plasmid, was only noted in 5 colonies out of the hundreds of micro colonies on the plate. This process was repeated until there was a cumulative total of 30 hyper growth colonies. Colonies were sequenced and there was an average number of 3 base substitutions per OLE1 ORF, however these did not confer any amino acid substitutions. Hyper growth was predicted to be due to other factors that would render the cell more resistant to F900742, for example a natural variation in influx or efflux pumps preventing intracellular drug build-up. This experiment was limited by the fact that only a low number of colonies were screened and only colonies that displayed a hyper growth phenotype. A more pertinent method would be to screen for hyper and hypo growth in a high throughput screen such that thousands of colonies (or more) could be efficiently tested.

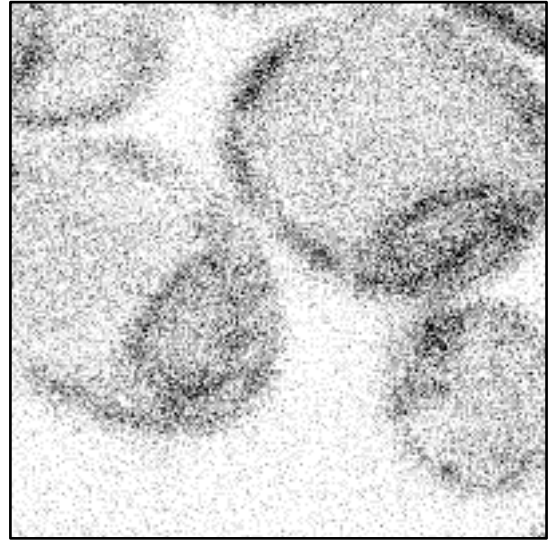
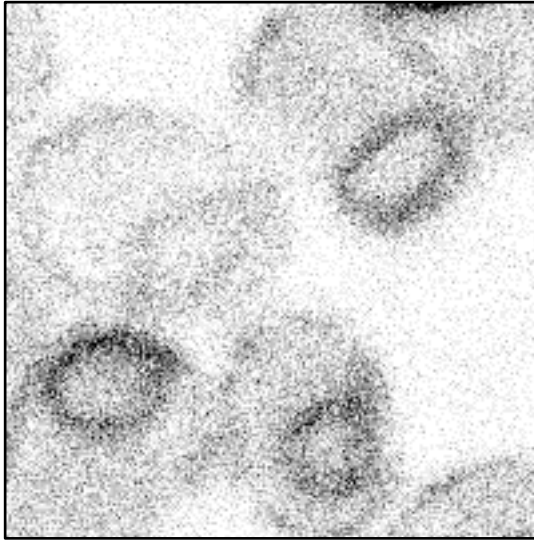


A)

BY  $\Delta ole1$  + pOLE1<sup>wt</sup>

Untreated

F900742



B)

BY mCherry-Sct1 + pOLE1<sup>wt</sup>

Untreated

F900742

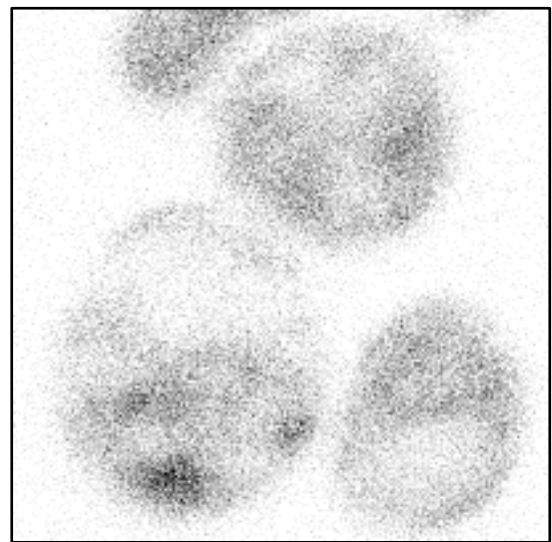
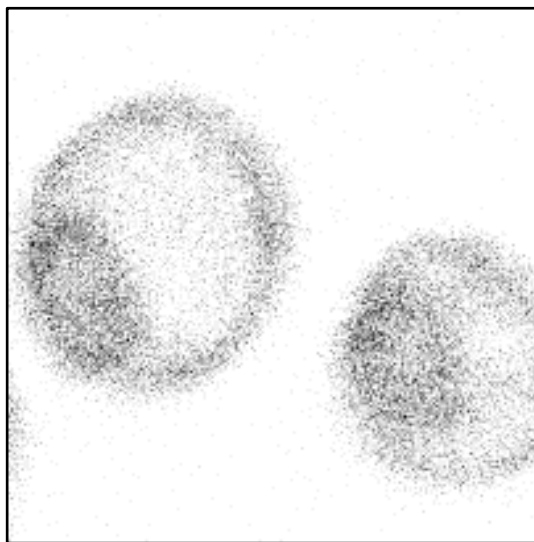


**Figure 5.10. Ole1p expressed off pOLE1<sup>wt</sup> did not relocalise.** The plasmid pOLE1<sup>wt</sup> contains the wild type OLE1 ORF followed by a GFP tag off a PHO5 promoter. pOLE1<sup>wt</sup> was transformed into BY  $\Delta ole1$  and into BY mCherry-Sct1. (A) Ole1p-GFP did not relocalise when pOLE1<sup>wt</sup> was expressed in BY  $\Delta ole1$  and grown in the presence of 100  $\mu$ g/ml F900742 for 4 hours. (B) Ole1p-GFP did relocalise to puncta when expressed in BY mCherry-Sct1. F900742 was added at 100  $\mu$ g/ml. Samples were incubated for 4 hours at 30 °C. N = 3.

### 5.2.6 Inducing mutations in OLE1

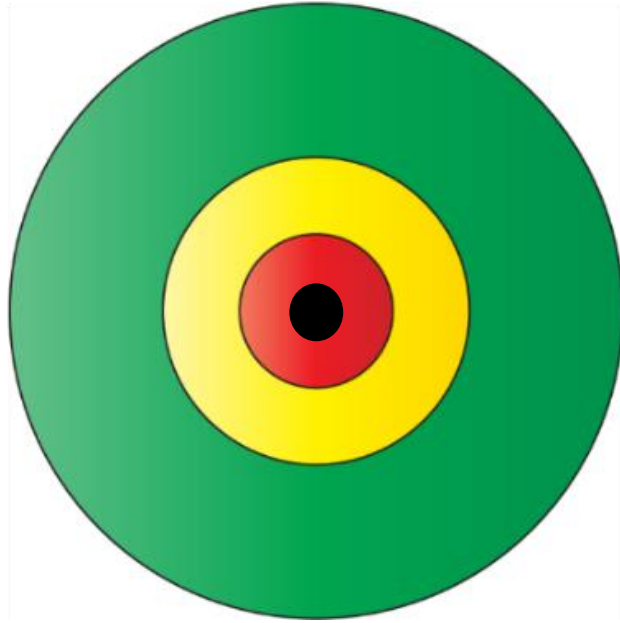
In parallel to screening for hyper growth mutations, a second approach to investigate residues essential for F900742 binding involved taking advantage of the ability of fungi to rapidly evolve antifungal drug resistance. Drug resistance is considered an unfavourable outcome in the clinic, however inducing resistance in experimental strains can prove a powerful tool to predict likely response to antifungal agents. One frequently annotated mechanism of drug resistance is through alterations to the drug binding site of the target protein. *S. cerevisiae* were repeatedly exposed to F900742 in an attempt to induce resistance. It was expected that a likely mechanism of resistance would be through base substitutions in the OLE1 ORF, therefore the ORF was sequenced to identify residues essential for F900742 binding.

Complete YPD agar plates were made. A hole was created in the middle of the plate using the wide end of a 1000 µl pipette tip. F900742 was added into the well to ensure a linear diffusion gradient of drug such that there was the highest concentration at the middle and the lowest concentration at the periphery of the plate (Figure 5.11A). To determine the optimum concentration of F900742 such that the gradient of drug induced no growth, limited growth, and high growth regions, F900742 was made at final concentrations from 10 mg/ml to 0.1 mg/ml. 100 µl of F900742 at the relevant concentration was added to the well and the plate allowed to rest for at least 6 hours at room temperature. 100 µl of log phase BY Ole1-GFP were evenly spread onto the agar and incubated for 48 hours. Dense growth was noted in the low drug concentration (green zone), reduced growth characterised by micro colonies in the middle (yellow zone), and very limited growth in the area immediately surrounding the well (red zone) in the plate containing 4 mg/ml F900742 (Figure 5.11B). Other concentrations of F900742 either caused an over growth so there was no zone of inhibition or insufficient growth (data not shown). A swab of approximately 30 colonies was collected from the zone of lowest growth. These colonies were resuspended in 100 µl of sterile water and re-plated on to a fresh drug concentration gradient plate. Plates were incubated at 30 °C for 48 hours. This process was repeated to exert a high

level of selective pressure onto the yeast. The swab from every 5<sup>th</sup> passage was also grown on a drug-free YPD agar plate. 3 colonies were isolated, and the MIC of these colonies was determined as previously described. In addition, the OLE1 ORF and promoter region of these colonies were sequenced. A total of 65 passages were completed. None of the passaged colonies had a MIC that was significantly different from that of BY Ole1-GFP (Figure 5.11C), nor any mutations in the OLE1 ORF (data not shown). Further to this, there was no significant difference in growth of passaged colonies when grown in the presence of F900742 relative to BY Ole1-GFP (Figure 5.11D) suggesting that 65 passages was not sufficient to induce mutations in *S. cerevisiae* that render the yeast more resistant to this drug. Furthermore, the localisation of Ole1p-GFP was also assessed in the isolated cells. Ole1p-GFP was normally localised in all cells observed at all passages.

The MIC and growth of passaged cells was not sufficiently different from BY Ole1-GFP to suspect that an alternative mechanism of resistance had been induced. However, it would be interesting to continue with the passages and determine how many rounds would be required to induce resistance. Whole genome sequencing would also be advantageous to identify possible alternative pathways that render the cell resistance. The passage method described here has been previously used by F2G to induce resistance in a clinically resistant isolate of *Aspergillus* to a novel antifungal compound that does not target fatty acid desaturation. Clinical isolates that have developed resistance to all antifungal drug classes already have a genome that is very susceptible to further mutations. As such, it is likely that resistance was induced faster in the *Aspergillus* isolate compared to *S. cerevisiae* due to the inherent differences in genome stability. Alternatively, there is substantial variation in the frequency of resistance between different drug classes and also between strains, therefore, it is also possible that there is an inherently lower chance of developing resistance to F900742. If a derivative of F900742 proceeds to clinical trials, it would also be of profound clinical use to determine the susceptibility of common *Candida* and *Aspergillus* species to develop resistance against this drug.

**A)**



**B)**



Figure 5.11 continues over page

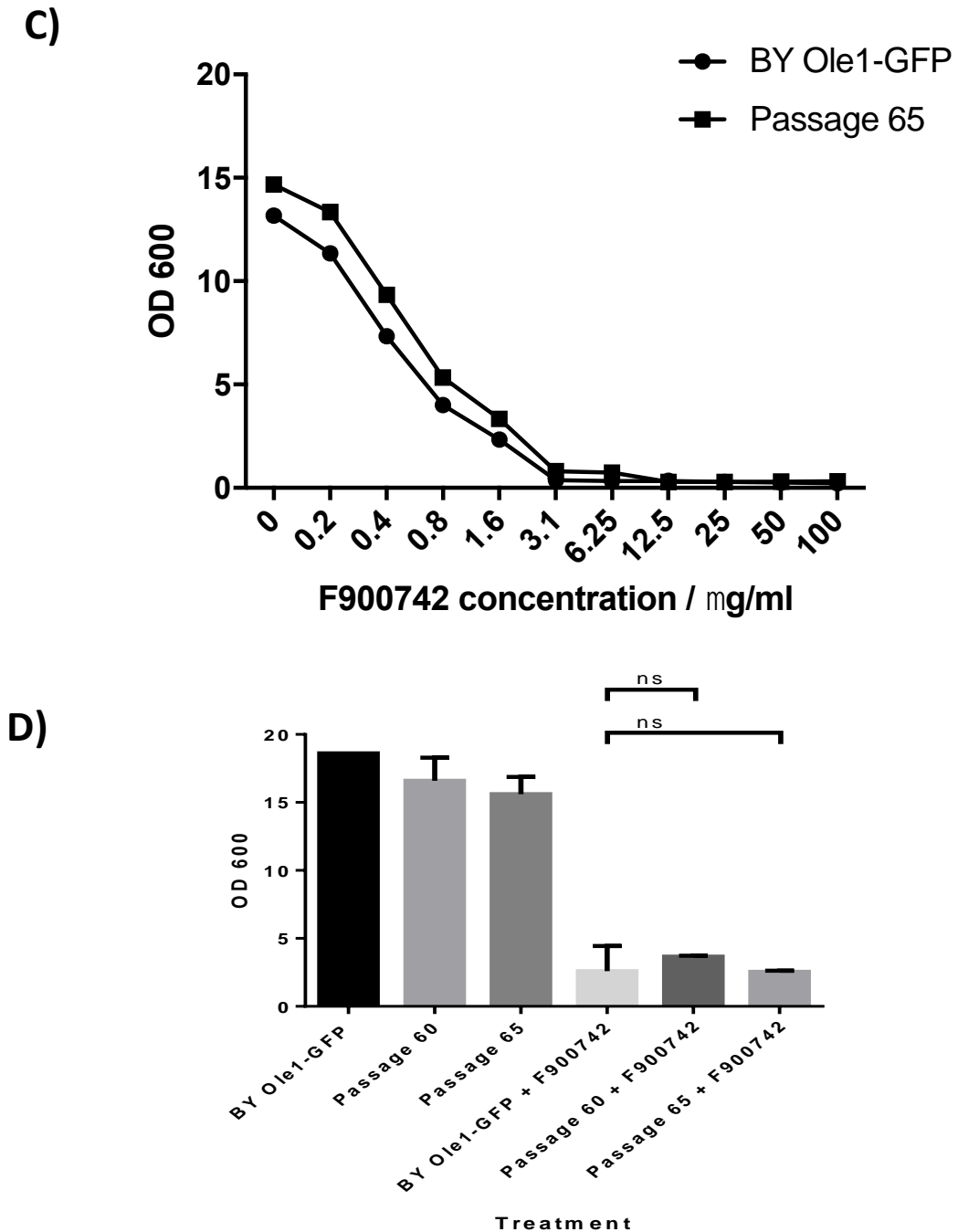


**Figure 5.11. Repeated exposure to F900742 to induce mutation in OLE1.** (A) Cartoon of YPD plates containing a gradient of F900742. Drug was added into a well in the middle of the plate (black) and allowed to diffuse to create an even gradient with the highest concentration of drug closest to the well (red) and the lowest at the periphery of the plate (green). (B) Representative passage plate. The highest density of yeast colonies was towards the edge of the plate where the lowest concentration of F900742. (C) The MIC of BY Ole1-GFP and the 60<sup>th</sup> and 65<sup>th</sup> passage were tested as previously described. There was no substantial difference in MIC between BY Ole1-GFP and the 60<sup>th</sup> nor 65<sup>th</sup> passage. MIC was determined as 25 µg/ml. (D) The growth of passage 60 and 65 was assessed relative to BY Ole1-GFP at 30 °C over a 24 hour period. The OD 600 was measured to infer cell growth. F900742 did not induce any significant differences in the growth of BY Ole1-GFP, passage 60, and passage 65. 25 µg/ml F900742 was added. N =3.

### 5.3 Discussion

The experiments presented in this chapter used genetic manipulation of the *S. cerevisiae*  $\Delta 9$  desaturase expression to investigate the target of F900742. Experiments confirmed that:

- 1) Ole1p was likely to be the target of F900742
- 2) F900742 also targeted the human  $\Delta 9$  desaturase Scd1

The expression of Ole1p was modulated through varying the promoter strength of OLE1 or SCT1 which enabled the characterisation of F900742 activity (Figure 5.4). This enabled the prediction of cellular Ole1p content. However, it must be noted that this study is limited by the fact that the expression of Ole1p was not measured. A quantitative approach to determine Ole1p expression, for example RT-PCR, could be used to validate the level of the desaturase in each strain and therefore enable more robust conclusions to be drawn. Further to this, the alterations to the lipidome in response to F900742 exposure in strains with varying amounts of Ole1p would have proven beneficial for a more conclusive data set. Despite these limitations, it is possible to link together data presented here with previously published data identifying alterations in expression of proteins in the Ole1p pathway and lipid profiles (91,147,157). As such, it was possible to predict the likely changes in the lipidome as a result of varying the promoter strength of OLE1 and the gene encoding the Ole1p competitor for saturated fatty acids, SCT1. De Smet et al have shown that deleting either OLE1 or SCT1 renders *S. cerevisiae* with a fatty acid profile that is skewed in favour of saturated fatty acids or unsaturated fatty acids, respectively, however, when both OLE1 and SCT1 were co-overexpressed the lipid profile appeared normal (147). From this piece of evidence, it was possible to infer that the lipid profile would be normal in BY mCherry-OLE1 and BY mCherry-SCT1, however the expression of both Ole1p and Sct1p was greater than when expressed from the respective wild type promoters. Both of the mCherry strains have the respective genes under the control of the TEF1 promoter. TEF1 is a highly expressing promoter relative to the endogenous OLE1 and SCT1 promoters as such the increase in expression of OLE1 would be balanced by an increase in expression of SCT1, and vice versa, to ensure the lipid

profile remains normal. BY mCherry-OLE1 was not sensitive to 50 µg/ml F900742, whereas all other strains tested were (Figure 5.4). It was expected that this was due to the expression of Ole1p being the highest in BY mCherry-SCT1 thereby overwhelming the inhibitory capacity of the drug. Alternatively it could be due to the greater expression of Sct1p sequestering saturated fatty acids into lipids, therefore lower amounts of lipotoxicity from free saturated fatty acids. Data in chapter 4 suggested that there was in fact a decrease in Sct1p expression after 4 hours (Figure 4.16), however it is plausible that this might in fact only be in the early stages of lipotoxicity and would be counterintuitive to cell survival over longer periods of time (24 hours). Overall, this data suggested that the greater the expression of Ole1p, the less active F900742 is in *S. cerevisiae*. Future experiments that confirmed the expression level of Ole1p and lipid profiles in the various strains would be beneficial to confirming the interpretation of these results.

Replacement of OLE1 with the gene encoding the human  $\Delta 9$  desaturase SCD1 provided the most striking result: there was no significant difference in growth between *S. cerevisiae* expressing either the endogenous or the human desaturase. Eukaryotic  $\Delta 9$  desaturases are predicted to be structurally similar, however, due to inherent difficulties with purifying membrane proteins, only truncated versions of the mouse and human Scd1 have been crystallised (125,128). The topology of Ole1p has been inferred from the solved mammalian structures. Human Scd1 and *S. cerevisiae* Ole1p have just 36% primary sequence identity (128), however there is substantial structural homology between the active sites of the enzymes which is not unexpected as they share common substrates. Differences between mammalian and fungal primary sequences were used to predict residue differences within the active site of the desaturases, and F2G used this to guide drug design with the aim that only the fungal enzyme was targeted.

In light of F900742 targeting a broad spectrum of fungi, moulds, and dermatophytes, as well as targeting Scd1 expressed in *S. cerevisiae* at the MIC of wild type, it is expected that F900742 is a pan-inhibitor of  $\Delta 9$  desaturases throughout eukaryotes. Yet, inhibition of HeLa cell growth was not observed at antifungal relevant

concentrations. Possible explanations for the discrepancy in response between HeLa cell and humanised yeast growth might be as follows: Firstly, F900742 inhibition of Scd1 in HeLa cells could activate feedback mechanisms that initiate the overexpression of the desaturase such that the protein overwhelms the inhibitory capacity of the drug. Such a feedback mechanism would not be present in the humanised strain as SCD1 was present on a plasmid in an *ole1* null background. Secondly, humans have two forms of the desaturase, SCD1 and SCD5, therefore HeLa cells have both isoforms encoded within the genome. SCD1 has been previously identified in HeLa cells (129). SCD5 was more recently identified. Very few studies have investigated the action of Scd5 and, thus far, it has been identified in the brain and pancreas, but no studies have ruled out its expression in cervical or HeLa cells (170). It is theoretically possible that Scd1 is the major isoform expressed in cells, however, in times of stress or Scd1 inhibition, Scd5 expression is upregulated and is able to compensate for the reduction in Scd1 activity. Sufficient structural differences between these isoforms could elicit Scd1 as a much more sensitive protein than Scd5, therefore the growth inhibition noted at lower F900742 concentrations in the humanised strain relative to HeLa cells could be a result of functional redundancy between the two human isoforms. It would be interesting to investigate whether the same growth phenotype is noted if *S. cerevisiae* expressed the alternative human SCD gene, SCD5, or if *S. cerevisiae* express both SCD isoforms together, or if the same results are observed when SCD1 or SCD5 is expressed in the genome. It is pertinent to note that HeLa cells are not representative of all human tissues. Future studies would also need to explore the action of F900742 in additional human cells lines, including ones derived from the brain and pancreas, and measure the expression level of both Scd1 and Scd5. Although experiments here do show that Scd1 is likely to be targeted by F900742 at concentrations relevant for *S. cerevisiae*, the concentrations of F900742 used here is over 100 times greater than the MIC in any of the tested *Aspergillus* or *Candida* species (Table 4.1). Therefore, an interesting future experiment would be to generate humanised *Aspergillus* and *Candida* strains that express the human  $\Delta 9$  desaturase. An alternative novel regulator of lipid metabolism cannot be eliminated as the target of F900742.



Data presented here has not unequivocally proven that Ole1p is the target of F900742, however it does remove the possibility of some of the alternative targets. The activity of the OLE1 pathway is regulated by multiple proteins and any one of these could be the target of F900742. Alternative targets that result in the indirect inhibition of the OLE1 pathway and relocalisation of Ole1p-GFP could be regulators of Ole1p expression such as protein synthesis or protein degradation machinery, a posttranslational modifier of Ole1p, or a protein that affects an entirely separate part of the lipidome which subsequently effects the OLE1 pathway. The likelihood of F900742 targeting these alternative targets will be discussed below.

Firstly, regulators of Ole1p expression (for example transcriptional (Ubx2p, Mga2p, Spt23p) or degradation elements) cannot be the target of F900742. Conditional inhibition of the OLE1 pathway by F900742 altered the subcellular localisation of Ole1p-GFP and was associated with an increase in desaturase expression that was shown to be a result of an increase in protein transcription (Figure 4.15). Taken together with the observation that F900742 also targeted Scd1 (expressed at high levels from the plasmid) and induced an increase in Ole1p expression, it is possible to conclude that the antifungal effects were not a result of low Ole1p levels and that F900742 did not induce a reduction in Ole1p expression through inhibiting any of the regulators of Ole1p expression, including proteins involved in transcription and translation. In addition, the sensitivity of the humanised strain eliminated the possibility that an alternative target was a transcriptional or translation regulator of Ole1p. The expression of the  $\Delta 9$  desaturase in the humanised strain is independent of the endogenous OLE1 transcriptional and translational elements, therefore their inhibition would not have affected the expression or activity of Scd1. Furthermore, the expression of Ole1p was shown to increase in response to F900742 which also eliminated the possibility that the target increased the rate of protein degradation. However, none of the data presented here can rule out that a common, but unidentified, posttranslational modifier of both Ole1p and Scd1 as a possible target, for example a kinase. Although an unidentified posttranslation protein is a possible alternative target, it is very unlikely as humans and yeast diverged one billion years ago, as such a common ancestral protein that regulates posttranslational modifications

that are essential for the function of both enzymes is improbable. In addition, to date, there have not been any posttranslational modifications noted for either proteins. Therefore, it is unlikely that F900742 attenuates its activity through inhibition of a direct regulator of Ole1p expression or activity.

An alternative theory is that F900742 inhibits a protein that sufficiently effects the saturation content of the lipidome which could induce lipotoxic effects and thus expression changes in Ole1p are as a counter response to rebalance the lipidome. Major progress has been made in the field of lipid metabolism, though there are still many remaining questions. Unidentified pathways that initiate an increase in saturated lipid content could be the true target of F900742, and the OLE1 pathway effects are a secondary response. The degree of membrane lipid saturation could be increased through several hypothetical, yet plausible pathways. Firstly, the inhibition of an unidentified sensor that detects the requirement to halt *de novo* lipid synthesis would render the cell in a perpetual state of *de novo* fatty acid synthesis. This would initiate an increase in Ole1p expression, but the rate at which saturated fatty acids are generated could still overwhelm the desaturation capacity of Ole1p resulting in a net saturated lipidome. Alternatively, F900742 could act through the inhibition of a protein that sequesters saturated fatty acids into lipids, thereby resulting in a pool of free saturated fatty acids. High levels of free saturated fatty acids could overwhelm the storage capacity of lipid droplets or the rate at which they are converted to triacylglycerol (TAG) thereby increasing the cytoplasmic content of free saturated fatty acids. The expression of Ole1p could increase to convert some of the saturated pool into unsaturated fatty acids and subsequent insertion into membrane lipids. If the target of F900742 was an alternative protein involved in lipid metabolism and effects to Ole1p are secondary, it is predicted that OLE1 transcriptional activation would be through membrane lipid sensing by Mga2p. Although this theory remains hypothetical, it has not been disproven. To date no pathways or proteins have been identified that would affect the lipid profile in a manner that would induce the overexpression of Ole1p. As such, it is most likely that Ole1p is the target of F90742, although an unidentified regulator of lipid biosynthesis remains a plausible alternative target to Ole1p.

Experiments to identify residues key for F900742 binding and for overcoming F900742 were unsuccessful. The approaches to express Ole1p with random mutations throughout the ORF and to induce mutations through repeated passaging are limited by the fact that these select only for mutants that render a hypergrowth phenotype. Mutants that render the yeast more sensitive would be lost. To compensate for the information that is lost by hypogrowth colonies, a more pertinent method to screen the mutant plasmid library would have been to plate the transformed yeast on to a plate containing YPD only and then grow individual colonies in YPD broth with drug. By measuring the OD 600, it would be possible to determine whether each colony has a hyper- or hypogrowth phenotype relative to wild type. The plasmid could then be extracted from colonies with either high or low growth and the OLE1 ORF sequenced to identify mutations that result in the aberrant growth profile.

Passaging has proven a successful technique to identify the likelihood that resistance will develop in previous studies by F2G (data not published). Difficulties in inducing mutations in OLE1 may stem from yeast species differences or differences in susceptibilities of genes to mutate. Currently no clinical or agricultural antifungal targets  $\Delta 9$  desaturases, therefore this pathway is unlikely to display clinical resistance as a result of use of crop treatments in the environment. However, one study has demonstrated that Ole1p is only essential in *S. cerevisiae* under aerobic conditions (171). Dekker et al demonstrated that the yeast had unsaturated fatty acid-independent growth in anaerobic conditions in an *ole1* null mutant, whereas Ole1p was required for growth in aerobic conditions. This suggests that yeast, or at least *S. cerevisiae*, are capable of activating unsaturated fatty acid independent growth pathways to adapt to conditions where the activity of Ole1p would be insufficient to sustain growth. The OLE1 promoter region and ORF was sequence of every 5<sup>th</sup> passage, but no alterations were noted in either region nor to the MIC. It is possible that more than 65 passages would be required to induce mutations in OLE1 and this would render F900742 ineffective. An alternative, plausible outcome of further passages would be that the unsaturated fatty acid independent pathway would be activated even under aerobic conditions and that Ole1p would be a redundant protein under

these conditions, therefore F900742 would not have any effect on inhibiting fungal cell growth. Further F900742 passages and additional studies to investigate the unsaturated fatty acid independent growth of yeast proposed by Dekker et al is required to fully investigate the possibility of resistance to  $\Delta 9$  desaturase inhibition. It is also possible that because OLE1 is the sole copy of an essential gene (at least under aerobic conditions), that this gene is very tightly regulated to ensure correct function. Greater than 80% of the active site sequence of  $\Delta 9$  desaturases is conserved throughout eukaryotes suggesting that there is little scope for mutations that prevent F900742 from binding, but do not affect the activity of the enzyme. However, the tight regulation of this gene may be met by a significant energy cost, as such a cost-fitness balance that eventually results in the resistance to F900742 is a possible outcome.

Overall, when taken together with data presented in chapter 4, this chapter provides compelling evidence that Ole1p is the target of F900742 and that it is unlikely that resistance would develop to this drug. Additional studies to verify this interpretation are required.

# CHAPTER 6

## Investigating the mechanism of action of F900742

### 6.1 Introduction

Chapters 4 and 5 identified that F900742 is likely to induce growth inhibitory effects through alterations to the OLE1 pathway. Ole1p is the sole desaturase in *S. cerevisiae* and it has been previously shown that its deletion generates an auxotroph that is lethal in a few cell divisions unless media is supplemented with unsaturated fatty acids (167). Inhibition of the activity of Ole1p, whether through the chemical or genetic means, has been previously shown to induce an imbalance of saturated to unsaturated membrane lipids which induces irreversible, lethal lipotoxicity unless the media is supplemented with unsaturated fatty acids (116). Lipotoxicity is defined here as the toxic consequences of abnormal lipid load which can induce cellular dysfunction or stress if not corrected and, in extreme cases, can lead to cell death. Lipotoxic events varies between lipid species and cause of the disruption to lipid metabolism. Lipid induced cell death as a consequence of fatty acid overload can occur via necrosis or through more regulated autophagic and apoptotic routes. It has been previously demonstrated that high doses of long chain saturated fatty acids are non-toxic to wild type *S. cerevisiae*, whereas low levels of unsaturated fatty acids are linked to the activation of processes such as the unfolded protein response (UPR) and reactive oxygen species (ROS) production (172,173). The precise mechanisms by which lipotoxic events are activated remain somewhat elusive; however, this must be a multifaceted, coordinated response as highlighted by lipid-induced activation of either the UPR or ROS production will induce the activation of the other.

This chapter investigated Aims 5 and 6. The mechanism of action of F900742 was inferred from a series of experiments investigating drug-induced ultrastructural defects.

## 6.2 Results

### 6.2.1 F900742 inhibited growth in logarithmic phase

Initially, the timing of the onset of the growth inhibitory activity of F900742 was investigated. The MIC of F900742 in wild type *S. cerevisiae* was determined as 50 µg/ml (Figure 4.2). Cells were grown to mid log phase (approximately OD 0.5) and diluted back to OD 0.1 before addition of 50 µg/ml F900742. The OD 600 was measured every 2 hours for the first 12 hours post-treatment and at 24 hours (Figure 6.1). There was no difference in growth rates between the treated and untreated samples for the first 2 hours, and only a slight, non-significant growth difference following 4 hours of treatment. The untreated sample continued in logarithmic growth phase for a further 6 hours. By 10 hours, the untreated yeast were predicted to have entered into stationary growth phase identified by a constant OD, which remained steady through to 24 hours. The untreated sample followed an expected growth pattern for the growth of wild type *S. cerevisiae*. In contrast, F900742 inhibited the cells from continuing logarithmic growth. Although there was a slight difference in growth between the two samples by 4 hours post treatment, the first significant difference was at 6 hours. Throughout the experiment, the OD remained relatively constant at approximately OD 0.6, less than 10% of the growth of the uninhibited sample. It was concluded that treated *S. cerevisiae* were unable to continue in logarithmic growth phase as observed in the untreated sample. Overall, *S. cerevisiae* were unaffected by F900742 for the first 4 hours of treatment, however F900742 inhibited any further growth of cells after this point.

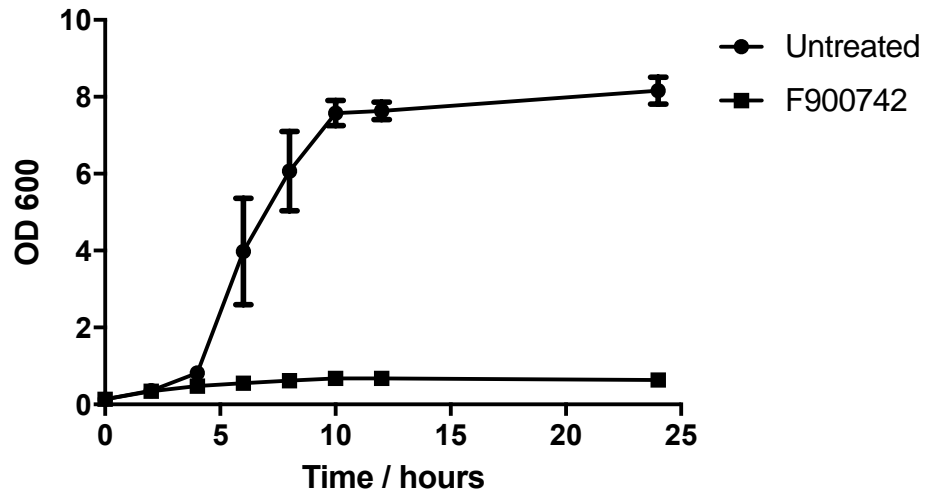


**Figure 6.1. F900742 inhibited growth in logarithmic phase.** The growth of BY4741 in the presence of 50  $\mu\text{g}/\text{ml}$  F900742 was assessed against an untreated sample by measuring the OD 600 every 2 hours for the first 12 hours and at 24 hours post treatment. A significant difference in optical density was first observed between the F900742 and untreated sample after 6 hours. There was a significant difference in every reading after this time point. There was no significant difference in growth for the first 4 hours of treatment. Significance not shown. Samples were grown at 30 °C. N = 3.

### 6.2.2 F900742 exerted a fungistatic mechanism of action

Antifungals can act through either fungistatic or fungicidal mechanisms, that is they can halt the growth of fungal cells and rely on the host to rid the live fungi through epithelial turnover or the antifungal can kill the cells, respectively (174). Fungicidal agents would be preferred over fungistatic as the majority of patients with invasive fungal infections are immunocompromised, therefore require more assistance from the drug. However, the majority of clinical antifungal agents act through a fungistatic mechanism, for example the azoles. The method for determining the fungistatic or fungicidal ability of a novel compound is to treat the sample for 24 hours at the MIC and then plate on to complete media agar without drug. If growth is observed, then the drug is fungistatic; if growth is not observed the drug is fungicidal.

BY4741 and BY Ole1-GFP were treated with F900742 at 50 and 25  $\mu\text{g}/\text{ml}$ , respectively, for 24 hours before being diluted and grown on YPD agar at 30 °C for 48 hours.

F900742 was identified as primarily a fungistatic inhibitor as there was growth in both BY4741 and BY Ole1-GFP samples that had been treated with F900742 (Figure 6.2). However, there was an 85% and 96% reduction in colony number in BY4741 and BY Ole1-GFP compared to their untreated counterpart at the greatest cell dilution which suggested some fungicidal activity as well. As suggested in earlier MIC and growth assessment experiments (Figure 4.2), BY Ole1-GFP was more sensitive to F900742 than BY4741.

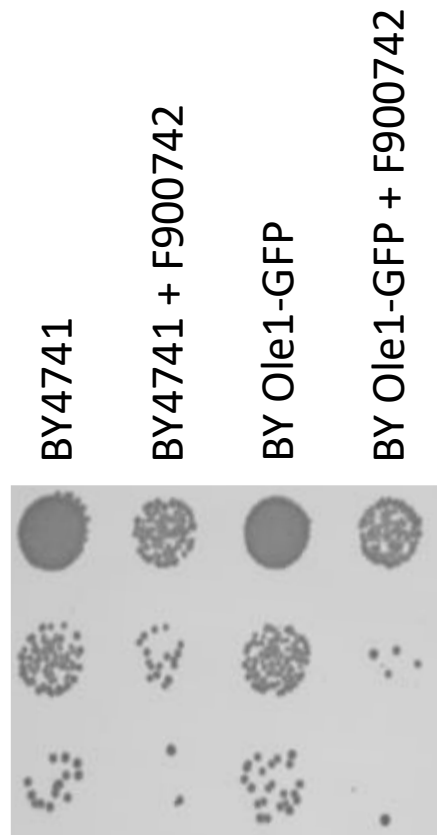


**Figure 6.2. F900742 exerted a fungistatic mechanism of action.** BY4741 and BY Ole1-GFP were treated at their respective MIC (50 and 25  $\mu\text{g/ml}$  F900742) for 24 hours at 30 °C prior to growth on complete media agar for 48 hours. There was growth in both of the treated samples: F900742 exerted a fungistatic mechanism of action. However, there was a substantial reduction in growth in both strains that had been treated with F900742 relative to their untreated counterpart which also suggested some fungicidal activity. BY Ole1-GFP was more sensitive to F900742 than BY4741. N = 3.



### 6.2.3 F900742 effects were selective for the OLE1 pathway

It has been demonstrated that there was a redistribution of Ole1p-GFP to dense puncta that were most often at the periphery of the cell following at least 2 hours of treatment with F900742, however it is somewhat unclear how this relocalisation occurs and indeed the exact region within the cell where these puncta reside. Ole1p is an integral ER membrane anchored protein. The ER can undergo a variety of morphological changes in response to a multitude of stresses and these alterations appear to be dependent on the type of insult. For example, ER stress induced by DTT initiates proliferation of the peripheral ER only (175), whilst whorl formation of the perinuclear ER has been observed by electron microscopy in cells containing a shortage of unsaturated fatty acids which are reversed on unsaturated fatty acid supplementation (91). In addition, Tatzert et al (157) describes Ole1p<sup>ts</sup> relocalising to unidentified membranous structures that are ER-like and derived from the ER following incubation at non-permissive temperatures.

The localisation of other ER resident membrane proteins was examined under conditions where Ole1p-GFP displayed subcellular relocalisation. ER morphology was assessed in *S. cerevisiae* strains that contained fluorescently tagged ER membrane proteins that are not involved with the OLE1 pathway. The tag was either incorporated into the genome after the ORF (BY Sec63-GFP, BY Scs2-GFP) or the strain contained a plasmid with a fluorescent tag before the transmembrane domain region of Scs2p (RFP-TMD). Neither the nuclear nor the peripheral ER appeared morphologically different to that of untreated cells following 2 or 4 hours of treatment with F900742 in any of the strains (Figure 6.3A) suggesting that the morphology of the ER was unaffected by the drug. To simultaneously detect an ER resident protein and Ole1p-GFP, BY Ole1-GFP was transformed with RFP-TMD. Under untreated conditions, RFP-TMD colocalised with the desaturase (Figure 6.3B). In comparison, F900742 induced Ole1p-GFP to redistribute to puncta that appeared in very close proximity with the nuclear and peripheral ER after 2 hours. No puncta were noted in cytoplasmic regions. This data suggested that the ER membrane is not affected by the drug and that Ole1p-

GFP is redistributing either to a specific area(s) on the ER or that Ole1p is in fact in an unidentified region of the cell that is in close proximity to the ER

A)

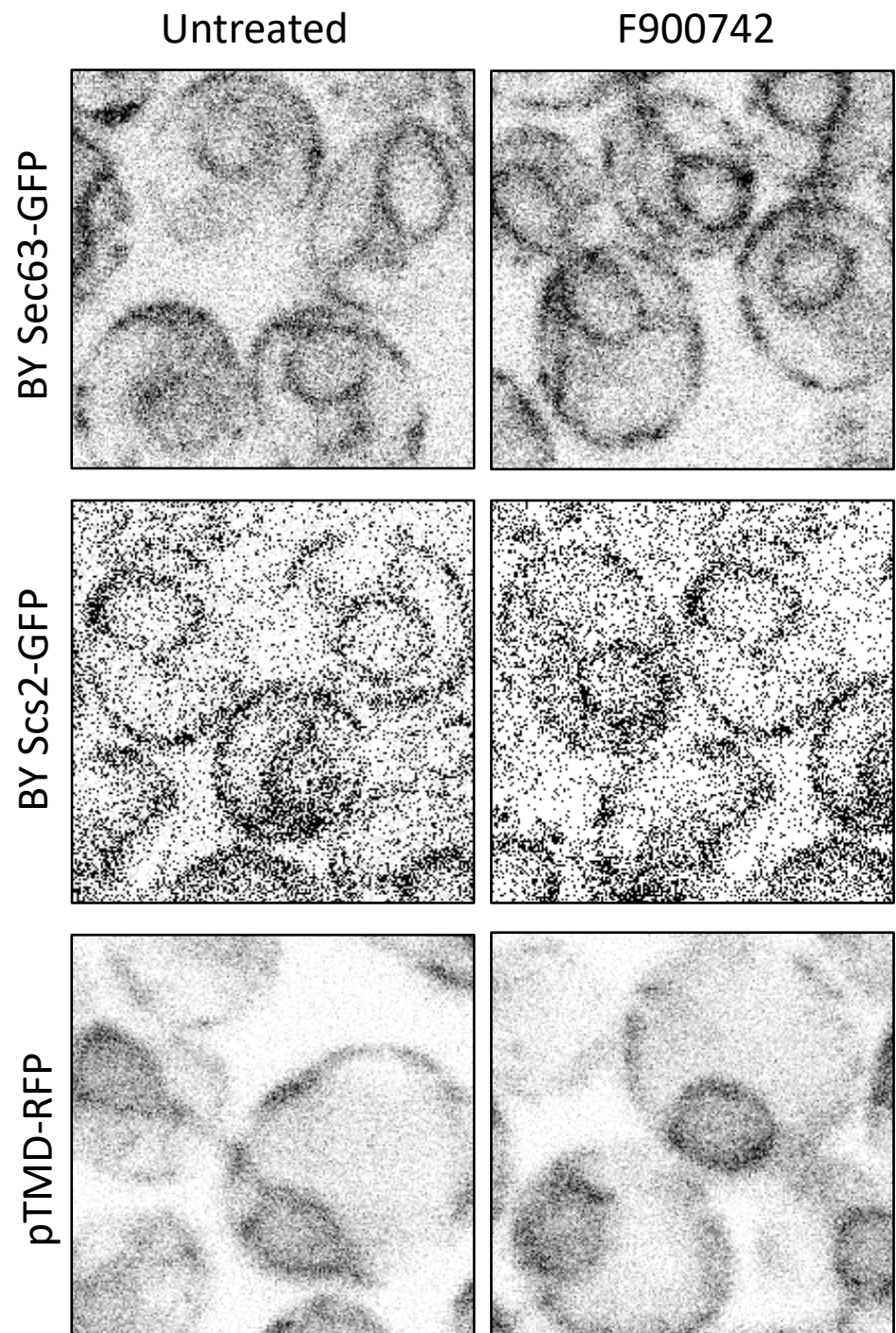
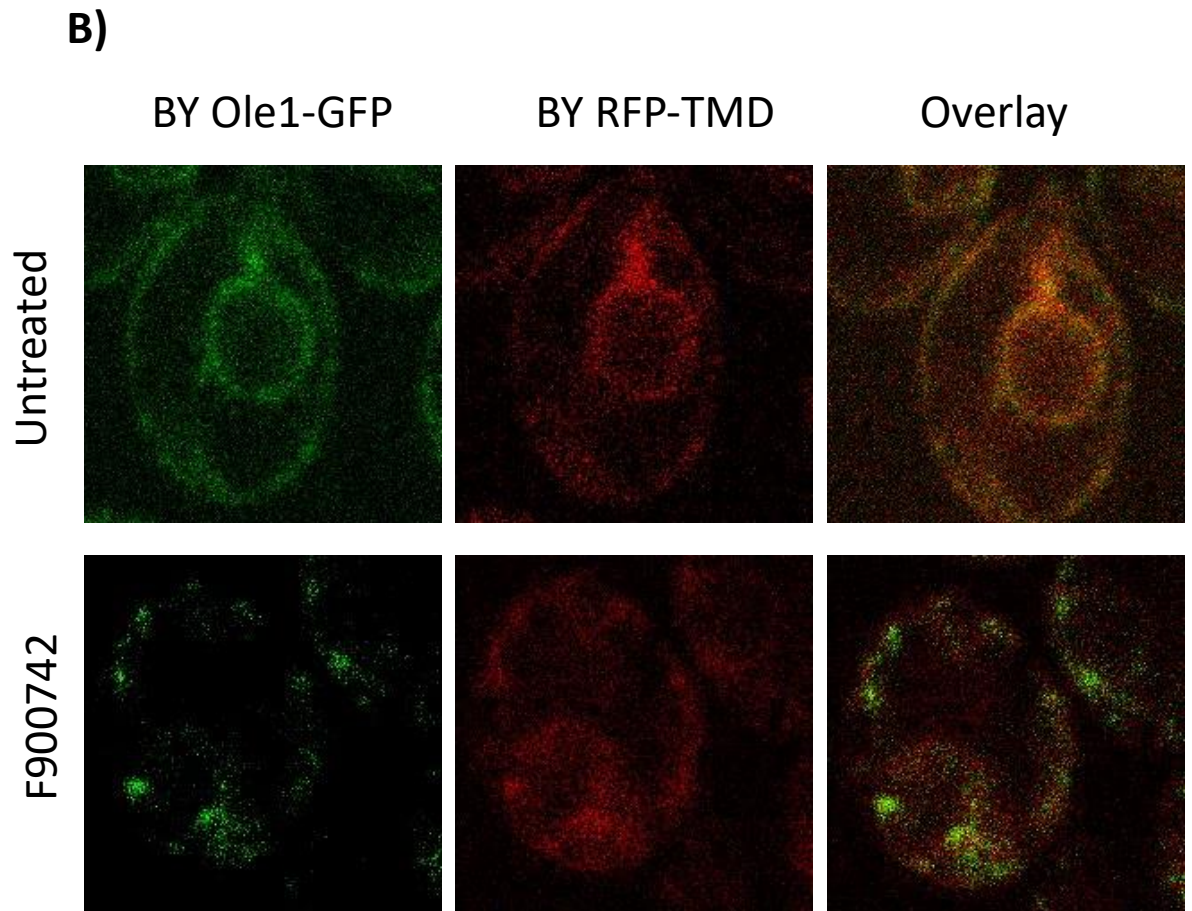


Figure 6.3 continues over page



**Figure 6.3. The localisation of ER membrane proteins was unaffected by F900742.** BY Sec63-GFP, BY Scs2-GFP, pTMD-RFP, and BY Ole1-GFP transformed with RFP-TMD were treated with 100  $\mu\text{g/ml}$  F900742 for 2 hours at 30  $^{\circ}\text{C}$ . (A) The localisation of the ER membrane resident proteins Sec63p and Scs2p was used to assess ER morphology through GFP-tagged strains or plasmids containing a truncated form of the protein such that only the transmembrane domain is expressed. There were no differences in protein distribution between the untreated and F900742 treated samples for any of the strains tested. N = 2. (B) BY Ole1-GFP was transformed with RFP-TMD. F900742 induced the relocalisation of Ole1p-GFP to regions that in close proximity to RFP-TMD. N = 3.

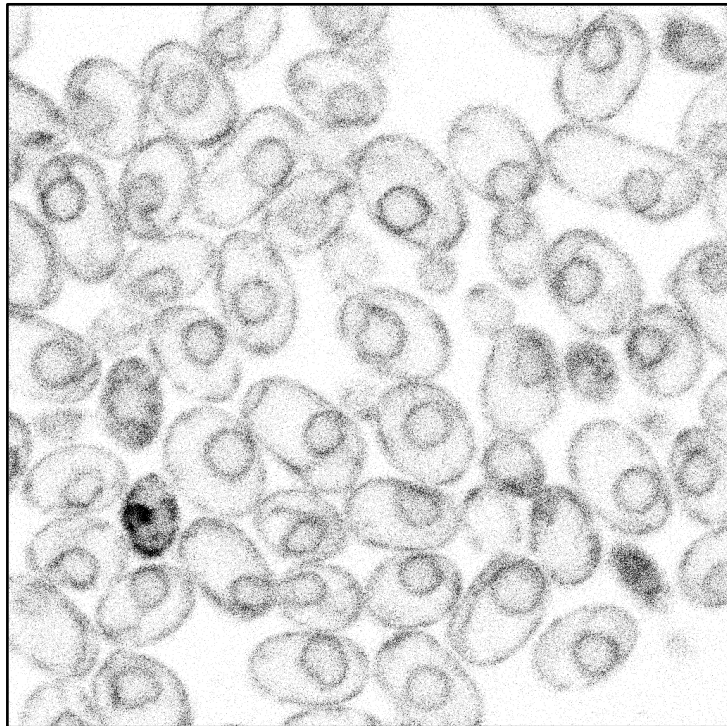
#### 6.2.4 F900742 induced the formation of unidentified structures

The localisation of the ER lumen marker HDEL was assessed. The ER luminal retention sequence HDEL is equivalent of the mammalian ER retention sequence KDEL. This sequence is a target peptide of a single histidine (H), aspartate (D), glutamate (E), and leucine (L) residues located at the C-terminal end of a protein. The HDEL sequence retains proteins in the lumen of the ER by preventing their secretion from the ER, as well as facilitating their return if accidentally exported. The RFP-HDEL sequence was inserted into the TRP1 locus of *S. cerevisiae* strains by digestion of RFP-HDEL and subsequent homologous recombination.

RFP-HDEL was transformed into *wild type* BY4741, as well as into the null strains of the regulators of Ole1p, BY  $\Delta ubx2$ , BY  $\Delta mga2$ , and BY  $\Delta spt23$ . The correct localisation of RFP-HDEL to the ER was confirmed by confocal microscopy. Strains were treated with F900742 for 2 hours prior to imaging. There was a clear peripheral and nuclear ER localisation in all untreated strains. In contrast to all tested ER integral membrane protein strains, F900742 induced the relocalisation of RFP-HDEL to tubular structures in over 90% of cells observed following 2 hours of treatment (Figure 6.4). There was at least one aberrant structure per cell in all background strains tested (Figure 6.5). This observation is not consistent with any previously published reports of altered ER morphology. The tubes were long, straight structures that extended between the poles of the cell and into the daughter cell of budding yeast. Cells containing more than one tube were most often observed with tubes intersecting to form a triangular shape (Figure 6.5F and Figure 6.6C). The tubes were unable to pass through the nucleus, instead they branched and passed around the nuclear membrane. Imaging cells as Z stacks, it was confirmed that the structures extended throughout the majority of the depth of the cell in greater than 75% of cells, however they were narrow in width in all cells observed. As can be inferred from the HDEL sequence, these structures are likely to be consistent with the lumen of the ER. There were no obvious differences in tube morphology between the different background strains.

BY4741 – RFP HDEL

Untreated



F900742

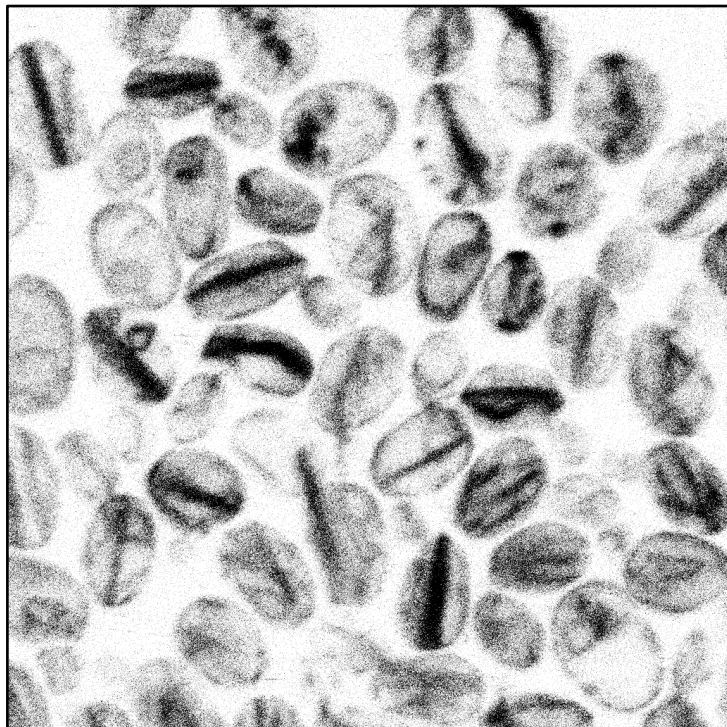
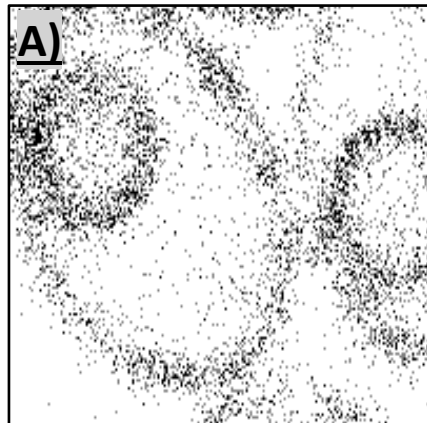


**Figure 6.4. F900742 induced the relocalisation of RFP-HDEL in wild type yeast.** Cells were treated with 100  $\mu\text{g/ml}$  F900742 for 2 hours at 30  $^{\circ}\text{C}$ . F900742 induced a redistribution of the ER luminal marker RFP-HDEL to unidentified tubular structures that extended between the poles of the cell. After 2 hours of treatment, the tubes were straight and wide. RFP-HDEL was mislocalised in greater than 90% of cells treated with F900742. N = 3.

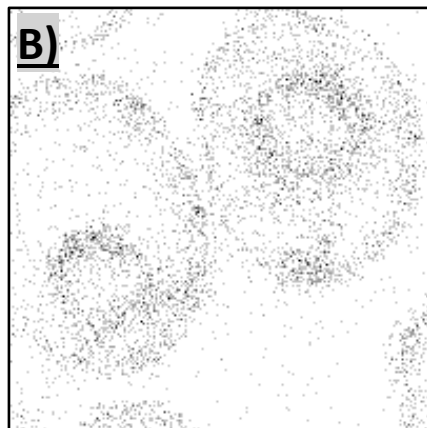
Untreated

F900742

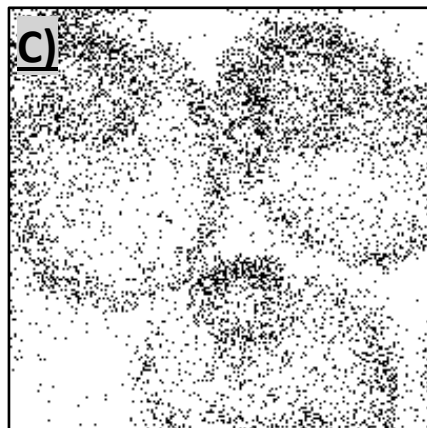
BY4741



$\Delta ubx2$



$\Delta mga2$



$\Delta spt23$

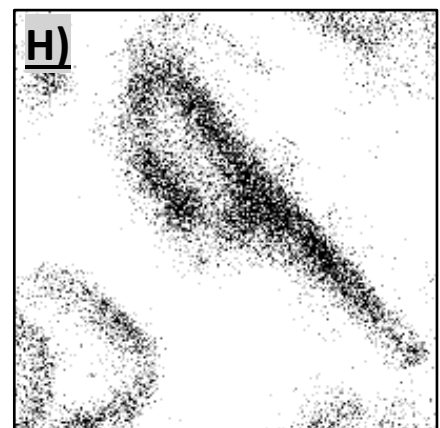
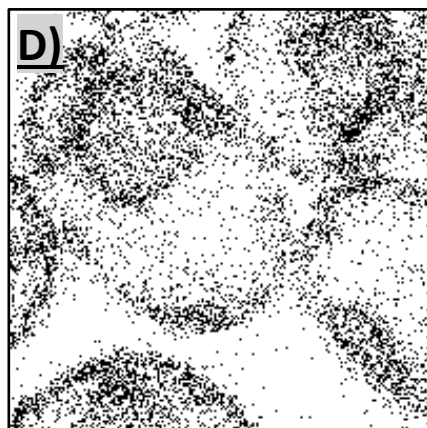


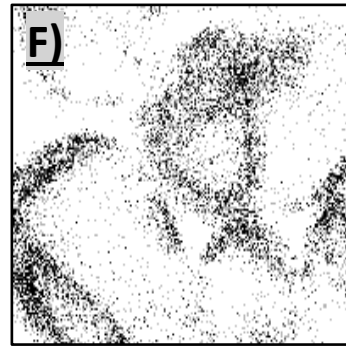
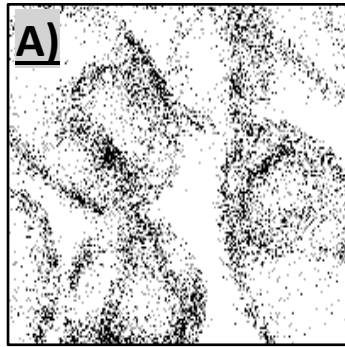
**Figure 6.5. F900742 induced the relocalisation of RFP-HDEL in OLE1 null pathway strains.** Strains were treated with 100µg/ml F900742 for 2 hours at 30 °C. BY4741 wild type and strains containing a deletion for a regulator of OLE1 were transfected with RFP-HDEL. RFP-HDEL localised to the nuclear and peripheral ER in all untreated samples. F900742 induced the relocalisation of RFP-HDEL to tubes that extended between the poles of the cell and into daughter cells in all strains. The tubes were relatively narrow, but extended throughout the majority of the depth of the cell. N = 3



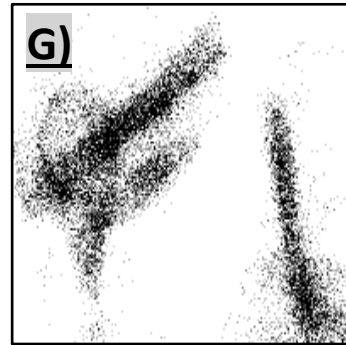
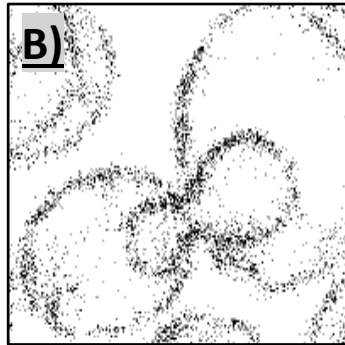
The tubular structures were first noted in a minority (less than 20%) of BY4741-HDEL cells after 30 minutes of treatment with F900742 (Figure 6.6F). Following 1 hour with the drug, almost all cells (greater than 80%) observed contained the tubes which appeared thicker and darker than at the previous time point (Figure 6.6G). Tubes were even thicker and darker at 2 hours and again at 4 hours post-treatment (Figure 6.6H and 6.6I). The formation of the tubes correlated with a decrease in amount of HDEL localised to the peripheral and nuclear ER. Following 4 hours of treatment, HDEL appeared as smaller, intense fragments and there was an increase in cytosolic background fluorescence. Following 24 hours of treatment there was some resemblance of classical nuclear and peripheral ER morphology, however there were still faint tubes. Furthermore, at this time point, there was also the appearance of peripheral and nuclear puncta that were not observed in any cells imaged at any other time point (Figure 6.6J). These puncta could possibly be the ends of tubes or they could be fragments of former long tubes. As with the 4 hour treatment, there was also a large amount of cytosolic staining at the 24 hour time point. The partial redistribution of HDEL to wild type ER distribution after 24 hours is consistent with F900742 being a fungistatic inhibitor. Fungistatic drugs halt the growth of the cell only until the point when the drug is no longer at inhibitory concentrations.

It has previously been demonstrated that Ole1p-GFP relocalisation was lipid dependent and that supplementation of either oleic acid or palmitoleic acid was sufficient for normal Ole1p-GFP distribution (Figure 4.9 to Figure 4.14). There were no tubes noted in any cell treated with oleic acid and F900742 for 2 hours (Figure 6.7D). Oleic acid alone did not affect HDEL localisation, nor amount (Figure 6.7B). Furthermore, oleic acid supplementation was sufficient to reverse this phenotype to normal ER distribution and amount (Fig 6.8).

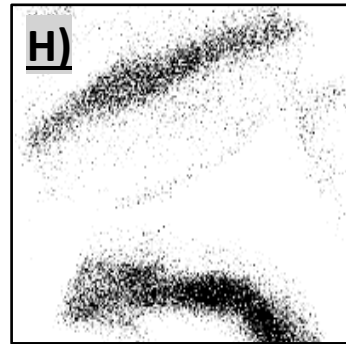
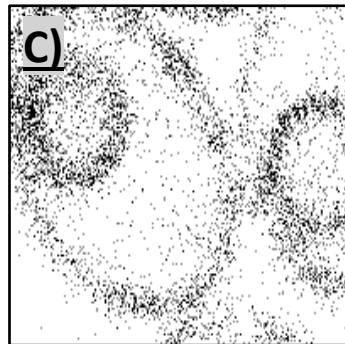
30 mins



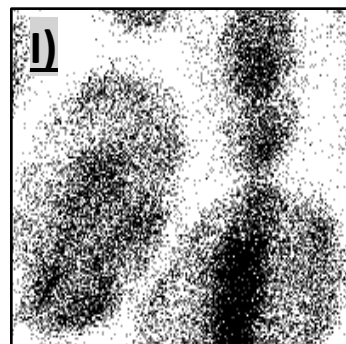
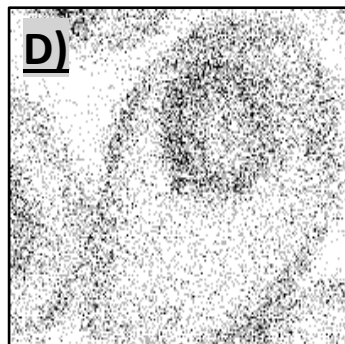
1 hour



2 hours



4 hours



24 hours

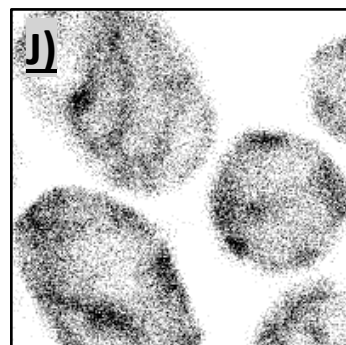


**Figure 6.6. F900742 induced a rapid relocalisation of RFP-HDEL.** Wild type BY4741 containing the integrated RFP-HDEL tag were treated with 100 µg/ml F900742 for 24 hours at 30 °C. Samples were taken after 30, 60, 120, and 240 minutes, as well as at 24 hours. The tubes were first noted in less than 20% of cells after 30 minutes of treatment. All cells imaged contained tubes that extended between the poles of the cell and into daughter cells by 2 hours. The tubes were denser by 4 hours, and some appeared to have fragmented. After 24 hours, the structures appeared as puncta rather than tubes. N = 3.

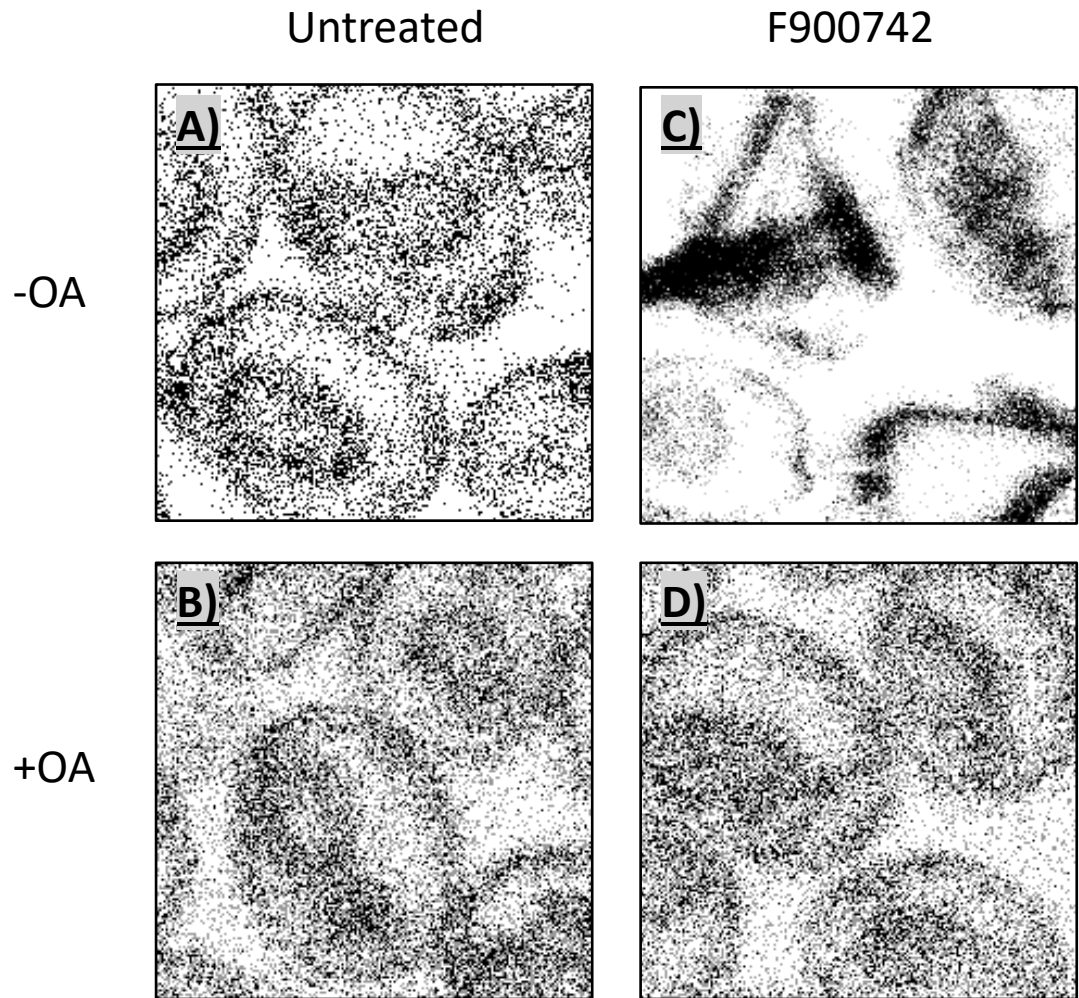
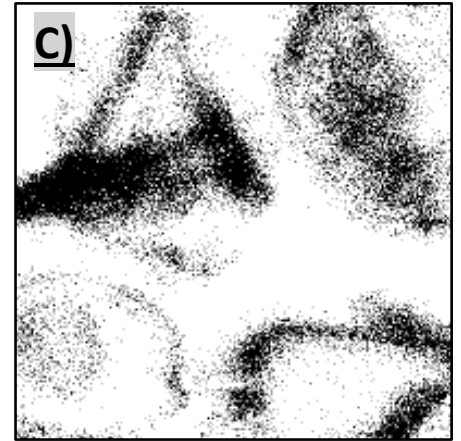
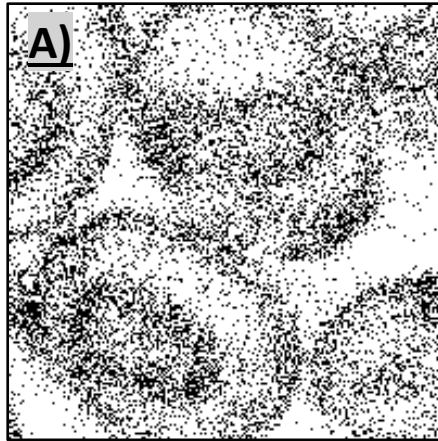
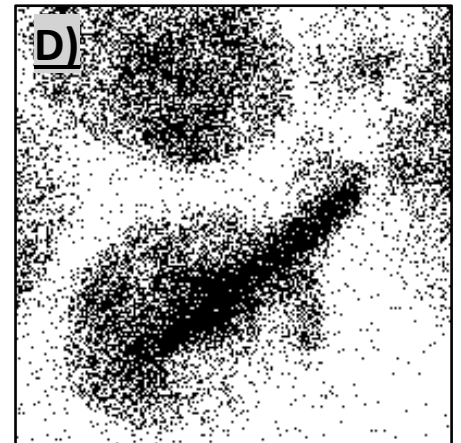
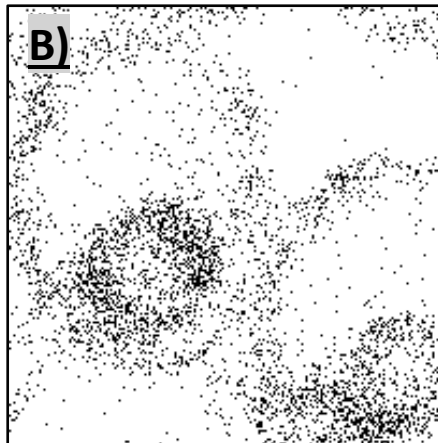


**Figure 6.7. Oleic acid inhibited RFP-HDEL relocalisation.** BY4741 cells containing RFP-HDEL were treated with 100  $\mu\text{g/ml}$  F900742 and 1 mM oleic acid for 2 hours at 30  $^{\circ}\text{C}$ . Oleic acid inhibited the formation of tubes in all cells observed. Oleic acid did not interfere with the normal localisation of RFP-HDEL to the ER. N = 3.

2 hours



4 hours



2 hours F9 -> 2 hours OA

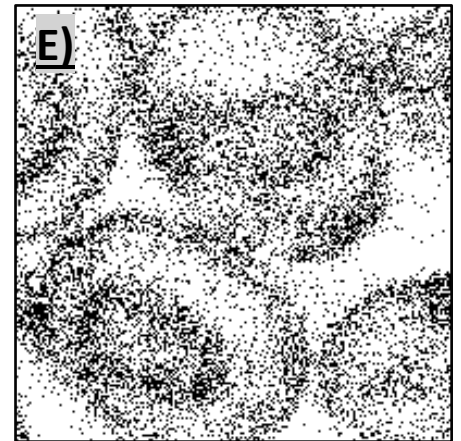


**Figure 6.8. Oleic acid reversed RFP-HDEL relocalisation.** BY4741 containing RFP-HDEL were treated with 100  $\mu\text{g/ml}$  F900742 for 2 hours before 1 mM oleic acid supplementation for a further 2 hours. Samples were grown at 30  $^{\circ}\text{C}$ . Oleic acid completely reversed the distribution of RFP-HDEL to tubes. No cells observed contained tubes after 2 hours with oleic acid. N = 3.

Thus far, I have demonstrated that chemical inhibition of the OLE1 pathway with F900742 induced the formation of aberrant tubular structures that extended throughout the cell in a variety of backgrounds. Discussions with Professor Robert Ernst (University of Saarland, Homburg, Germany) revealed that his group has observed a similar tubular phenotype in untreated  $\Delta mga2$  cells tagged with HDEL grown in complete media liquid after 24 hours. This phenotype could also be rescued by 90 minutes of oleate supplementation (unpublished data). Their interpretation is that chronic reduction in desaturase activity (through the deletion of Mga2p (91)) over a 24 hour period is sufficient to substantially skew the fatty acid content of  $\Delta mga2$  cells in favour of saturated fatty acids, thereby rendering toxic levels of free saturated fatty acids and saturated lipids. They predict that the tubes are a “gel phase” of ER - ER that contains high levels of saturated fatty acids making it less fluid - that is a side compartment to the normal ER. Professor Ernst has suggested that the purpose of a gel phase ER could be twofold: firstly, the structure would sequester toxic levels of saturated fatty acids in order to protect the nuclear and peripheral ER from any alterations in lipid balance and, therefore, ensures normal function; secondly, the structure is very large and extends throughout the cell which could provide a physical force that pushes cytosolic content towards the periphery of the cell, increasing the availability of required substrates and cellular metabolism in times of stress. Alternatively, the formation of tubes could be a process that occurs to separate regions of ER containing very high saturated acyl chain content from areas of normal lipid composition. This would ensure the isolation of lipotoxic regions of membrane and that ER processes are unaffected by the alterations in lipid content. Though unlikely, it also plausible that tube formation is a passive process that has no physiological benefit in sick yeast.

Based on Professor Ernst’s observation that HDEL relocalises to tubes in  $\Delta mga2$  cells after 24 hours, it was expected that tubes would also be observed in null cells for the alternative transcriptional activator of OLE1  $\Delta spt23$  tagged with RFP-HDEL. BY  $\Delta spt23$  was treated with F900742 for 24 hours. F900742 induced the formation of demi tubes that extended only part way across the cell (Figure 6.9). Untreated  $\Delta spt23$  had

morphologically normal nuclear and peripheral ER with small tubes that appeared to extend from the nucleus. None of the untreated imaged cells contained long tubes as observed in the samples treated for 2 hours. There was also an increase in HDEL content within the nucleus, as well as a slight increase in cytosolic HDEL in areas surrounding the nucleus relative to the periphery. The formation of tubes in untreated BY  $\Delta mga2$  has not been tested, but it would be interesting to see whether tubes also develop in this background after 24 hours in untreated samples, and whether these tubes are morphologically similar to those induced by F900742. It was expected that the relocalisation of HDEL was a result of an increase in saturated fatty acid content in both the genetic knock out strains and F900742 treated samples. The differences in timing of tube formation is likely due to F900742 inducing a complete inhibition of Ole1p activity after 4 hours, whilst a knockout of either *mga2* or *spt23* induces a less rapid effect due to functional redundancy between the transcriptional regulators: deletion of either gene is associated with a reduction in OLE1 mRNA rather than a complete inhibition of Ole1p synthesis (91).

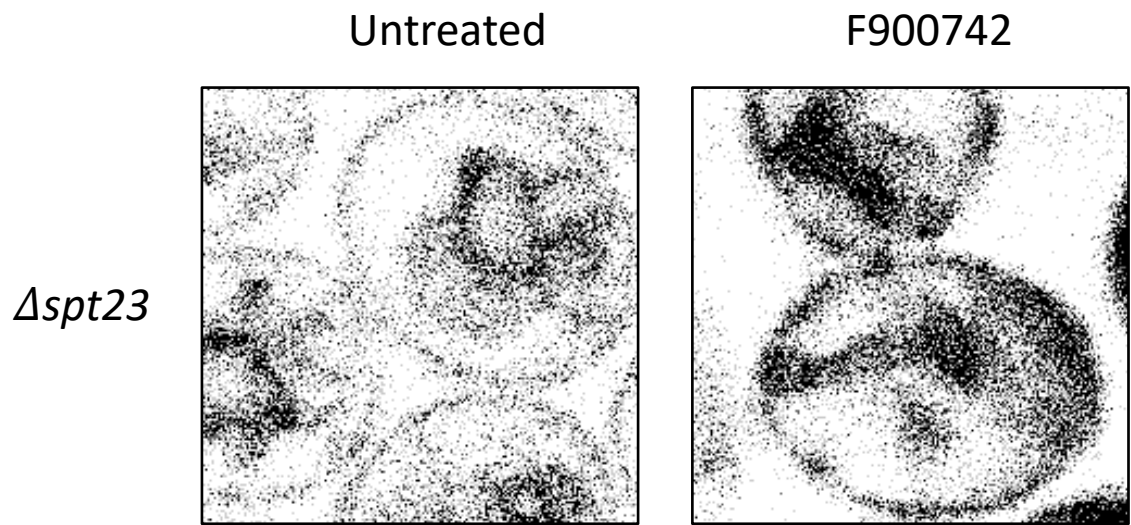


**Figure 6.9. Deletion of SPT23 was not sufficient to induce the relocalisation of RFP-HDEL.** 100  $\mu\text{g/ml}$  F900742 was required for the redistribution of RFP-HDEL. Small tubes extending from the nucleus were noted in the untreated sample after 24 hours. Samples were grown at 30 °C. N = 2.



It would be expected that *ole1* null cells would enter a similar state of stress responses in media lacking unsaturated fatty acids as those that have had Ole1p chemically inhibited by F900742. It has been previously demonstrated that *ole1* null cells are able to survive for a few cell divisions without the addition of exogenous unsaturated fatty acids (167). It was predicted that 2 hours of growth in the absence of oleic or palmitoleic acid would initiate early lipotoxic stress response pathways. BY  $\Delta ole1$  cells were grown in complete liquid media for 2 hours in the absence or presence of F900742 and oleic acid. Tubes that appeared morphologically similar in length and shape to ones previously described were observed in the untreated  $\Delta ole1$  sample. F900742 did not have any effect on tube formation in BY  $\Delta ole1$  (Figure 6.10A and Figure 6.10C). The addition of oleic acid to both the F900742 treated and untreated samples prevented the formation of the tubes and HDEL assumed classical ER localisation (Figure 6.10B and 6.10D).

BY  $\Delta ole1$

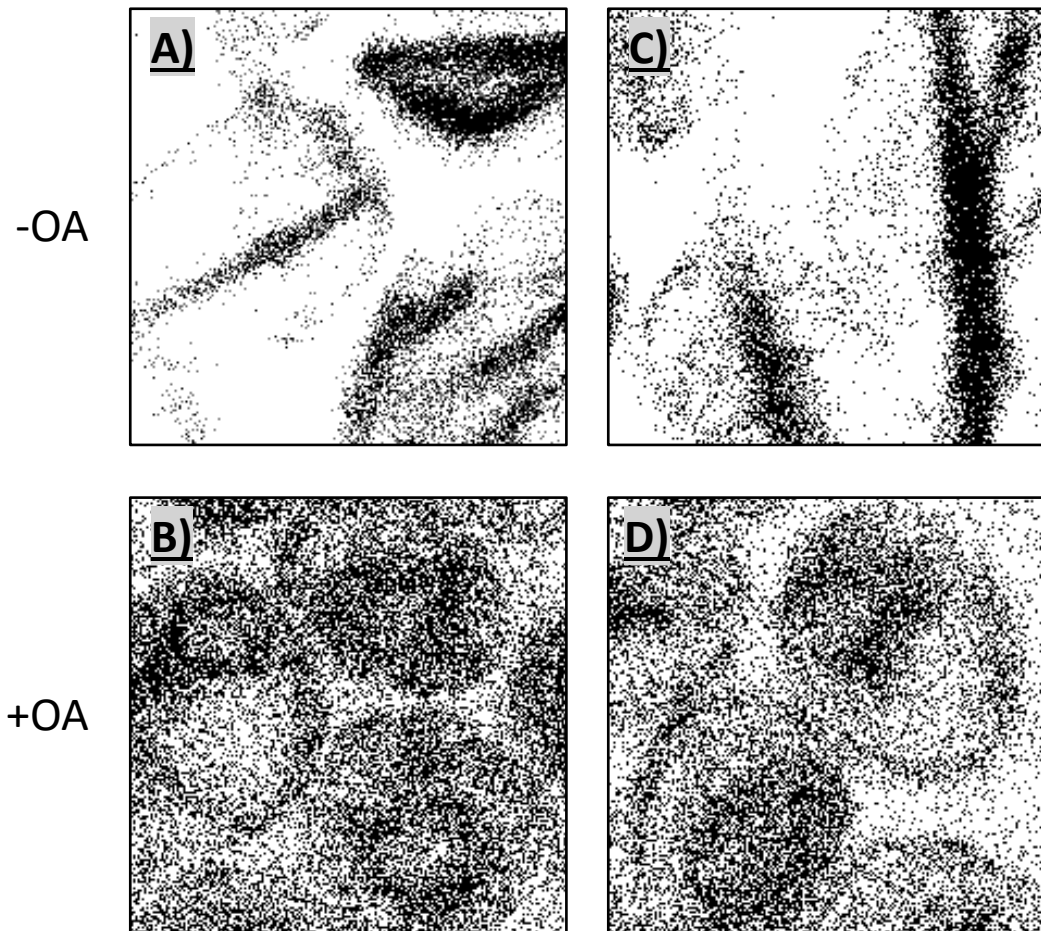
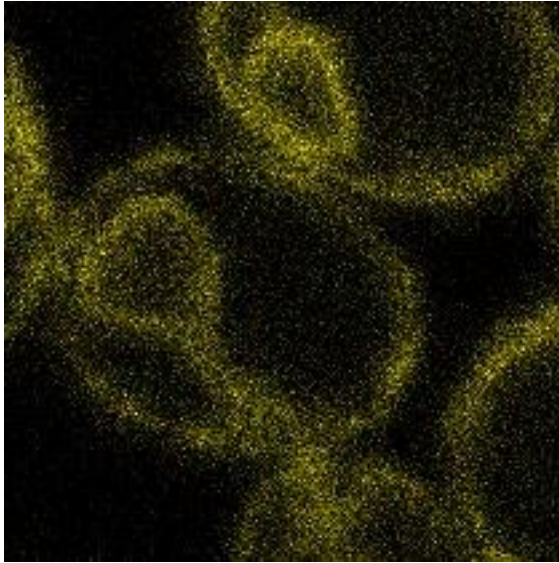


**Figure 6.10. Deletion of OLE1 induced the redistribution of RFP-HDEL.** There were no morphological differences in the relocation of RFP-HDEL between the sample treated with F900742 and untreated. Oleic acid was sufficient to prevent the redistribution of the ER luminal marker. F900742 was added at 100  $\mu\text{g/ml}$ . Oleic acid was added at 1 mM. Samples were grown at 30  $^{\circ}\text{C}$  for 2 hours. N = 3.

To determine whether Ole1p-GFP relocated to areas that colocalised with the tubular HDEL compartments, BY Ole1-GFP was transformed with HDEL. Ole1p-GFP and RFP-HDEL co-localised in untreated samples. F900742 induced the formation of tubes as observed in all other genetic backgrounds, however it was difficult to clearly identify Ole1p-GFP localisation in the majority of cells due to a high amount of background. Of note, this was the only experiment where difficulties in observing Ole1p-GFP localisation occurred. In a minority of cells, Ole1p-GFP was apparent. In these cells, Ole1p-GFP localised near to or adjacent to the tubes in all cells (Figure 6.11). However, it is unclear whether this is because of the difficulty in clearly detecting both fluorescent tags. Therefore, Ole1-GFP was mated with BY4741-HDEL. To this point, all HDEL studies had been conducted in haploid strains; the Ole1-GFP-BY-HDEL strain is a diploid, therefore contains two copies of OLE1 - one copy of OLE1-GFP and one copy of untagged OLE1. It was assumed that the diploid would be less sensitive to F900742 than the haploid due to an increase in amount of Ole1p in the diploid. To circumnavigate this potential problem, cells were also treated with a higher concentration of F900742 (100 µg/ml and 200 µg/ml). Tubes were observed as previously noted, however it was still difficult to clearly identify Ole1p-GFP localisation. Ole1p-GFP tubes did colocalise with HDEL, whereas Ole1p-GFP puncta appeared in close proximity to HDEL tubes. The possibility of cross-channel bleed through was eliminated by checking for fluorescence in both channels with strains containing either a red or a green tag (Figure 6.12).

Untreated



F900742

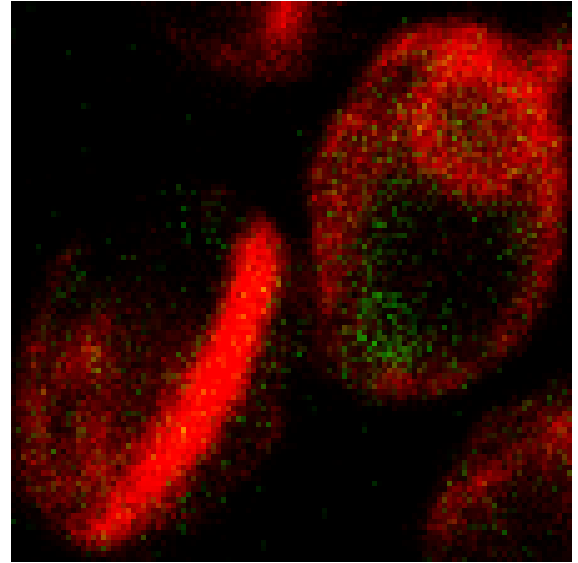


**Figure 6.11. Ole1p-GFP relocalised to RFP-HDEL.** BY Ole1-GFP expressing RFP-HDEL was treated with 100  $\mu\text{g/ml}$  F900742 for 2 hours. Ole1p-GFP relocalised to areas in close proximity to RFP-HDEL. All cells observed contained relocalised HDEL. Not all cells contained relocalised Ole1p-GFP. Samples were grown at 30  $^{\circ}\text{C}$ . N = 2.

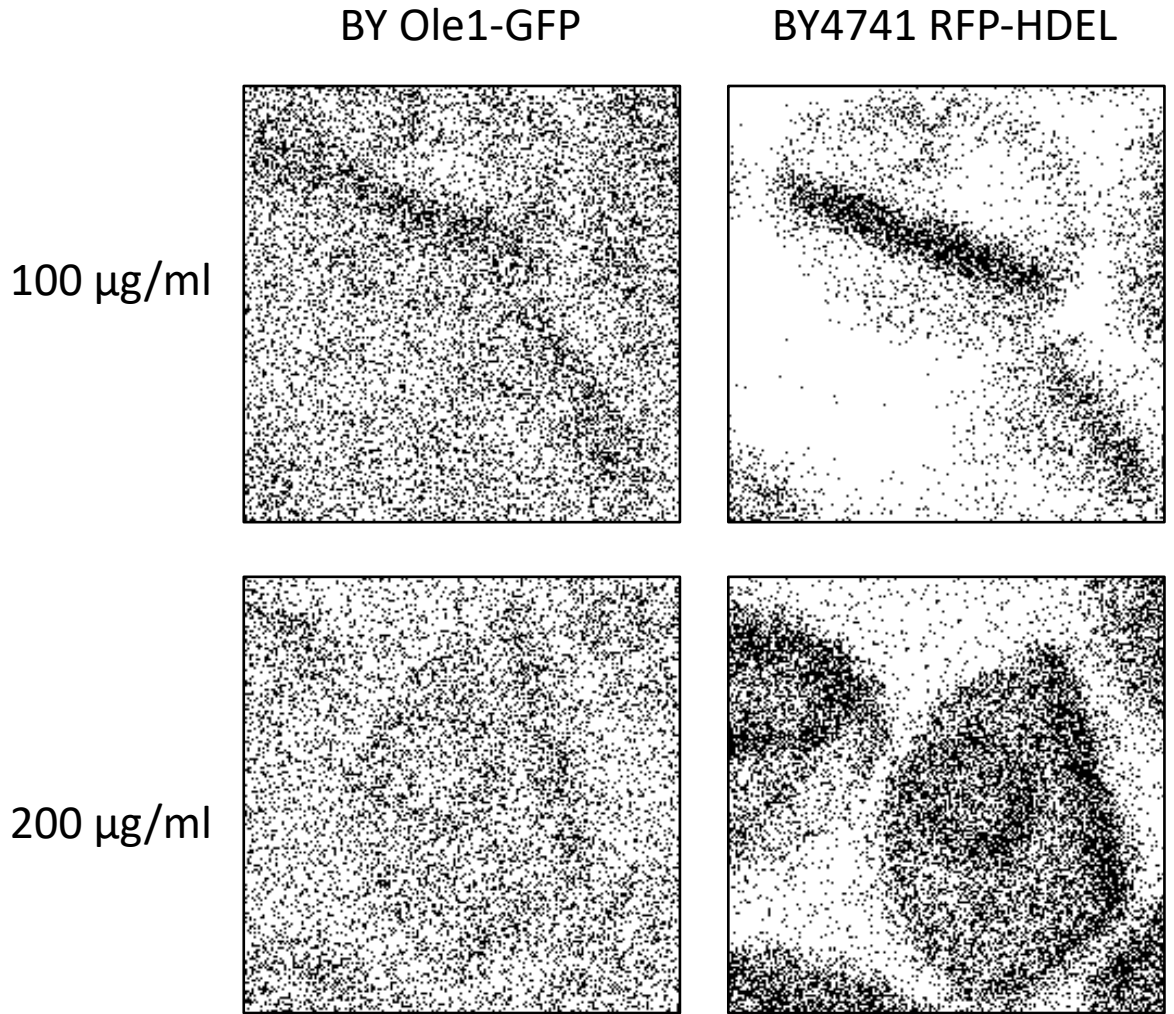


**Figure 6.12.** Ole1p-GFP relocated to RFP-HDEL in the diploid Ole1-GFP RFP-HDEL. BY Ole1-GFP was mated with BY4741-RFP-HDEL and treated with F900742 for 2 hours at 30 °C. Ole1p-GFP relocated to tubes that colocalized with RFP-HDEL.

### 6.2.5 Ole1p-GFP did not relocalise to lipid droplets

Previous studies have demonstrated that altering the expression of components of the OLE1 pathway, either through deletion or overexpression, does render an abnormal cellular fatty acid profile. For example, deletions of either *ubx2* or *mga2* results in a significant increase in the amount of saturated fatty acids at the expense of unsaturated fatty acids. Previous studies have demonstrated that excess saturated fatty acids are stored in lipid droplets (172). It was speculated that Ole1p-GFP was relocalising nearby to pools of saturated lipids stored in lipid droplets in an attempt to normalise the cell's balance of saturated and unsaturated fatty acids. Erg6p is a marker of lipid droplets. A haploid strain that contained a plasmid with ERG6 and a red fluorescent marker was mated with BY Ole1-GFP such that the diploid expressed both Ole1p-GFP and Erg6p-RFP. F900742 induced a substantial increase in the size, but a reduction in number of lipid droplets (Figure 6.13). Ole1p-GFP was observed in close proximity to some lipid droplets in some cells, however co-localisation between the desaturase and lipid droplets was not observed.

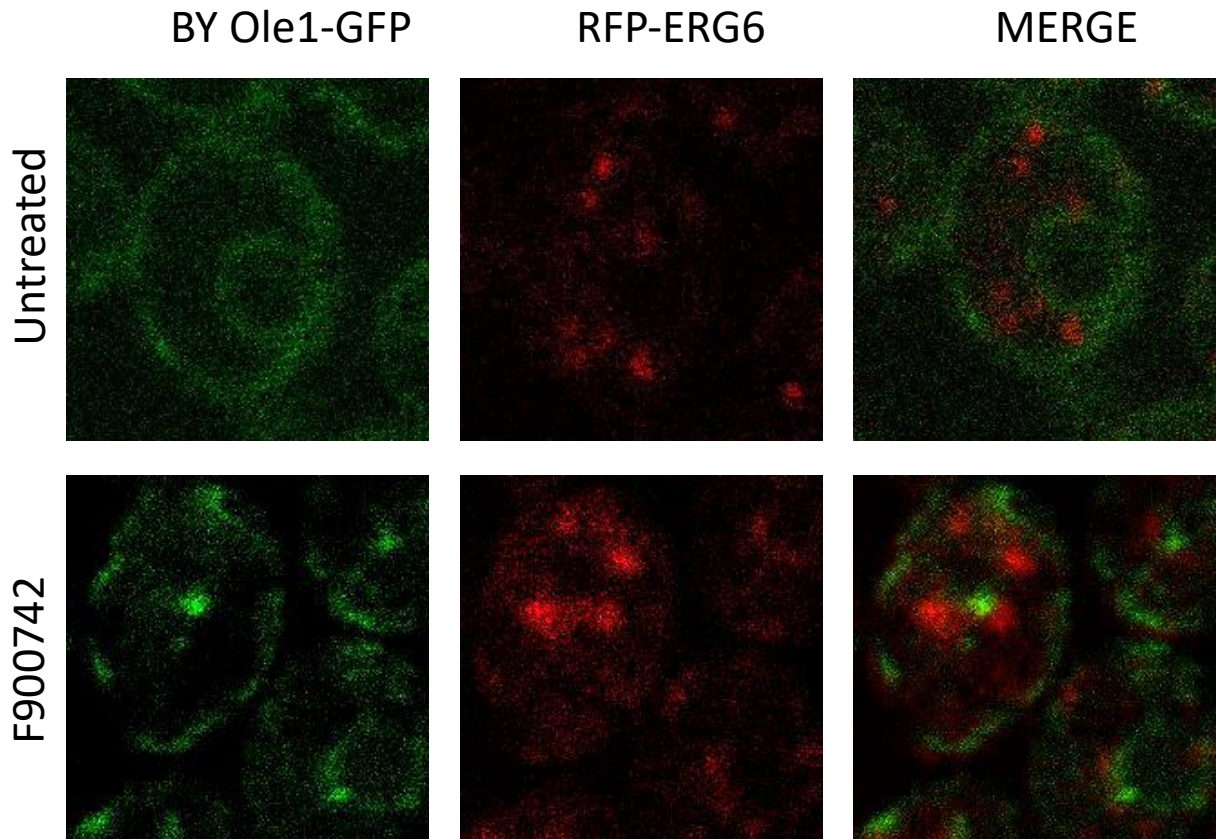


**Figure 6.13. Ole1p-GFP did not relocalise to lipid droplets.** BY Ole1-GFP was mated with RFP-ERG6. The diploid was treated with 100  $\mu\text{g/ml}$  F900742 for 2 hours at 30  $^{\circ}\text{C}$ . F900742 induced an increase in the size of lipid droplets, but a reduction in the number per cell. Ole1p-GFP relocalised to areas in close proximity to lipid droplets. N = 3

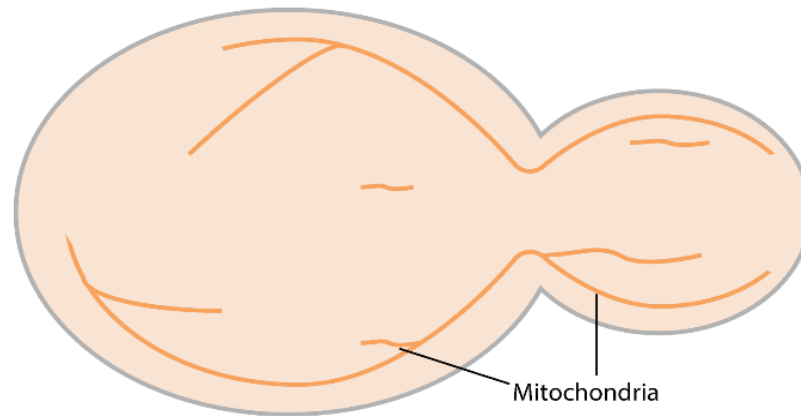
### 6.2.6 F900742 induced mitochondria fission

The alternative name for Ole1p is Mdm2, or Mitochondrial Distribution and Morphology 2 (MDM2). McConnell et al initially identified a temperature-sensitive *mdm* strain that resulted in a failure to deliver mitochondria to daughter cells along with extensively clumped mitochondria and altered morphology in both mitotic and non-mitotic cells following 90 minutes at nonpermissive conditions (176). Stewart et al then demonstrated that there was a significantly different fatty acid profile in the *mdm2* strain with a vast increase in the amount of saturated C16 and C18 fatty acids at the expense of their unsaturated counterparts (109). They also demonstrated that both the inherited and morphological mitochondrial phenotypes could be inhibited by the addition of 1 mM oleate prior to incubation at non-permissive temperature. Together these data suggest there is a direct a role for fatty acids in the regulation of mitochondrial movement, distribution, and inheritance as the aberrant phenotype can be rescued by the addition of unsaturated fatty acids.

The mitochondria are essential organelles in eukaryotic cells. Their most prominent function is to generate energy for the cell via oxidative phosphorylation, as well as a variety of other metabolic processes. The structure of mitochondria is complex: they are double membrane-bound organelles with a highly dynamic morphology and distribution that reflects the energy requirements of the cell. The mitochondria in *S. cerevisiae* is maintained by a series of fusion and fission events in response to the cell's metabolic status. During periods of high energy requirement, mitochondria fuse to form a highly branched network that ensures sufficient energy output. Mitochondria fusion also allows for healthy mitochondria to compensate for defects in others through the sharing of components. Conversely, mitochondria fission results in the segregation of mitochondria to regulate a lower energy output during times of low metabolic activity, and, importantly for this work, fission also facilitates the protection of the healthy network from irreversibly damaged mitochondria (177). Figure 6.14A illustrates the mitochondria morphology distribution between a mother and daughter cell.



**A)**



**B)**

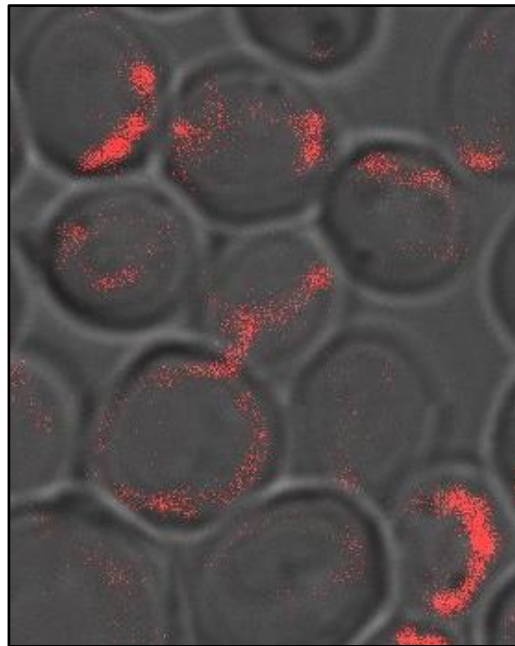


**Figure 6.14. Mitochondria morphology and distribution in wild type *S. cerevisiae*.** (A) Cartoon to represent the morphology and distribution of the mitochondria in budding yeast mother and daughter cells. (B) Tom6p-RFP distribution in wild type, log phase *S. cerevisiae*.

The mitochondria were examined by assessing the localisation of the outer mitochondrial membrane protein Tom6p (Figure 6.14B). Untreated, log phase samples contained mitochondria that appeared mostly continuous, indicative of a more fused mitochondria morphology. In stark contrast, F900742 induced fragmentation of mitochondria indicating that one mechanism that *S. cerevisiae* evoke in response to desaturase inhibition are mitochondrial fission events (Figure 6.15). Mitochondria fission was observed in all cells imaged after 30 minutes. The mitochondria fragments appeared morphologically the same and of comparable fluorescence at both 30 minutes and 1 hour after treatment. The average size of the clumps appeared larger by 2 hours, suggesting that several had fused together or were in very close proximity. The timings of the mitochondria fragmentation suggested that mitochondrial fission is an early cellular stress response to F900742 and it occurred prior to Ole1p-GFP relocalisation. 1 mM of oleic acid was sufficient to completely inhibit this phenotype when added with F900742 (Figure 6.16). Oleic acid alone did not have any effect on mitochondria morphology or distribution. Furthermore, one hour of incubation with oleic acid was sufficient for the mitochondria to resume a wild type morphology and distribution following 2 hours of incubation with F900742 (Figure 6.17). This data suggested that one mechanism by which F900742 exerted lipotoxicity was through the disruption of mitochondria and corroborated earlier discussions on the regulatory role of fatty acids on the mitochondria.

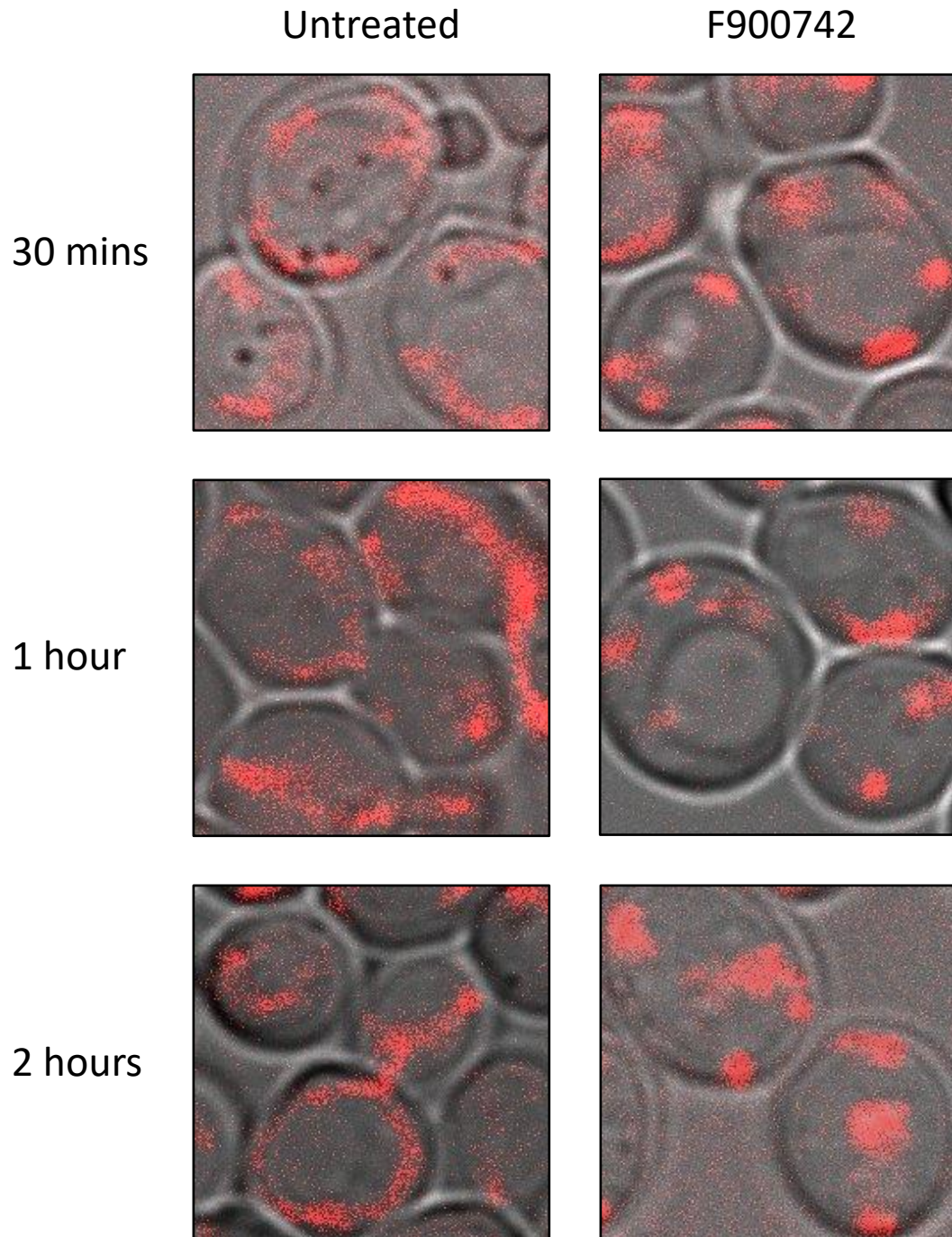


**Figure 6.15. F900742 induced mitochondrial fission.** Mitochondria fragmentation was first observed after 30 minutes of incubation with 100  $\mu\text{g/ml}$  F900742. The fragments appeared larger as though mitochondria fragments had clumped after 2 hours which was associated with an increase in brightness of Tom6p-RFP. Mitochondria were observed in daughter cells treated with F900742. Samples were incubated at 30  $^{\circ}\text{C}$ . N = 3.

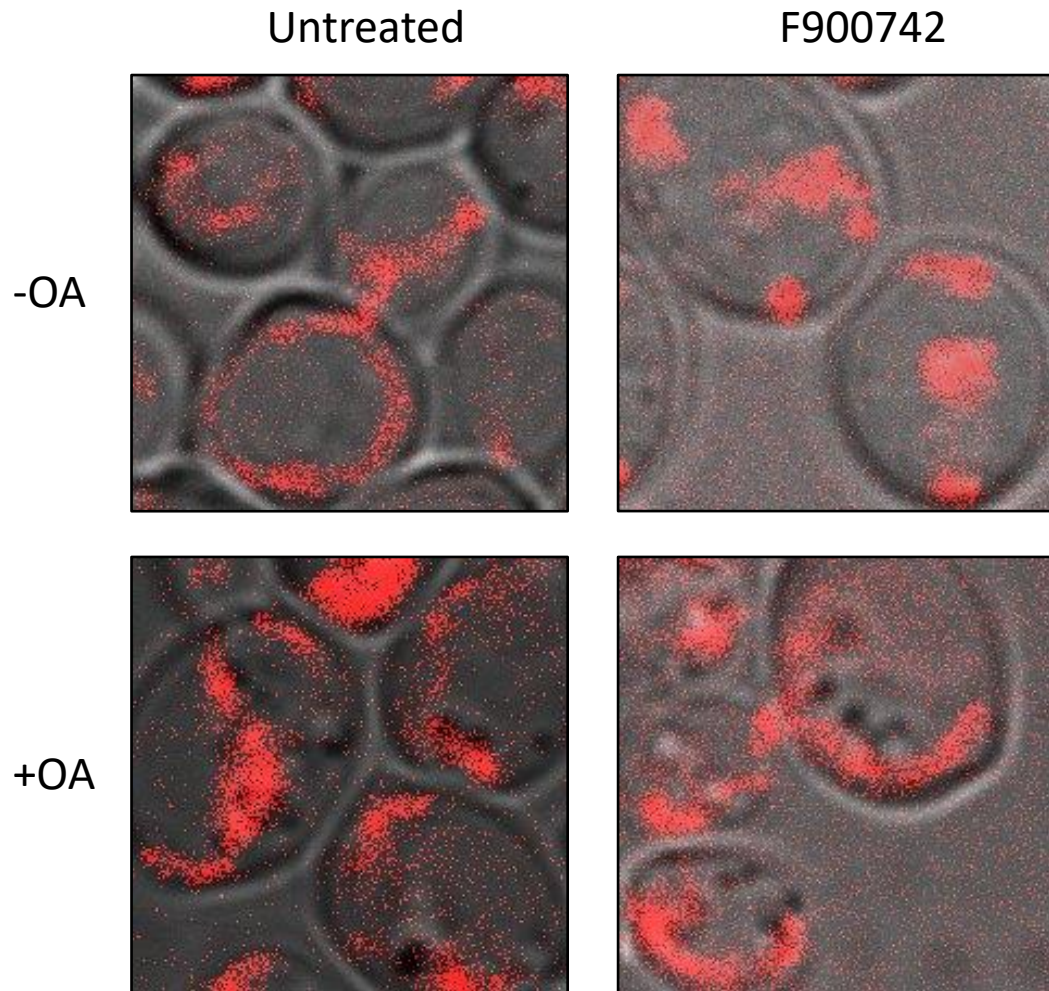


**Figure 6.16. Oleic acid inhibited F900742-induced mitochondrial fission.** There were no morphological differences in mitochondrial morphology between untreated cells and samples treated with 100  $\mu\text{g/ml}$  F900742 and 1 mM oleic acid. Mitochondria appeared continuous in the presence of oleic acid. Oleic acid alone did not affect the mitochondrial morphology. Samples were incubated at 30  $^{\circ}\text{C}$ . N = 3.



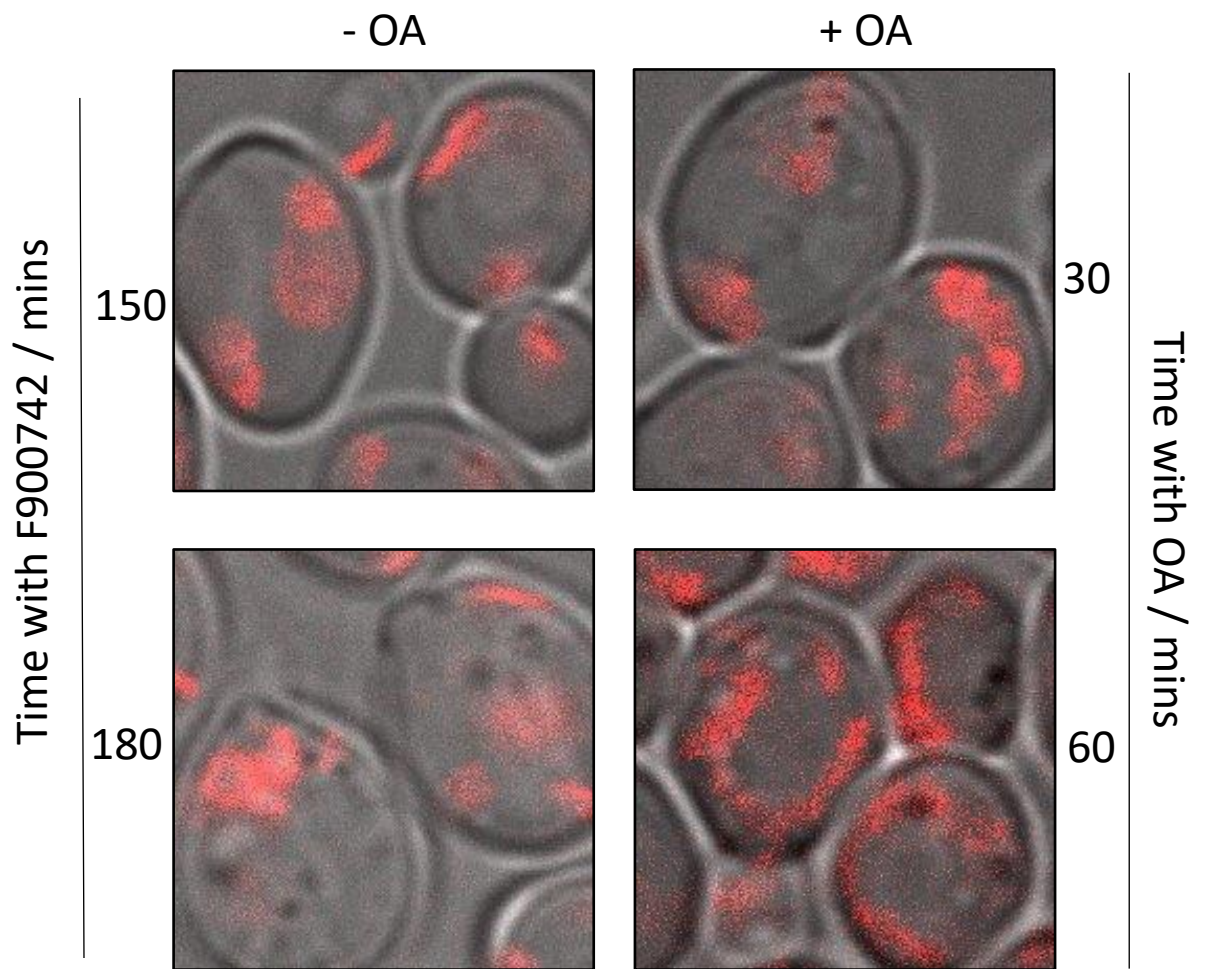


**Figure 6.17. Oleic acid reversed F900742-induced mitochondrial fission.** There was a complete reversal in mitochondrial morphology to that of wild type following 60 minutes of incubation with 1mM oleic acid. Samples were pre-treated with 100  $\mu\text{g/ml}$  F900742 for 2 hours prior to oleic acid addition. Samples were incubated at 30  $^{\circ}\text{C}$ . N = 3.

### **6.2.7 The morphology of other organelles was unaffected by F900742**

Organelles each have a unique membrane lipidome and proteome. Organelles synchronise their metabolic processes to fit with cellular requirements to ensure the maintenance of proper cellular function. F900742 induced morphological defects to the mitochondria and lipid droplets, and also the formation of an unidentified ER-derived compartment which are all lipid-dependent alterations. Inhibition of the OLE1 pathway could also have profound effects on the structures and functions of other subcellular structures. It was next investigated whether the organelle membranes of the cis Golgi (BY Mnn9-GFP), nucleus (BY NmaIII-GFP), peroxisome (BY Pex3-GFP), and vacuole (BY Vac4-GFP), as well as actin (BY Sec6-GFP) were also affected by F900742 using the strains of GFP-tagged proteins indicated. F900742 did not induced any differences in the localisation of these protein markers in any of the organelles observed after 4 hours (Figure 6.18). It was concluded that 4 hours was insufficient time for morphological differences to be induced for these organelles, however it would be interesting to observe the protein localisation after longer incubations with the drug.

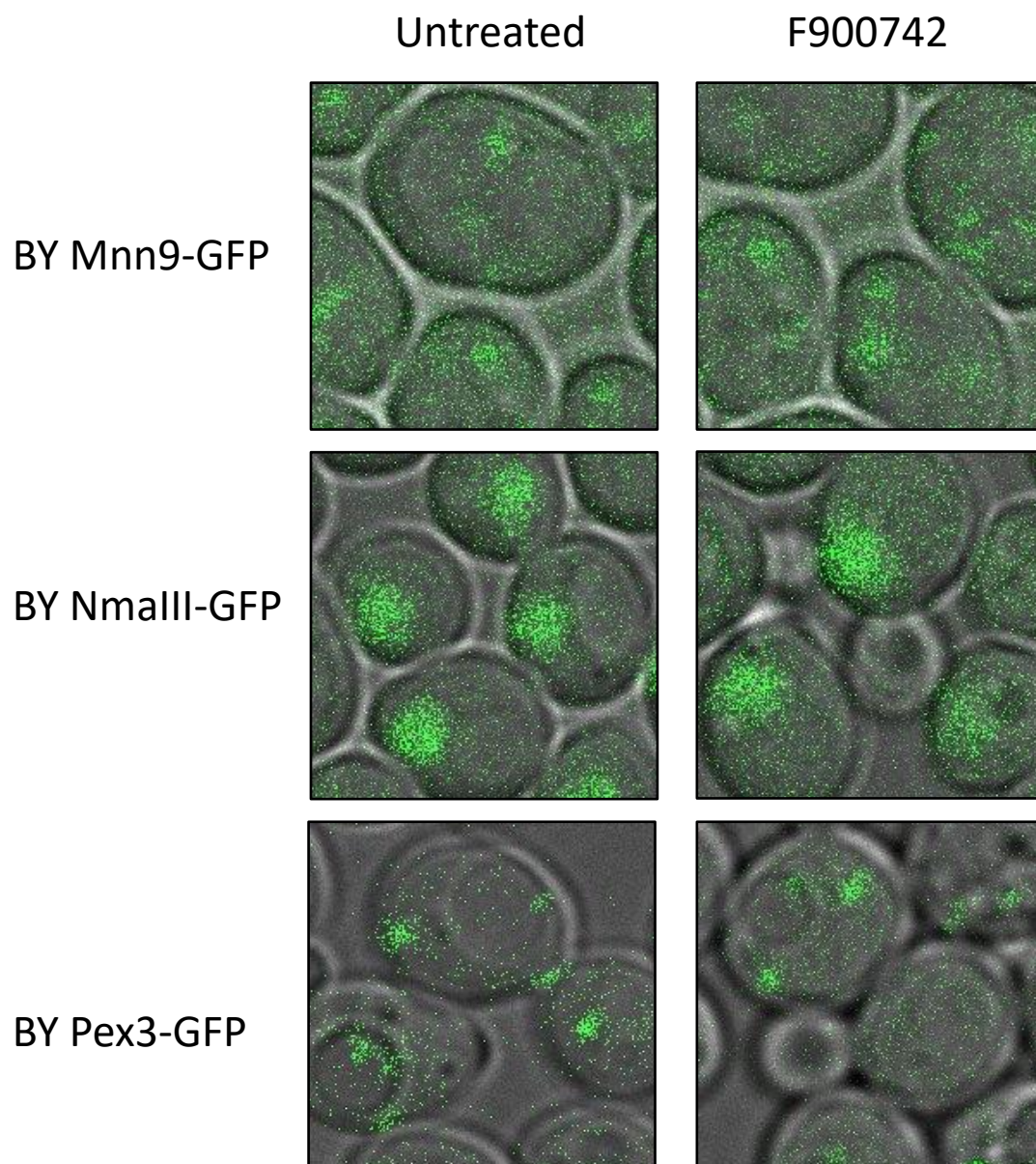
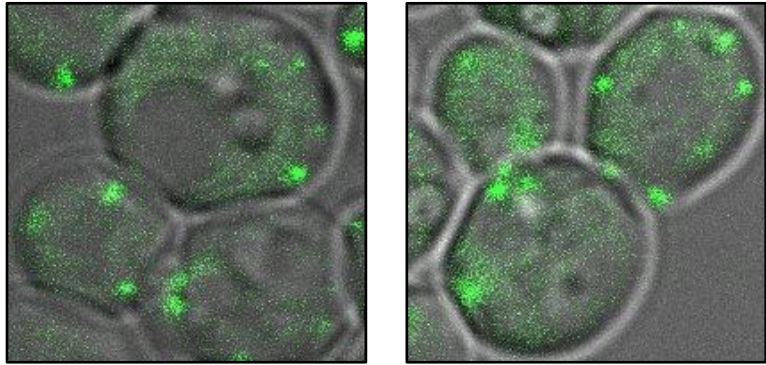
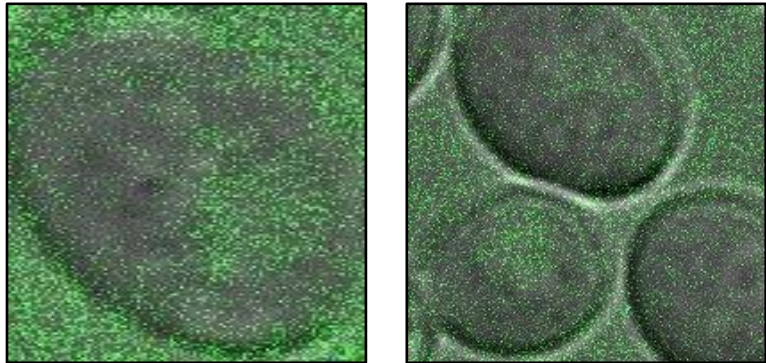


Figure 6.18 continues over page

BY Sac6-GFP



BY Vac4-GFP



**Figure 6.18. F900742 did not induce morphological defects to other organelles.** The localisation of nuclear, peroxisome, Golgi, vacuolar, and actin proteins was used to assess morphological defects to these organelles induced by F900742. There were no differences in protein distribution in any of the strains tested after 4 hours of treatment. F900742 was added at 100  $\mu\text{g}/\text{ml}$ . Samples were incubated at 30 °C. N = 2.



### 6.2.8 Ultrastructural analysis of F900742 treated fungi

Ole1p-GFP is an integral membrane protein that relocalised to unidentified cellular compartments in the presence of F900742. In addition, ER membrane proteins that are involved in the OLE1 pathway also exhibited subcellular relocalisation along with the formation of aberrant compartments that are consistent with the lumen of the ER, as well as mitochondrial fission. Previous studies by Tatzer et al demonstrated the mislocalisation of *ole1p<sup>ts</sup>* to aberrant puncta within the cytosol and adjacent to the nuclear and peripheral membranes upon growth at nonpermissive temperatures or when the OLE1 pathway was inhibited with the iron chelators sodium azide or potassium cyanide in wild type *S. cerevisiae*. Furthermore, they showed the formation of “..aberrant membranous structures in close proximity to the nuclear membrane and in the cytosol..” when looking at the temperature sensitive strain by EM (157). It was expected that Ole1p and HDEL were relocalising to a similar sort of membranous structure(s) as to those observed by Tatzer et al.

To further investigate ultrastructural defects induced by F900742 in *S. cerevisiae*, and to explore whether similar morphologies were observed in *C. albicans* and *A. fumigatus*, these strains were treated with F900742, fixed, and prepared for electron microscopy.

#### 6.2.8.1 *S. cerevisiae*

BY Ole1-GFP *S. cerevisiae* were treated with 100 µg/ml F900742 for 2 or 4 hours. At both incubation times, Ole1p-GFP relocalisation was confirmed by confocal microscopy (Figure 6.19). Briefly, samples were prepared for EM by first staining them in 1.5% potassium permanganate before dehydration in increasing amounts of acetone. Dr. Matt Hayes kindly fixed the samples in Spurr’s resin, sectioned them, and imaged the *S. cerevisiae* samples. Untreated control samples were prepared in the same manner.

Ultrastructural analysis revealed that F900742 induced multiple morphological phenotypes within *S. cerevisiae* that were not observed in control samples. The most striking feature was the formation of a long, double membrane-enclosed structure that

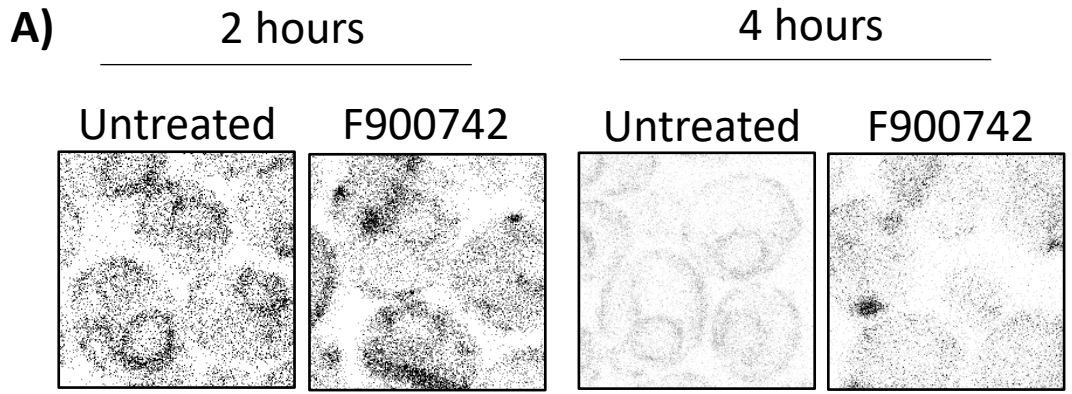
stretched throughout the cytoplasm of cells after 2 hours of treatment (white arrow, Figure 6.19C). Greater than 90% of cells contained one aberrant compartment only at this time point. These structures often came into very close proximity with other cellular membranes, for example the nucleus and plasma membrane, yet they remained as separate entities that did not fuse with organelles in any of the imaged cells. Most often they were relatively straight, wider than the lumen of the ER, and runs between the poles of the cell, however some cells contained shorter tubes (Figure 6.19D), whilst other cells had much wider membrane-bound compartments (Figure 6.19F). Despite slight morphological differences between cells, it was assumed that these structures would all serve the same purpose and the differences were either due to observing alternative planes of the cell or were a result of inherent differences in the rate of cellular responses. These structures could not be assigned to any organelle, nor any aberrant feature described in the literature. These aberrant structures were observed in approximately 90% of analysed sections that had been treated with F900742 for 2 hours and only one was observed per cell. Surprisingly, there were tubular structures in a minority of the daughter buds imaged, despite RFP-HDEL containing tubes transcending into the buds in the majority of imaged cells. 4 hours of treatment induced the formation of further aberrant tubes with a greater proportion of cells containing multiple structures that appeared wider, longer, and less linear than at 2 hours. Based on the morphology of the aberrant compartments, it seemed likely that this is where HDEL was relocating to and, therefore, it was predicted that the structures originated from the ER.

There were additional abnormal ER morphologies such as the presence of ER whorls in the cytoplasm and at the nuclear membrane which were larger and more frequently noted at 4 hours than 2 hours (Figure 6.19J, orange arrow). Large membrane delineated structures that were associated with the nuclear membrane were noted at 4 hours in the majority of cells imaged (Figure 6.19H and 6.19J, orange arrow head). Smaller, membrane-enclosed structures were observed at or in very close proximity to the nuclear membrane in a minority of the cells imaged after 2 hours of treatment (Figure 6.19E, orange arrow head). Furthermore, similar round, membrane-enclosed structures were observed in the cytosol in cells treated for 2 hours (Figure 6.19D and

6.19E black arrow head), however these were not observed in any cells from the 4 hour sample. There was the appearance of very electron dense round structures that were in close proximity to the cell periphery, cytosol, and at the nuclear membrane after 4 hours (Figure 6.19H and 6.19J, light blue arrow head). It was predicted that the electron dense regions developed from the membrane enclosed structures observed at 2 hours.

It was somewhat surprising that only a limited number of cells displayed an obvious increase in the number and size of lipid droplets (Figure 6.19C, light blue). However, F900742 induced the accumulation of content at the inner and outer nuclear membranes in a minority of cells that is likely to be lipid content (Figure 6.19C and 6.19D, white arrow head). In addition, there appeared to be an increase in vacuolar material in both of the treated samples relative to the untreated.

At least one of the described alterations was observed in all sections analysed. There were no similar membrane alterations in any of the untreated sections analysed, indicating that these aberrant membrane-enclosed structures were as a result of F900742 inhibition of the OLE1 pathway. Although this wasn't analysed, it would be interesting to confirm the confocal microscopy results demonstrating that unsaturated fatty acids inhibited morphological differences by EM.



2 hours

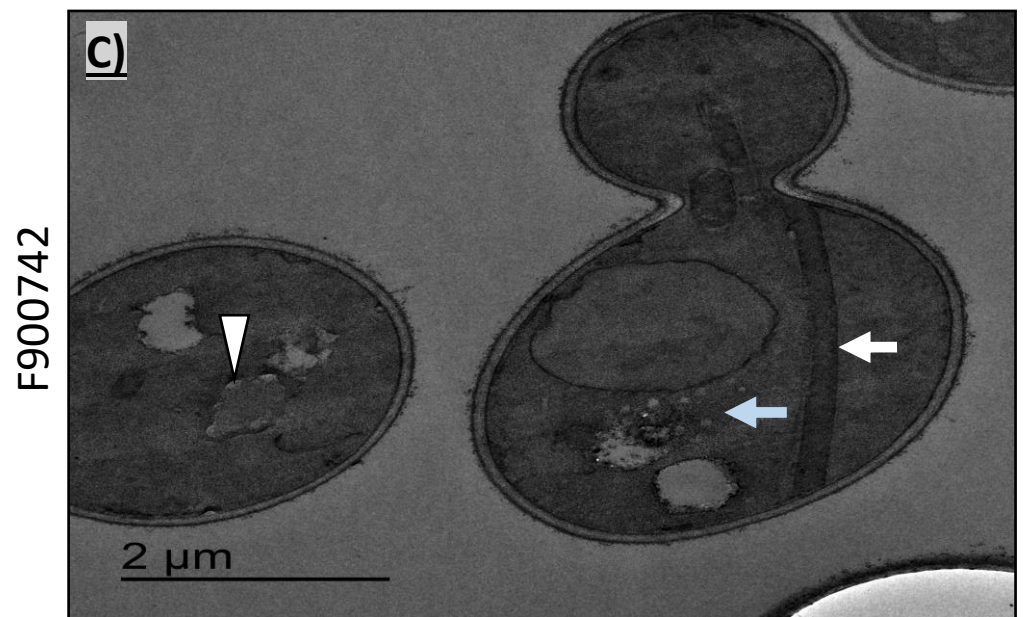
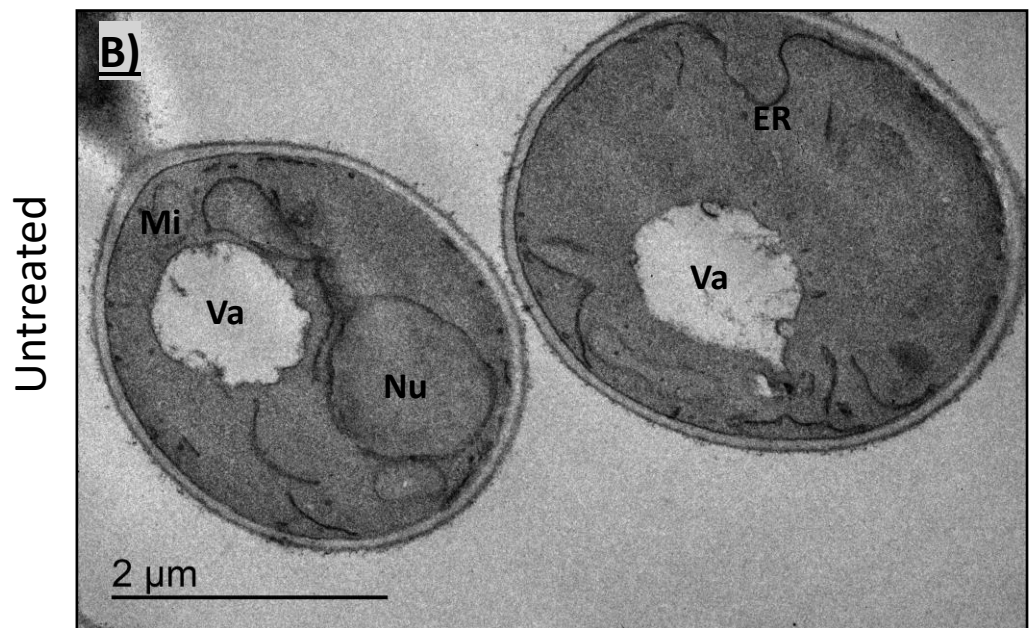


Figure 6.19 continues over page



2 hours F900742

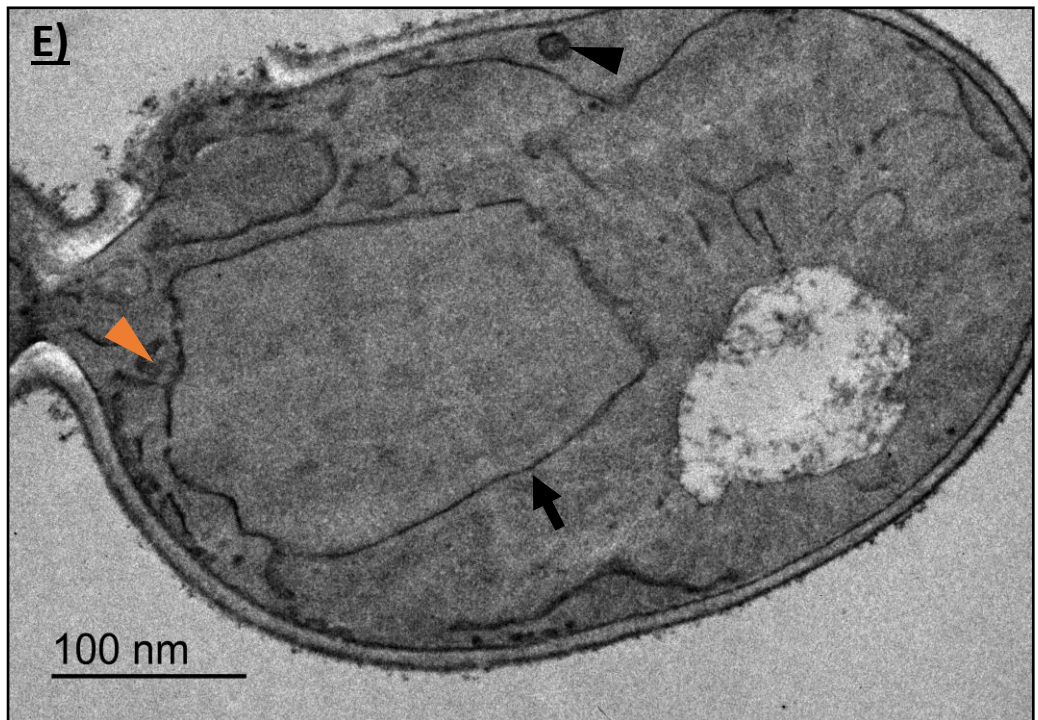
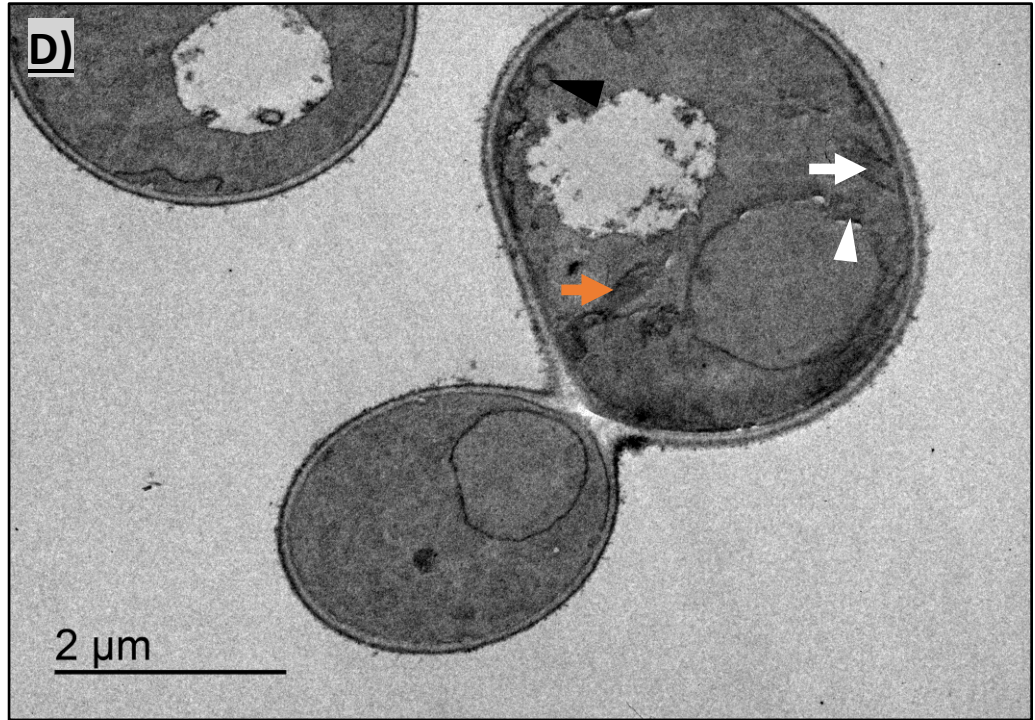


Figure 6.19 continues over page

2 hours + F900742

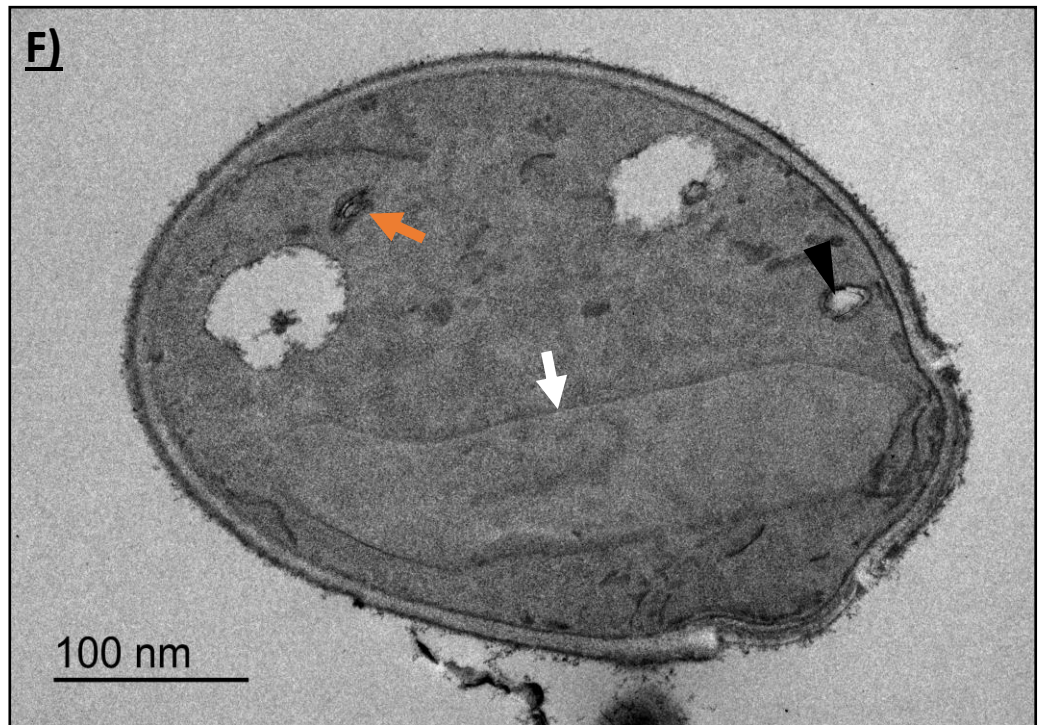


Figure 6.19 continues over page



4 hours

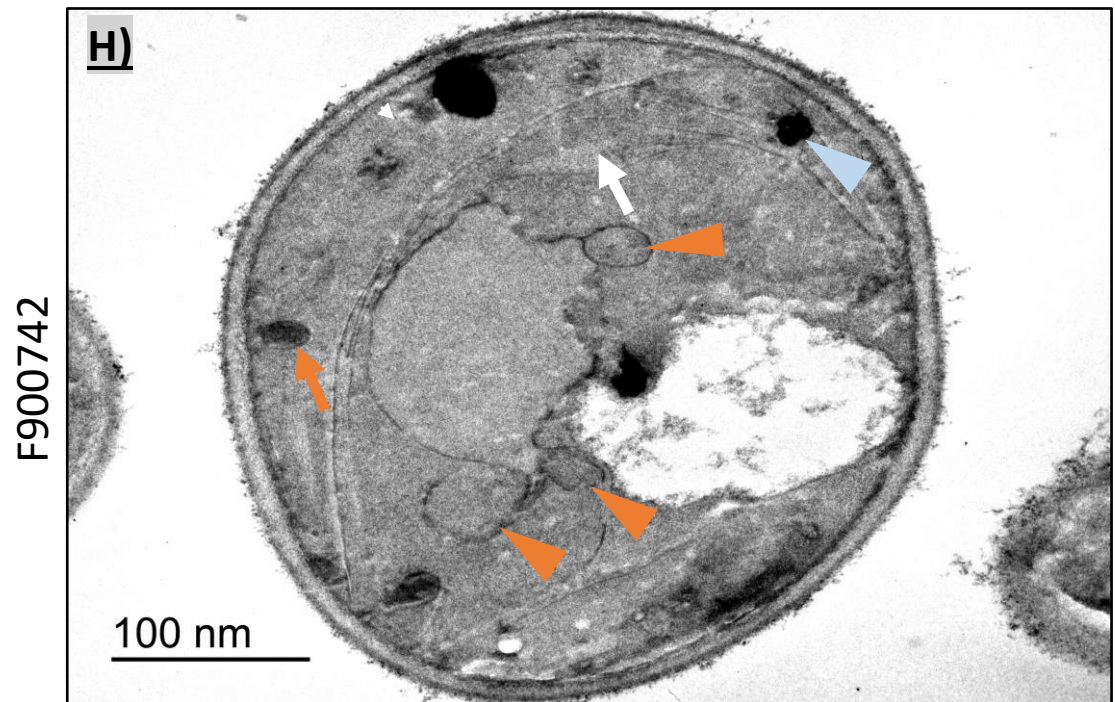
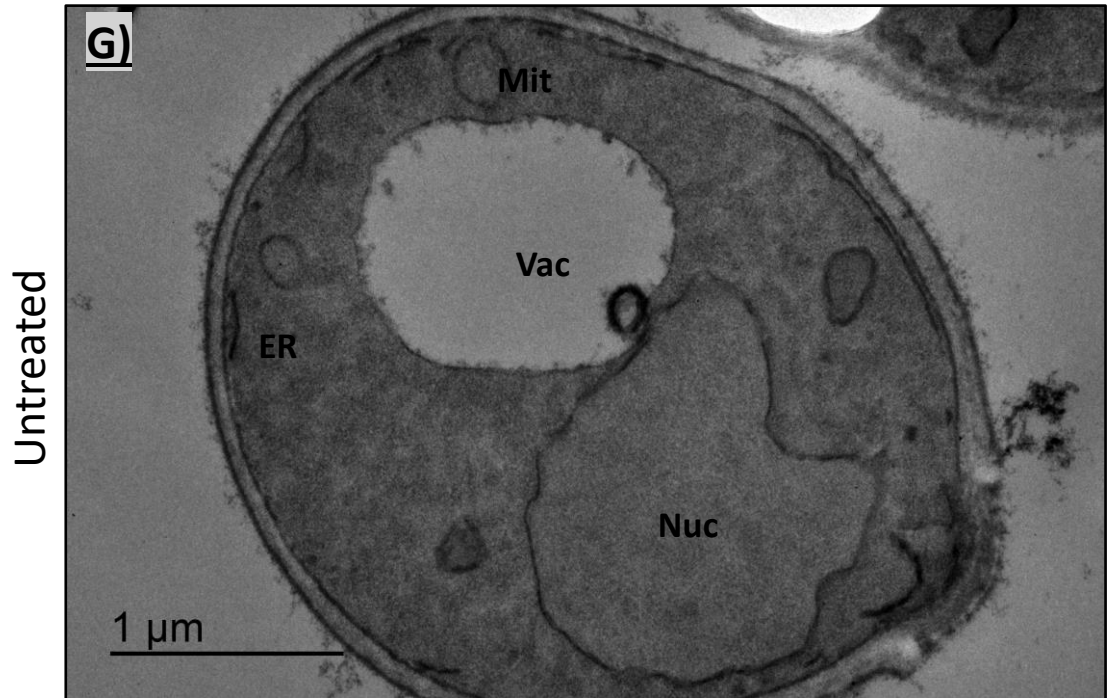
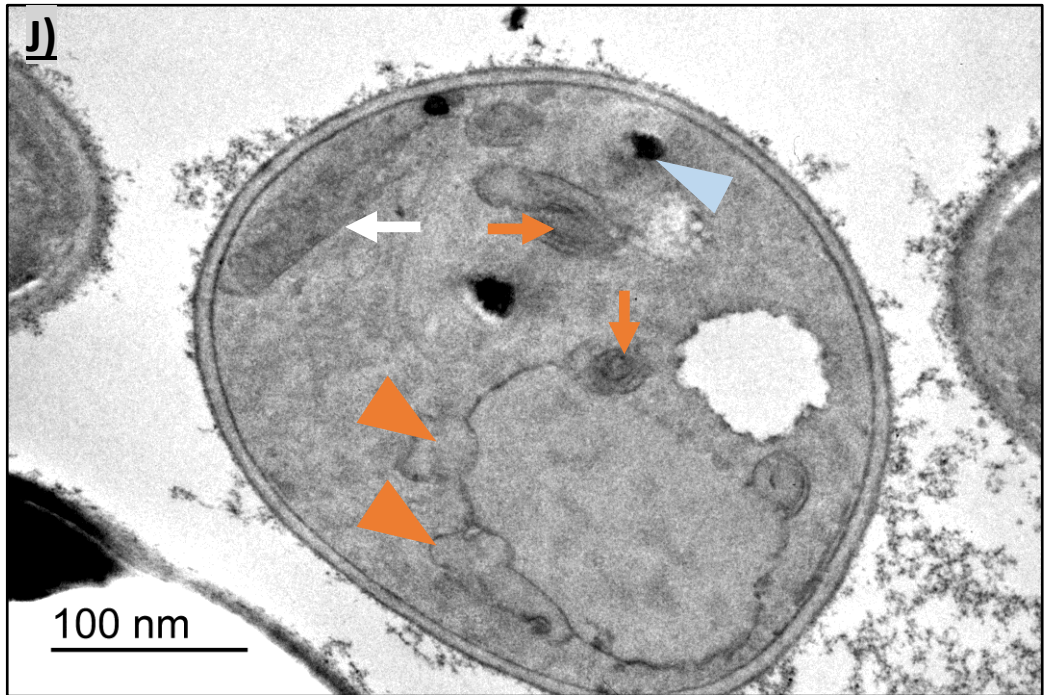
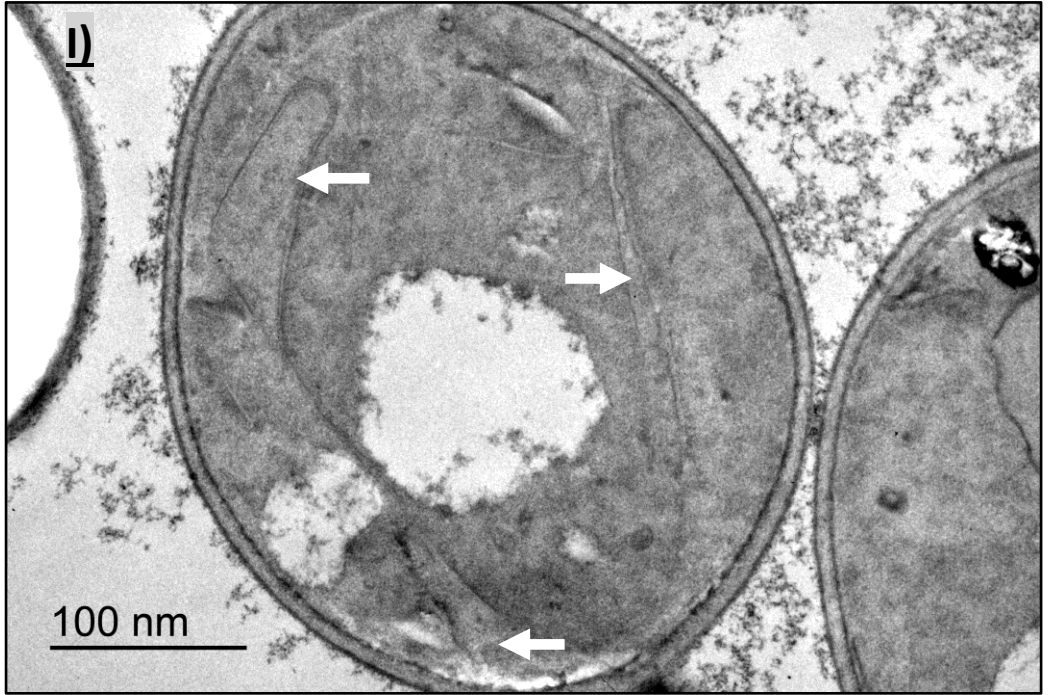


Figure 6.19 continues over page

4 hours F900742





**Figure 6.19. Ultrastructural analysis of F900742-induced morphological phenotypes in *S. cerevisiae*.** BY Ole1-GFP was treated with 100 µg/ml F900742 for 2 or 4 hours prior to preparation for EM. Samples were incubated at 30 °C. (A) It was confirmed that F900742 induced Ole1p-GFP relocalisation. (B and G) The subcellular morphology appeared as wild type in the untreated 2 and 4 hour samples. F900742 induced severe morphological phenotypes. Previously unidentified tubes were observed in the majority of cells (white arrow) (C,D,F,H,I,J). F900742 induced an accumulation of lipid content at the nuclear membrane (white arrow head) (C,D) and lipid droplets in the cytosol (light blue arrow) (C). F900742 induced the formation of membrane bound cytosolic structures near to the cell periphery (black arrow head) (D,E,F,) Small ER whorls (orange arrow) were noted in 2 hour samples (D,F) which were larger in cells treated with 4 hours (H,J), and alterations to the shape of the nucleus (black arrow) was noted in a minority of cells (E). Nuclear membrane extensions were noted in cells treated for 4 hours with F900742 (orange arrow head). Electron dense regions were noted in the 4 hour sample (blue arrow head) (H, I). Images taken by Dr. Matt Hayes.

White arrow = tube ; White arrow head = lipid deposits at the nucleus ; Black arrow = funky nuclear membrane shaped ; Black arrow head = membrane-enclosed cytoplasmic structures ; Orange arrow = ER whorls ; Orange arrow head = Nuclear membrane attachments ; Light blue arrow head = electron dense blob?! ; Blue arrow = lipid droplets ; Blue arrow head = electron dense regions.

### 6.2.8.2 *C. albicans*

*C. albicans* are the most common cause of pathogenic fungal infection, accounting for over 700000 cases and 350000 deaths worldwide per year. Although previous investigations used *S. cerevisiae* to study the effects of F900742, this drug has very good efficacy against *C. albicans* and represents a promising series of  $\Delta 9$  desaturase inhibitors for the treatment of life-threatening fungal infections. Although not been investigated in this study, it was assumed that F900742 would induce similar relocalisation patterns of Ole1p and aberrant morphological phenotypes in *C. albicans* as observed in *S. cerevisiae*. The ultrastructural morphological changes were investigated in a patient isolate of *C. albicans*. Cells were treated with 10  $\mu\text{g/ml}$  F900742 for 4 hours and samples were prepared for EM. Dr. Matt Hayes kindly embedded these samples in Spurr's resin and sectioned them. An untreated control sample was prepared using the same method.

*C. albicans* ultrastructural analysis identified several similar aberrant morphologies as described in *S. cerevisiae* (Figure 6.20). The majority of imaged cells (greater than 75%) contained one extended tube (Figure 6.20C, white arrow). In line with observations with the 4 hour *S. cerevisiae* sample, the structures were not linear and with varying widths throughout the structure, however they were shorter in length than in *S. cerevisiae* – none were observed to cross between the poles of the cell. It was expected that these structures also descended from micro-sections of stressed ER. ER whorls were also noted in a minority of cells (Figure 6.20D, orange arrow). Small, rounded, membrane-enclosed content was observed in the cytosol in many cells (Figure 6.20D, black arrow head), along with very electron dense black puncta (Figure 6.20C, blue arrow head). There was a large reduction in the number of lipid droplets which was associated with a substantial increase in size (Figure 6.20C, labelled LD). There were no obvious lipid deposits at the nuclear membrane in any cells.

One of the most contrasting phenotypes to that of *S. cerevisiae* is the appearance of ring-shaped or donut mitochondria. Donut mitochondria were observed in 80% of cells. Donut mitochondria have been previously reported in response to increased

mitochondrial ROS production (178). It was also reported that donut mitochondria are more able to recover normal morphology and function when the source of cell stress is removed (179). It was expected that the formation of donut mitochondria in *C. albicans* was as a consequence of F900742-induced ROS production as a result of mitochondria stress and dysfunction.

Consistent with *S. cerevisiae*, there were no obvious changes in the size or the shape of the yeast after treatment. *C. albicans* samples were not taken 2 hours after treatment, therefore no comments can be made on the development of structures throughout this experiment.

*Candida albicans*

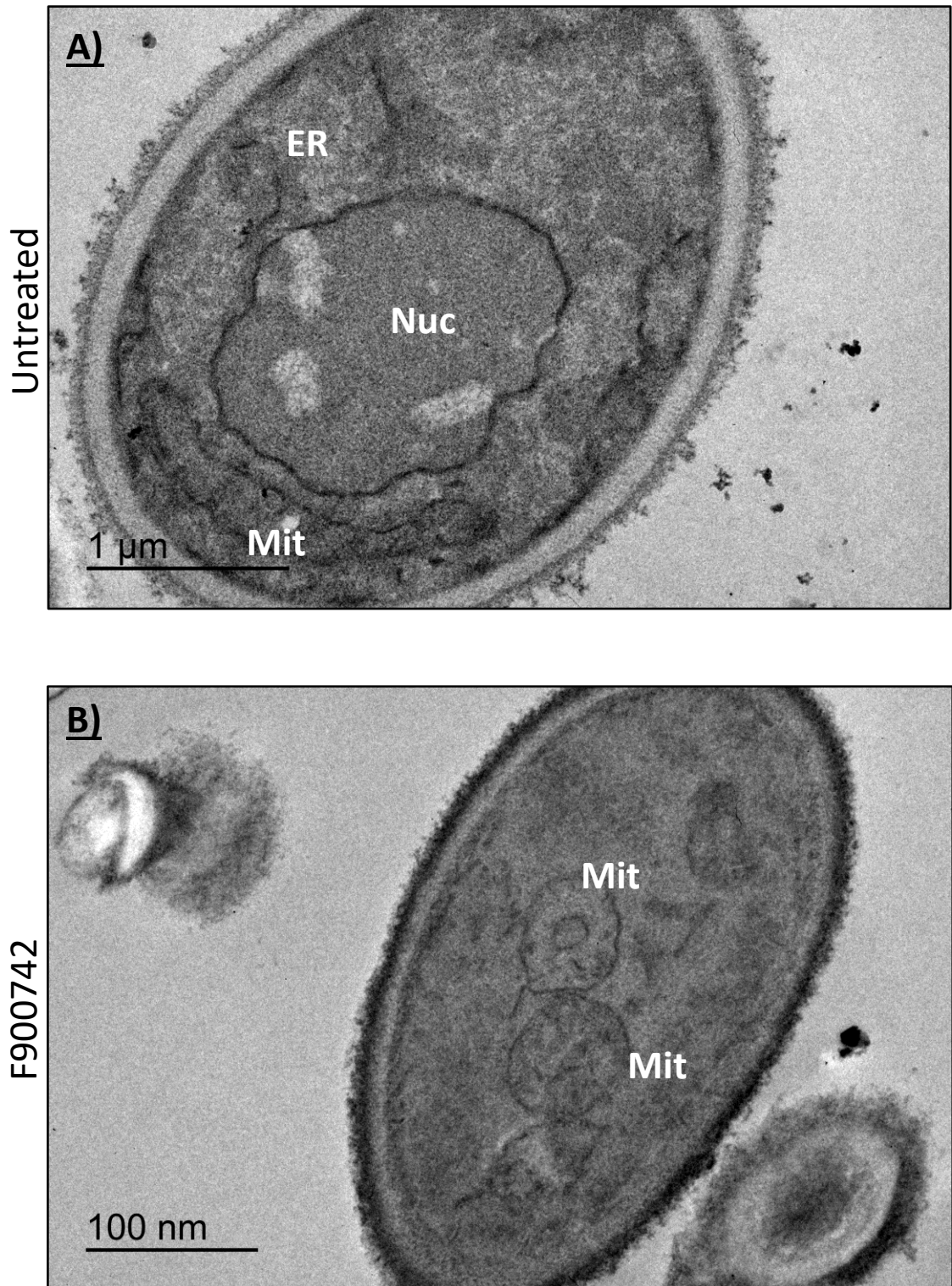
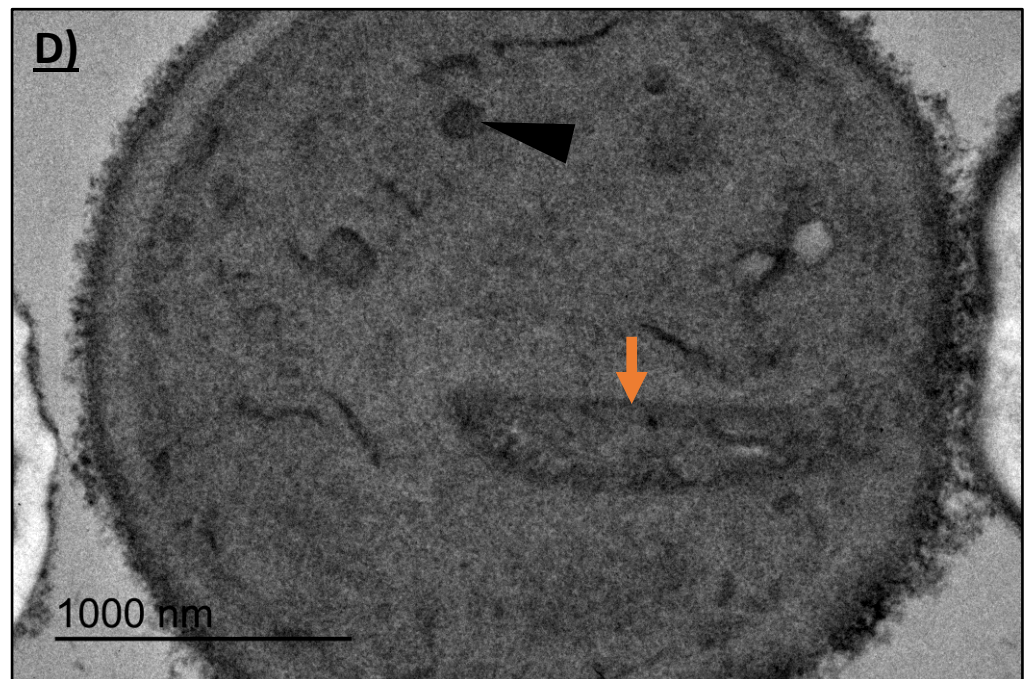


Figure 6.20 continues over page

*Candida albicans*

F900742



**Figure 6.20 Ultrastructural analysis of F900742-induced morphological phenotypes in *C. albicans*.** *C. albicans* were treated with 10  $\mu\text{g/ml}$  F900742 for 4 hours and incubated at 35  $^{\circ}\text{C}$ . A) No aberrant morphological features were noted in the untreated sample. (B-D) F900742 induced the formation of donut mitochondria, the formation of large lipid droplets (LD), electron dense regions (blue arrow head), membrane-bound cytosolic structures (black arrow head), and unidentified structures (orange arrow).

### 6.2.8.3 *A. fumigatus*

*A. fumigatus* 243 is a patient isolate that was resistant to all clinical treatments. F900742 demonstrated good *in vitro* antifungal efficacy with an MIC of 0.8 µg/ml. As with *C. albicans*, it was hypothesised that F900742 would induce similar cellular responses in *A. fumigatus* as *S. cerevisiae* although this wasn't tested, but would be an interesting investigation for future work. *A. fumigatus* were treated with 10 µg/ml F900742 for 4 hours. Sample and control were prepared for EM as previously described.

Tubular structures were not noted in any *A. fumigatus* cells (Figure 6.21). The majority of ultrastructural abnormalities induced by F900742 were enlargements of organelles resulting in a more densely packed cytosol. There was an increase in average size of the nucleus (N) and mitochondria (M) in treated samples relative to untreated. This was visually assessed. F900742 also induced a greater amount of disordered material within the nucleus, that is possibly lipid content. There was also an increase in the number of mitochondria per cell. Lipid droplets (LD) appeared small or not identifiable in the untreated sample, whereas there was one large lipid droplet in every cell imaged that had been treated with drug. F900742 induced changes in nucleus, mitochondria, and lipid droplet morphology, as well as the accumulation of unidentified cytosolic material.



*Aspergillus fumigatus*

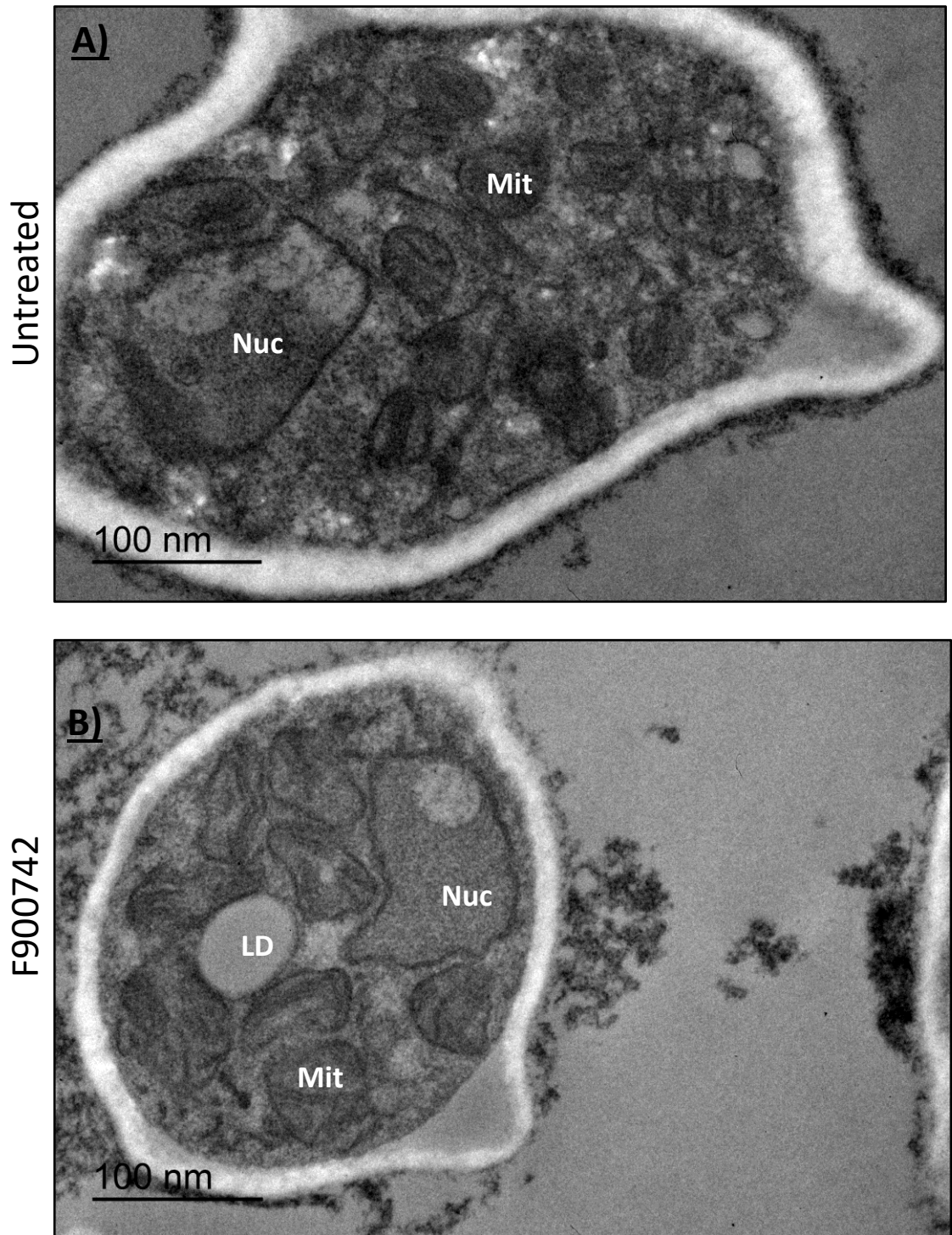
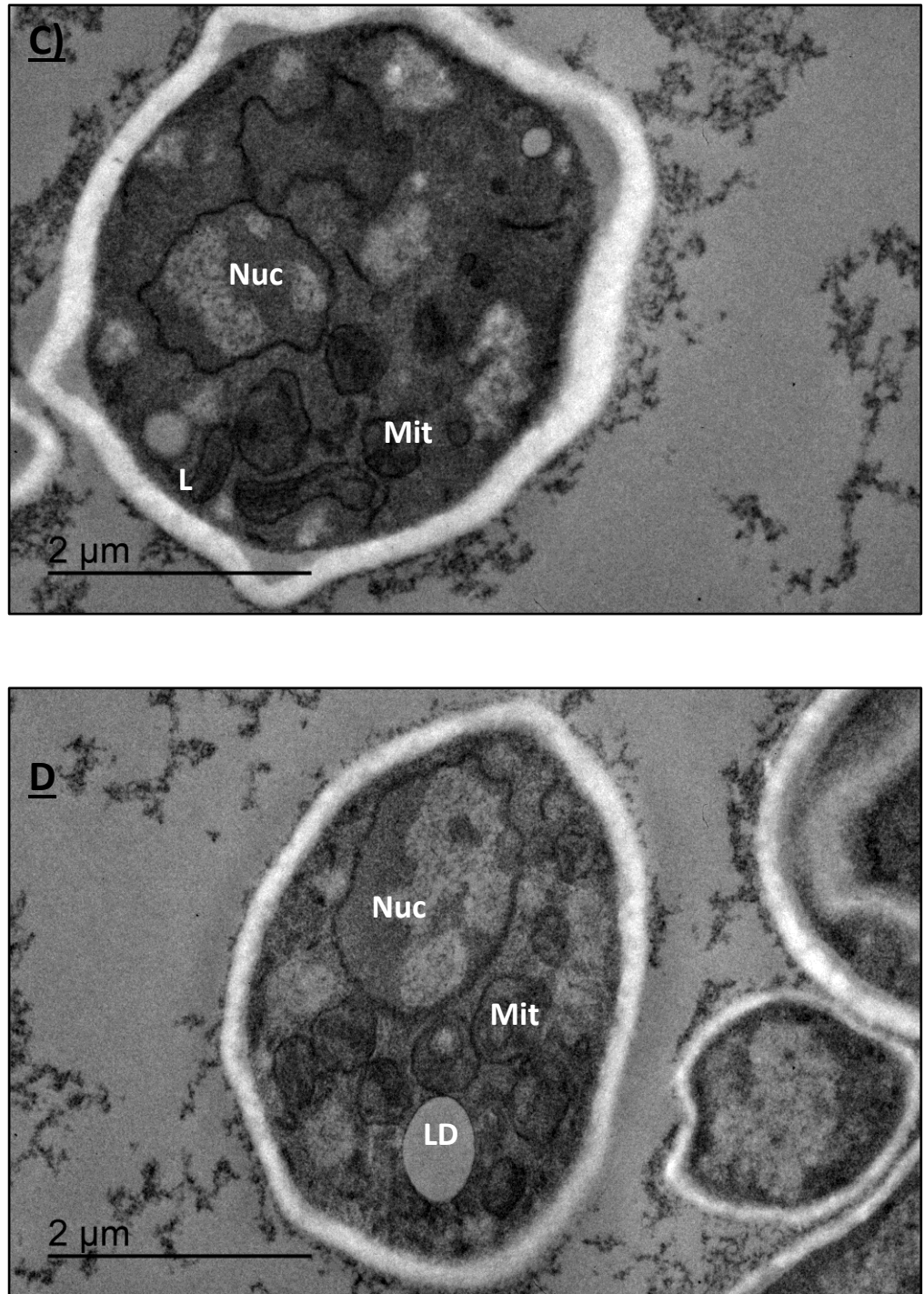


Figure 6.21 continues over page

*Aspergillus fumigatus*

F900742



**Figure 6.21. Ultrastructural analysis of F900742-induced morphological phenotypes in *A. fumigatus*.** (A) There were no aberrant morphological features in the untreated sample. (B-D) *A. fumigatus* were treated with 10 µg/ml F900742 for 4 hours and incubated at 35 °C. F900742 induced an increase in size and number of mitochondria and an increase in the size of lipid droplets. There was an increase in the amount of unidentified cytosolic non-membrane bound content as well as in the nucleus. LD = lipid droplet ; Mit = mitochondria ; Nuc = nucleus



## 6.2.9 Mechanism of action

### 6.2.9.1 F900742 induced the production of ROS

Energy, in the form of ATP, is produced at the inner mitochondrial membrane during oxidative phosphorylation, but this process is associated with the production of highly reactive oxygen molecules known as reactive oxygen species (ROS). ROS have important roles in cell signalling and homeostasis, however high levels of ROS, or oxidative stress, is associated with substantial cellular damage to nucleic acids, proteins and lipids, and is implicated in many human diseases (180). Eukaryotes have developed multiple lines of defence against ROS. One mechanism is via the abundant and ubiquitously expressed antioxidant glutathione. Glutathione can exist in both oxidised and reduced states depending on the cell's redox state. In the reduced state, glutathione is able to donate an electron to reduce oxidised molecules, such as reactive oxygen species, thereby neutralising them. Glutathione synthesis is limited by the availability of cysteine. Compounds such as N-acetyl cysteine (NAC) regenerate the reduced form of glutathione, thereby acting as an antioxidant itself.

Mitochondria are the major source of cellular ROS and disruption to mitochondrial morphology is associated with an increased production of ROS. It has previously been shown that F900742 disrupted mitochondrial morphology (Figure 6.15), therefore a proposed mechanism of drug action could be via alterations in the cellular redox state and the generation of ROS. To investigate the relevance of ROS following treatment with F900742, the fluorescent dye 2',7'-dichloro-dihydrofluorescein diacetate (H<sub>2</sub>-DCFDA) was used to visualise cellular ROS production in the presence or absence of the antioxidant NAC. H<sub>2</sub>-DCFDA is cell permeable and is a reduced form of fluorescein. Following oxidation, the acetate is cleaved by intracellular esterases resulting in the non-fluorescent H<sub>2</sub>DCFDA being converted into the highly fluorescent 2',7'-dichlorofluorescein (DCF), which is retained in cells. Cells were treated with H<sub>2</sub>DCFDA following a 2 hour incubation with F900742. Consistent with the induction of mitochondrial defects, BY4741 cells treated with F900742 there was a far greater amount of ROS production than the untreated control group (Figure 6.22A). Greater

than 90% of observed cells exposed to F900742 displayed high levels of cellular ROS. In contrast, there was no detection of ROS in the untreated samples. Further to this, cells treated with F900742 and the antioxidant NAC also demonstrated very low levels of ROS production such that there were no obvious differences relative to the untreated cells. This data suggested that a substantial increase in ROS production was likely to play a significant role in the mechanism of action of F900742. It was, therefore, investigated whether NAC was sufficient to inhibit F900742.

The inhibitory activity of NAC on F900742 was investigated by two growth assays: one method measured the amount of growth in 24 hours in liquid culture by OD 600, the other determined the growth of strains on YPD agar following 24 hours of treatment. BY4741 was treated with F900742, NAC, or F900742 and NAC for 24 hours. There was a large difference in OD between samples treated with F900742 only and F900742 and NAC (Figure 6.22B). The optical density of samples treated with NAC or NAC and F900742 was similar to that of the untreated cells. There was a slight decrease in optical density between the untreated sample and NAC + F900742, however there was a slightly greater difference with NAC alone suggesting that the decrease is due to the addition of NAC rather than F900742 activity. This suggested that, in liquid culture, NAC was sufficient to prevent F900742-induced growth inhibition as determined by optical density. Further to this, there was a substantial decrease in the number of colonies that grew on YPD agar following 24 hours of treatment with F900742 compared to F900742 and NAC (Figure 6.22C). F900742 prevented the growth of any colonies in the most dilute cell number (Figure 6.22C, bottom row), and there were just 5 colonies in the middle dilution (Figure 6.22C, middle row). In contrast, NAC inhibited the activity of F900742 to the extent there were no differences in colony number at the most dilute cell concentration to the untreated sample. Furthermore, NAC also inhibited the relocalisation of Ole1p-GFP to puncta and tubes in F900742 treated cells, but did not interfere with the localisation of the desaturase the ER when added without the drug (Figure 6.22D). This data further corroborated that NAC was sufficient to inhibit the activity of F900742, therefore suggested that a major mechanism of action of F900742 was via the production of ROS. Overall these experiments identified that F900742 induced mitochondrial ROS production and that

ROS inhibition did result in a reduction in F900742 activity. However, it is important to note that experiments in figure 6.22B-D have only been performed once. In order to draw statistically robust conclusions, they would need to be repeated at least another two times.

Activation of one stress response pathway can lead to a snowball effect such that multiple responses are activated. For example, mitochondria stress and lipotoxicity both can induce ER stress and activate cell survival processes linked to this organelle.

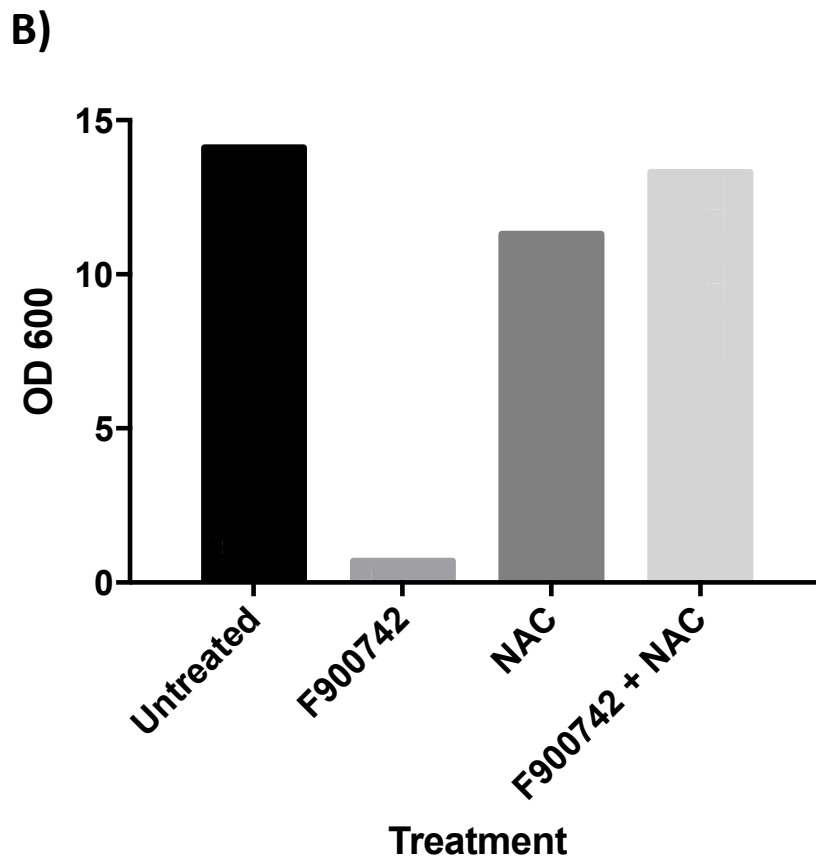
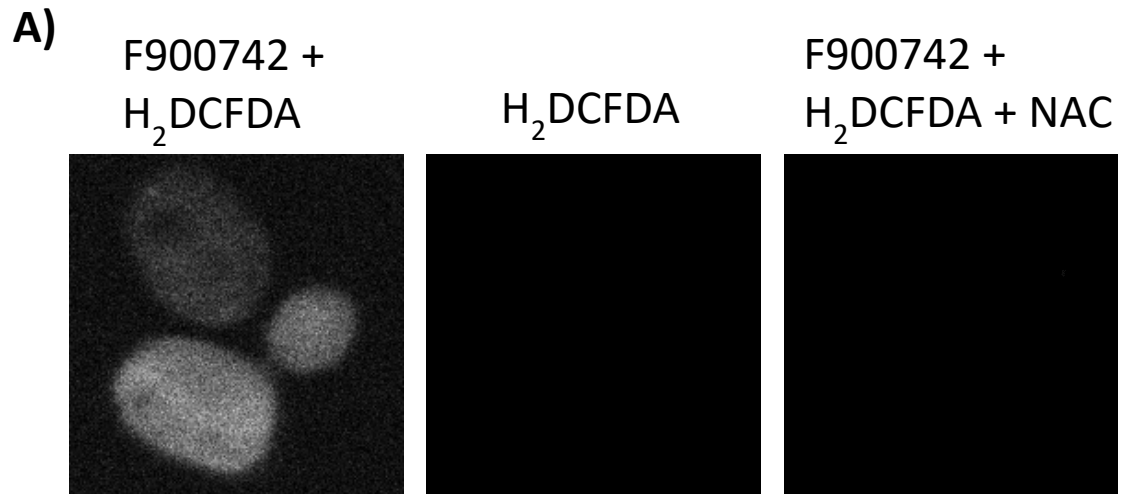
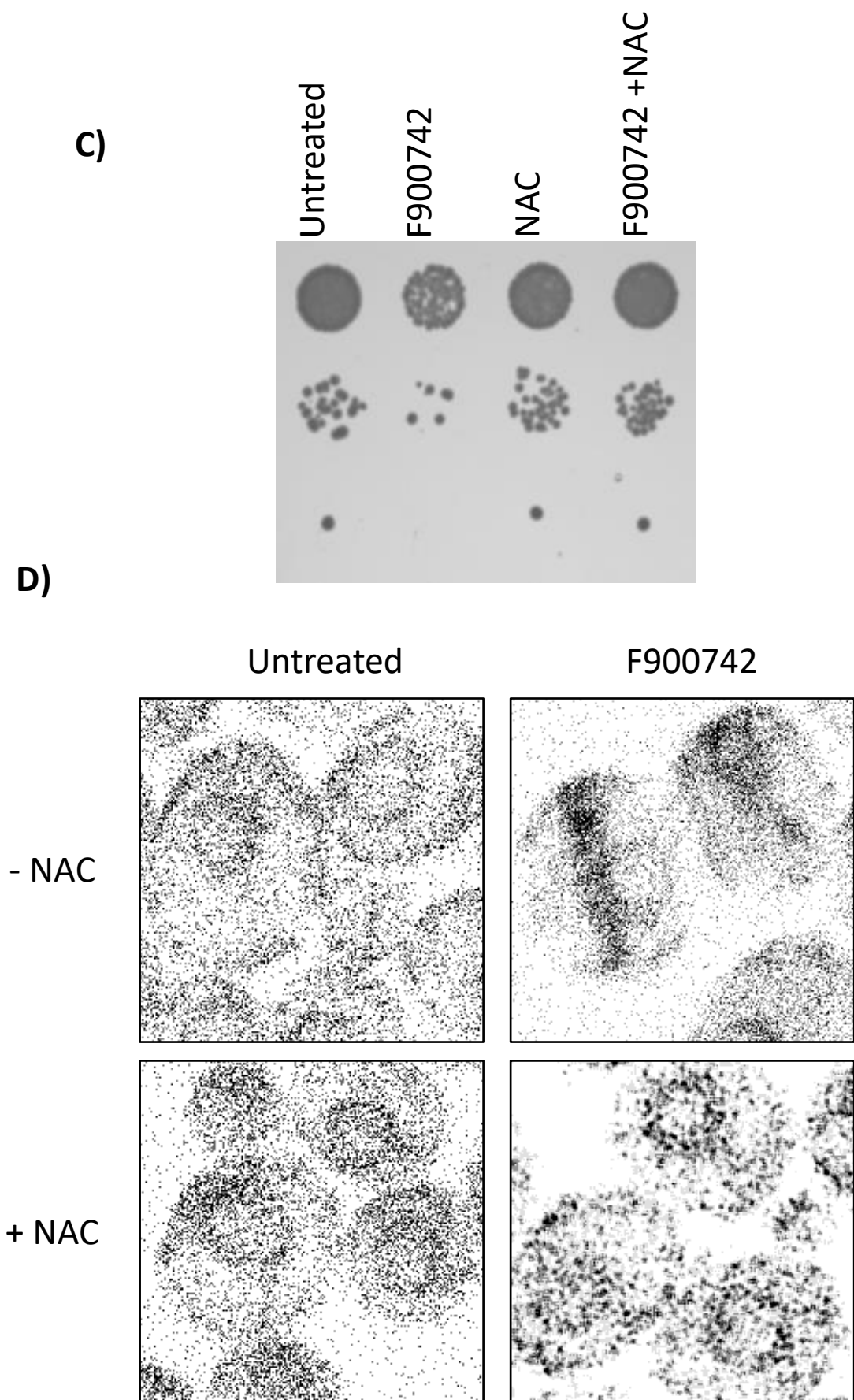


Figure 6.22 continues over page



**Figure 6.22. F900742 induced the generation of ROS.** (A) Treatment with F900742 induced ROS production as visualised by the fluorescent dye H<sub>2</sub>DCFDA. Cells treated with both F900742 and the antioxidant NAC did not result in the production of ROS. N = 3. (B and C) The antioxidant NAC was sufficient to inhibit the growth suppressing activity of F900742 in both liquid (B) and on agar (C). N = 1. (D) NAC inhibited the relocalisation of Ole1p-GFP to tubes and puncta. F900742 added at 100 µg/ml. H<sub>2</sub>DCFDA added at 50 µM. NAC added at 150 mM. Samples were incubated at 30 °C. N = 1.

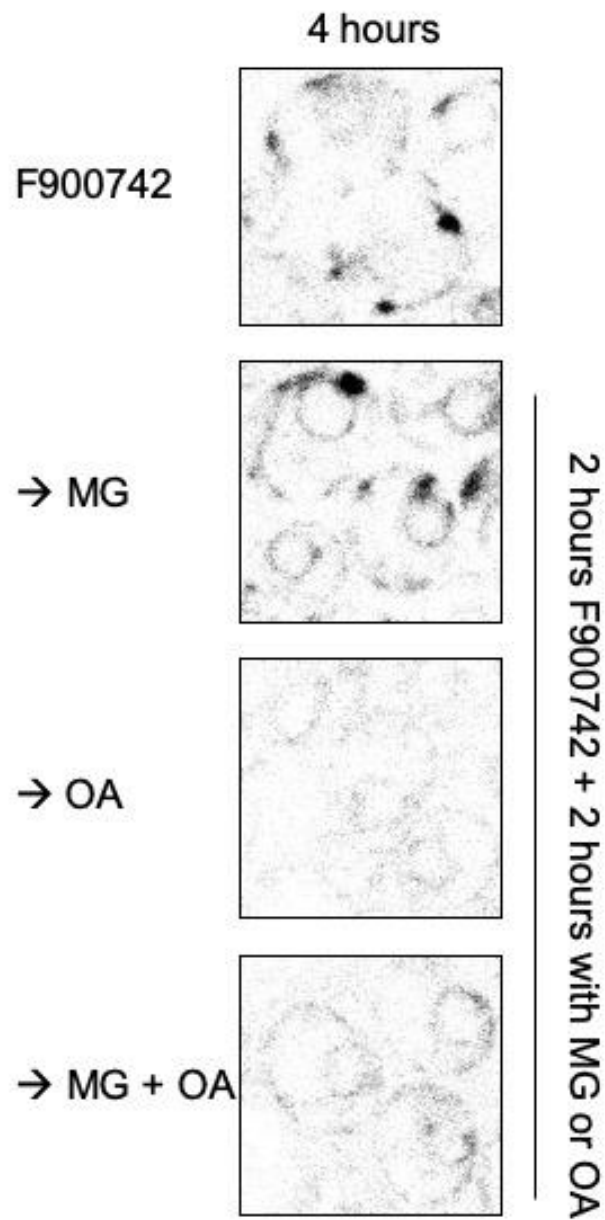
### 6.2.10 Ole1p-GFP was degraded by the proteasome

When cells contain an optimum fatty acid profile, Ole1p is rapidly degraded to almost undetectable levels (181). The majority of eukaryotic ER membrane-bound proteins are degraded by the ubiquitin-proteasome system. Initially, proteins are tagged for degradation by the addition of a series of ubiquitin molecules followed by degradation in the 26S proteasome. ER localised proteins that undergo proteasomal degradation do so via the Endoplasmic Reticulum Associated Degradation (ERAD) pathway. Braun et al demonstrated that Ole1p is at least partially degraded via ERAD using expression shut-off *S. cerevisiae* strains for different ERAD mutants (165). Therefore, it was suspected that the monounsaturated fatty acid-induced reduction in Ole1p-GFP expression was proceeding via proteasomal degradation.

To test whether the reduction in Ole1p-GFP expression following addition of monounsaturated fatty acids was a result of Ole1p degradation via ERAD, cells were treated with F900742 for 2 hours prior to addition of MG132, a potent inhibitor of the 26S proteasome complex (Methods 21.8). MG132 was added either by itself or in conjunction with oleic acid. 2 hours with MG132 and oleic acid was sufficient to substantially reduce the number of cells containing relocalised Ole1p-GFP puncta, but not sufficient to completely reverse the relocalisation of Ole1p-GFP to the same extent as oleic acid only. Furthermore, there was a substantial reduction in the amount of Ole1p-GFP in this sample that is comparable to the amount in the oleic acid only treatment (Figure 6.23A). MG132 alone did not have any effect on the size or distribution of Ole1p-GFP puncta. Contrary to Braun's findings (165), when quantified, proteasomal inhibition by MG132 was not sufficient to significantly inhibit Ole1p degradation in the strain BY Ole1-GFP (Figure 6.23B). The amount of fluorescence in cells treated with MG132 and oleic acid was not significantly different compared to cells treated with oleic acid only suggesting that proteasomal inhibition is not the only pathway involved in the degradation of Ole1p. In addition, MG132 was not sufficient to prevent the reduction in Ole1p induced by oleic acid in cells that were not pre-treated with F900742 (Figure 6.24A). Furthermore, as yeast proceed through the growth phases, various metabolic shifts occur. One of these effects is a stabilisation of

the fatty acid profile and subsequent reduction in Ole1p expression. There was also no significant difference in amount Ole1p when MG132 only was added to cells over a 4 hour period (Figure 6.24B). These results were somewhat unexpected. Previous studies have demonstrated that genetic disruption of pumps involved in influx or efflux of content or increasing the permeability of the cell membrane are all associated with greater MG132 efficacy due to a higher cellular content of the proteasome inhibitor (182,183). Altering the permeability of the cell does not represent an ideal experiment as many of the pumps and cell membrane are non-selective and, therefore, would also result in an increase in the cellular content of F900742. Other studies have suggested that 150  $\mu$ M MG132 is sufficient to overcome any uptake or efflux barriers in *S. cerevisiae* (184). Experiments were repeated with the higher concentration of MG132, however no significant inhibition of Ole1p-GFP degradation was observed (data not shown). Therefore, the experiment was repeated in a strain that has been previously shown to have an enhanced permeability to MG132.

A)



B)

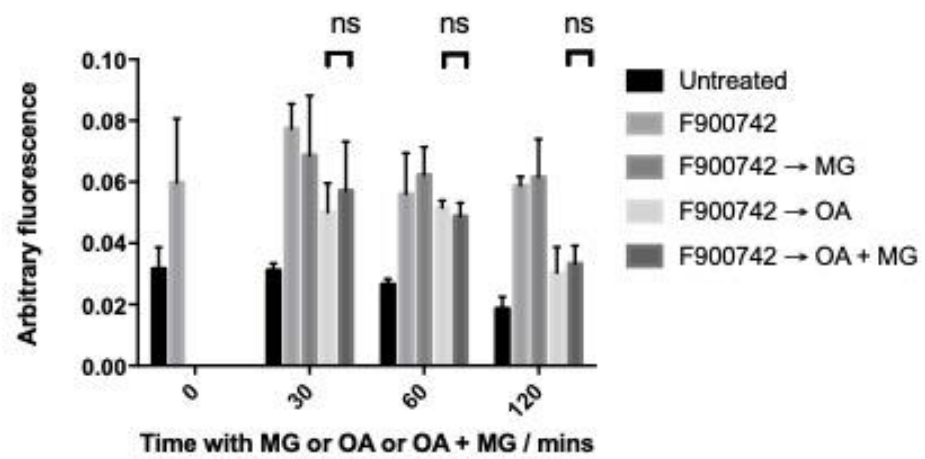
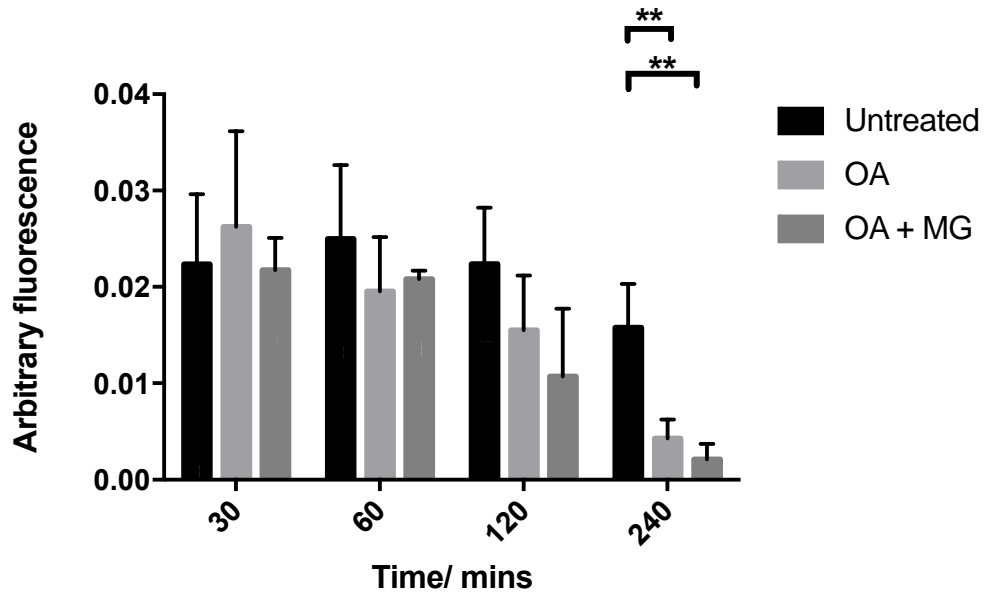




**Figure 6.23. MG132 did not inhibit oleic acid-induced turnover of Ole1p in BY Ole1-GFP.** BY Ole1-GFP were treated with 100  $\mu\text{g/ml}$  F900742 for 2 hours and incubated at 30 °C. Cells were washed and resuspended in fresh YPD supplemented with either 50  $\mu\text{M}$  MG132, 1 mM oleic acid, or 50  $\mu\text{M}$  MG132 and 1 mM oleic acid. (A) MG132 did not inhibit the reduction in Ole1-GFP expression induced by exogenous fatty acid supplementation, however puncta were still apparent in a minority of cells. No puncta were observed in any cells treated with oleic acid only and this sample was associated with the visually greatest decrease in Ole1p-GFP expression. Supplementation of MG132 alone did not affect the relocalisation of Ole1p to puncta. (B) There was no significant difference in Ole1p-GFP expression in cells treated with MG132 and oleic acid or oleic acid alone for 2 hours following a 2 hour incubation with F900742. N = 4.

A)



B)

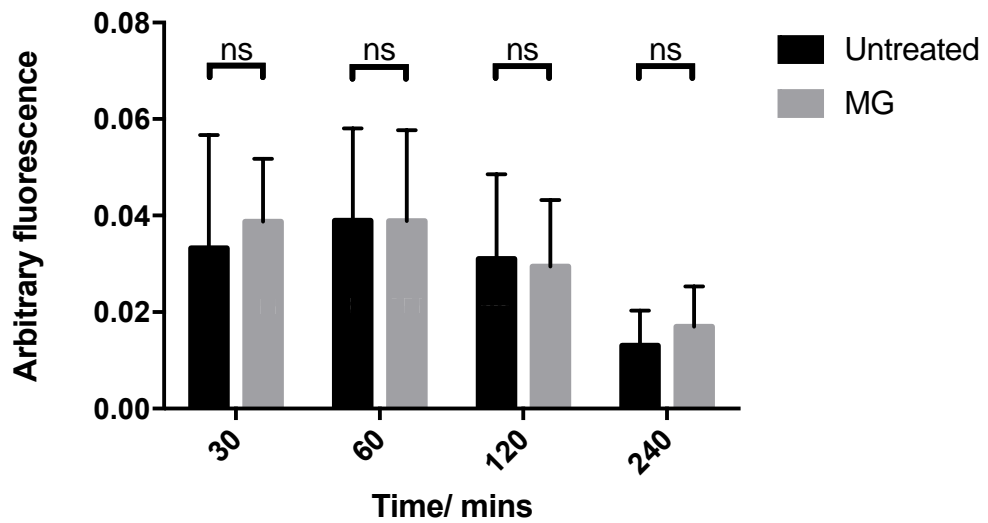
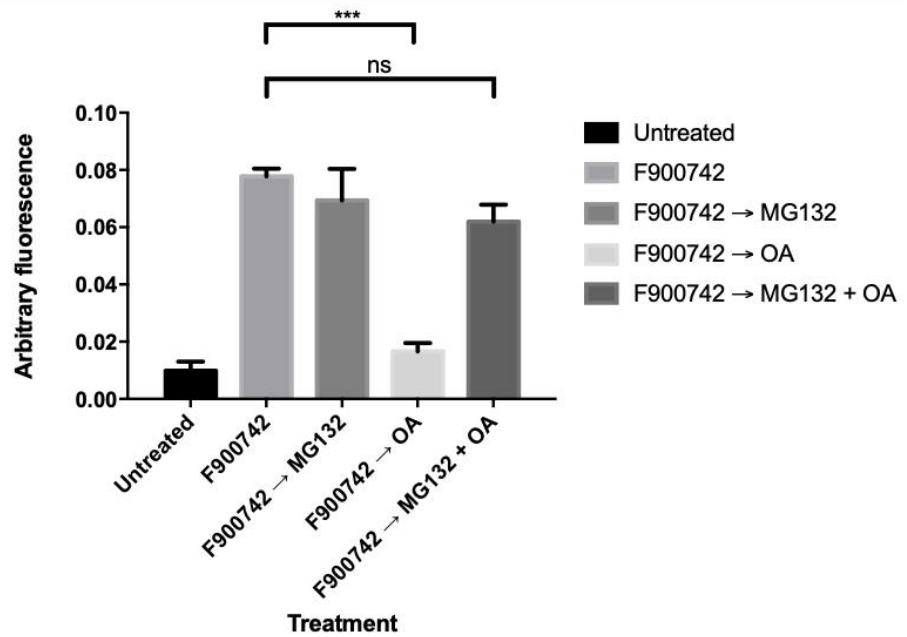


**Figure 6.24. MG132 did not inhibit the degradation of Ole1p in BY Ole1-GFP.** (A) 50  $\mu$ M MG132 did not inhibit the reduction in Ole1p-GFP induced by 1 mM oleic acid. There was no significant difference in Ole1p-GFP expression between cells treated with oleic acid only or oleic acid and MG132. Non-significant differences not labelled. (B) 50  $\mu$ M MG132 was also unable to prevent the reduction in Ole1p-GFP through the natural cycling of the protein. Samples were incubated at 30  $^{\circ}$ C for 4 hours. N = 3.

Ergosterol (encoded by *ERG*) is the major yeast sterol in the plasma and mitochondrial membranes. The primary functions of ergosterol is to regulate membrane fluidity, permeability, and structure (185). Specifically, Erg6p catalyses the formation fecosterol from zymosterol. Of relevance to this thesis, ergosterol is not present in mammalian cells. Instead, mammals produce cholesterol and, therefore, this distinction makes the ergosterol biosynthesis pathway an attractive antifungal target. *ERG6* is a non-essential gene: null strains are viable, but are characterised by an accumulation of aberrant sterols leading to an increase in susceptibility to many xenobiotics, including MG132 (183). BY  $\Delta$ *erg6* was transformed with the *OLE1* wild type plasmid pOLE1<sup>wt</sup> (416 $\phi$ >OLE1-GFP). Successful transformants were isolated and the expression and correct localisation of Ole1p-GFP was confirmed (data not shown). Cells were treated with F900742 for 2 hours prior to the addition of either MG132 or oleic acid or both as described above. Samples were taken 2 hours after the addition of MG132 and or oleic acid (Figure 6.25A). As previously shown in BY Ole1-GFP, the addition of oleic acid did result in a significant decrease in Ole1p-GFP relative to the drugged sample, however in the  $\Delta$ *erg6* background MG132 inhibited the degradation of Ole1p-GFP sufficiently such that there was no significant difference in protein amount compared to the treated sample. There was no significant difference between samples treated with F900742 or F900742 and MG132. A caveat to this experiment is the levels of Ole1p were expected to be greatly over expressed due to Ole1p expression being regulated by the PHO5 promoter on the plasmid in addition to the presence of a genomic copy of *OLE1*. The increased expression of Ole1p did not appear to differ from previously observed desaturase response to F900742, however this strain was associated with only a limited amount of desaturase relocalisation which is likely to be due to the greater initial expression of Ole1p-GFP (Figure 6.25B). A more accurate way to have approached this experiment would be to have knocked out *ERG6* from BY Ole1-GFP. Alternatively, there have been suggestions that using inhibitors of the proteasome that inhibit its caspase-like and tryptic-like activities would be more suitable to avoid any concurrent cellular effects as a result of the deletion of *ERG6* and subsequent membrane defects (186).

A)



B)

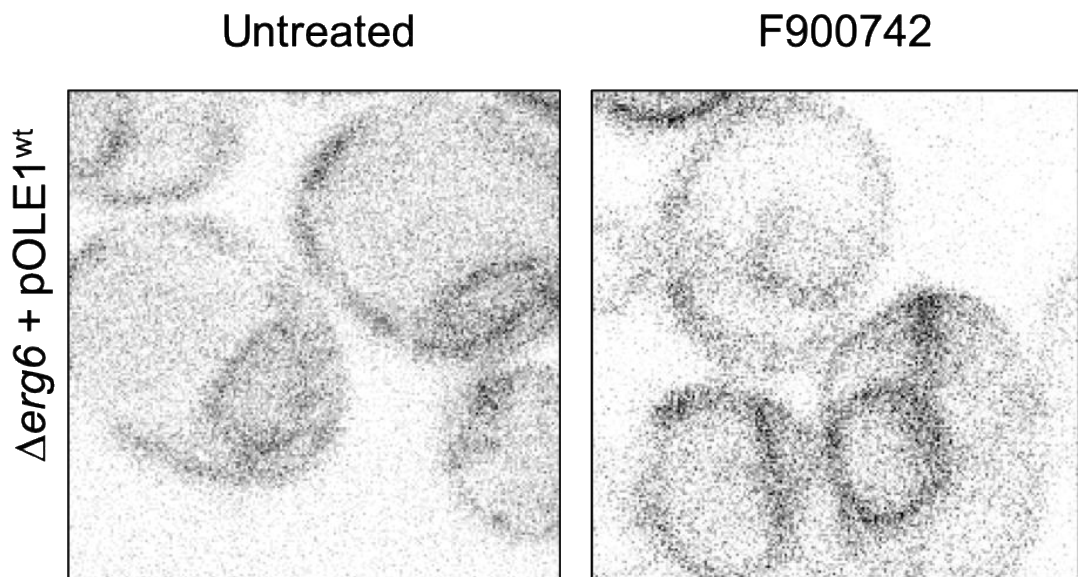


**Figure 6.25. MG132 inhibited Ole1p degradation in  $\Delta$ erg6.**  $\Delta$ erg6 were transfected with pOLE1<sup>wt</sup> and treated with 100  $\mu$ g/ml F900742, 50  $\mu$ M MG132 or 1 mM oleic acid for 2 hours and incubated at 30 °C. (A) There was no significant difference in fluorescence between cells treated with F900742 only or supplemented with oleic acid and MG132 for 2 hours. There was a significant difference between samples treated with F900742 or oleic acid only. (B) There was limited relocalisation of Ole1p-GFP expressed off the plasmid pOLE1<sup>wt</sup>. N = 3.

There are multiple pathways to ensure that correct protein function is maintained through the constant removal, recycling, and regeneration of proteins. Disruption of any element of protein regulation is associated with profound cellular stress and can induce devastating diseases (187). The most common forms of protein regulation are through autophagy, the proteasome, and vacuolar degradation. Braun et al implied that other pathways are also involved in the removal of Ole1p, therefore, the role of alternative protein regulation pathways in the turnover of Ole1p were also investigated.

The vacuole in *S. cerevisiae* has a number of different roles, including nutrient storage, detoxification, and its principle role in protein degradation. Vacuole function is essential under normal physiological conditions, but also under conditions of nutrient stress and cell growth (188). The vacuole ensures protein homeostasis by degrading damaged proteins and those with needless function. Autophagy is essential for many cellular processes, including adaptation to starvation, through the degradation of cytoplasmic contents. There are various forms of autophagy, one of which, termed macroautophagy, involves the formation of autophagosomes. Autophagosomes envelop target contents and then fuse with vacuoles to offload their contents for degradation. The Atg proteins are essential for the formation of autophagosomes and are conserved from yeast to humans (189). Atg9p is a transmembrane protein that is essential for autophagosome formation (190). Recently, it was demonstrated by Ogasawara et al that monounsaturated fatty acids are essential for the correct formation of autophagosomes likely because of their membrane curvature-inducing in mammalian cells and that Ole1p is required for starvation-induced macroautophagy through the proper delivery of Atg9p to the pre-autophagosome (191).

It was investigated whether vacuolar degradation or autophagy were involved in the oleic acid-induced degradation of Ole1p-GFP.  $\Delta atg1$  and  $\Delta vac4$  were also transformed with wild type Ole1p-GFP and expression of the plasmid was confirmed by confocal microscopy (data not shown). The experiment was performed as before with cells treated for 2 hours with F900742 prior to oleic acid supplementation. There was a significant reduction in the amount of desaturase when either vacuolar degradation or

autophagy were inhibited, suggesting that neither of these are essential, or at least the sole required process, for the turnover of Ole1p-GFP (Figure 6.26). Alternatively, as previously mentioned, there could be a substantial amount of redundancy between the remaining vacuolar proteins in this pathway that are masking the true role of this pathway. Ole1p is required for Atg9p delivery during autophagy (191). Although it is unlikely that autophagy plays a role in the turnover of Ole1p, it would be interesting to investigate whether F900742 inhibits the formation of the autophagosome through the mislocalisation of Atg9p. There was a discrepancy between the increase in fluorescence induced in the  $\Delta erg6$  background compared to  $\Delta atg1$  and  $\Delta vac4$  with a far greater increase in Ole1p-GFP in the  $\Delta erg6$  strain relative to either  $\Delta atg1$  or  $\Delta vac4$ . A possible explanation for this is all three delete strains contain a greater amount of Ole1p due to the presence of the over expressing plasmid and OLE1 in the genome. Therefore, compared to BY Ole1-GFP there is substantially greater amount of Ole1p per drug molecule. Therefore, it is not as necessary to increase the expression of Ole1p as much in these cells due an increased protein to drug ratio. However, deletion of ERG6 disrupts cellular membrane sufficiently to alter the permeability of the membrane (185), therefore it was likely that there was a greater internal content of F900742 in  $\Delta erg6$  than either  $\Delta atg1$  or  $\Delta vac4$  resulting in a greater F900742 inhibition of the desaturase and therefore less increase in protein expression is required in the  $\Delta atg1$  or  $\Delta vac4$  background strains.

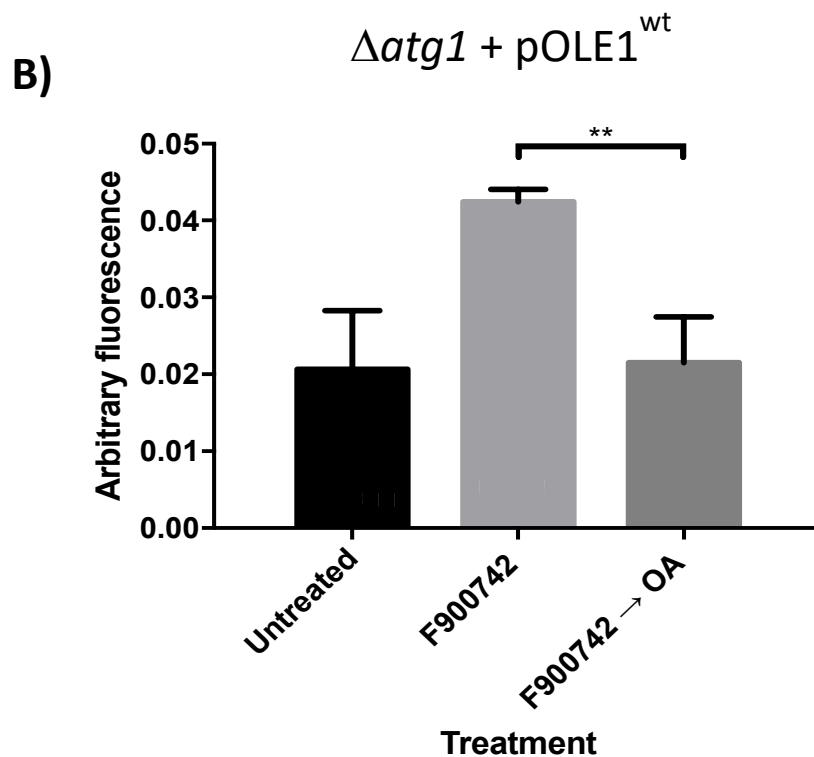
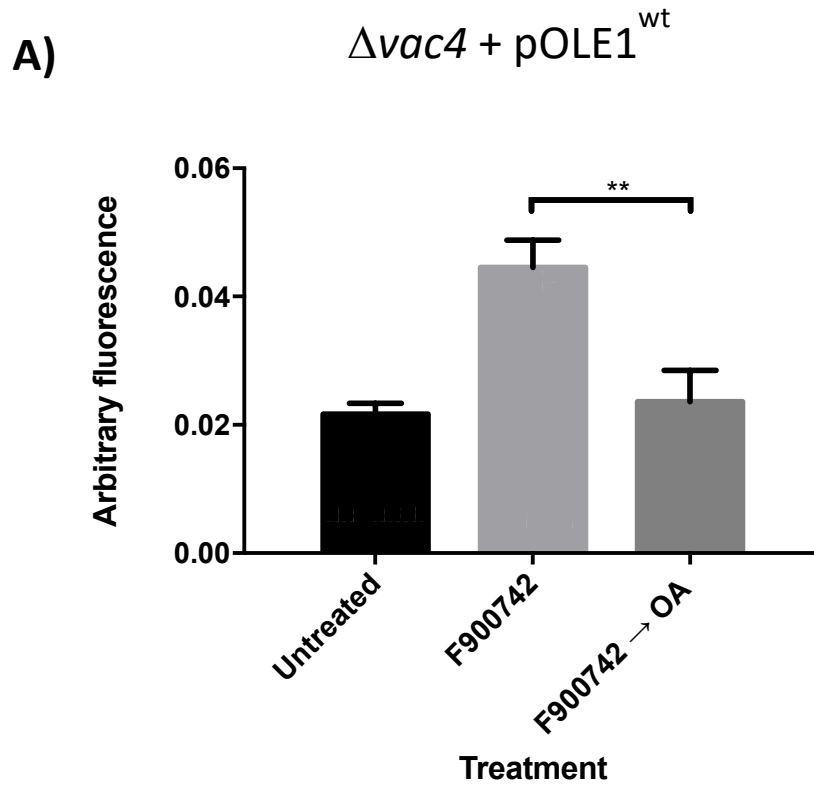


**Figure 6.26. Ole1p-GFP turnover was not via vacuolar degradation or autophagy.** (A) VAC4 was deleted to inhibit vacuolar degradation. Inhibition of vacuolar degradation did not prevent the degradation of Ole1p-GFP. (B) ATG1 was deleted to inhibit autophagic degradation. Inhibition of autophagy did not prevent the degradation of Ole1p-GFP. (A) and (B) F900742 added at 100  $\mu\text{g/ml}$ . Oleic acid added at 1 mM. Samples incubated at 30  $^{\circ}\text{C}$  for 2 hours. N = 3.

### 6.3 Discussion

The work presented in this chapter confirmed that:

- 1) Inhibition of *de novo* fatty acid synthesis induced the formation of an unidentified cytosolic structure that is likely to be derived from the ER
- 2) F900742 exerted a fungistatic mechanism of action less than 6 hours after treatment
- 3) The major mechanism of action of F900742 was via ROS generation

Confocal and transmission electron microscopy were used to study the ultrastructural defects induced by F900742 in *S. cerevisiae*, *C. albicans*, and *A. fumigatus*. Unsaturated fatty acids are well established as regulators of membrane fluidity and are essential for maintaining physiochemical properties and ensuring correct cellular processes.

Lipotoxicity, as a result of improper lipid metabolism, has been associated with a diverse set of stress conditions, including nutrient limitation. No previous studies have provided a comprehensive investigation into the early stress response pathways initiated as a result of OLE1 pathway inhibition in *S. cerevisiae*. This study identified how F900742 exerts antifungal effects through a mechanism that connects inhibition of lipid desaturation and ROS production that is mediated by ER and mitochondria membrane stress. It is expected that other  $\Delta 9$  desaturase inhibitors, whether direct or indirect inhibitors of the enzyme, would also induce similar morphological phenotypes.

EM studies identified that F900742 induced a variety of ultrastructural, morphological responses, the most striking of which was the formation of an unidentified cytosolic compartment that, based on consistencies with RFP-HDEL, Ole1p-GFP, Ubx2p-GFP, and Sct1p-GFP relocalisation, was likely to be derived from the ER. Additional evidence that this compartment is a result of Ole1p inhibition, was the appearance of RFP-HDEL tubes in BY  $\Delta ole1$  even in the absence of F900742. Similar structures were identified by Pineau in a strain of *S. cerevisiae* devoid of heme synthesis through the deletion of *hem1* (BY  $\Delta hem1$ ) (146). Pineau noted that there was a significant decrease in the unsaturated fatty acid content and an increase in saturated fatty acids, and these were associated with an increase in phosphatidylinositol at the expense of



phosphatidylethanolamine. These alterations to the lipidome are not unexpected given that Ole1p has a di-iron heme centre at the active site that is essential for catalytic function. Pineau also described dilated cisternae that were detached from the periphery of the cell and clefts that expand throughout the cytoplasm after 8 hours. They also noted that the plasma membrane was indented. The physiological benefit of this structure observed in both this study and by Pineau, if any, remains to be determined. It is likely that the compartment functions as an active cellular response to limit lipotoxicity by isolating regions of ER membrane containing unusually high saturated lipid content thus maintain function, or to store high levels of saturated fatty acid pools to avoid membrane incorporation. However, it is also plausible that it is a non-functional response to ER membrane stress. This structure has not been identified in any previous reports of unsaturated fatty acid induced lipotoxicity through deletion of *ole1*, *mga2*, or *ubx2* which brings into question whether it is a product that occurs rapidly and is then lost, or if it is part of a cohort of responses to cellular stress that has previously been missed. Cells were observed after a relatively short incubation with F900742, just 2 or 4 hours, therefore the reported morphological phenotypes are early responses to Ole1p inhibition, however Pineau reported the structures after 8 hours. Alterations to membrane lipid synthesis as a result of conditional Ole1 mutation have also been previously described by Tatzer et al. They identified that the *de novo* synthesis of glycerophospholipids is unaffected in OLE1<sup>ts</sup> mutant strains grown at non-permissive temperatures, however these lipids were more frequently associated with the incorporation of saturated fatty acids despite normally being highly unsaturated (157). It would be expected that similar shifts in membrane lipids incorporating saturated acyl chains would also be observed in cells treated with F900742 and this would be associated with a more rigid membrane. To assess this theory, fluidity probes, such as laurdan could be used. Future studies could correlate changes in the lipid and protein content of the ER membrane and appearance of aberrant compartments at various time points over long-term treatment with F900742.

The formation of ER-derived aberrant compartments challenges the way ER stress should be viewed: it cannot simply be assumed as a global response throughout the organelle. Here, ER stress is defined as the disturbance of normal organelle

morphology which is predicted to be a result of alterations in the lipid content of the membrane. It has been previously suggested that alterations to ER membrane lipid content can occur at microregions resulting in areas of altered activity. A suggestion could be that lipid alterations in ER microdomains are tolerated up to a threshold; beyond this, ER stress responses are activated unless the membrane balance is restored. A plausible function of the aberrant compartment is as a short-term store of saturated lipids to remove excess saturated lipids from the membrane and maintain normal ER processes. Further to this, Tatzert et al demonstrated that one of the major ER functions, the secretory pathway, was unaffected by the conditional mutation of *OLE1<sup>ts</sup>* after 30 minutes. Taken together with data presented here and the survival of *ole1* null cells for several cell divisions, it is not expected that ER function would be affected in the first 4 hours of treatment with F900742, and this would be consistent with the suggestion that the aberrant compartments serve a short-term protective function such that ER function is unaffected by an increase in saturated lipid membrane content. The function of the ER was not tested, therefore whether ER processes such as the secretory pathway or protein trafficking are affected remain to be determined. However, 24 hours of treatment with F900742 induced some fungicidal activity and this is likely to be through the activation of processes such as the UPR. Initially the UPR exerts a protective response from cell death. However, persistent or excessive ER stress can trigger cell death, and this is typically via apoptosis (192). Future work could test the effect of F900742 on ER pathways through investigating the formation of the aberrant compartments in *sec* mutants and the localisation of proteins containing a glycosylphosphatidylinositol anchor (GPI). It is expected that incubation with F900742 over longer periods of time would produce effects to other organelles. The long-term morphological effects of F900742, or *OLE1<sup>ts</sup>* conditional deletion, on the aberrant compartments and ER function remain to be determined. It would be interesting to investigate whether ER processes such as the localisation of newly synthesised proteins or proteins containing a GPI anchor (for example Gas1p) also relocalise to the aberrant structure. Assuming the aberrant compartment provides a protective role to the ER membrane, it would be expected that chronic exposure, longer than 4 hours, with F900742 would eventually overwhelm the storage capability of the compartment thus chronic ER stress would be induced.

Taken with data suggesting that by 6 hours F900742 induced a significant growth inhibitory defect, it is likely that significant ER stress would occur less than 6 hours post treatment. At this time, it is expected that additional ultracellular ER phenotypes would be observed (for example ER whorls), along with alterations to pathways such as the secretory pathway and activation of the UPR.

During periods of nutrient starvation, there is a shift from a predominantly glycolysis-driven metabolism to relying on fatty acid breakdown by the mitochondria which corresponds with a model in which fatty acids are released by autophagic degradation of membranous organelles and stored into new lipid droplets (193). F900742 induced an increase in size of lipid droplets and in the production of ROS which suggested that 2 hours was sufficient for a transition into oxidative phosphorylation. The mitochondria are expected to influence cell survival in several, but opposing, ways: the mitochondria are associated with the activation of cell survival pathways, including the UPR, in response to unsaturated fatty acid nutrient starvation, however the generation of ROS can shorten cell survival. Further to this, Ole1p activity has been previously identified as essential for mitochondrial distribution and morphology through undefined mechanisms (109). Irrespective of the cause of the mitochondrial phenotype, F900742 induced significant mitochondria fission which is likely to be a result of damage caused by ROS or as a result of an increase in saturated lipid content. The mitochondria fission exerts a protective response to ensure that the network isolates damaged mitochondria and is associated with halting cell growth thus providing a likely mechanism of action for F900742. The activation of stress response pathways in the mitochondria or the ER have been shown to positively feedback to activate the other, as such it is suggested that F900742 exerted antifungal activity through the generation of ER and mitochondrial stress which activates pathways to halt cell growth. This is discussed more in the final discussion.

Overall, this work demonstrated a novel cellular response that is likely through the direct inhibition of Ole1p that results in the formation of aberrant cytoplasmic structures that are ER-derived. Through this, and the identification of increased ROS

production, it is possible to infer that the likely mechanism of F900742 action is through ER and mitochondrial stress.

# CHAPTER 7

## *In vivo* analysis of F900742

### 7.1 Introduction

There are approximately 611000 types of fungi that account for almost 7% of the total number of eukaryotic species on Earth. Just 600 species, less than 0.001%, of fungi are human pathogens (194,195). Pathogenic fungi range from eliciting mild infection to those that have the potential to cause life threatening systemic infections which are responsible for more than 1.5 million deaths annually (9). Many opportunistic fungi, for example *Candida albicans* and *Candida krusei*, live as part of the normal human microbial flora, whilst other, such as *Aspergillus fumigatus* and *Aspergillus terreus*, are found within the environment without eliciting infection. Immunocompromised individuals, premature neonates, diabetics, and patients who require extended stays in healthcare settings are at a far greater risk of developing a lethal fungal infection. With rising numbers of people living full lives in an immunosuppressed state, the mortality rate from opportunistic fungal infections will only increase.

Currently there are just four classes of clinical antifungal drugs, each targets a single requirement for fungi cell survival. Issues with these current classes include adverse toxicity, drug-drug interactions, and variable pharmacokinetics both between patients and within the same individual. Moreover, the selective pressure on a single pathway has resulted in the development of resistance to every clinical treatment which poses a grave threat to many already vulnerable individuals. The problem of antifungal drug resistance has been exacerbated by the generation and selection of strains that display high levels of innate resistance, for example *Candida auris* (55). The ease of global travel in the 21st century aids the spreading of these clinically resistant pathogens such that this is a worldwide concern. Azoles, such as voriconazole (VOR), display low toxicity and a high efficacy against a range of fungi, including *Candida albicans*,

however due to extensive use in the clinic as part of both preventative and curative treatment plans, drug resistance to this class is commonplace and drug resistance frequently emerges. For example, it was reported in China that the number of clinical *C. albicans* isolates that were resistant to voriconazole doubled between 2010 to 2014 (0.7% to 1.5%). This poses a significant risk to patient outcome as these species are more likely to be resistant to antifungal treatments and therefore cause large scale epidemics (196).

F2G, an antifungal drug development company based in Manchester, UK, ran a high throughput screen of 340292 compounds for activity against a variety of *Candida* and *Aspergillus* species. Hits were defined as compounds that displayed antifungal activity at a concentration of 50 µg/ml or less. Hits from this screen were used to drive the computational design of many new series of compounds based on structure-activity relationships and the *in vitro* activity. This process led to F2G's major current lead drug F901318, Olorofim (OLR). Olorofim is the first in a novel class of antifungals known as the orotomides that act by inhibiting the pyrimidine biosynthesis enzyme dihydroorotate dehydrogenase (DHODH) (77). A unique feature of this compound is that it displays activity against *Aspergillus*, but not *Candida* species. Of note, early antifungal screens are typically initially performed in *Candida* only, therefore the discrepancy in antifungal activity between these species may partially explain why there has been a 17 year gap between now and when the last novel drug class, the echinocandins, was discovered. Therefore, it is important for developers to assess antifungal activity of novel compounds in both *Aspergillus* and *Candida* species. It is also likely that many discarded compounds would be active in species other than *Candida*.

After initial screening and *in vitro* testing, hit compounds enter into an *in vivo* phase of investigations. *In vivo* pharmaceutical studies are frequently performed using mammals, however invertebrate models have proven to be considerably useful in many microbiological studies, including for invasive fungal infections. The larvae of the wax moth *Galleria mellonella* has been described as an *in vivo* infection model to study novel antifungal drug efficacy against pathogenic fungi, including *Aspergillus*, *Candida*,

*Cryptococcus*, and *Fusarium* species, as well as for biofilm formation. *G. mellonella* possess many advantages over mammalian fungal models: they are cheaper and easier to maintain, they can withstand a large range of relevant incubation temperatures (15-37 °C), they provide treatment efficacy data quickly due to their short lifespan, and experiments with *G. mellonella* do not require ethical approval (197). Of particular importance, *G. mellonella* larvae have both a cellular and humoral immune response akin to that in mammals (198). Furthermore, the hemocoel content of both fungal inoculum and treatment can easily be controlled through administering an injection into the prolags of *G. mellonella*. However, the *G. mellonella* genome has not been fully sequenced yet and there are no methods for creating mutant strains. The generation of mutant strain and fluorescent *G. mellonella* libraries would provide an exciting line of new *in vivo* experiments to study host genetic responses to fungal infection and drug treatment.

Healthy *G. mellonella* are turgid to touch and are flesh coloured (Figure 7.1A and 7.1B). The underside of *G. mellonella* has two parallel rows of multiple prolags. The prolags lead into the larvae haemolymph, a fluid equivalent to blood in invertebrates (Figure 7.1A). Inoculum, drug, and control liquids were all injected into the haemolymph through the prolags using a Hamilton syringe. As candidiasis ensues, *G. mellonella* turn a grey-brown colour and are less mobile (Figure 7.1C). As the infection develops, the colouring darkens, and the larvae become more stationary and less responsive to light and physical stimuli. Sick *G. mellonella* are a dark brown-grey (Figure 7.1D) which darkens further to a deep black post mortem (Figure 7.1E).

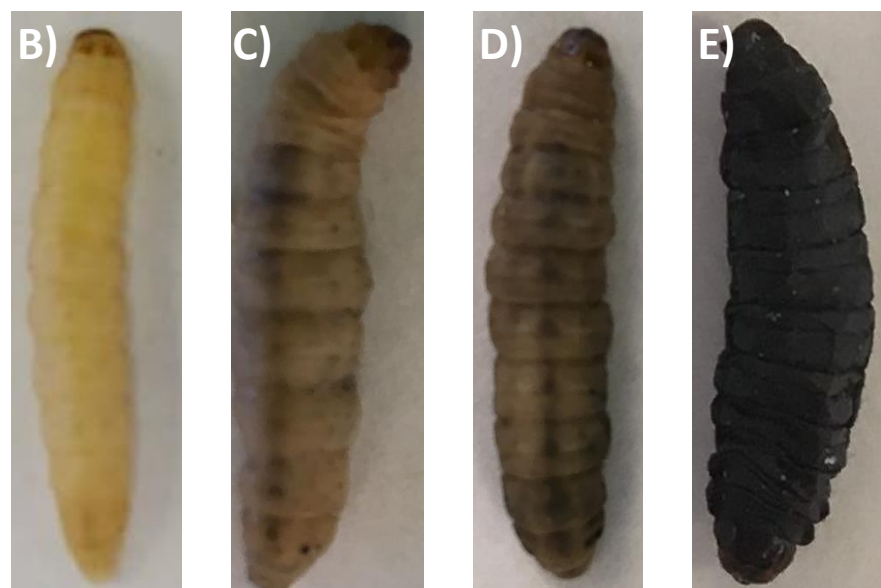
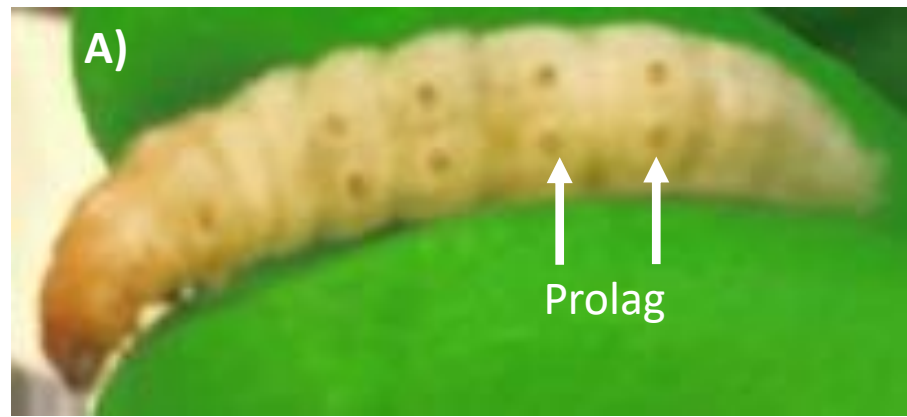


**Figure 7.1. Physiological changes to *G. mellonella* larvae following infection with *C. albicans*.** (A) The under side of *G. mellonella* larvae have two columns of multiple prolags. 10  $\mu$ l was injected into the larvae haemocoel via a prolag using a Hamilton syringe. (B) Healthy *G. mellonella* are flesh coloured, turgid, and responsive to physical stimuli. (C) As *G. mellonella* become sick, they darken and are less mobile. The darker the colour, the more sick the larvae. (D) Dead *G. mellonella* are a dark grey and are flaccid. (E) *G. mellonella* turn a very dark black a couple of days post mortem from invasive fungal infections.



## 7.2 Results

### 7.2.1 F900742 activity in the fungal model *G. mellonella*

#### 7.2.1.1 Pilot inoculum study

*In vitro* studies demonstrated that F900742 had a good potency against a range of pathogenic fungi, with limited cytotoxic effects in HeLa cells. In this study, the larvae of *G. mellonella* were used as a model of early stage candidiasis elicited by the fungal pathogen *C. albicans* to determine the *in vivo* antifungal efficacy of F900742. The length of *G. mellonella* survival is dependent on the size of the *C. albicans* inoculum. Preliminary experiments were carried out to determine the optimum inoculum size, as well as the larvae tolerance to F900742. Previous studies have reported an 10 µl of  $5 \times 10^4$  CFU/ml *C. albicans* to be lethal within several days (199), therefore, this was used as a guide inoculum size. *G. mellonella* were inoculated with either  $5 \times 10^4$ ,  $1 \times 10^4$ , or  $5 \times 10^3$  CFU/ml of *C. albicans* and incubated at 37 °C. One larva death was noted at both 24 and 48 hours in the  $5 \times 10^4$  CFU/ml group, and there was just a 20% survival rate by 72 hours. No further larvae died between the 3 and 6 day time point in this group. By the time of death, larvae were a deep grey-black which deepened post-mortem. The only surviving larva in this group was grey and minimally responsive to physical stimuli suggesting it was sick. In contrast, larvae inoculate with either  $1 \times 10^4$  or  $5 \times 10^3$  CFU/ml the first and only deaths were noted at 48 hours and 144 hours respectively; there was an 80% survival rate by day 6. All surviving larvae appeared healthy as determined by colouring and responsiveness to physical stimuli. There were no deaths noted in either of the control groups (Figure 7.2). Owing to the rapid onset of fatal candidiasis in 80% of larvae by 72 hours, it was determined that  $5 \times 10^4$  CFU/ml of *C. albicans* was the optimum inoculum concentration to use in the *G. mellonella* survival assay. This concentration of *C. albicans* was used in all candidiasis experiments hereon.

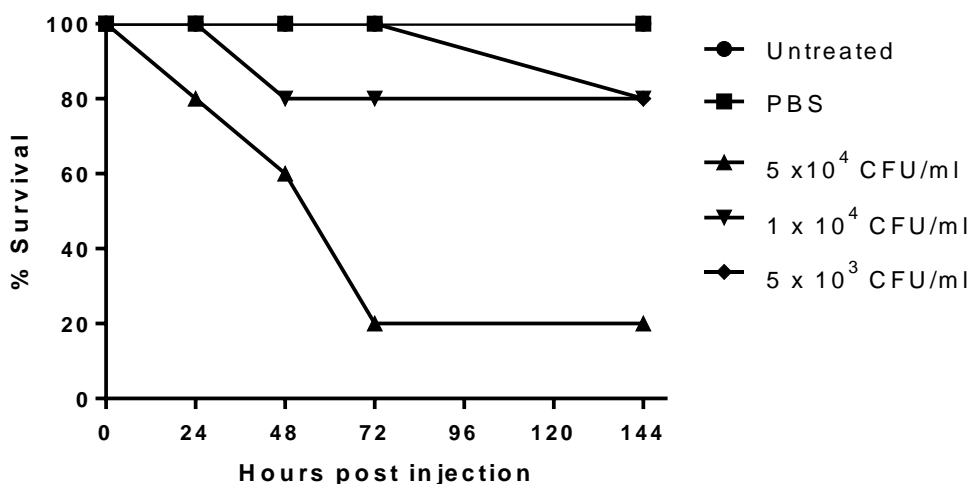


**Figure 7.2. *C. albicans* inoculum size testing.** 5 *G. mellonella* were inoculated with 10  $\mu$ l of either  $5 \times 10^4$ ,  $1 \times 10^4$ , or  $5 \times 10^3$  CFU/ml *C. albicans*. 20% of *G. mellonella* died by 24 hours and 40% by 48 hours in the  $5 \times 10^4$  inoculum. There was just a 20% survival rate of *G. mellonella* in this group after 72 hours.  $1 \times 10^4$  CFU/ml was sufficient to cause 20% death by 48 hours, but no further were noted. There was 20% death in the group treated with  $5 \times 10^3$  after 72 hours, however no additional deaths were noted throughout the duration of the experiment. No deaths were noted in either of the control groups. It was concluded that  $5 \times 10^4$  CFU/ml was the optimum inoculum size.

### 7.2.1.2 F900742 tolerance pilot study

The MIC of F900742 in *C. albicans* was determined as 0.8  $\mu$ g/ml (Table 4.1). The pharmacokinetic and distribution properties of F900742 in *G. mellonella* are currently unknown, therefore to overcome any apparent reduction in antifungal efficacy that is in fact a result of poor distribution to infection sites, double the MIC, 1.6  $\mu$ g/ml, was also tested for tolerance. The *G. mellonella* used in this study were not inoculated with *C. albicans*. To assess the cytotoxicity of F900742 at these concentrations, *G. mellonella* were injected with 10  $\mu$ l of F900742 at either 0.8  $\mu$ g/ml or 1.6  $\mu$ g/ml. No *G. mellonella* died in either treatment groups, or in either of the control groups, as such it was concluded that both drug concentrations were non-toxic to larvae over a 6 day period (Table 7.1).

		Hours post injection						
		0	24	48	72	96	120	144
F900742 concentration								
Untreated	Number alive	5	5	5	5	5	5	5
	Number dead	0	0	0	0	0	0	0
	Percentage survival	100	100	100	100	100	100	100
PBS	Number alive	5	5	5	5	5	5	5
	Number dead	0	0	0	0	0	0	0
	Percentage survival	100	100	100	100	100	100	100
0.8 µg/ml	Number alive	5	5	5	5	5	5	5
	Number dead	0	0	0	0	0	0	0
	Percentage survival	100	100	100	100	100	100	100
1.8 µg/ml	Number alive	5	5	5	5	5	5	5
	Number dead	0	0	0	0	0	0	0
	Percentage survival	100	100	100	100	100	100	100

**Table 7.1. F900742 tolerance pilot study.** 5 uninfected *G. mellonella* were injected with either 0.8 µg/ml or 1.6 µg/ml of F900742. No deaths were observed in either of the treatment or control groups.

### 7.2.1.3 F900742 demonstrated *in vivo* antifungal efficacy

F900742 has demonstrated a low MIC against a range of clinically relevant pathogenic fungi *in vitro*. The *G. mellonella*-*C. albicans* pathosystem was used to assess single dose treatments of F900742 against a clinically relevant *C. albicans* strain that is multidrug resistant. To evaluate the *in vivo* antifungal efficacy of F900742, 40 *G. mellonella* larvae were inoculated with *C. albicans* one hour prior to drug treatment. The hour incubation enabled the initiation of early candidiasis and gave the larvae time to recover from the inoculum injection. Larvae were then treated with either 0.8 or 1.6 µg/ml F900742 or sterile PBS (candidiasis control). To limit the amount of trauma due to injections, the inoculum injection was into the last left proleg and the drug injection was into the last right proleg. Two control groups were used, one was untreated and the other had an injection with sterile PBS at the time of inoculum or drug. A single dose of F900742 at either concentration was able to significantly increase the survival of *C. albicans* infected larvae after just 24 hours. There was no significant difference in survival between either of the F900742 groups. There was just a 55% survival rate in the untreated candidiasis group by 24 hours, which decreased to 45% by 48 hours and 30% by 72 hours. In contrast, the groups that were treated with 0.8 or 1.6 µg/ml F900742 both had a 90% and 92.5% survival rate after 24 hours and at 72 hours. There was a final survival rate of just 22.5% in the infected larvae that did not receive F900742, and an 82.5% and 85% in the 0.8 and 1.6 µg/ml treatment groups at the 6 day time point. The surviving larvae in both treatment groups appeared healthy as determined by colour, turgidity, and response to physical stimuli. The surviving larvae in the candidiasis group were less mobile and less responsive to physical stimuli. This data suggested that F900742 was effective at preventing the onset of candidiasis *in vivo* in the model organism *G. mellonella* (Figure 7.3).

There was a rapid onset of candidiasis in the untreated groups within the first 72 hours, with the greatest number of larvae dying within the first 24 hours. There were no deaths noted between 72 and 96 hours, and less than 8% between 96 and 144 hours. This suggested that candidiasis infections are rapid onset and fatal, however there is some inter-individual variability in susceptibility to candidiasis, demonstrated

by at least 20% of larvae surviving pathogenic fungal infection 6 days post inoculation. Mutant libraries of *G. mellonella* would be useful to investigate the humoral and adaptive immune responses to pathogenic fungal infections, and subsequently to identify novel drug targets.

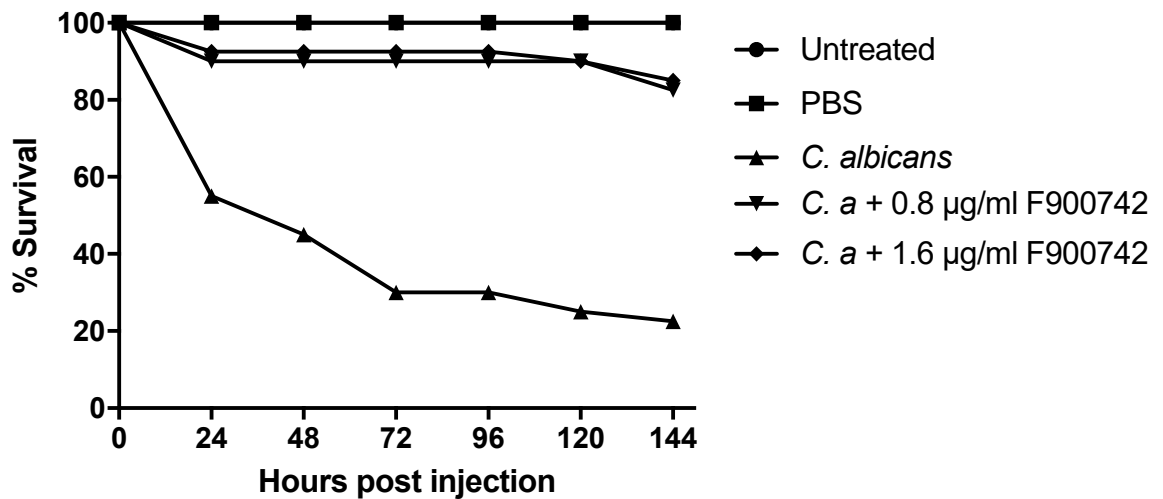


**Figure 7.3.** F900742 had good *in vivo* efficacy in the *G. mellonella* model of candidiasis. 40 *G. mellonella* over 3 experiments were inoculated with *C. albicans* one hour prior to treatment with F900742 at either 0.8 or 1.6 µg/ml. The survival rate was noted at 24 hour intervals. F900742 did induce a significant protective effect to infected *G. mellonella*. The 6 day survival rate was 22.5% in untreated infected larvae, where as it was greater than 80% in both samples that received an injection of F900742. No deaths were observed in either of the control groups (untreated or PBS).

F900742 demonstrated significant *in vivo* efficacy as demonstrated in figure 7.3. Differences between the immune responses of larvae resulted in a large wave of candidiasis-induced deaths in the first 72 hours and a smaller number in the following 3 days. Although it is possible the second wave was due to injection trauma or natural aging - there were a couple of deaths in the PBS control groups within this time period in the following experiment (Figure 7.4) - alternatively it could be due to *C. albicans* overwhelming the immune response at this time point. Next it was investigated whether an additional injection of F900742 improved the survival of *Candida*-inoculated larvae relative to a single dose (Figure 7.4). To assess the possibility that F900742 treatment on sequential days increased the survival of *G. mellonella*, larvae were

inoculated with *C. albicans* and treated as described above with 0.8 µg/ml F900742 on day 1, but then an additional injection of 0.8 µg/ml F900742 was administered through the penultimate bottom left proleg 24 hours later. As in figure 7.3, there was a significant increase in survival of *G. mellonella* treated with F900742 relative to the untreated control group after just 24 hours and throughout the course of the experiment. There was no difference in survival between the single or double treatment groups for the first 96 hours. However, there was one additional larval death at 120 hours in the single dose group, whereas there were no further deaths noted in the double dose group after 96 hours. The final 144 hour survival rates for the single and double F900742 groups were 80% and 90% respectively. This experiment was performed with just 10 larvae, therefore it is unclear whether a single larval death at 120 hours in the single dose group represents a significant result. However, the *G. mellonella* double dose group appeared more healthy in colour and movement than those that received the single dose. 5 of the alive single dose group were very grey and seemingly more lethargic than those that received the double dose. These results suggested that a second dose of F900742 slightly increased the overall survival of *G. mellonella* infected with *C. albicans* over a 144 hour period. Based on the responsiveness and colouring of the double dose group, but it is tempting to speculate that there would be a larger number of *G. mellonella* surviving candidiasis when treated with two rounds of F900742 than just one over a longer time course.

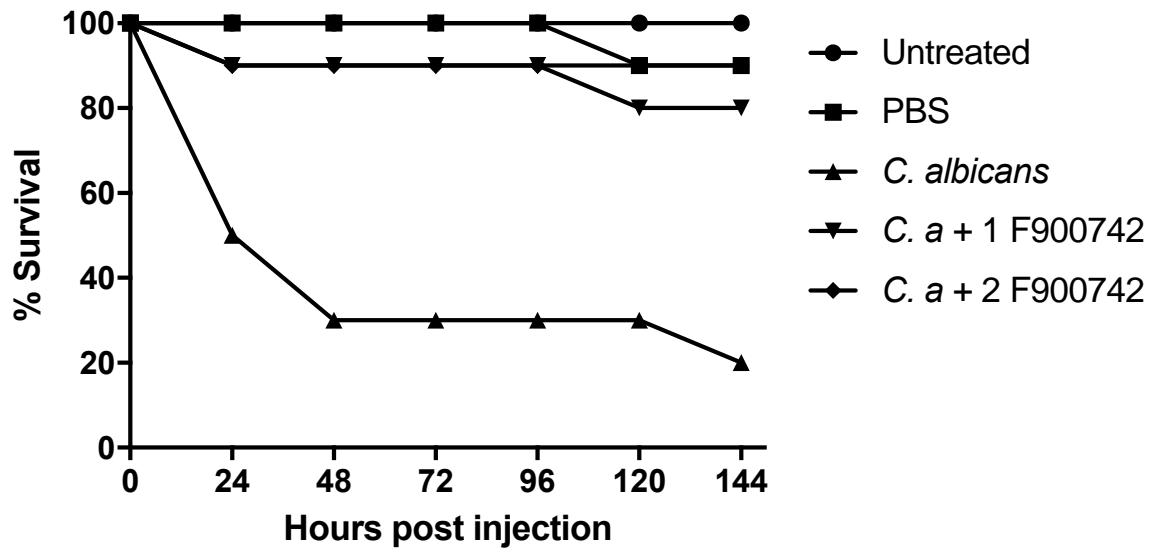


**Figure 7.4. A second dose of F900742 exerted a greater *in vivo* protective effect.** 10 *G. mellonella* were inoculated with *C. albicans* an hour prior to treatment with F900742 at 0.8 µg/ml. 24 hours later, 10 were injected with a second dose of F900742 at the same concentration. The survival rate was noted at 24 hour intervals. There was a 90% 6 day survival rate in *G. mellonella* that received the second injection of F900742, whereas there was an 80% survival rate was noted in the single dose group and just 22.5% in untreated infected larvae. No deaths were observed in the untreated control group; 1 was noted in the PBS control group.

### 7.2.2 Fungal burden analysis in *G. mellonella* treated with F900742

3 *G. mellonella* from the double dose group and 4 from both of the single dose groups (Figure 7.4) from various stages of candidiasis were culled and homogenised with a pestle and mortar. Water was added to the residual mix and 20 fold dilutions were made. 1.5 µl of each dilutant was added to a SAB agar plate and incubated at 30 °C for 48 hours. There was a total reduction in the fungal burden in all 3 alive larvae that were treated with two rounds of F900742 such that no colonies grew (Figure 7.5). There was the greatest residual fungal burden in the dead larvae in the single 0.8 µg/ml dose. In contrast, there was no growth at the most dilute number of fungi in the group that received a single dose of 1.6 µg/ml. The lowest dilution of fungal growth from this larva was observed one dilution fold higher than the 0.8 µg/ml larvae. Interestingly, alive larvae at the single 0.8 µg/ml doses had a similar fungal burden to that of the sick larvae at both 0.8 and 1.6 µg/ml single dose, however this alive larva

did not display obvious signs of infection. Sick larvae from both the 1.6 and 0.8  $\mu\text{g/ml}$  groups had a similar fungal burden. 3 untreated larvae (no inoculum or drug) and 3 larvae used as a candidiasis controls (inoculated with *C. albicans* but not given drug) were also analysed for fungal burden. There was no growth of fungi in the untreated larvae and growth in all 5 dilutants in the candidiasis control larvae, similar growth to that observed in the dead single 0.8  $\mu\text{g/ml}$  larvae (data not shown).



2 doses			1 dose (1.6)				1 dose (0.8)			
Alive	Alive	Alive	Dead	Sick	Sick	Alive	Dead	Sick	Sick	Alive



**Figure 7.5. Fungal burden analysis in *G. mellonella*.** Larvae were inoculated with *C. albicans* and treated with either a single dose of 0.8 or 1.6  $\mu\text{g/ml}$  of F900742 or two doses of 0.8  $\mu\text{g/ml}$  at 24 hour intervals. *G. mellonella* were homogenised and grown on SAB agar in 20 fold dilutions. No fungal growth was observed in any of the larvae treated with two doses of F900742. There was a one dilution fold reduction in the fungal burden in the dead larvae that received 1.6  $\mu\text{g/ml}$  relative to the dead larvae that received 0.8  $\mu\text{g/ml}$  F900742. There was similar fungal burden in all sick larvae that were treated with a single dose at either 0.8 or 1.6  $\mu\text{g/ml}$ . There was a substantial decrease in fungal burden between the larvae that received a single dose of 1.6  $\mu\text{g/ml}$  of F900742 relative to 0.8  $\mu\text{g/ml}$ . No growth was observed in the untreated *G. mellonella* (data not shown).

### 7.2.3 F900742 activity in mammalian models

The *G. mellonella* studies suggested significant *in vivo* potential of F900742 as an antifungal agent, however mice studies were not so promising (data not included). The mammalian studies were designed by F2G and carried out by a contract research organisation. The mice did not respond at all to F900742 against any pathogenic fungi, even when the experiment was skewed heavily in favour of the drug. Further analysis revealed F900742 had a very poor volume of distribution and a significant amount was secreted in the urine.

To ascertain whether serum factors were responsible for the poor volume of distribution of F900742 noted in the mammalian studies, wild type *S. cerevisiae* was grown in YPD and F900742 supplemented with either 10% FBS or 0.5% BSA (Figure 7.6). The addition of FBS was sufficient to reverse the growth inhibitory effect induced by F900742. BSA induced a partial reversal of F900742 activity. There was a similar amount of growth observed when either FBS or BSA was supplemented to YPD and F900742 relative to the YPD only sample. FBS had a greater F900742 inhibitory effect than BSA, suggesting that BSA is a major cause of serum inhibition, however it is likely that other unidentified factors further this effect. The addition of BSA or FBS to YPD only did not alter the growth of the yeast. It should be noted that both BSA and FBS are of bovine origin and not murine (the mammalian model of candidiasis used). Therefore, it is expected that the majority of the serum content will be very similar, if not identical, however it is likely that there are differences between bovine and murine serum content. This experiment was only performed once as such statistically robust conclusions cannot be made.

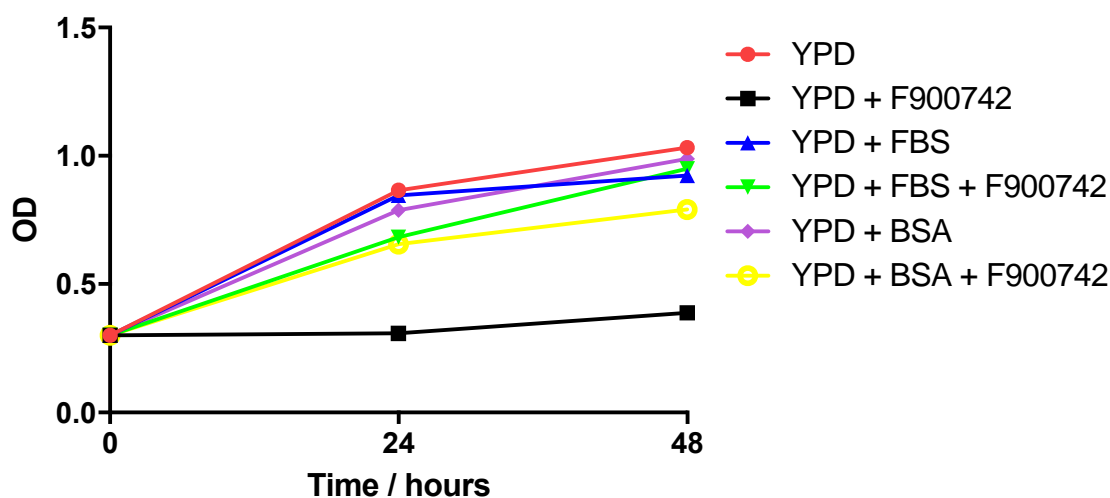
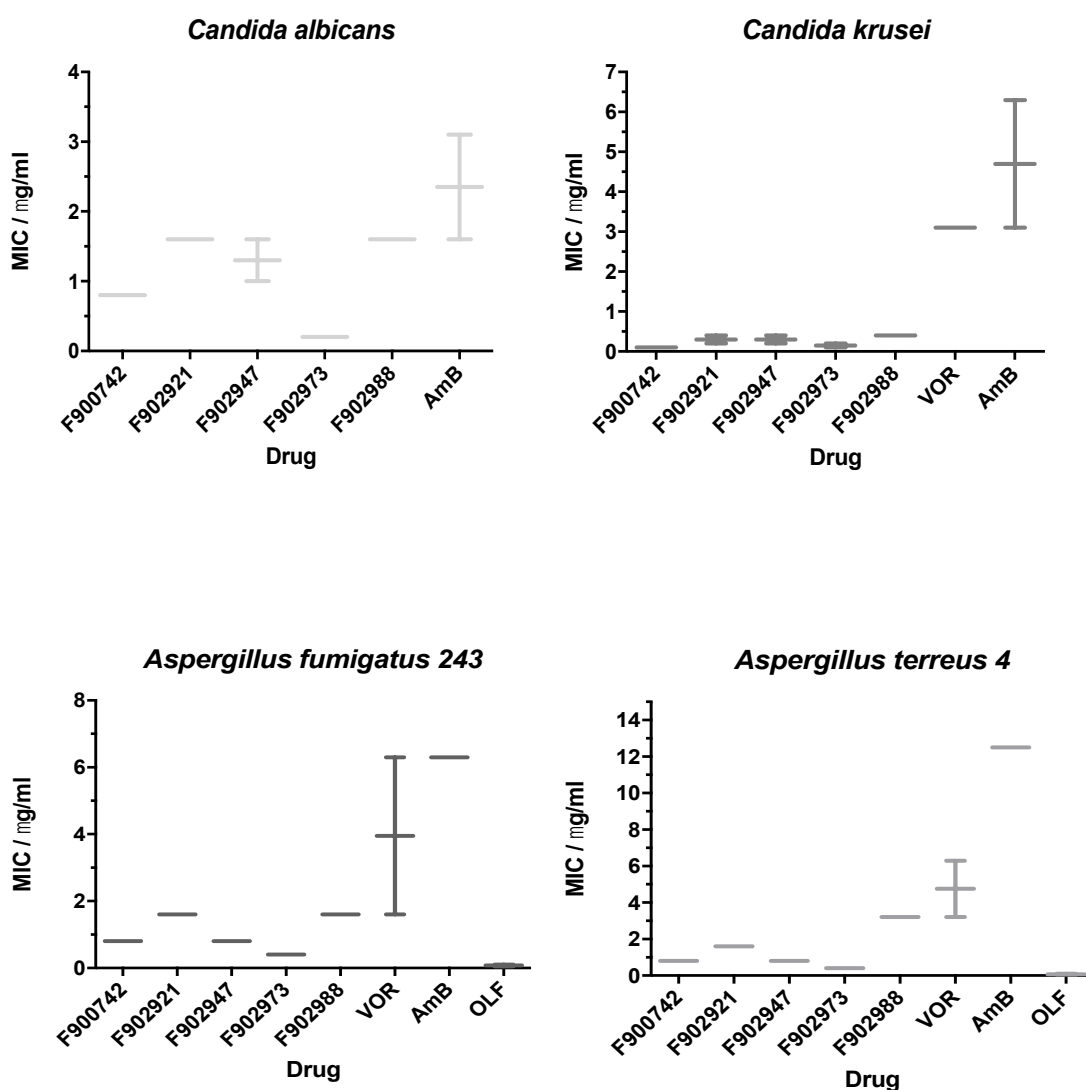


**Figure 7.6. FBS or BSA supplementation was sufficient to inhibit F900742.** FBS or BSA were added to YPD media containing F900742. FBS induced a greater F900742-inhibitory effect than BSA alone. N = 1.

#### 7.2.4 Investigating the activity of novel F6 series compounds

F900742 is part of the “F6” series. F900742 is very water soluble (greater than 75 mg/ml), therefore it is likely that the high solubility is at least part of the reason why F900742 demonstrated high levels of secretion in mammalian studies (data not shown). Further modifications to improve physicochemical properties, antifungal potency, and toxicology profile of F900742 has led to the production of many daughter compounds that also target  $\Delta 9$  desaturase. New compounds are designed in-house at F2G via *in silico* structure-activity driven design. Novel compounds are initially screened for their antifungal activity (MIC) against a range of pathogenic fungi and referenced against current clinical compounds. The MIC was determined by observing no growth of fungi in a plate containing serial, two-fold dilutions such that the concentration range of the F6 series drugs was 50  $\mu\text{g/ml}$  to 0.05  $\mu\text{g/ml}$ , voriconazole was 8 to 0.008  $\mu\text{g/ml}$ , amphotericin B was 2 to 0.002  $\mu\text{g/ml}$ , and olorofim was 4 to 0.004  $\mu\text{g/ml}$  (Figure 7.7). Voriconazole was not used in the *Candida albicans* screen due to the high levels of resistance described in previous studies. *Candida* species are not sensitive to olorofim, therefore this drug was not included as a reference

compound for either *C. albicans* or *C. krusei*. As initially identified by F2G (Table 4.1), *C. krusei* was the most sensitive to F900742 with an MIC of 0.1 µg/ml. *C. albicans*, *A. fumigatus* 243, and *A. terreus* 4 all had a MIC of 0.8 µg/ml. All F6 drugs showed significant antifungal efficacy at low concentrations. The MIC of all F6 compounds in both *Candida* species was lower than any of the current clinical treatments. Furthermore, there was substantial variation response to amphotericin B and voriconazole noted in both *Candida* strains, and a large variation in *A. fumigatus* response to voriconazole, whereas there was limited variation in response to the F6 compounds for any strain. F902973 had the most potent antifungal effect in all four strains and, of particular note, in *A. fumigatus* it had the same MIC as the current clinical trial compound olorofim (0.1 µg/ml). F902947 was the next most potent antifungal treatment in both *A. fumigatus* and *A. terreus* with an average MIC of 0.4 µg/ml in both species, with a similar MIC of 0.3 µg/ml noted in *C. krusei*. However, there was a substantially greater MIC of F902947 in *C. albicans*. F902988 displayed the least antifungal efficacy throughout all tested strains. F902921 had one fold lower antifungal activity than F900742 in all strains. Of note, in both *Aspergillus* species, olorofim was more potent than any of the F6 series compounds and current clinical treatments. *C. krusei* is been associated with significant multidrug resistance, and this strain most commonly leads to a fatal clinical outcome. *C. krusei* was the most sensitive strain to all F6 compounds tested. This suggested that  $\Delta 9$  desaturase inhibition is a very promising line of therapy, especially for patients presenting with *C. krusei* infection.



Treatment	F900742	F902921	F902947	F902973	F902988	Voriconazole	Amphotericin	Olorfim
Species								
<i>Candida albicans</i>	0.8	1.6	1.3	0.2	1.6	>50	2.4	>50
<i>Candida krusei</i>	0.1	0.3	0.3	0.1	0.4	3.1	4.7	>50
<i>Aspergillus fumigatus 243</i>	0.8	1.6	0.8	0.4	1.6	4	6.3	0.1
<i>Aspergillus terreus 4</i>	0.8	1.6	0.8	0.4	3.2	4.7	12.5	0.06

**Figure 7.7. Antifungal efficacy of novel F6 series compounds.** The MIC of 4 novel F6 series compounds that are derivatives of F900742 was determined in *C. albicans*, *C. krusei*, *A. fumigatus 243*, and *A. terreus 4*. The clinical compounds voriconazole and amphotericin B, as well as the clinical trial drug olorofim, were used as reference drugs. N = 2.

### 7.3 Discussion

Currently there are a limited number of treatment options available for patients with life threatening candidiasis. *C. albicans* is the most frequently isolated strain from patients presenting with nosocomial fungal infections. *C. albicans* is associated with high levels of acquired drug resistance and often to multiple drugs and drug classes thereby overwhelming any form of clinical intervention. Recent estimates suggest that *C. albicans* is associated with an annual mortality rate greater than 50% (over 350000 people). As the prevalence of novel strains of *Candida* that are associated with inherent resistance increases there will be a concurrent demand for novel drug classes and rising mortality rates tending.

The larvae of the wax moth *G. mellonella* provide a medically relevant alternative model to assess the efficacy of novel antifungal agents *in vivo* without the use of mammals. *G. mellonella* have been previously described as a clinically important model of *C. albicans* infection owing to, but not limited to, similarities with the human immune system, ease of control of candidiasis, correlations to mammalian models, and the quick generation of data (199).

Data presented here suggested that the F6 series of drugs represents a novel class of antifungals with significant *in vivo* efficacy in the fungal infection model *G. mellonella*. Overall, this suggested that F900742 does have significant *in vivo* efficacy at preventing candidiasis in *G. mellonella* when administered one hour after *C. albicans* inoculum. This study was designed to demonstrate that F900742 does have *in vivo* efficacy through preventing candidiasis onset, however it is not possible to conclude whether F900742 has curative effects in *G. mellonella*. To investigate the potential of F900742 as a clinical treatment, it would be required that candidiasis is fully established in *G. mellonella* prior to treatment. Visual cues such as darkening of larvae colour, dampened response to physical and light stimuli, and limited movement could be used to guide severity of candidiasis. At this stage, it is tempting to speculate that a derivative of F900742 that has overcome albumin binding could be used as a prophylactic treatment in patients deemed at high risk of developing fungal infections,

but to confirm this theory it would require much further *in vivo* testing in both mammalian and non-mammalian models. Interesting additional investigations could compare the efficacy of F900742 to current clinical compounds, for example voriconazole and amphotericin B or clinical trial drugs such as olorofim, in *G. mellonella* and investigate differences in response to alternative *Candida* or *Aspergillus* strains.

20% of *G. mellonella* were inherently more resistant to candidiasis infection 6 days post inoculum. Although recent years have witnessed a substantial increase in the understanding of antifungal immunity, considerable challenges remain. The discovery that phagocytes, and in particular dendritic cells, modulate the adaptive immunity have led to recent advances in the development of antifungal vaccines that could prove lifesaving for many thousands of immunocompromised patients each year (200). However, no vaccines are currently available for clinical use and it has been over 30 years since the first and only vaccine entered into a clinical trial (201). The timely and costly analysis of *in vivo* vaccine development mean that it is unlikely that a vaccine will be widely available in the near future. The development fungal infection models that are easy to genetically manipulate and cheap to house will prove invaluable for the design of vaccines and aid the design of novel therapies to treat these infections. The generation of mutant libraries and immunological assays to identify innate resistant factors in models such as *G. mellonella* will substantially aid this process.

There are often substantial discrepancies between *in vitro* and *in vivo* responses, and also clinical outcomes. This was highlighted here by variations in response to F900742 in mammalian *in vivo* experiments. *G. mellonella* studies demonstrated that F900742 had significant *in vivo* potential, whilst mammalian studies in a mouse model were less promising: F900742 was ineffective in a mouse model of systemic candidiasis. A previous study by Knechtle et al demonstrated that a novel compound, EV-086, was likely to inhibit  $\Delta 9$  desaturase and displayed broad spectrum activity against a range of pathogens *in vitro* and in an *in vivo* guinea pig model of *T. mentagrophytes* skin infection, but was ineffective in the mouse and rat systemic models of candidiasis (202). Of note, Knechtle used different types of fungal pathogens in the skin and

systemic models, as such it was not proven whether EV-086 is active in any *in vivo* model of candidiasis.

The therapeutic efficacy of a drug is limited by factors such as rate of renal clearance, accumulation at the site of action, degradation, and side effects to the patient. Albumin is the most abundant protein within human blood and functions as a transport protein for multiple ligands, including fatty acids, and xenobiotics, for example warfarin (203). Many drugs that mimic endogenous targets of albumin (such as Levemir mimicking fatty acids) exploit the natural transport function and multiple binding sites of albumin to ensure correct delivery to the target site and increase drug efficacy (204). This mechanism requires the dissociation of the drug over time to ensure therapeutic bioavailability and distribution. Conversely, if the drug does not dissociate from albumin then a reduction in drug efficacy would be observed. F900742 and EV-086 both demonstrated poor efficacy in mammalian *in vivo* studies. *In vitro* analysis revealed F900742 activity was reversed by the supplementation of BSA or FBS to YPD suggesting that at least a majority of the reason for unfavourable result in mammalian studies was due to albumin binding to F900742 and subsequent poor bioaccumulation at the site(s) of infection. Although it was not discussed by the authors, it is expected that as with F900742 the poor systemic response to EV-086 was likely due to serum factors which could highlight a possible difficulty in the development of all  $\Delta 9$  desaturase inhibitors for systemic fungal infections due to structural similarities with endogenous albumin ligands. Furthermore, F900742 is highly water soluble (> 75 mg/ml). Derivatives of F900742 would require to be designed to facilitate rapid dissociation from albumin and to reduce the hydrophilicity of the drug. Taken together with F900742 reversal data in (Figures 4.14 – 4.18), poor systemic activity could also be due to *C. albicans* overcoming F900742 inhibition by uptake of serum unsaturated fatty acids. However, it would be expected that this would also be demonstrated in the *G. mellonella* model data presented here and the guinea pig skin model in (202), as such it seems a somewhat unlikely mechanism. An initial step to ascertain whether compounds from the F6 series display activity in *in vivo* mammalian models, would be to utilise the guinea pig skin model. Based on



current data, it would be expected that F900742, or at least more potent derivatives of this drug, would display antifungal activity in this model.

At least two  $\Delta 9$  desaturase inhibitors have displayed good *in vitro* efficacy and in *in vivo* models of non-systemic infection. This suggests that compounds targeting  $\Delta 9$  desaturase represents a promising line of treatment at least for dermal infections. Furthermore, studies have suggested that Ole1p is essential for *Candida* virulence which suggests  $\Delta 9$  desaturase represents a good antifungal target, but further development of these inhibitors are required to ensure systemic efficacy in mammalian organisms (166,205).

Additional *in vivo* investigations into the antifungal efficacy of F900742 are unlikely, but this compound has proven useful for confirming that  $\Delta 9$  desaturase is a promising target for antifungal treatments. Derivatives of F900742 that also target this enzyme displayed very good *in vitro* efficacy relative to clinical compounds in clinically resistant isolates. Of particular note, *Candida krusei*, which displays high levels on innate and acquired resistance to treatments and is most often associated with a fatal patient outcome, was the most sensitive to all of the F6 series drugs in *in vitro* studies. It will be interesting to follow this series of drugs into the *in vivo* testing phases in both non-mammalian and mammalian systems of both aspergillosis and candidiasis.

# Discussion

# CHAPTER 8

## Final Discussion

The overall aims of this thesis were:

- 1) Identify the target of F900742;
- 2) Elucidate the mechanism of antifungal action of F900742;
- 3) Determine whether F900742 could represent the inaugural member of a novel class of clinical antifungals.

This thesis demonstrated that Ole1p is the likely target of F900742. Inhibition of Ole1p exerted significant morphological phenotypes that cumulated in the increased production of ROS suggesting this as a major mechanism of action. Although all *in vitro* and insect *in vivo* data presented here provided promising results that F900742 is a hopeful clinical compound, its activity was reversed by both unsaturated fatty acids and albumin suggesting that it would be unsuitable for the treatment of invasive fungal infections in patients. It has also been confirmed by F2G that F900742 had poor efficacy in mammalian studies. Despite the limited clinical potential of F900742, an insect *in vivo* model suggested that  $\Delta 9$  desaturase inhibitors do represent a promising and novel class of antifungals.

Development of future  $\Delta 9$  desaturase inhibitors for use as antifungal treatment is not without major difficulties, not least of which stems from issues in verifying the target protein beyond reasonable doubt. Data presented here is compatible with the hypothesis that Ole1p is the direct target of F900742. Although advances have been made in the field of lipid metabolism, there are still large gaps in our understanding: theories that were accepted are being challenged and replaced. The most pertinent unanswered question in relation to this thesis is: is there another regulator(s) of lipid desaturation or *de novo* lipid synthesis? At this stage it cannot be ruled out that an

unknown protein that is involved in the regulation of lipid saturated acyl chain metabolism via an unidentified mechanism is in fact the target of F900742. A drug-protein crystal structure would unquestionably confirm Ole1p as the target of F900742, however, to date, no group has reported the successful purification of the fungal  $\Delta 9$  desaturase. Membrane bound proteins represent approximately 30% of all genomes, yet there are few crystal structures for this group (206). The solubilisation and purification of this group of proteins, in particular integral membrane proteins, are associated with significant technical difficulties due to the high hydrophobicity, relatively low cellular levels, and susceptibility to degradation by proteases. In turn, this does not produce sufficient protein quantities for crystallisation. Based on current difficulties in purifying such highly hydrophobic proteins as Ole1p, it might be necessary to initially purify a truncated version of Ole1p, as with the mouse and human Scd1 isoforms, until methods for protein isolation improve. Alternatively, a phenotypic growth screen that enables high throughput screening of Ole1p mutants would prove useful for identifying residues that are essential for F900742 binding. Residues that are conserved throughout eukaryotic  $\Delta 9$  desaturases are highlighted in figure 1.6 and figure 1.7. Site directed mutagenesis at these conserved residues may be sufficient to reduce the affinity of the drug to the desaturase. However, some of these residues have been previously shown to be essential for  $\Delta 9$  desaturase function, for example all 9 of the conserved histidines (128), therefore it must be ensured that enzyme activity has not been effected by mutagenesis at these sites. The mutagenic plasmid library purchased for this study could still be utilised for this purpose by transforming the library into yeast and growing them on YPD only. Subsequently selecting individual colonies and growing them in YPD broth supplemented with F900742 will make it possible to determine whether the plasmid is inducing a hyper- or hypogrowth phenotype. Colonies displaying an altered growth phenotype would have the plasmid isolated and sequenced such that a library of base mutations could be built. However, experiments here were somewhat hindered by the OLE1 ORF in the mutagenic library not being expressed off its endogenous promoter. Future experiments should ensure that the library is designed such that the endogenous OLE1 promoter is used. Although this study did not unequivocally confirm that Ole1p is the target of F900742, previous studies have demonstrated similar cellular responses

when chemically or genetically interfering with the OLE1 pathway (146,157). This provides additional evidence supporting the hypothesis that Ole1p is the target of F900742.

This study also identified a novel cellular response to lipotoxic stress through the direct inhibition of the OLE1 pathway. It has previously been demonstrated that identical cellular responses were initiated when desaturase expression was chemically or genetically inhibited. Tatzer noted the relocalisation of Ole1p<sup>ts</sup> to aberrant regions within the cell when grown at non-permissive temperatures, and that these responses were also apparent when cells were grown in the presence of cyanides or azides (157). The inhibition of the OLE1 pathway via the temperature sensitive allele or addition of cyanides or azides was associated with a reduction in desaturase activity and skewed the lipid profile in favour of saturated lipids. Indirect inhibition of the OLE1 pathway was also achieved by Pienau through the inhibition of heme synthesis using the  $\Delta$ hem1 strain. Both Tatzer and Pienau identified aberrant, cytosolic, membrane bound structures by EM. F900742 induced the formation of RFP-HDEL, Ole1p-GFP, Ubx2p-GFP, and Sct1p-GFP containing tubes and aberrant cytosolic, membranous compartments. The formation of these structures is predicted to be in-line with data reported by Tatzer and Pienau. It is predicted that F900742 inhibits Ole1p and results in an increase in saturated lipid content inducing regions of suboptimal fluidity and micro-stress in the ER membrane as a result of containing an unusually high saturated to unsaturated lipid content. Micro-stress is defined here as small areas of membrane containing an aberrant lipid profile that induces alterations to the physicochemical properties in that region and subsequently effect membrane processes. Small regions of micro-stress are expected to be tolerable, however as these regions grow or there are more regions, they are likely to interfere with the physicochemical properties of the ER and essential cellular processes.

All experiments performed here were in log phase cells as such it would be expected that there would be a high requirement for *de novo* lipid synthesis. During unsaturated fatty acid starvation, yeast have been shown to maintain membrane fluidity through the incorporation of saturated acyl chains with smaller head groups. However, chronic

low levels of unsaturated fatty acids lead to lipotoxicity and cell death, in contrast high doses of saturated fatty acids have been shown to be non-toxic to *S. cerevisiae* (109,207). It is predicted that it was low levels of unsaturated fatty acids that instigated F900742-induced lipotoxicity rather than high levels of membrane saturated fatty acids. To protect the majority of the ER and its function, it is expected that ER membrane containing abnormally high levels of saturated lipids separated from the main ER which resulted in a side compartment containing high levels of membrane lipids with saturated acyl chains. This would ensure that the main ER would be composed of a normal ratio of saturated to unsaturated fatty acids and able to continue with normal functions. It is also plausible that *de novo* free saturated fatty acids are sequestered into these structures to avoid their incorporation into new lipids. Future work could investigate the physiological implications of these structures: do they effect ER processes such as the secretory pathway? Do other ER membrane anchored proteins, for example glycosylphosphatidylinositol (GPI) anchored proteins, relocate to the aberrant compartments? Is there any physiological role for the compartments? Does inhibition of lipid metabolism through other pathways also produce these structures? Investigations into the timings and morphological developments of these compartments would be of great interest and aid understanding of cellular responses to unsaturated fatty acids starvation. However, it must be noted that this study is substantially limited by the fact that the lipid profile was not assessed in any cell type. It would be of paramount importance for future work to determine the alterations to the lipidome and changes in Ole1p activity.

The selective relocalisation of Ole1p-GFP, Ubx2p-GFP, and Sct1-GFP to tubes and puncta supports the theory that the unidentified compartments could contain high levels of saturated acyl chains (the substrates of Ole1p and Sct1p) and that the proteins are relocalising within the ER to restore the saturated:unsaturated lipid balance. It would be interesting to investigate whether Scd1-GFP expressed in *ole1* null yeast relocalises in a similar pattern to Ole1p-GFP. Once protocols have developed to successfully purify Ole1p from the ER membrane, cells expressing a protein-A tagged desaturase could be used to assess the immunogold localisation of the desaturase. This would confirm whether Ole1p was relocalising to the unidentified structures.

Along with lipid analysis, confirmation that Ole1p was redistributing to the compartments would provide an insight into the physiological function of these regions. However, it is plausible that the compartments are of no physiological relevance and are a passive pathological consequence of acute unsaturated fatty acid starvation. On the other hand, if these structures do provide a physiological and protective role to the cell then data presented here demonstrated a novel cellular response to direct unsaturated fatty acid-induced lipotoxicity. Similar structures have not been described in any study investigating fatty acid induced lipotoxicity either through genetic knock out of enzymes involved in the OLE1 pathway, nor when yeast are grown in media supplemented with high levels of saturated fatty acids. It is possible that these aberrant compartments have not been noted before as they are a rapidly appearing phenotype, whereas most studies have investigated longer term effects. Investigations into the ultrastructural defects following long-term treatment with F900742 would be expected to induce further phenotypes, for example the degradation of the nuclear envelope and other organelle membranes. OLE1 pathway mutants have been previously shown to disintegrate the nuclear envelope inducing irreversible cell damage (207). Furthermore, Zhang et al observed severe morphological defects in *ole1* null *S. cerevisiae* after 6 hours. Stukey had previously identified that these cells contained less than 10% of wild type levels of unsaturated fatty acids (208). Assuming F900742 does effect the lipidome through a reduction in unsaturated fatty acid levels, it would be expected that morphological defects observed by Zhang would also be noted in cells treated with F900742 after comparable treatment times. Of note, the morphological features of F900742-treated cells are limited by drug availability, as such it would be expected that drug concentration could limit morphological phenotypes after a certain time point.

RFP-HDEL relocalisation was first observed after just 30 minutes, whilst an increase in Ole1p-GFP transcription was noted after 1 hour and relocalisation after 2 hours. This data provides a possible feedback mechanism in response to low levels of membrane unsaturated lipids whereby cells evoke the formation of saturated lipid rich structures as stores of a finite amount of lipid, but when the storage capacity limit is nearing and fewer saturated lipids are sequestered from the ER, changes to the ER membrane

physicochemical properties are sensed by Mga2p which initiates the transcription of Ole1p. It is plausible that the large size of these structures induced lateral pressure on to the ER membrane. In an attempt to generate *de novo* membrane lipids containing unsaturated acyl chains, Ole1p could relocalise to the structures to desaturate acyl chains. However, in the presence of F900742, desaturase activity is inhibited, thus Ole1p is unable to restore the balance of membrane acyl chain saturation. It would be interesting to investigate the correlative timings between variations in the ER lipidome, relocalising of Ole1p, and the formation of the aberrant compartments. Concurrent with the redistribution of RFP-HDEL after 30 minutes, mitochondrial fission was observed which was associated with significant ROS production. NAC was sufficient to inhibit the reduction in growth suggesting that at least a major mechanism of F900742 action is via the generation of ROS. It is currently unclear what the role of Ole1p is in mitochondrial distribution and morphology. It also remains to be determined whether mitochondrial fission is activated by the inhibition of an unknown Ole1p activity in the mitochondria, or through the activation of ER stress, or as a result of low unsaturated fatty acid content, or a combination.

Overall, the proposed mechanism of action of F900742 is fast-acting and lipid-dependent. Lipotoxic-induced cellular stress was expected to be exerted through an inhibition of Ole1p. It is predicted that over the first 4 hours of treatment, cells overcame the growth inhibitory effects of F900742 by utilising unsaturated fatty acid stores. However, due to the large requirement for unsaturated fatty acids in log phase growing cells, the unsaturated fatty acid stores quickly deplete to a level that initiated early lipotoxic responses after 30 minutes, such as mitochondrial fission and alterations to the ER morphology. The reduction in unsaturated:saturated lipid content in the ER induced the formation of aberrant compartments derived from the ER just 30 minutes after treatment with F900742. These are expected to have a protective, short-term role. 2 hours of treatment was predicted to induce significant alterations to the ER membrane physicochemical properties which were sensed by Mga2p and resulted in an increase in Ole1p and Ubx2p transcription. Ole1p relocalised to the aberrant compartments containing high levels of substrate (saturated acyl chains) to balance the shift towards a more saturated membrane lipidome. Ubx2p also localised to the



compartments to enable further activation of OLE1 transcription as required. It is unclear whether ER stress induced mitochondrial fission or whether this was a result of Ole1p inhibition, or both. Mitochondria fission induced the production of ROS which is expected to be the major mechanism of action. Further lipotoxicity would be expected to initiate substantial ER expansion through the generation of ER whorls, as well as increase the amount of ROS production and the degradation of the organelle membranes. It would be expected that pathways such as the unfolded protein response (UPR) would be activated. Pineau showed significant activation of the UPR in  $\Delta hem1$  that paralleled changes in the lipidome to more saturated content. Further investigations into the activation of pathways such as the UPR would be interesting to provide a complete picture for the mechanism of action of F900742. Figure 8.1 summarises the suggested mechanism of action of F900742.

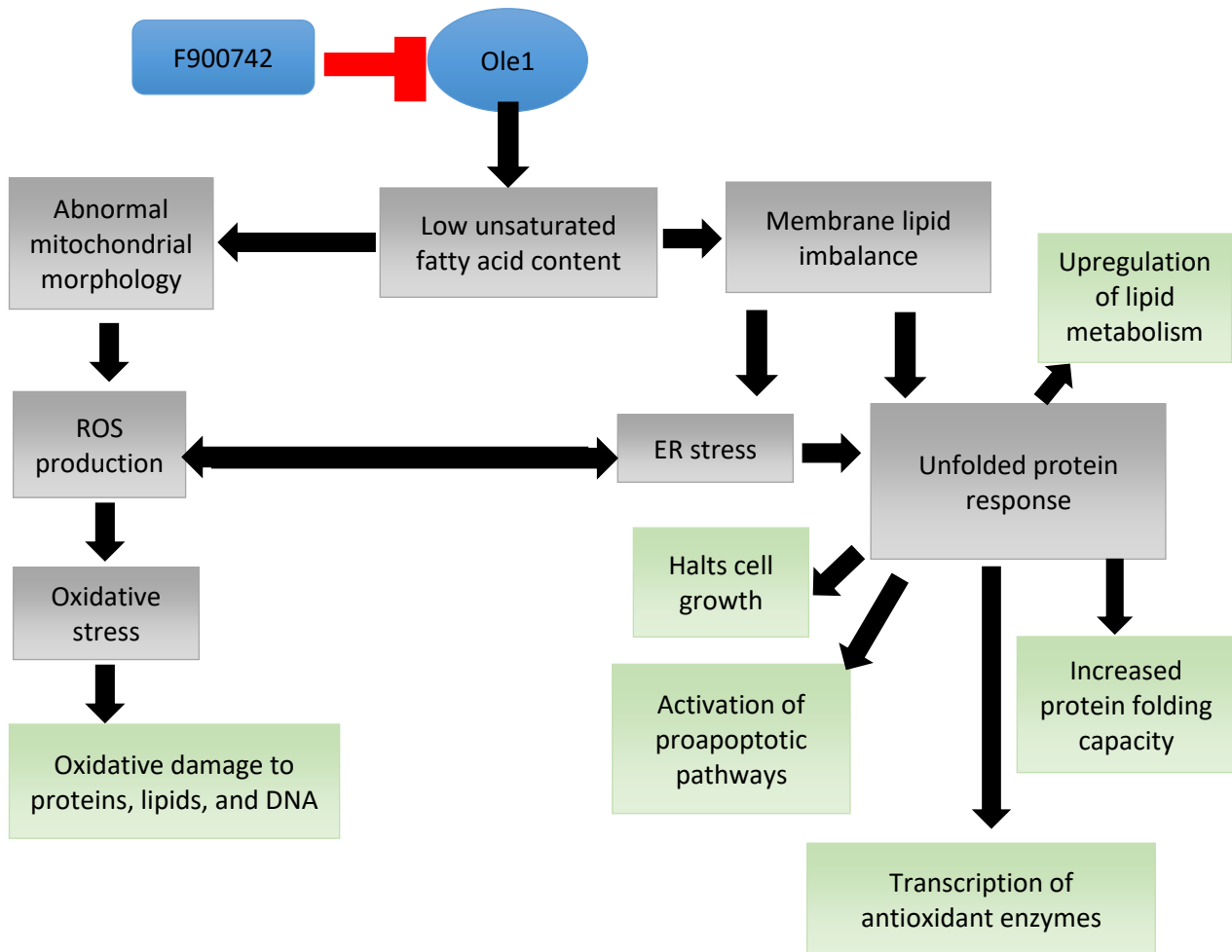


**Figure 8.1. Proposed mechanism of action of F900742.** It is predicted that Ole1p is the target of F900742. Inhibition of Ole1p would drive alterations to the lipidome such that there would be a low unsaturated fatty acid content. The membrane imbalance would induce ER stress which causes morphological phenotypes such as ER whorls and the formation of ER-derived, cytosolic compartments. ER stress induces process such as the unfolded protein response. The UPR mounts a myriad of responses to initially attempt to promote cell survival through the activation of pathways such as increase protein folding capacity, the transcription of antioxidant enzymes, and the upregulation of lipid metabolism genes. If the cost-benefit becomes such that the energy expense is too great, the unfolded protein response activates pathways that halt cell growth and eventually proapoptotic pathways. Inhibition of Ole1p can also trigger mitochondrial fission. Mitochondrial fission induces the production of ROS and subsequent oxidative stress to proteins, lipids and DNA. ER stress can also initiate the production of ROS, as well as ROS activate ER stress.

F900742 demonstrated good *in vitro* efficacy as a broad-spectrum, fungistatic inhibitor. However, there is no clinical potential for this compound: either oleic acid or palmitoleic acid, FBS or BSA was sufficient to reverse the activity of F900742 *in vitro*. It is expected that similarities between the structure and physical parameters of the drug and fatty acids (an endogenous substrate of albumin) resulted in F900742 being sequestered by albumin and that this was the major factor resulting in poor mammalian studies for invasive, systemic fungal infection. It is also expected that the serum factors were responsible for the significantly higher MIC in HeLa cells relative to any fungal strain. Retesting the MIC of HeLa cells in unsaturated fatty acid-free and serum-free media would verify whether F900742 also targets Scd1 in this mammalian cell line. Derivatives of F900742 could target allosteric sites of  $\Delta 9$  desaturase to overcome albumin binding or be made more insoluble through formulation as a salt or emulsion or made as a complex with cyclodextrins. The correct delivery of  $\Delta 9$  desaturase inhibitors to therapeutic site of action has been demonstrated in mammalian models of obesity (209), type 2 diabetes (210), and cancers (211). However, to date, no Scd1 inhibitor has been trialled in humans. Data presented here has not investigated the possibility of F900742 binding to Scd5, the second human  $\Delta 9$  desaturase. Additional studies to verify the activity of F900742 against Scd5 would also be essential for predicting any potential adverse drug effects through non-specific desaturase binding. The F6 series is a promising line of therapy as demonstrated by *in vivo* studies using *G. mellonella*. Derivatives of F900742 have also demonstrated good antifungal potency in *in vitro* assays against clinically relevant strains, and have shown to have the same, if not better, efficacy than some of the frequently used clinical drugs. In an era associated with large scale, widespread, and growing antifungal resistance, it is paramount that novel drug classes with good efficacy are developed.

Although F900742 does not represent a good candidate drug for antifungal use due to its Scd1 binding properties, data presented in this thesis does suggest that derivatives of this drug could be useful for conditions that display aberrant Scd1 activity. SCD1 represents a novel therapeutic target for the treatment of conditions such as cancers (212). One hallmark of cancer cells is an altered cell metabolism, one of which is the increased demand for fatty acids to meet the energy expensive process of rapid cell

proliferation. Studies have shown that increased lipid metabolism is linked to the metastatic potential of the tumour (213). To ensure the large lipid requirements are met, cancer cells synthesise the majority of lipids *de novo* (214). SCD1 overexpression has been observed in a large number of cancers. Scd1 promoters many features of cancers that are associated with a poor patient outcome, including promoting cancer cell proliferation, migration, and metastasis. Furthermore, Scd1 is associated with maintaining many of the characteristics of cancer stem cells and subsequently driving resistance to chemotherapy and cancer progression. Expanding the realms of therapeutic potential of the F6 series to include diseases such as cancers could be of great benefit to many patients with ailments other than invasive fungal infections (215).

Irrespective of its potential as a clinical agent, F900742 has potential for enhancing our understanding of lipotoxic stress response pathways *in vitro*. F900742 induced rapid changes to the lipid profile which induced the formation of aberrant structures that are predicted to exert immediate, short-term protective relief to the cell. It is expected that the novel compartments are derived from the ER, yet questions still remain as to their function. Do they contain a high portion of saturated fatty acids? Does Ole1p relocalise to within these structures or in close proximity to an opening, if at all? What is the maximum size these compartments can reach before they exert damaging physical strain on the cell? Does the cell respond in the same manner if the lipidome is skewed towards high levels of unsaturated acyl chains? Further beyond the formation of the compartments, what morphological features ensue if the acyl chain balance is not restored? In relation to the development of antifungal drugs, this study has demonstrated that although insect fungal models do provide a significant wealth of data, they are not currently sufficient to accurately predict *in vivo* mammalian efficacy. Prior to mammalian studies, and to keep adhere to the replacement, reduction, and refinement (3Rs) framework for animal research, antifungal drugs should have their *in vitro* efficacy tested in mammalian serum. The development of insect models of for the human innate and humoral response to fungal pathogens will prove valuable for the development of vaccines for high-risk patients and identifying drugs that harness the most effective barrier to fungal infection: the healthy human immune system.

# References

1. Brown GD, Denning DW, Gow NAR, Levitz SM, Netea MG, White TC. Hidden killers: Human fungal infections. *Sci Transl Med*. 2012 Dec 19;4(165):1–9.
2. Schelenz S, Barnes RA, Barton RC, Cleverley JR, Lucas SB, Kibbler CC, et al. British Society for Medical Mycology best practice recommendations for the diagnosis of serious fungal diseases. *Lancet Infect Dis*. 2015;15(4):461–74.
3. Clancy CJ, Jaber RA, Leather HL, Wingard JR, Staley B, Wheat LJ, et al. Bronchoalveolar lavage galactomannan in diagnosis of invasive pulmonary aspergillosis among solid-organ transplant recipients. *J Clin Microbiol*. 2007 Jun 1;45(6):1759–65.
4. Robbins N, Caplan T, Cowen LE. Molecular Evolution of Antifungal Drug Resistance. *Annu Rev Microbiol*. 2017 Sep 8;71(1):753–75.
5. Wisplinghoff H, Bischoff T, Tallent SM, Seifert H, Wenzel RP, Edmond MB. Nosocomial Bloodstream Infections in US Hospitals: Analysis of 24,179 Cases from a Prospective Nationwide Surveillance Study. *Clin Infect Dis*. 2004 Aug 1;39(3):309–17.
6. Perlin DS, Rautemaa-Richardson R, Alastruey-Izquierdo A. The global problem of antifungal resistance: prevalence, mechanisms, and management. *Lancet Infect Dis*. 2017 Dec 1;17(12):383–92.
7. Sarvepalli AK, Dharana PK. Spectrum of opportunistic infections with correlation to CD4 counts in newly diagnosed HIV seropositive cases. *Int J Adv Med*. 2017 Jan 23;4(1):252–8.
8. Vincent J-L, Rello J, Marshall J, Silva E, Anzueto A, Martin CD, et al. International Study of the Prevalence and Outcomes of Infection in Intensive Care Units. *JAMA*. 2009 Dec 2;302(21):2323–9.
9. Bongomin F, Gago S, Oladele R, Denning D, Bongomin F, Gago S, et al. Global and Multi-National Prevalence of Fungal Diseases—Estimate Precision. *J Fungi*. 2017 Oct 18;3(57):1–29.
10. Pfaller MA, Diekema DJ, Gibbs DL, Newell VA, Ellis D, Tullio V, et al. Results from the ARTEMIS DISK Global Antifungal Surveillance Study, 1997 to 2007: a 10.5-Year Analysis of Susceptibilities of *Candida* Species to Fluconazole and Voriconazole as Determined by CLSI Standardized Disk Diffusion. *J Clin Microbiol*. 2010;48(4):1366–77.
11. Paulo S, Colombo AL, de Almeida Júnior JN. Fungal infections 2 *Candida* and invasive mould diseases in non-neutropenic critically ill patients and patients with haematological cancer. *Ser Lancet Infect Dis*. 2017;17(17):30443–50.
12. Rosales C, Demarex N, Lowell CA, Uribe-Querol E. Neutrophils: Their Role in Innate and Adaptive Immunity. *J Immunol Res*. 2016 Feb 24;2016:1–2.
13. Perlroth J, Choi B, Spellberg B. Nosocomial fungal infections: Epidemiology, diagnosis, and treatment. *Med Mycol*. 2007;45(4):321–46.
14. Köhler JR, Casadevall A, Perfect J. The spectrum of fungi that infects humans. *Cold Spring Harb Perspect Med*. 2015 Nov 3;5(1):1–22.
15. Mayer FL, Wilson D, Hube B. *Candida albicans* pathogenicity mechanisms. *Virulence*. 2013;4(2):119–28.

16. Pasqualotto AC. Differences in pathogenicity and clinical syndromes due to *Aspergillus fumigatus* and *Aspergillus flavus*. *Med Mycol*. 2009;47(1):261–70.
17. Chawla K, Kosaraju K, Rayasam S, Mukhopadhyay C. Clinico-Microbiological Profile of Chronic Pulmonary Aspergillosis from a Tertiary Care Centre in Southern India Microbiology Section. *J Clin Diagnostic Res*. 2013;7(12):2712–5.
18. Lamoth F. *Aspergillus fumigatus*-related species in clinical practice. *Front Microbiol*. 2016;7(MAY):683.
19. Levitz SM, Diamond RD. Mechanisms of resistance of *Aspergillus fumigatus* conidia to killing by neutrophils in vitro. *Journal of Infectious Diseases*. 1985;152(1):33–42.
20. Aimanianda V, Bayry J, Bozza S, Knemeyer O, Perruccio K, Elluru SR, et al. Surface hydrophobin prevents immune recognition of airborne fungal spores. *Nature*. 2009 Aug 27;460(7259):1117–21.
21. Armstrong-James D, Brown GD, Netea MG, Zelante T, Gresnigt MS, van de Veerdonk FL, et al. Immunotherapeutic approaches to treatment of fungal diseases. *Lancet Infect Dis*. 2017;17(12):393–402.
22. Bowen AD, Davidson FA, Keatch R, Gadd GM. Induction of contour sensing in *Aspergillus niger* by stress and its relevance to fungal growth mechanics and hyphal tip structure. *Fungal Genet Biol*. 2007 Jun;44(6):484–91.
23. Kathuria S, Singh PK, Sharma C, Prakash A, Masih A, Kumar A, et al. Multidrug-Resistant *Candida auris* Misidentified as *Candida haemulonii*: Characterization by Matrix-Assisted Laser Desorption Ionization-Time of Flight Mass Spectrometry and DNA Sequencing and Its Antifungal Susceptibility Profile Variability by Vitek 2, CLSI Broth Microdilution, and Etest Method. *J Clin Microbiol*. 2015 Jun 1;53(6):1823–30.
24. Perfect JR. The antifungal pipeline: a reality check. *Nat Rev Drug Discov*. 2017 Sep;16(9):603–16.
25. Mizusawa M, Miller H, Green R, Lee R, Durante M, Perkins R, et al. Can multidrug-resistant *Candida auris* be reliably identified in clinical microbiology laboratories? *J Clin Microbiol*. 2017;55(2):638–40.
26. Drain PK, Hyle EP, Noubary F, Freedberg KA, Wilson D, Bishai WR, et al. Diagnostic point-of-care tests in resource-limited settings. *Lancet Infect Dis*. 2014;14(3):239–49.
27. Fisher MC, Hawkins NJ, Sanglard D, Gurr SJ. Worldwide emergence of resistance to antifungal drugs challenges human health and food security. *Science (80- )*. 2018 May 18;360(6390):739–42.
28. Brown GD. Innate Antifungal Immunity: The Key Role of Phagocytes. *Annu Rev Immunol*. 2011;29:1–21.
29. Verma A, Wüthrich M, Deepe G, Klein B, Giri G. Adaptive immunity to fungi. *Cold Spring Harb Perspect Med*. 2015;5(3):1–14.
30. Carvalho A, Cunha C, Pasqualotto AC, Pitzurra L, Denning DW, Romani L. Genetic variability of innate immunity impacts human susceptibility to fungal diseases. *Int J Infect Dis*. 2010 Jun;14(6):460–8.
31. Hardison SE, Brown GD. C-type lectin receptors orchestrate antifungal immunity. *Nat Immunol*. 2012 Sep 21;13(9):817–22.
32. Day JN, Chau TTH, Wolbers M, Mai PP, Dung NT, Mai NH, et al. Combination Antifungal Therapy for Cryptococcal Meningitis. *N Engl J Med*. 2013 Apr

- 4;368(14):1291–302.
33. Anderson TM, Clay MC, Cioffi AG, Diaz KA, Hisao GS, Tuttle MD, et al. Amphotericin forms an extramembranous and fungicidal sterol sponge. *Nature Chemical Biology* 2014 p. 400–6.
  34. Denning DW, Hope WW. Therapy for fungal diseases: opportunities and priorities. *Trends Microbiol.* 2010 May 1;18(5):195–204.
  35. Paul O Gubbins. Triazole antifungal agents drug–drug interactions involving hepatic cytochrome P450. *Expert Opin Drug Metab Toxicol.* 2011;7(11):1411–29.
  36. Huh W-K, Falvo J V., Gerke LC, Carroll AS, Howson RW, Weissman JS, et al. Global analysis of protein localization in budding yeast. *Nature.* 2003;425(6959):686–91.
  37. Birnbaum JE. Pharmacology of the allylamines. *Journal of the American Academy of Dermatology.* 1990;23(4):782-785.
  38. Kyle AA, Dahl M V. Topical therapy for fungal infections. *American Journal of Clinical Dermatology.* 2004;5(6):443-451.
  39. Van Paassen J, Russcher A, In't Veld-Van Wingerden AW, Verweij PE, Kuijper EJ. Emerging aspergillosis by azole-resistant *aspergillus fumigatus* at an intensive care unit in the Netherlands, 2010 to 2013. *Eurosurveillance.* 2016;21(30).
  40. Patterson TF, Thompson GR, Denning DW, Fishman JA, Hadley S, Herbrecht R, et al. Practice guidelines for the diagnosis and management of aspergillosis: 2016 update by the infectious diseases society of America. *Clin Infect Dis.* 2016;63(4):e1–60.
  41. Pappas PG, Kauffman CA, Andes DR, Clancy CJ, Marr KA, Ostrosky-Zeichner L, et al. Clinical Practice Guideline for the Management of Candidiasis: 2016 Update by the Infectious Diseases Society of America. *Clin Infect Dis.* 2015;62(4):1–50.
  42. Vincent BM, Lancaster AK, Scherz-Shouval R, Whitesell L, Lindquist S. Fitness Trade-offs Restrict the Evolution of Resistance to Amphotericin B. Mitchell AP, editor. *PLoS Biol.* 2013 Oct 29;11(10):1–17.
  43. Shapiro RS, Robbins N, Cowen LE. Regulatory Circuitry Governing Fungal Development, Drug Resistance, and Disease. *Microbiol Mol Biol Rev.* 2011 Jun 1;75(2):213–67.
  44. Fanos V, Cataldi L. Amphotericin B-induced nephrotoxicity: A review. *J Chemother.* 2000;12(6):463–70.
  45. Hamill RJ. Amphotericin B formulations: A comparative review of efficacy and toxicity. Vol. 73, *Drugs.* 2013. p. 919–34.
  46. Network RP. Trends and Challenges in Pesticide Resistance Detection. *Trends Plant Sci.* 2016 Oct;21(10):834–53.
  47. Lucas JA, Hawkins NJ, Fraaije BA. The Evolution of Fungicide Resistance. *Adv Appl Microbiol.* 2015;90:29–92.
  48. Sanglard D, Ischer F, Koymans L, Bille J. Amino Acid Substitutions in the Cytochrome P-450 Lanosterol 14 $\alpha$ -Demethylase (CYP51A1) from Azole-Resistant *Candida albicans* Clinical Isolates Contribute to Resistance to Azole Antifungal Agents. *Antimicrob Agents Chemother.* 1998 Feb 1;42(2):241–53.
  49. Shor E, Perlin DS. Coping with Stress and the Emergence of Multidrug Resistance in Fungi. Heitman J, editor. *PLoS Pathog.* 2015 Mar 19;11(3):1–7.
  50. Krcmery V, Barnes AJ. Non-*albicans* *Candida* spp. causing fungaemia:

- pathogenicity and antifungal resistance. *J Hosp Infect.* 2002 Apr;50(4):243–60.
51. Berger S, Chazli Y El, Babu AF, Coste AT. Azole resistance in *Aspergillus fumigatus*: A consequence of antifungal use in agriculture? *Front Microbiol.* 2017 Jun 7;8(JUN):1–6.
  52. Sanglard D, Kuchler K, Ischer F, Pagani JL, Monod M, Bille J. Mechanisms of resistance to azole antifungal agents in *Candida albicans* isolates from AIDS patients involve specific multidrug transporters. *Antimicrob Agents Chemother.* 1995;39(11):2378–86.
  53. Sanglard D, Ischer F, Monod M, Bille J. Cloning of *Candida albicans* genes conferring resistance to azole antifungal agents: Characterization of CDR2, a new multidrug ABC transporter gene. *Microbiology.* 1997;143(2):405–416.
  54. Coste A, Turner V, Ischer F, Morschhäuser J, Forche A, Selmecki A, et al. A mutation in Tac1p, a transcription factor regulating CDR1 and CDR2, is coupled with loss of heterozygosity at chromosome 5 to mediate antifungal resistance in *Candida albicans*. *Genetics.* 2006 Apr;172(4):2139–56.
  55. Chowdhary A, Sharma C, Meis JF. *Candida auris*: A rapidly emerging cause of hospital-acquired multidrug-resistant fungal infections globally. Hogan DA, editor. *PLoS Pathog.* 2017 May 18;13(5):1–10.
  56. Lockhart SR, Etienne KA, Vallabhaneni S, Farooqi J, Chowdhary A, Govender NP, et al. Simultaneous emergence of multidrug-resistant *Candida auris* on 3 continents confirmed by whole-genome sequencing and epidemiological analyses. *Clin Infect Dis.* 2017;64(2):134–40.
  57. Casadevall A, Kontoyiannis DP, Robert V. On the emergence of *Candida auris*: climate change, azoles, swamps, and birds. *MBio.* 2019;10(4):1–10.
  58. Owusu Obeng A, Egelund EF, Alsultan A, Peloquin CA, Johnson JA. CYP2C19 polymorphisms and therapeutic drug monitoring of voriconazole: Are we ready for clinical implementation of pharmacogenomics? *Pharmacotherapy.* 2014 Jul;34(7):703–18.
  59. Hawkins NJ, Cools HJ, Sierotzki H, Shaw MW, Knogge W, Kelly SL, et al. Paralog re-emergence: A novel, historically contingent mechanism in the evolution of antimicrobial resistance. *Mol Biol Evol.* 2014;31(7):1793–802.
  60. Selmecki A, Gerami-Nejad M, Paulson C, Forche A, Berman J. An isochromosome confers drug resistance in vivo by amplification of two genes, ERG11 and TAC1. *Mol Microbiol.* 2008 May;68(3):624–41.
  61. Esquivel BD, Smith AR, Zavrel M, White TC. Azole drug import into the pathogenic fungus *Aspergillus fumigatus*. *Antimicrob Agents Chemother.* 2015;59(6):3390–8.
  62. Hamamoto H, Hasegawa K, Nakaune R, Lee YJ, Makizumi Y, Akutsu K, et al. Tandem repeat of a transcriptional enhancer upstream of the sterol 14 $\alpha$ -demethylase gene (CYP51) in *Penicillium digitatum*. *Appl Environ Microbiol.* 2000 Aug 1;66(8):3421–6.
  63. Snelders E, Karawajczyk A, Verhoeven RJA, Venselaar H, Schaftenaar G, Verweij PE, et al. The structure–function relationship of the *Aspergillus fumigatus* cyp51A L98H conversion by site-directed mutagenesis: The mechanism of L98H azole resistance. *Fungal Genet Biol.* 2011 Nov 1;48(11):1062–70.
  64. Hoot SJ, Smith AR, Brown RP, White TC. An A643V amino acid substitution in Upc2p contributes to azole resistance in well-characterized clinical isolates of



- Candida albicans*. *Antimicrob Agents Chemother*. 2011 Feb;55(2):940–2.
65. Morio F, Pagniez F, Besse M, Gay-Andrieu F, Miegerville M, Le Pape P. Deciphering azole resistance mechanisms with a focus on transcription factor-encoding genes TAC1, MRR1 and UPC2 in a set of fluconazole-resistant clinical isolates of *Candida albicans*. *Int J Antimicrob Agents*. 2013 Nov;42(5):410–5.
  66. Marichal P, Koymans L, Willemsens S, Bellens D, Verhasselt P, Luyten W, et al. Contribution of mutations in the cytochrome P450 14 $\alpha$ -demethylase (Erg11p, Cyp51p) to azole resistance in *Candida albicans*. *Microbiology*. 1999;145(10):2701–13.
  67. Coste A, Selmecki A, Forche A, Diogo D, Bougnoux ME, D’Enfert C, et al. Genotypic evolution of azole resistance mechanisms in sequential *Candida albicans* isolates. *Eukaryot Cell*. 2007 Oct;6(10):1889–904.
  68. Cannon RD, Lamping E, Holmes AR, Niimi K, Baret P V, Keniya M V, et al. Efflux-mediated antifungal drug resistance. *Clin Microbiol Rev*. 2009 Apr;22(2):291–321, Table of Contents.
  69. Holmes AR, Cardno TS, Strouse JJ, Ivnitski-Steele I, Keniya M V, Lackovic K, et al. Targeting efflux pumps to overcome antifungal drug resistance. *Future Med Chem*. 2016;8(12):1485–501.
  70. Nett JE, Crawford K, Marchillo K, Andes DR. Role of Fks1p and Matrix Glucan in *Candida albicans* Biofilm Resistance to an Echinocandin, Pyrimidine, and Polyene. *Antimicrob Agents Chemother*. 2010;54(8):3505–8.
  71. Chowdhary A, Voss A, Meis JF. Multidrug-resistant *Candida auris* : ‘new kid on the block’ in hospital-associated infections? *J Hosp Infect*. 2016 Nov;94(3):209–12.
  72. Sharma C, Kumar N, Pandey R, Meis JF, Chowdhary A. Whole genome sequencing of emerging multidrug resistant *Candida auris* isolates in India demonstrates low genetic variation. *New Microbes New Infect*. 2016 Sep;13:77–82.
  73. Mabey D, Peeling RW, Ustianowski A, Perkins MD. Diagnostics for the developing world. *Nat Rev Microbiol*. 2004 Mar;2(3):231–40.
  74. Lockhart SR, Etienne KA, Vallabhaneni S, Farooqi J, Chowdhary A, Govender NP, et al. Simultaneous emergence of multidrug-resistant *Candida auris* on 3 continents confirmed by whole-genome sequencing and epidemiological analyses. *Clin Infect Dis*. 2017 Jan 15;64(2):134–40.
  75. Sharma C, Kumar N, Pandey R, Meis JF, Chowdhary A. Whole genome sequencing of emerging multidrug resistant *Candida auris* isolates in India demonstrates low genetic variation. *New microbes new Infect*. 2016 Sep;13:77–82.
  76. Chatterjee S, Alampalli SV, Nageshan RK, Chettiar ST, Joshi S, Tatu US. Draft genome of a commonly misdiagnosed multidrug resistant pathogen *Candida auris*. *BMC Genomics*. 2015 Sep 7;16(1):686–9.
  77. Oliver JD, Sibley GEM, Beckmann N, Dobb KS, Slater MJ, McEntee L, et al. F901318 represents a novel class of antifungal drug that inhibits dihydroorotate dehydrogenase. *Proc Natl Acad Sci U S A*. 2016 Nov 8;113(45):12809–14.
  78. Warrilow AGS, Hull CM, Parker JE, Garvey EP, Hoekstra WJ, Moore WR, et al. The clinical candidate VT-1161 is a highly potent inhibitor of *Candida albicans* CYP51 but fails to bind the human enzyme. *Antimicrob Agents Chemother*. 2014

- Dec 1;58(12):7121–7.
79. Monk BC, Keniya M V., Sabherwal M, Wilson RK, Graham DO, Hassan HF, et al. Azole resistance reduces susceptibility to the tetrazole antifungal VT-1161. *Antimicrob Agents Chemother.* 2019 Jan 1;63(1):1–19.
  80. Warrillow AGS, Parker JE, Price CL, Nes WD, Garvey EP, Hoekstra WJ, et al. The investigational drug VT-1129 is a highly potent inhibitor of *Cryptococcus* species CYP51 but only weakly inhibits the human enzyme. *Antimicrob Agents Chemother.* 2016;60(8):4530–8.
  81. Nielsen K, Vedula P, Smith KD, Meya DB, Garvey EP, Hoekstra WJ, et al. Activity of VT-1129 against *Cryptococcus neoformans* clinical isolates with high fluconazole MICs. *Med Mycol.* 2017 Sep 24;55(4):453–6.
  82. Schell WA, Jones AM, Garvey EP, Hoekstra WJ, Schotzinger RJ, Alexander BD. Fungal CYP51 inhibitors VT-1161 and VT-1129 exhibit strong in vitro activity against *Candida glabrata* and *C. krusei* isolates clinically resistant to azole and echinocandin antifungal compounds. *Antimicrob Agents Chemother.* 2017 Mar 1;61(3):1–3.
  83. Scorzoni L, de Paula e Silva ACA, Marcos CM, Assato PA, de Melo WCMA, de Oliveira HC, et al. Antifungal therapy: New advances in the understanding and treatment of mycosis. *Front Microbiol.* 2017;8(JAN):1–23.
  84. Edwards JE. Fungal cell wall vaccines: An update. *J Med Microbiol.* 2012;61(PART7):895–903.
  85. Kumaresan PR, Manuri PR, Albert ND, Maiti S, Singh H, Mi T, et al. Bioengineering T cells to target carbohydrate to treat opportunistic fungal infection. *Proc Natl Acad Sci U S A.* 2014;111(29):10660–5.
  86. Van Meer G, Voelker DR, Feigenson GW. Membrane lipids: Where they are and how they behave. *Nat Rev Mol Cell Biol.* 2008;9(2):112–24.
  87. Escribá P V., González-Ros JM, Goñi FM, Kinnunen PKJ, Vigh L, Sánchez-Magraner L, et al. Membranes: a meeting point for lipids, proteins and therapies. *J Cell Mol Med.* 2008 Jun 1;12(3):829–75.
  88. Czabany T, Athenstaedt K, Daum G. Synthesis, storage and degradation of neutral lipids in yeast. *Biochim Biophys Acta - Mol Cell Biol Lipids.* 2007 Mar 1;1771(3):299–309.
  89. Holthuis JCM, Menon AK. Lipid landscapes and pipelines in membrane homeostasis. *Nature.* 2014;510(7503):48–57.
  90. Payet LA, Pineau L, Snyder ECR, Colas J, Moussa A, Vannier B, et al. Saturated fatty acids alter the late secretory pathway by modulating membrane properties. *Traffic.* 2013;14(12):1228–41.
  91. Surma MA, Klose C, Peng D, Shales M, Mrejen C, Stefanko A, et al. A lipid E-MAP identifies Ubx2 as a critical regulator of lipid saturation and lipid bilayer stress. *Mol Cell.* 2013;51(4):519–30.
  92. Gross RW, Han X. Shotgun lipidomics of neutral lipids as an enabling technology for elucidation of lipid-related diseases. *Am J Physiol - Endocrinol Metab.* 2009;297(2):297–303.
  93. Unger RH. Lipotoxic Diseases. *Annu Rev Med.* 2002;53(1):319–36.
  94. Volmer R, Ron D. Lipid-dependent regulation of the unfolded protein response. *Curr Opin Cell Biol.* 2015 Apr;33:67–73.
  95. Giaever G, Chu AM, Ni L, Connelly C, Riles L, Véronneau S, et al. Functional

- profiling of the *Saccharomyces cerevisiae* genome. *Nature*. 2002 Jul;418(6896):387–91.
96. Steinmetz LM, Scharfe C, Deutschbauer AM, Mokranjac D, Herman ZS, Jones T, et al. Systematic screen for human disease genes in yeast. *Nat Genet*. 2002;31(4):400–4.
  97. Ballweg S, Ernst R. Control of membrane fluidity: the OLE pathway in focus. *Biol Chem*. 2017;398(2):215–28.
  98. Klose C, Surma MA, Gerl MJ, Meyenhofer F, Shevchenko A, Simons K. Flexibility of a eukaryotic lipidome - insights from yeast lipidomics. Polymenis M, editor. *PLoS One*. 2012 Apr 18;7(4):1–11.
  99. Tehlivets O, Scheuringer K, Kohlwein SD. Fatty acid synthesis and elongation in yeast. *Biochim Biophys Acta - Mol Cell Biol Lipids*. 2007;1771(3):255–70.
  100. Lykidis A. Comparative genomics and evolution of eukaryotic phospholipid biosynthesis. *Prog Lipid Res*. 2007;46(3–4):171–99.
  101. López Alonso D, García-Maroto F, Rodríguez-Ruiz J, Garrido JA, Vilches MA. Evolution of the membrane-bound fatty acid desaturases. *Biochem Syst Ecol*. 2003;31:1111–24.
  102. Klug L, Daum G. Yeast lipid metabolism at a glance. *FEMS Yeast Res*. 2014;14(3):369–88.
  103. Nakamura T, Nguyet VTA, Kato S, Arie Y, Akino T, Izawa S. Trans 18-carbon monoenoic fatty acid has distinct effects from its isomeric cis fatty acid on lipotoxicity and gene expression in *Saccharomyces cerevisiae*. *J Biosci Bioeng*. 2017 Jan 1;123(1):33–8.
  104. Stukey JE, McDonough VM, Martin CE. Isolation and Characterization of Ole1, a Gene Affecting Fatty-Acid Desaturation from *Saccharomyces-Cerevisiae*. *J Biol Chem*. 1989;264(28):16537–44.
  105. Ernst R, Ejsing CS, Antonny B. Homeoviscous Adaptation and the Regulation of Membrane Lipids. *J Mol Biol*. 2016 Dec 4;428(24):4776–91.
  106. Martin CE, Oh CS, Jiang Y. Regulation of long chain unsaturated fatty acid synthesis in yeast. *Biochim Biophys Acta - Mol Cell Biol Lipids*. 2007;1771(3):271–85.
  107. Holthuis JCM, Menon AK. Lipid landscapes and pipelines in membrane homeostasis. *Nature*. 2014;510(7503):48–57.
  108. Suutari M, Liukkonen K, Laakso S. Temperature adaptation in yeasts: The role of fatty acids. *Journal of General Microbiology*. 1990;136(8):1469-1474.
  109. Stewart LC, Yaffe MP. A Role for Unsaturated Fatty Acids in Mitochondrial Movement and Inheritance. *JCB*. 1991;115(5):1249–57.
  110. Rockenfeller P, Ring J, Muschett V, Beranek A, Büttner S, Carmona-Gutierrez D, et al. Fatty acids trigger mitochondrion-dependent necrosis. *Cell Cycle*. 2010 Jul 15;9(14):2908–14.
  111. Bloomfield DK, Bloch K. The formation of delta 9-unsaturated fatty acids. *J Biol Chem*. 1960;235(2):337–45.
  112. Holloway PW, Katz JT. A Requirement for Cytochrome b5 in Microsomal Stearyl Coenzyme a Desaturation. *Biochemistry*. 1972;11(20):3689–96.
  113. P. W. Holloway, Wakil SJ. Requirement for Reduced Diphosphopyridine Nucleotide-Cytochrome bs Reductase in Stearyl Coenzyme A Desaturation. *J Biol Chem*. 1970;245(7):1862–5.

114. Strittmatter P, Spatz L, Corcoran D, Rogers MJ, Setlow B, Redline R. Purification and properties of rat liver microsomal stearyl coenzyme A desaturase. *Proc Natl Acad Sci U S A*. 1974;71(11):4565–9.
115. Enoch HG, Catala A, Strittmatter P. Mechanism of rat liver microsomal stearyl CoA desaturase. Studies of the substrate specificity, enzyme substrate interactions, and the function of lipid. *J Biol Chem*. 1976;251(16):5095–103.
116. Stuke JE, McDonough VM, Martin CE. The OLE1 gene of *Saccharomyces cerevisiae* encodes the delta9 fatty acid desaturase and can be functionally replaced by the rat stearyl-CoA desaturase gene. *J Biol Chem*. 1990;265(33):20144–9.
117. Tuller G, Nemeč T, Hraštnik C, Daum G. Lipid composition of subcellular membranes of an FY1679-derived haploid yeast wild-type strain grown on different carbon sources. *Yeast*. 1999;15(14):1555–64.
118. Mitchell AG, Martin CE. A novel cytochrome b5-like domain is linked to the carboxyl terminus of the *Saccharomyces cerevisiae* delta-9 fatty acid desaturase. *J Biol Chem*. 1995 Dec 15;270(50):29766–72.
119. Kaestner KH, Ntambi JM, Kelly TJ, Lane MD. Differentiation-induced gene expression in 3T3-L1 preadipocytes. A second differentially expressed gene encoding stearyl-CoA desaturase. *J Biol Chem*. 1989;264(25):14755–61.
120. Ntambi JM. The regulation of stearyl-CoA desaturase (SCD). *Prog Lipid Res*. 1995;34(2):139–50.
121. Zheng Y, Prouty SM, Harmon A, Sundberg JP, Stenn KS, Parimoo S. Scd3 - A novel gene of the stearyl-CoA desaturase family with restricted expression in skin. *Genomics*. 2001;71(2):182–91.
122. Mihara K. Structure and Regulation of Rat Liver Microsomal Stearyl-CoA Desaturase Gene. *J Biochem*. 1990;108:1022–9.
123. Zhang L, Ge L, Parimoo S, Stenn K, Prouty SM. Human stearyl-CoA desaturase : alternative transcripts generated from a single gene by usage of tandem polyadenylation sites. *Biochem J*. 1999;340:255–64.
124. James M. Ntambia, Makoto Miyazaki and AD. Regulation of stearyl-CoA desaturase expression. *Lipids*. 2004;39(11):1061–5.
125. Wang H, Klein MG, Zou H, Lane W, Snell G, Levin I, et al. Crystal structure of human stearyl-coenzyme A desaturase in complex with substrate. *Nat Struct Mol Biol*. 2015 Jul 22;22(7):581–5.
126. Shanklin J, Whittle E, Fox BG. Eight Histidine Residues Are Catalytically Essential in a Membrane-Associated Iron Enzyme, Stearyl-CoA Desaturase, and Are Conserved in Alkane Hydroxylase and Xylene Monooxygenase. *Biochemistry*. 1994;33(43):12787–94.
127. Sperling P, Ternes P, Zank TK, Heinz E. The evolution of desaturases. *Prostaglandins Leukot Essent Fat Acids*. 2003 Feb;68(2):73–95.
128. Bai Y, McCoy JG, Levin EJ, Sobrado P, Rajashankar KR, Fox BG, et al. X-ray structure of a mammalian stearyl-CoA desaturase. *Nature*. 2015 Aug 22;524(7564):252–6.
129. Man WC, Miyazaki M, Chu K, Ntambi JM. Membrane topology of mouse stearyl-CoA desaturase 1. *J Biol Chem*. 2006 Jan 13;281(2):1251–60.
130. Zhang S, Skalsky Y, Garfinkel DJ. MGA2 or SPT23 is required for transcription of the  $\Delta 9$  fatty acid desaturase gene, OLE1, and nuclear membrane integrity in

- Saccharomyces cerevisiae*. *Genetics*. 1999;151(2):473–83.
131. Choi JY, Stukey J, Hwang SY, Martin CE. Regulatory elements that control transcription activation and unsaturated fatty acid-mediated repression of the *Saccharomyces cerevisiae* OLE1 gene. *J Biol Chem*. 1996 Feb 16;271(7):3581–9.
  132. Gonzalez CI, Martin CE. Fatty acid-responsive control of mRNA stability. Unsaturated fatty acid-induced degradation of the *Saccharomyces* OLE1 transcript. *J Biol Chem*. 1996 Oct 18;271(42):25801–9.
  133. Nakagawa Y, Sakumoto N, Kaneko Y, Harashima S. Mga2p is a putative sensor for low temperature and oxygen to induce OLE1 transcription in *Saccharomyces cerevisiae*. *Biochem Biophys Res Commun*. 2002;291(3):707–13.
  134. Kwast KE, Burke P V, Poyton RO. Oxygen sensing and the transcriptional regulation of oxygen-responsive genes in yeast. *J Exp Biol*. 1998;201:1177–95.
  135. Bossie MA, Martin CE. Nutritional regulation of a yeast  $\Delta$ -9 fatty acid desaturase activity. *J Bacteriol*. 1989;171(12):6409–13.
  136. Zhang SR, Burkett TJ, Yamashita I, Garfinkel DJ, Kohlwein SD. Genetic redundancy between SPT23 and MGA2: Regulators of Ty-induced mutations and Ty1 transcription in *Saccharomyces cerevisiae*. *Mol Cell Biol*. 1997 Aug;17(8):4718–29.
  137. Auld KL, Brown CR, Casolari JM, Komili S, Silver PA. Genomic Association of the Proteasome Demonstrates Overlapping Gene Regulatory Activity with Transcription Factor Substrates. *Mol Cell*. 2006;21:861–71.
  138. Hentze MW, Muckenthaler MU, Andrews NC. Review Balancing Acts: Molecular Control of Mammalian Iron Metabolism sequences of systemic iron overload result from chronic iron accumulation in tissues. Systemic iron imbalance is not a sine qua non for. *Cell* 2004 p. 285–97.
  139. Rape M, Hoppe T, Gorr I, Kalocay M, Richly H, Jentsch S. Mobilization of Processed, Membrane-Tethered SPT23 Transcription Factor by CDC48UFD1/NPL4, a Ubiquitin-Selective Chaperone. *Cell*. 2001 Nov 30;107(5):667–77.
  140. Covino R, Ballweg S, Stordeur C, Michaelis JB, Puth K, Wernig F, et al. A Eukaryotic Sensor for Membrane Lipid Saturation. *Mol Cell*. 2016;63(1):49–59.
  141. Ballweg S, Sezgin E, Wunnicke D, Hänelt I, Ernst R. Regulation of lipid saturation without sensing membrane fluidity. *bioRxiv*. 2019;(5):706556.
  142. Bhattacharya S, Shcherbik N, Vasilescu J, Smith JC, Figeys D, Haines DS. Identification of Lysines within Membrane-Anchored Mga2p120 that Are Targets of Rsp5p Ubiquitination and Mediate Mobilization of Tethered Mga2p90. *J Mol Biol*. 2009;385(3):718–25.
  143. Shcherbik N, Haines DS. Cdc48pNpl4p/Ufd1p Binds and Segregates Membrane-Anchored/Tethered Complexes via a Polyubiquitin Signal Present on the Anchors. *Mol Cell*. 2007 Feb 9;25(3):385–97.
  144. Kolawa N, Sweredoski MJ, Graham RLJ, Oania R, Hess S, Deshaies RJ. Perturbations to the ubiquitin conjugate proteome in yeast  $\delta$ ubx mutants identify Ubx2 as a regulator of membrane lipid composition. *Mol Cell Proteomics*. 2013 Oct;12(10):2791–803.
  145. Richly H, Rape M, Braun S, Rumpf S, Hoegge C, Jentsch S. A Series of Ubiquitin Binding Factors Connects CDC48/p97 to Substrate Multiubiquitylation and Proteasomal Targeting to mobilize ubiquitylated substrates from the cytosolic.

- Cell. 2005;120:73–84.
146. Pineau L, Colas J, Dupont S, Beney L, Fleurat-Lessard P, Berjeaud J-M, et al. Lipid-Induced ER Stress: Synergistic Effects of Sterols and Saturated Fatty Acids. *Traffic*. 2009 Jun 1;10(6):673–90.
  147. De Smet CH, Vittone E, Scherer M, Houweling M, Liebisch G, Brouwers JF, et al. The yeast acyltransferase Sct1p regulates fatty acid desaturation by competing with the desaturase Ole1p. *Mol Biol Cell*. 2012;23(7):1146–56.
  148. Kajiwara S, Aritomi T, Suga K, Ohtaguchi K, Kobayashi O. Overexpression of the OLE1 gene enhances ethanol fermentation by *Saccharomyces cerevisiae*. *Appl Microbiol Biotechnol*. 2000;53(5):568–74.
  149. Pagac M, Vazquez HM, Bochud A, Roubaty C, Knöpfli C, Vionnet C, et al. Topology of the microsomal glycerol-3-phosphate acyltransferase Gpt2p/Gat1p of *Saccharomyces cerevisiae*. *Mol Microbiol*. 2012 Dec;86(5):1156–66.
  150. Westermann B. Mitochondrial inheritance in yeast. *Biochim Biophys Acta - Bioenerg*. 2014 Jul 1;1837(7):1039–46.
  151. Levine TP, Munro S. Dual Targeting of Osh1p, a Yeast Homologue of Oxysterol-binding Protein, to both the Golgi and the Nucleus-Vacuole Junction. *Mol Biol Cell*. 2001;12:1633–44.
  152. Loewen CJR, Young BP, Tavassoli S, Levine TP. Inheritance of cortical ER in yeast is required for normal septin organization. *J Cell Biol*. 2007 Nov 5;179(3):467–83.
  153. Gatta AT, Wong LH, Sere YY, Calderón-Noreña DM, Cockcroft S, Menon AK, et al. A new family of StART domain proteins at membrane contact sites has a role in ER-PM sterol transport. *Elife*. 2015 May 22;4:1–46.
  154. Sikorski RS, Hieter P, Garfinkel DJ. A system of shuttle vectors and yeast host strains designed for efficient manipulation of DNA in *Saccharomyces cerevisiae*. *Genetics*. 1989 May 1;122(1):19–27.
  155. Singh M V., Weil PA. A method for plasmid purification directly from yeast. *Anal Biochem*. 2002;307(1):13–7.
  156. Keith AD, Resnick MR, Haley AB. Fatty acid desaturase mutants of *Saccharomyces cerevisiae*. *J Bacteriol*. 1969;98(2):415–20.
  157. Tatzler V, Zellnig GN, Kohlwein SD, Schneiter R. Lipid-dependent Subcellular Relocalization of the Acyl Chain Desaturase in Yeast. *Mol Biol Cell*. 2002;13:4429–42.
  158. Oshino N, Imai Y, Sato R. Electron-transfer mechanism associated with fatty acid desaturation catalyzed by liver microsomes. *Biochim Biophys Acta - Enzymol Biol Oxid*. 1966 Oct;128(1):13–28.
  159. Baker Brachmann C, Davies A, Cost GJ, Caputo E, Li J, Hieter P, et al. Designer Deletion Strains derived from *Saccharomyces cerevisiae* S288C: a Useful set of Strains and Plasmids for PCR-mediated Gene Disruption and Other Applications. *Yeast*. 1998;14(14):115–32.
  160. EUCAST. EUCAST antifungal MIC method for yeasts. EUCAST Definitive Doc EDEF 731. 2015;(December):1–21.
  161. Oliveira JA, West CP, Afif E, Palencia P. Method for the determination of broth dilution minimum inhibitory concentrations of antifungal agents for conidia forming moulds. Vol. 9, EUCAST E.DEF. Scientific Data Coordinator; 2017.
  162. Bojsen R, Regenber B, Folkesson A. *Saccharomyces cerevisiae* biofilm tolerance towards systemic antifungals depends on growth phase. *BMC Microbiology*.

- 2014;14(1):1-10.
163. Aravind L, Watanabe H, Lipman DJ, Koonin E V. Lineage-specific loss and divergence of functionally linked genes in eukaryotes. *Proc Natl Acad Sci U S A*. 2000;97(21):11319–24.
  164. Los DA, Murata N. Structure and expression of fatty acid desaturases. *Biochim Biophys Acta - Lipids Lipid Metab*. 1998 Oct 2;1394(1):3–15.
  165. Braun S, Matuschewski K. Role of the ubiquitin-selective CDC48UFD1/NPL4 chaperone (segregase) in ERAD of OLE1 and other substrates. *EMBO J*. 2002;21(4):615–21.
  166. Xu D, Sillaots S, Davison J, Hu W, Jiang B, Kauffman S, et al. Chemical genetic profiling and characterization of small-molecular compounds that affect the biosynthesis of unsaturated fatty acids in *Candida albicans*. *J Biol Chem*. 2009 Jul 17;284(29):19754–64.
  167. Stukey JE, McDonough VM, Martins CE. Isolation and Characterization of OLE 1 , a Gene Affecting Fatty Acid Desaturation from *Saccharomyces cerevisiae*. 1989;264(28):16537–44.
  168. Senyilmaz-Tiebe D, Pfaff DH, Virtue S, Schwarz K V., Fleming T, Altamura S, et al. Dietary stearic acid regulates mitochondria in vivo in humans. *Nat Commun*. 2018 Dec 7;9(1):3129.
  169. Schneider-Poetsch T, Ju J, Eyler DE, Dang Y, Bhat S, Merrick WC, et al. Inhibition of eukaryotic translation elongation by cycloheximide and lactimidomycin. *Nat Chem Biol*. 2010 Mar;6(3):209–17.
  170. Wang J, Yu L, Schmidt RE, Su C, Huang X, Gould K, et al. Characterization of HSCD5, a novel human stearyl-CoA desaturase unique to primates. *Biochem Biophys Res Commun*. 2005 Jul;332(3):735–42.
  171. Dekker WJC, Wiersma SJ, Bouwknecht J, Mooiman C, Pronk JT. Anaerobic growth of *Saccharomyces cerevisiae* CEN.PK113-7D does not depend on synthesis or supplementation of unsaturated fatty acids. *FEMS Yeast Res*. 2019 Sep 1;19(6):1–10.
  172. Petschnigg J, Wolinski H, Kolb D, Zellnig G, Kurat CF, Natter K, et al. Good fat, essential cellular requirements for triacylglycerol synthesis to maintain membrane homeostasis in yeast. *J Biol Chem*. 2009 Nov 6;284(45):30981–93.
  173. Ariyama H, Kono N, Matsuda S, Inoue T, Arai H. Decrease in membrane phospholipid unsaturation induces unfolded protein response. *J Biol Chem*. 2010 Jul 16;285(29):22027–35.
  174. Ben-Ami R, Lewis RE, Kontoyiannis DP. Immunocompromised Hosts: Immunopharmacology of Modern Antifungals. *Clin Infect Dis*. 2008 Jul 15;47(2):226–35.
  175. Bernales S, McDonald KL, Walter P. Autophagy counterbalances endoplasmic reticulum expansion during the unfolded protein response. *PLoS Biol*. 2006;4(12):2311–24.
  176. McConnell SJ, Stewart LC, Talin A, Yaffe MP. Temperature-sensitive yeast mutants defective in mitochondrial inheritance. *J Cell Biol*. 1990;111(3):967–76.
  177. Youle RJ, Van Der Bliek AM. Mitochondrial Fission, Fusion, and Stress. 2012.
  178. Long Q, Zhao D, Fan W, Yang L, Zhou Y, Qi J, et al. Modeling of Mitochondrial Donut Formation. *Biophysj*. 2015;109:892–9.
  179. Liu X, Hajnóczky G. Altered fusion dynamics underlie unique morphological

- changes in mitochondria during hypoxia–reoxygenation stress. *Cell Death Differ.* 2011 Oct 4;18(10):1561–72.
180. Ray PD, Huang B-W, Tsuji Y. Reactive oxygen species (ROS) homeostasis and redox regulation in cellular signaling. *Cell Signal.* 2012 May;24(5):981–90.
  181. Oshino N, Sato R. The dietary control of the microsomal stearyl CoA desaturation enzyme system in rat liver. *Arch Biochem Biophys.* 1972;149(2):369–77.
  182. Thrower JS, Hoffman L, Rechsteiner M, Pickart CM, Yokosawa H, Toh-e A, et al. Recognition of the polyubiquitin proteolytic signal. *EMBO J.* 2000 Jan 4;19(1):94–102.
  183. Liu C, Apodaca J, Davis LE, Rao H. Proteasome inhibition in wild-type yeast *Saccharomyces cerevisiae* cells. *Biotechniques.* 2007;42(2):158–62.
  184. Cavellini L, Meurisse J, Findinier J, Erpapazoglou Z, Belgareh-Touzé N, Weissman AM, et al. An ubiquitin-dependent balance between mitofusin turnover and fatty acids desaturation regulates mitochondrial fusion. *Nat Commun.* 2017;8(May 2016):1–15.
  185. Kodedová M, Sychrová H. Changes in the sterol composition of the plasma membrane affect membrane potential, salt tolerance and the activity of multidrug resistance pumps in *Saccharomyces cerevisiae*. *PLoS One.* 2015;10(9):1–19.
  186. Collins GA, Gomez TA, Deshaies RJ, Tansey WP. Combined chemical and genetic approach to inhibit proteolysis by the proteasome. *Yeast.* 2010 Nov;27(11):965–74.
  187. Ho N, Xu C, Thibault G. From the unfolded protein response to metabolic diseases - lipids under the spotlight. *J Cell Sci.* 2018;131(3):1–9.
  188. Thumm M. Structure and function of the yeast vacuole and its role in autophagy. *Microsc Res Tech.* 2000 Dec 15;51(6):563–72.
  189. Nakatogawa H, Suzuki K, Kamada Y, Ohsumi Y. Dynamics and diversity in autophagy mechanisms: lessons from yeast. 2009 Jul 3;10(7):458–67.
  190. Noda T, Kim J, Huang W-P, Baba M, Tokunaga C, Ohsumi Y, et al. Apg9p/Cvt7p Is an Integral Membrane Protein Required for Transport Vesicle Formation in the Cvt and Autophagy Pathways. *J Cell Biol.* 2000;148(3):465–79.
  191. Ogasawara Y, Kira S, Mukai Y, Noda T, Yamamoto A. Ole1, fatty acid desaturase, is required for Atg9 delivery and isolation membrane expansion during autophagy in *Saccharomyces cerevisiae*. *Biol Open.* 2017;6(1):35–40.
  192. Bravo R, Parra V, Gatica D, Rodriguez AE, Torrealba N, Paredes F, et al. Endoplasmic Reticulum and the Unfolded Protein Response. Dynamics and Metabolic Integration. *Int Rev Cell Mol Biol.* 2013;301:215–90.
  193. Nguyen TB, Louie SM, Daniele JR, Tran Q, Dillin A, Zoncu R, et al. DGAT1-Dependent Lipid Droplet Biogenesis Protects Mitochondrial Function during Starvation-Induced Autophagy. *Dev Cell.* 2017 Jul 10;42(1):9–21.
  194. Mora C, Tittensor DP, Adl S, Simpson AGB, Worm B. How many species are there on earth and in the ocean? *PLoS Biol.* 2011;9(8):1–8.
  195. Brown GD, Denning DW, Levitz SM. Tackling human fungal infections. *Science* (80- ). 2012 May 11;336(6082):647.
  196. Xiao M, Sun Z-Y, Kang M, Guo D-W, Liao K, C-A Chen S, et al. Five-Year National Surveillance of Invasive Candidiasis: Species Distribution and Azole Susceptibility



- from the China Hospital Invasive Fungal Surveillance Net (CHIF-NET) Study. *J Clin Microbiol*. 2018;56:577–95.
197. Champion OL, Wagley S, Titball RW. *Galleria mellonella* as a model host for microbiological and toxin research. *Virulence*. 2016;7(7):840–5.
  198. Wojda I. Immunity of the greater wax moth *Galleria mellonella*. *Insect Sci*. 2017 Jun 1;24(3):342–57.
  199. Kavanagh K, Sheehan G. The use of *Galleria mellonella* larvae to identify novel antimicrobial agents against fungal species of medical interest. *J Fungi*. 2018 Sep 19;4(3):1–13.
  200. Roy RM, Klein BS. Dendritic Cells in Antifungal Immunity and Vaccine Design. *Cell Host Microbe*. 2012 May;11(5):436–46.
  201. Pappagianis D. Evaluation of the Protective Efficacy of the Killed *Coccidioides immitis* Spherule Vaccine in Humans . *Am Rev Respir Dis*. 1993 Sep 17;148(3):656–60.
  202. Knechtle P, Diefenbacher M, Greve KB V, Brianza F, Folly C, Heider H, et al. The Natural Diyne-Furan Fatty Acid EV-086 Is an Inhibitor of Fungal Delta-9 Fatty Acid Desaturation with Efficacy in a Model of Skin Dermatophytosis Downloaded from. *Antimicrob Agents Chemother*. 2014;58(1):455–66.
  203. Moman RN, Varacallo M. *Physiology, Albumin*. StatPearls. StatPearls Publishing; 2019.
  204. Larsen MT, Kuhlmann M, Hvam ML, Howard KA. Albumin-based drug delivery: harnessing nature to cure disease. *Mol Cell Ther*. 2016;4(1):2–12.
  205. Nguyen LN, Gacser A, Nosanchuk JD. The stearoyl-coenzyme A desaturase 1 is essential for virulence and membrane stress in *Candida parapsilosis* through unsaturated fatty acid production. *Infect Immun*. 2011 Jan 1;79(1):136–45.
  206. Wallin E, Heijne G Von. Genome-wide analysis of integral membrane proteins from eubacterial, archaean, and eukaryotic organisms. *Protein Sci*. 2008 Dec 31;7(4):1029–38.
  207. Zhang S, Skalsky Y, Garfinkel DJ. MGA2 or SPT23 is required for transcription of the  $\Delta 9$  fatty acid desaturase gene, OLE1, and nuclear membrane integrity in *Saccharomyces cerevisiae*. *Genetics*. 1999;151(2):473–83.
  208. Stuke JE, McDonough VM, Martin CE. The OLE1 gene of *Saccharomyces cerevisiae* encodes the  $\Delta 9$  fatty acid desaturase and can be functionally replaced by the rat stearoyl-CoA desaturase gene. *J Biol Chem*. 1990;265(33):20144–9.
  209. Brown JM, Chung S, Sawyer JK, Degirolamo C, Alger HM, Nguyen T, et al. Inhibition of stearoyl-coenzyme A desaturase 1 dissociates insulin resistance and obesity from atherosclerosis. *Circulation*. 2008 Sep 30;118(14):1467–75.
  210. Iida T, Ubukata M, Mitani I, Nakagawa Y, Maeda K, Imai H, et al. Discovery of potent liver-selective stearoyl-CoA desaturase-1 (SCD1) inhibitors, thiazole-4-acetic acid derivatives, for the treatment of diabetes, hepatic steatosis, and obesity. *Eur J Med Chem*. 2018 Oct 5;158:832–52.
  211. Mason P, Liang B, Li L, Fremgen T, Murphy E, Quinn A, et al. SCD1 inhibition causes cancer cell death by depleting mono-unsaturated fatty acids. Lebedeva I V., editor. *PLoS One*. 2012 Mar 22;7(3):1–8.
  212. Tracz-Gaszewska Z, Dobrzyn P. Stearoyl-CoA desaturase 1 as a therapeutic target for the treatment of cancer. Vol. 11, *Cancers*. MDPI AG; 2019. p. 1–25.
  213. Röhrig F, Schulze A. The multifaceted roles of fatty acid synthesis in cancer. Vol.

- 16, Nature Reviews Cancer. Nature Publishing Group; 2016. p. 732–49.
214. Medes G, Thomas A, Weinhouse S. Metabolism of Neoplastic Tissue. IV. A Study of Lipid Synthesis in Neoplastic Tissue Slices in Vitro. *Cancer Res.* 1953 Jan 1;13(1):27–9.
215. Zhang Z, Dales NA, Winther MD. Opportunities and challenges in developing stearoyl-coenzyme A desaturase-1 inhibitors as novel therapeutics for human disease. *J Med Chem.* 2014 Jun 26;57(12):5039–56.